NASA Technical Memorandum 100726

Tunneling Calculations for GaAs-$Al_xGa_{(1-x)}As$ Graded Band-Gap Sawtooth Superlattices

K.A. Forrest and P.H.E. Meijer

April 1991

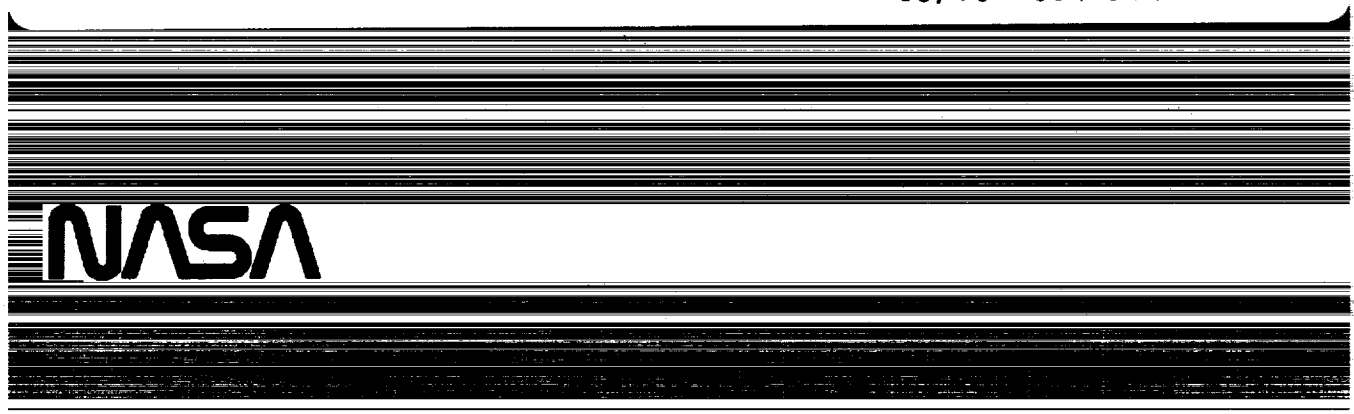

NASA Technical Memorandum 100726

Tunneling Calculations for GaAs-$Al_xGa_{(1-x)}As$ Graded Band-Gap Sawtooth Superlattices

K.A. Forrest
NASA-Goddard Space Flight Center
Greenbelt, Maryland

P.H.E. Meijer
The Catholic University of America
Washington, D.C.

National Aeronautics and
Space Administration

Goddard Space Flight Center
Greenbelt, MD

1991

FIGURES

10. The Difference Between Multiple Step Barriers and Multiple Quantum Wells (MQW).

For energies E below the top of the barriers or well, respectively, MSB's can have only virtual, or quasi-bound, states, while MQW's can have true bound states. Both types of heterostructure can support resonances for E greater than the barrier or well height.

11. Bound States and Resonances of a Single Quantum Well

a. $E > 0$: Transmission coefficients for uniform and varying effective masses. Resonances in T.

b. $E < 0$: Criterion for bound states. Eigenvalue condition on M_{11} gives bound states.

12. Transfer Matrix Method Applied to Arbitrary, Real Potential V(z).

The potential is broken into intervals Δz wide. Transfer matrices M_j at each step are multiplied to give overall transfer matrix M.

13. Single Quantum Well and Barrier in Uniform Electric Field F_{ap}

14. Transfer Matrix Method Applied to Finding Bound States of a Single Quantum Well in Uniform Electric Field F_{ap}

The region inside the well is divided into intervals where plane-wave transfer matrices are calculated. In the regions outside the well, the solutions of the Schroedinger equation are the Airy functions.

15. The Airy Function and Derivative with Negative Argument

a. Ai(-x)

b. Ai'(-x)

16. The Bairy Function and Derivative with Negative Argument

a. Bi(-x)

b. Bi'(-x)

17. Single Quantum Well in a Localized Electric Field.

The applied field is zero far from the well.

18. Deformation of a Single Quantum Well in a Localized Electric Field.

The applied field shifts the bound and quasi-bound levels to lower energy.

a. Low field strength, with true bound states at E_0 and E_1

b. Moderate field strength, with one true bound state at $E_0 - \Delta$, and a quasi-bound state at $E_1 - \Delta$.

c. High field strength, only quasi-bound states remain.

19. Transfer Matrix Method Applied to Single Quantum Well in Localized Field

The well and a small surrounding area over which the field extends are broken into intervals. At each step a transfer matrix M_i is calculated; the overall transfer matrix M is the product of all the M_i.

20. Transfer Matrix Method Applied to Multiple Step Barrier with N Periods in an External, Localized Electric Field F_{ap}.

21. Transfer Matrix Method Applied to Sawtooth Superlattice with N Periods in an External, Localized Electric Field F_{ap}.

22. Energy Band Structure of Pure GaAs (<100> and <111> directions) (33)

23. Complex Energy Band Structures of pure GaAs and AlAs (34)

i. (110) interface: a. GaAs b. AlAs

ii. (100) interface: a. GaAs b. AlAs

24. Energy Gap in Al(x)Ga(1-x)As as a Function of AlAs Mole Fraction x (19)

The x-dependence of the direct conduction band Γ_{1c} is shown by the solid line; that of the indirect gap X_{1c} by the dashed line. The direct and indirect minima are equal at x = 0.37

25. The Fraction of Conduction Electrons in Γ_{1c} of Al(x)Ga(1-x)As as a Function of AlAs Mole Fraction x.(18)

Data are taken at 300 K. Dotted line is for degenerate case with $N = 4\times10^{17}$ cm^{-3} ; solid line is for nondegenerate case with $N = 4\times10^{16}$ cm^{-3}.

26. Band-Edge Alignments at GaAs-Al(x)Ga(1-x)As Heterojunctions (R. Miller, ATT-Bell Laboratories)

a. ΔE_c, conduction band misalignment

b. ΔE_v, valence band misalignment

27. Esaki-Tsu Multiple Step Barrier Geometry (11)

a. Zero applied electric field

b. Applied field strength F = F_{ap} over the length l of the MSB

28. T-E Data for Single Step Barrier

Barrier is 10 nm wide, 0.33 eV high. Effective mass is uniform and equal to free electronic mass m_0.

29. T-E Data for Single GaAs-Al(0.4)Ga(0.6)As Step Barrier

Barrier is 10 nm wide and 0.33eV high. Effective mass is m_{in} = 0.0871 inside the barrier, m_{out} = 0.0636 outside.

30. T-E Data for Single Step Barriers 10nm Wide and 0.33 eV High.

a. Superposed T-E curves for GaAs-Al(0.4)Ga(0.6)As barrier, and barrier with uniform effective mass $m_{eff} = m_0$ everywhere. Curve 1: GaAs-Al(0.4)Ga(0.6)As, m_{in} = 0.0871, m_{out} = 0.0636; Curve 0: $m_{eff} = m_0$

b. Superposed T-E curves for GaAs-Al(0.4)Ga(0.6)As barrier, and barrier with uniform effective mass m_{eff} = 0.0636 everywhere. Curve 0: GaAs-Al(0.4)Ga(0.6)As; Curve 1: m_{eff} = 0.0636

31. Effects of Applied Electric Field on Transmission Coefficient of Single Step Barrier.

Barrier is 10 nm wide, 0.33 eV high. Effective mass = m_0 everywhere.

a. $F_{ap} = 0$

b. $F_{ap} = 2 \times 10^{-2}$ eV/nm

c. $F_{ap} = 5 \times 10^{-2}$ eV/nm

32. Effects of Applied Electric Field on Transmission Coefficient of Single GaAs-Al(0.4)Ga(0.6)As Step Barrier.

Barrier is 10 nm wide, 0.33 eV high. Inside the barrier m_{eff} = 0.0871, outside the barrier m_{eff} = 0.0636. Curve 0: $F_{ap} = 0$; Curve 1: $F_{ap} = 2 \times 10^{-2}$ eV/nm; Curve 2: $F_{ap} = 5 \times 10^{-2}$ eV/nm

33. Applied Field and Effective Mass Effects on Transmission Coefficient of Single Step Barriers.

Barriers are 10nm wide, 0.33 eV high. The two curves in each figure are for a barrier with uniform effective mass $m_{eff} = m_0$, and a GaAs-Al(0.4)Ga(0.6)As barrier: Curve 0: $m_{eff} = m_0$; Curve 1: m_{in} = 0.0871, m_{out} = 0.0636

a. Applied field $F_{ap} = 2 \times 10^{-2}$ eV/nm

b. Applied field $F_{ap} = 5 \times 10^{-2}$ eV/nm

34. Total Transfer Matrix Element M_{11} for Single GaAs-Al(0.5)Ga(0.5)As Quantum Well: Bound State.

Well is 3 nm wide, 0.4 eV deep. This calculation took account of the effective mass variation at the well edges: the effective masses inside and outside the well are m_{in} = 0.094, m_{out} = 0.0636. The minimum of M_{11} gives a bound state energy of -0.197 eV below the top of the well.

35. Bound State Energy as a Function of the Effective Mass Inside Well.

Well is the same as that of Figure 34. The effective mass, however, is taken in this calculation as 0.0636 inside and outside the well. The new bound state energy is -0.217 eV below the top of the well, instead of -0.197 eV.

Curve 0: Effective mass = 0.0636 everywhere. E_0 = -0.217 eV.

Curve 1: Effective mass = 0.094 inside the well, 0.0636 outside the well.E_0 = -0.197 eV.

36. Bound States in Single Quantum Well.

Well is 3nm wide, 0.4 eV deep. Effective mass is uniform and equal to m_0. The minima in M_{11} correspond to bound states. Using the free-electronic mass results in four bound states, in agreement with equation 139.

37. Total Transfer Matrix Element M_{11} as a Function of Localized Field Strength.

Data are for single GaAs-Al(0.5)Ga(0.5)As quantum well, 3 nm wide and 0.4 eV deep. Effective mass taken as 0.0636 everywhere. Each curve corresponds to a different field strength. Minima shift to energies deeper in the well as the field strength is increased.

Curve 0: F_{ap} = 0; Curve 1: $F_{ap} = 1 \times 10^{-2}$ eV/nm; Curve 2: $F_{ap} = 2 \times 10^{-2}$ eV/nm;

Curve 3: $F_{ap} = 3 \times 10^{-2}$ eV/nm; Curve 4: $F_{ap} = 4 \times 10^{-2}$ eV/nm;

Curve 5: $F_{ap} = 5 \times 10^{-2}$ eV/nm

38. Stark Shift of Bound State Energy Level under Localized Field.

Data are for single GaAs-Al(0.5)Ga(0.5)As quantum well, 3 nm wide and 0.4 eV deep. Effective mass taken as 0.0636 everywhere. In this figure the Stark shift (referred to the zero-field bound state energy) is plotted as a function of the applied field strength. The Stark shift is linear in the field strength.

39. The Ratio (F/E) as a Function of Energy and Applied Field Strength.

Data are for single GaAs-Al(0.5)Ga(0.5)As quantum well, 3 nm wide and 0.4 eV deep. Effective mass taken as 0.0636 everywhere; field is uniform and unrestricted. Each curve is for a different

field strength; the maxima in the data correspond to quasi-bound states of the quantum well. Maxima shift to energies deeper in the well as the field strength increases.
Curve 0: F_{ap} = 1.0 $\times 10^{-2}$ eV/nm; Curve 1: F_{ap} = 1.5 $\times 10^{-2}$ eV/nm;
Curve 2: F_{ap} = 2.0 $\times 10^{-2}$ eV/nm; Curve 3: F_{ap} = 2.5 $\times 10^{-2}$ eV/nm;
Curve 4: F_{ap} = 3.0 $\times 10^{-2}$ eV/nm

40. Stark Shift of Bound State Energy Level under Uniform, Unrestricted Field.
From Figure 39, the energy levels of the maxima in (F/E) are plotted as function of the applied field strength. The bound state energies are quadratically dependent on the applied field strength.

41. Stark Shift of Bound State Energy Levels under Uniform, Unrestricted Field.
From Figure 40, the Stark shift relative to the zero-field level is plotted as a function of the applied field strength. Also shown are the data of Austin and Jaros (41) for an identical quantum well.

42. Stark Shifts under Localized and Unrestricted Uniform Fields Compared.
From Figures 38 and 41, the Stark shifts calculated for a 3nm, 0.4 eV Al(0.5)Ga(0.5)As quantum well are plotted together.

43. T-E Curves for Two-, Three-, and Five-Barrier GaAs-Al(0.5)Ga(0.5)As Multiple Step Barriers.
These are the results of transfer matrix calculations for step barrier superlattices identical to those of Esaki and Tsu (11). Barriers are 2 nm wide, 5 nm apart, and 0.5 eV high. Effective mass in the barriers is m_{in} = 0.094, between the barriers m_{out} = 0.0636. Modified connection rules are used. Figures a, b, and c are for two, three and five barriers, respectively.

44. T-E curves for Two- and Five- Barrier Esaki-Tsu Type MSB's
The T-E curves from Figure 43 for two and five barriers superposed. Note the splitting of single resonances into four, caused by coupling between wells.

45. T-E Curves for Two-, Three-, and Five-Barrier MSB's Calculated By Esaki and Tsu (11).
Note the close agreement between these curves and those of Figure 43.

46. J-V Curves for Two- and Three-Barrier GaAs-Al(0.5)Ga(0.5)As MSB's
These curves are calculated for the same MSB's whose T-E curves appear in Figure 43.

47. J-V Curves for Two- and Three-Barrier MSB's Calculated by Esaki and Tsu (11).

Note the agreement between these curves and those of Figure 46.

48. T-E Curves of Two-Barrier MSB's: Influence of Effective Mass.

Both curves are for two-barrier MSB's with barriers 2 nm wide,5 nm apart, and 0.5 eV high. Curve 0 is for GaAs-Al(0.5)Ga(0.5)As MSB with effective mass variations taken into account, and Curve 1 is for MSB with effective mass uniform and equal to m_0.

49. T-E and J-V Curves of Two-Barrier MSB's: Effect of Neglecting the Effective Mass Step at Heterojunctions.

Data are for GaAs-Al(0.5)Ga(0.5)As Esaki-Tsu-type MSB's. Figures a and b are T-E and J-V curves respectively. In Curve 0, the effective mass is taken as uniform and equal to 0.0636. In Curve 1, the effective mass is 0.094 inside the barriers, and 0.0636 in the wells.

50. T-E and J-V Curves for GaAs-Al(0.4)Ga(0.6)As and GaAs-Al(0.5)Ga(0.5)As Two-Barrier MSB's: Effects of Composition

Data are for MSB's with barriers 2 nm wide, 5 nm apart. Figures a and b are T-E and J-V curves respectively. Curve 0 is for GaAs-Al(0.4)Ga(0.6)As. Curve 1 is GaAs-Al(0.5)Ga(0.5)As.

51. T-E Curves for Sawtooth and Step Barriers Compared.

Sawtooth barrier is 10 nm wide at the base, step barrier is 10 nm wide. Both are 0.33 eV high.

Figure a. Effective mass is uniform and equal to m_0. Curve 1 is for the sawtooth, Curve 2 is for the step barrier.

Figure b. Barriers are made of GaAs-Al(0.4)Ga(0.6)As. Effective mass is 0.0636 in GaAs, 0.0871 in Al(0.4)Ga(0.6)As. Curve 0 is for step barrier, Curve 1 is for the sawtooth.

52. T-E Curves for GaAs-Al(0.4)Ga(0.6)As Sawtooth Barriers: Influence of the Effective Mass.

Both barriers are 10 nm wide at the base and are 0.33 eV high. Curve 0 is for GaAs-Al(0.4)Ga(0.6)As with effective mass variations taken account of, and Curve 1 is for effective mass uniform and equal to m_0. Note the similarity between the two curves, as opposed to the same data for step barriers.

53. T-E Curves for Sawtooth Single Step Barriers: Influence of Effective Mass and Applied Electric Field Strength.

All data is for barriers 10 nm wide at the base and 0.33 eV high. Curve 0: $F_{ap} = 0$, $m_{eff} = m_0$. Curve 2: $F_{ap} = 0$, GaAs-Al(0.4)Ga(0.6)As Curve 3: $F_{ap} = 0.02$ eV/nm, $m_{eff} = m_0$. Curve 4: $F_{ap} = 0.02$ eV/nm, GaAs-Al(0.4)Ga(0.6)As Curve 5: $F_{ap} = 0.05$ eV/nm, $m_{eff} = m_0$. Curve 6: $F_{ap} = 0.05$ eV/nm, GaAs-Al(0.4)Ga(0.6)As .

54. Deformation of Single Sawtooth Barrier under Applied Electric Field.

The shape of the barrier under $F_{ap} = 0$, 0.02, and 0.05 eV/nm is shown in Figures a, b, and c, respectively. At $F_{ap} = 0.05$ eV/nm the barrier is actually a staircase.

55. T-E Curve for Two-Barrier Sawtooth Superlattice

Bases are 4.5 nm wide, heights are 0.5 eV. Effective mass is uniform and equal to m_0.

56. T-E Curves for Two-Barrier Sawtooth Superlattices: Influence of Effective Mass.

Bases are 4.5 nm wide, heights are 0.5 eV. Figure a is for $m_{eff} = m_0$, Figure b is for GaAs-Al(0.5)Ga(0.5)As superlattice.

57. T-E Curves for Sawtooth and Step Two-Barrier GaAs-Al(0.5)Ga(0.5)As Superlattices.

Curve 0: MSB with barriers 2 wide, 5 nm apart, and 0.5 eV high

Curve 1: Sawtooth superlattice with 4.5 nm wide bases.

58. T-E Curves for Sawtooth and Step Five-Barrier GaAs-Al(0.5)Ga(0.5)As Superlattices.

Curve 0: Sawtooth superlattice with 4.5 nm wide bases.

Curve 1: MSB with barriers 2 wide, 5 nm apart, and 0.5 eV high

59. J-V Curves for Two-Barrier GaAs-Al(0.5)Ga(0.5)As Sawtooth and Step Superlattices.

Curve 0: Sawtooth superlattice with 4.5 nm bases, 0.5 eV high

Curve 1: MSB with barriers 2 nm wide, 5 nm apart, 0.5 eV high

60. Deformation of Two-Barrier Sawtooth Superlattice under Applied Electric Field.

In Figures a, b, and c the applied field strength F_{ap} is 0, 0.02 and 0.05 eV/nm, respectively. At $F_{ap} = 0.05$ eV/nm the structure is a staircase.

61. T-E Curve for Two-Barrier GaAs-Al(0.5)Ga(0.5)As Superlattice
Bases are 4.5 nm wide, heights are 0.5 eV. The applied field strength is 0.052 eV/nm (applied voltage = 0.47 V).

62. T-E Curves for Two-Barrier Sawtooth Superlattices: Effects of Composition.
Data for GaAs-Al(0.4)Ga(0.6)As and GaAs-Al(0.5)Ga(0.5)As superlattices are shown in Curves 0 and 1 respectively. Bases are 4.5 nm wide.

63. J-V Curves for Two-Barrier Sawtooth Superlattices: Effects of Composition.
Data for GaAs-Al(0.4)Ga(0.6)As and GaAs-Al(0.5)Ga(0.5)As superlattices are shown in Curves 0 and 1, respectively. Bases are 4.5 nm wide.

1. INTRODUCTION

Recently there has been much interest in semiconductor heterojunction superlattices both theoretically and practically. The theoretical interest lies in the fact that quantum effects are observable in these macroscopic structures (1-3). The practical interest lies in the application of these superlattices as novel electronic devices with desirable characteristics (3-8).

The quantum mechanical effects displayed by semiconductor superlattices are manifestations of both quantum size effects and tunneling (1-11). Quantum confinement of electrons and holes in structures which are of the same order as the de Broglie wavelength of the particle results in quantization of the energy eigenvalues where previously a continuum existed. The degree of quantization depends on the number of dimensions in which the confinement exists. The motion of the confined particle then has a reduced dimensionality depending on whether the quantum confinement is present in more than one dimension. For instance, confinement in one direction results in approximately two-dimensional motion with partial quantization of energy eigenvalues. If the particle is confined in all three dimensions, the energy levels can be sharply quantized.(See Figure 1)

Tunneling is the process whereby a quantum particle can cross a potential barrier, which classically would be completely impenetrable because of its higher energy, to a state of equal or lower energy. The wave function of the particle extends into or even through the barrier when the barrier potential is finite. A non-zero particle current density through the barrier then results from the tunneling process. Quantum mechanical tunneling has been the basis of many semiconductor devices, starting with the Esaki tunnel diode, named for its inventor Leo Esaki, and introduced in 1958 (12). A discussion of the evolution of tunneling theory from 1928 up to the early seventies has been presented by L. Esaki (3, pp. 47-77).

When a particle interacts with and is confined by two or more barriers of finite height and not too great thickness, its wave is reflected multiply off each potential barrier reached by tunneling. When the confining region's dimension is some multiple of the wavelength, the particle "resonates" in the regions where its energy is greater than the local potential. At these wavelengths the tunneling current is amplified. Actually, both size quantization effects and resonance result from the same source: the constructive interference of forward and backward waves. This is the source of the quantized energy levels that result from the confinement of the particle.

Resonant tunneling figures prominently in the transport of carriers through semiconductor superlattices, and to understand it is not only desirable theoretically, but is also central to the application of these structures as electronic devices. Resonant tunneling of electrons and holes in the conduction and valence bands leads to formation of sub- or mini-

bands, whose widths and energy levels will affect the operation of superlattice devices. Tunneling calculations for semiconductor superlattices can provide this information, which can then be implemented in design of improved structures. By finding the transmission coefficient through the structure as a function of energy for either carrier, one can locate the energy levels of the resonances. It is also possible to find the effects of an external electric field on the transmission coefficient, and hence upon the resonance energy levels. Much effort has already been directed to this end for step superlattices; however, the sawtooth or graded band-gap superlattice proposed by F. Capasso (3) has up until now not been studied theoretically, except for an analysis of the multiplication noise associated with its use as a photo-detector. This is the aim of the present study.

A resurgence of interest in resonant tunneling in heterojunction semiconductors has been spurred by recent advances in molecular beam epitaxy, (MBE), which provides abrupt interfaces (on the order of a monolayer) as well as very uniform layer thicknesses (4-8,13). MBE is used to make superlattices of multiple barriers and wells in which the energy levels of the virtual states are consistent from well to well, leading to miniband formation and therefore to efficient transport of carriers through the structure. The energy levels in quantum wells and superlattices have been most recently and thoroughly reviewed by Altarelli (2). Excellent discussions of the devices which can be made from semiconductor superlattices grown by MBE, and the relationship of the superlattice structure to energy levels and resultant device performance are given by Capasso et alia (4-8).

The earliest theoretical exploration of resonant tunneling in semiconductor heterojunction superlattices was published by L. Esaki and R. Tsu in 1970 (9), who predicted negative conductance, caused by electron transport into negative effective mass regions of the minizone, and Bloch oscillations. The first experimental observation of resonant tunneling through a double barrier was made by Chang, Esaki, and Tsu in 1974 (10).

A fairly comprehensive body of work addressing carrier transport through GaAs-AlGaAs step superlattices exists with which comparisons may be made when studying other kinds of superlattice, starting with the work of Esaki and Tsu cited above. In a paper published in 1973 (11), they presented the calculated transmission coefficient as a function of incident energy, and tunneling current as a function of applied voltage, for two, three, and five GaAs-Al(0.5)Ga(0.5)As step barriers. A transfer matrix method was used for this work. Their computations were for thin layers (50 and 20 A wells and barriers,respectively), neglecting the potential gradients caused by the applied field within each layer, but taking account of the total potential drop between successive periods. They took account of effective mass variations throughout the superlattice. The correlation of the current peaks in the calculated J-V curves with the resonance energy levels

in the transmission data indicates a Stark shift in the levels that is linear in the electric field strength.

More recently, Marsh (14) applied an empirical pseudopotential formulation to tunneling calculations through a GaAs-Al(x)Ga(1-x)As double heterostructure step barrier under zero external electric field, and compared the results to those obtained by the effective mass approximation. In taking account of the effective mass variations throughout the heterostructure, Marsh made the distinction between an effective mass approximation which uses conventional wave function connection rules at interfaces where there is a sharp change in effective mass, and one which uses the modified connection rules suggested by Kroemer and Zhu (15,16). The latter, about which more will be said below, maintain particle flux continuity through the interface. Marsh found good agreement between the effective mass approximation and the empirical pseudopotential when the modified connection rules are used, and the aluminum concentration in the barrier layer is such that it is still a direct gap material. Significant discrepancies were observed between the two methods when direct-indirect interfaces were studied, and in all cases when the unmodified connection rules were used.

A modified scattering matrix formalism was recently applied to calculating the resonance energy spectra for electrons in multiple GaAs-AlGaAs quantum wells (17). The Stark shift of the levels was also calculated and found to be linear in the field strength. Although in that work the effective masses appropriate to each region were used, it appears that the conventional wave-function connection rules were used in deriving the scattering matrices, which may have resulted in some error in the computed energy levels.

MBE growth of these structures provides very precise control of the aluminum concentration in AlGaAs even at the monolayer level, allowing linear and even parabolic grading of the band-gap. Several novel electronic devices using both linearly and parabolically graded-gap materials have recently been described in the literature (4-6). A superlattice proposed by Capasso for use as a low-noise, high-gain solid-state avalanche photodiode is described in (7). In this structure, the conduction and valence band edges in each stage describe a sawtooth profile, that is, the band-gap in each layer is approximately linearly graded. (refer to Figure 2) This is achieved by varying the aluminum content linearly within the layer.At each interface there is a band-gap mismatch between pure GaAs and Al(x)Ga(1-x)As which is taken up mostly in the alignment of the conduction bands. Five or six stages are contained between n and p doped GaAs cladding layers. In operation, photo-electrons are accelerated down the structure by a strong external reverse bias. At each interface, because of the built-in potential drop afforded by the conduction band misalignment, the electron acquires enough kinetic energy to impact-ionize a lattice atom and liberate another electron. In this way the electrons multiply at each stage. The small valence band discontinuity in AlGaAs prevents the impact ionization of the holes. The larger the conduction

band discontinuity, the higher the probability that each electron will impact-ionize at each stage. This means that very low-noise multiplication can be achieved, approaching the light- detection performance of a photomultiplier tube.

The size of the potential mismatch at each interface in this device is determined by the amount of aluminum in the Al(x)Ga(1-x)As at the end of each stage. For x greater than approximately 0.4 (18,19), Al(x)Ga(1-x)As is an indirect gap material; pure AlAs has an indirect bandgap, and pure GaAs is a direct-gap material. The problem of electron tunneling through a direct- indirect gap interface must be handled differently than the simpler case of transport between two direct-gap layers, as the work by Marsh cited above indicates. Physically, the transport of electrons may be hindered by the competition of the direct and indirect bands in the high aluminum material. This may partially undo the advantage of the large conduction band discontinuity associated with high aluminum content. Hence consideration of Al(x)Ga(1-x)As sawtooth superlattices was limited in this study to compositions with x no greater than 0.4.

Sawtooth superlattices achieved by compositional grading differ from step superlattices in several important ways. One effect of the compositional grading is that the effective mass of the carriers is nowhere constant throughout the structure. In step superlattices the effective mass is constant within each layer, but there is a sharp change at each boundary. In sawtooth superlattices in AlGaAs the effective mass of the electron in the direct band is a quadratic function of the amount of aluminum. Since the aluminum content is linearly graded, there is a quadratic variation of the effective mass and the band-gap within each layer, and a large discontinuity at the end of each stage as well (18,19).

Another significant difference between the step and sawtooth superlattices is the presence of internal or "quasi" fields associated with the band-gap grading. One of these is a constant field which is the gradient of the band-gap. This field accelerates electrons and holes in the direction of the narrowest bandgap, and opposes the reverse bias applied to the device.

$$F_e = -\frac{dE_c}{dz} \tag{1a}$$

$$F_h = -\frac{dE_v}{dz} \tag{1b}$$

Ec(z) and Ev(z) are the conduction and valence band edge energies, respectively. This field is practically much less than the applied reverse bias for direct-gap AlGaAs-GaAs sawtooth superlattices.

Furthermore, the varying effective mass of the carriers gives rise to another quasi-field which assists the external reverse bias in accelerating carriers through the structure. This field is given by:

$$F_e = \frac{d}{dz}\left(\frac{3}{2} k T \ln\left(\frac{m_{eff,e}}{m_o}\right)\right) \quad (2a)$$

$$F_h = \frac{d}{dz}\left(\frac{3}{2} k T \ln\left(\frac{m_{eff,h}}{m_o}\right)\right) \quad (2b)$$

where $m_{eeff}(z)$ and $m_{heff}(z)$ are the electron and hole effective masses, respectively. For electrons in a direct-gap AlGaAs-GaAs sawtooth, this field strength is much less than that due to the band-gap gradient, and these two quasi-fields offset one another somewhat.

One more major difference between step and sawtooth superlattices is the way they deform under high external fields. Figure 3 illustrates this difference.In a step superlattice, no matter how strong the field, the barriers remain such that there is always a well between them. Resonances can in principal always be formed in these wells even under strong fields. The sawtooth, on the other hand, becomes a staircase structure at applied voltages greater than the sum of the conduction band discontinuities over all the stages. Then the triangular wells between the sawtooth barriers no longer exist. The electron still interacts with the staircase, but tunneling is no longer occurring between the barriers. Therefore it is expected that the transition from sawtooth to staircase should be signalled by some feature in the current-voltage characteristic.

An analysis of tunneling through a graded gap superlattice should thus take account of not only the external electric field and structural parameters such as number of stages, layer widths, composition, and interfacial conduction band discontinuities, but also of the quasi-fields caused by the gradients in the band-gap and effective mass. The differences between step and sawtooth superlattices should be reflected in the results of tunneling calculations.

It is the central purpose of the work described here to study the resonant energy levels of graded band gap GaAs-Al(x)Ga(1-x)As superlattices for x less than or equal to 0.4 (i.e. for direct gap material only), as a function of the applied and quasi-fields discussed above. A transfer matrix method is used to calculate the transmission coefficient and tunneling current for conduction electrons in sawtooth superlattices similar to those which might be used as avalanche photodiodes. Tunneling calculations are also presented for the same kind of step superlattice investigated by Tsu and Esaki (11). These are shown to agree with those previously obtained, and are also used to illustrate the differences and similarities between sawtooth and step superlattices with similar compositions and structural parameters. Throughout this work particular

attention is paid to role of the effective mass in electron transport through these structures. The justification for using the modified wave function connection rules when effective mass discontinuities are encountered at interfaces, is discussed. The effects of neglecting effective mass variations, or using inappropriate connection rules, are also explored.

2. THEORY OF TUNNELING IN SUPERLATTICES

2.A. Quantum Mechanical Tunneling

In quantum mechanical tunneling, a particle of energy E is incident on one or more potential barriers of arbitrary shape and height.Its behavior is described by the Schroedinger equation; specifically, the wave function inside and outside the barrier, energy eigenvalues and resonances, the transmission and reflection coefficients, and transmitted and reflected probability density currents may be calculated. In the problem of tunneling in superlattices, the salient features are essentially one dimensional: most often the superlattice is formed of parallel layers alternating in one dimension, say the z direction. The tunneling barriers then extend in the z direction, while momenta in the x and y directions are constants of the motion. The one-dimensional Schroedinger equation is then used to describe the motion of the tunneling particle:

$$\frac{-\hbar^2}{2m_{eff}} \frac{d^2\psi}{dz^2} + (V(z) - E)\,\psi = 0 \tag{3}$$

where ψ is the wave function, V(z) is the potential due to the superlattice, and m_{eff} is the mass of the incident particle (20,21).

In superlattices formed of real solids, the mass in the expression above is the effective mass appropriate to each layer. In the effective mass approximation, the ionic potential of the crystalline lattice is not dealt with directly, but instead is taken account of by the parameters of the effective mass and the energy band edge.(22)

The solution to the Schroedinger equation in regions of constant potential where $V(z) = V_j$, is the set of plane waves:

$$\psi_j = A_j e^{ik_j z} + B_j e^{-ik_j z} \tag{4}$$

where:

$$k_j = \frac{\sqrt{2m_{eff}(E - V_j)}}{\hbar} \tag{5}$$

When the energy E is greater than the potential V_j, $(E - V_j) > 0$ and the general solution above is composed of plane waves propagating to the right: $\exp(ik_j z)$, and to the left: $\exp(-ik_j z)$.

The particle propagates throughout this region like a free particle. This is characteristic of the motion of the particle in the regions outside the barriers.

When the particle encounters regions where its energy is lower than the potential, then $(E - V_j) < 0$, and the solution to the Schroedinger equation is the sum of exponentially growing and decaying parts:

$$\psi_j = A_j e^{-k_j z} + B e^{k_j z} \tag{6}$$

where κ_j is:

$$k_j = i k_j z = i \frac{\sqrt{2m_{eff}(E - V_j)}}{\hbar} \tag{7}$$

This wave function describes the penetration of the particle into a barrier. When the effective mass m_{eff} of the particle is constant from region to region, the coefficients A_j and B_j are found by applying the standard connection rules of matching the wave functions and first derivatives at each boundary:

$$\psi_j(z) = \psi_{j+1}(z) \tag{8a}$$

$$\psi_j'(z) = \psi_{j+1}'(z) \tag{8b}$$

In semiconductors the effective mass is dependent on composition. In semiconductor superlattices, the effective mass therefore makes a discontinuous jump at each interface between dissimilar materials. When this is the case, the standard wave function matching procedure above will not result in conservation of the probability density current through the interface (15,16,23). The connection rules must be modified so that this current is conserved. One approach (15,16) to this is to redefine the wave functions on either side of the interface as:

$$\chi_j = \sqrt{\frac{m_o}{m_{eff}}}\ \psi_j \tag{9}$$

Once this is done, the standard practice of matching the wave functions and their first derivatives can be applied to the χ_j to obtain the coefficients A_j and B_j. To summarize, the former wave function ψ is not continuous at each boundary when the effective mass of the particle changes abruptly there, but the renormalized wave function χ, used with the standard connection rules, results in coefficients which maintain the continuity of particle flux J through the boundaries:

$$J_j = J_{j+1} \tag{10}$$

$$\frac{-i\hbar}{2m_o}\left(\chi_j^* \frac{d\chi_j}{dz} - \chi \frac{d\chi^*}{dz}\right) = \frac{-i\hbar}{2m_o}\left(\chi_{j+1}^* \frac{d\chi_{j+1}}{dz} - \chi_{j+1} \frac{d\chi^*_{j+1}}{dz}\right) \tag{11}$$

2.B. Transfer matrix method

2.B.1. General properties of the transfer matrix

Transfer matrices can be derived describing the propagation of a wave through a superlattice of wells and barriers. The formalism is identical to that used in optics, where ray matrices are applied to the propagation of light through optical elements. (24)

The transfer matrix M used in the present work is closely related to the scattering matrix S that is applied to three-dimensional problems of nuclear scattering. The S matrix is most useful for formulating symmetry properties, whereas the M matrix is best applied to the one-dimensional problems dealt with here. It has been used in tunneling calculations for semiconductor multiple step barriers (MSB's), by Esaki and Tsu (11) and C. Schwartz (17), and for electrode-polymer interfacial layers by Meijer and Van Roggen (25,26).

The wave functions on either side of a potential step at z = 0 are written:

$$\psi_j = A_j e^{ik_j z} + B_j e^{-ik_j z} \qquad z < 0 \tag{12a}$$

$$\psi_{j+1} = A_{j+1} e^{ik_{j+1} z} + B_{j+1} e^{-ik_{j+1} z} \qquad z \geqslant 0 \tag{12b}$$

There are two linear, homogeneous equations relating the coefficients on either side of the step. The transfer matrix M expresses these equations:

$$\begin{pmatrix} A_j \\ B_j \end{pmatrix} = \begin{pmatrix} M_{11} & M_{12} \\ M_{21} & M_{22} \end{pmatrix} \begin{pmatrix} A_{j+1} \\ B_{j+1} \end{pmatrix} \tag{13}$$

The origin of the M_{ij} are the matching conditions at the step. M is determined to be:

$$M = \frac{1}{2}\sqrt{\frac{m_j}{m_{j+1}}} \begin{pmatrix} \left(1 + \frac{k_{j+1}}{k_j}\right) e^{i(k_{j+1} - k_j)z} & \left(1 - \frac{k_{j+1}}{k_j}\right) e^{-i(k_{j+1} + k_j)z} \\ \left(1 - \frac{k_{j+1}}{k_j}\right) e^{i(k_{j+1} + k_j)z} & \left(1 + \frac{k_{j+1}}{k_j}\right) e^{-i(k_{j+1} - k_j)z} \end{pmatrix} \tag{14}$$

Note that m_j/m_{j+1} is a factor of unity when there is no effective mass change at the interface. An overall transfer matrix through an arbitrary number N of steps, is just the product of the N such matrices found by matching at each step:

$$M = \prod_{j=1}^{N} M_j \tag{15}$$

Some general statements may be made about the properties of M, without knowing the details of its form, as long as the potential to which it is applied is real, goes to zero at infinity, and is symmetric about the origin. (See reference 20 for the discussion to follow.) It is important to note that the latter two conditions do not apply when a uniform electric field is present, nor when there is an asymmetric effective mass gradient throughout the structure, as is the case for the sawtooth superlattice. In that case, and in the case of the MSB under a uniform electric field, tunneling calculations are complicated somewhat by this lack of symmetry.

The scattering matrix S for a one-dimensional potential is:

$$\begin{pmatrix} B_j \\ A_{j+1} \end{pmatrix} = \begin{pmatrix} S_{11} & S_{12} \\ S_{21} & S_{22} \end{pmatrix} \begin{pmatrix} A_j \\ B_{j+1} \end{pmatrix} \tag{16}$$

This matrix relates the magnitudes of the outgoing waves to those of the incoming ones, and is easily related to the M matrix when the probability current density is conserved. In that case, S can be shown to be unitary, and symmetric as a consequence of the time reversibility of the Schroedinger equation for a real potential. M is then related to S as:

$$M = \begin{pmatrix} \frac{1}{S_{12}} & \frac{S^*_{11}}{S^*_{12}} \\ \frac{S_{11}}{S_{12}} & \frac{1}{S^*_{12}} \end{pmatrix} \tag{17}$$

When the potential is even, the Schroedinger equation is invariant under space reflection. Then $S_{11} = S_{22}$ and $S_{12} = S_{21}$. This fact combined with the unitarity and symmetry of S, leads to the relationships between the M_{ij}:

$$M_{11} = M^*_{22}$$

$$M_{12} = M^*_{12} = -M_{12} = M^*_{21}$$

$$\det(M) = 1$$

To summarize, the expressions above apply to transfer matrices for real, even, potentials which go to zero at infinity, and for which the probability current density is conserved.

Making the assumption that there is no wave incident on the barrier from the right implies that $B_{j+1} = 0$. Then the transmission coefficient T, defined as the magnitude squared of the ratio of the transmitted to the incident wave amplitudes A_{j+1}/A_j, is:

$$T = \left| \frac{A_t}{A_i} \right|^2 = |M_{11}|^{-2} \tag{18}$$

When $M_{11} = 1$, then the barrier is effectively transparent to the incident particle, and transmission is at a maximum of 1. This phenomenon is known as resonance. When M_{11} is very large, the barrier is effectively opaque, and most of the incident energy is reflected. Thus the transmission coefficient is related to the total transfer matrix M via the element M_{11}.

The transfer matrix is also used to calculate the ratio of the transmitted to the incident current densities. Applying equation 11 for the probability current density, to the incident and transmitted components of the wave functions Ai and At on either side of the interface, gives the incident and transmitted current densities:

$$J_j = \frac{\hbar k_i}{m_i} |A_i|^2 \tag{19a}$$

$$J_t = \frac{\hbar k_t}{m_t} |A_t|^2 \tag{19b}$$

The ratio of the transmitted to incident current density is then:

$$J = \left(\frac{k_t}{k_i}\right)\left(\frac{m_t}{m_i}\right)|M_{11}|^{-2} \tag{20}$$

J is often referred to as the tunneling current. It is the actual property of physical interest in tunneling problems, and is proportional to the transmission coefficient. Thus the element M_{11} of the total transfer matrix determines the tunneling current through semiconductor superlattices.

The presence of the effective mass should be noted in the expression above for the tunneling current: the ratio of the effective masses in the initial and final media will affect the current. Tunneling from high to low effective mass is less probable than tunneling in the opposite direction, for instance. This is anticipated in equation 2 for the quasi-field caused by effective mass variations:

$$V = \frac{3}{2} k T \ln \left(\frac{m_{eff}(z)}{m_o} \right)$$

The potential difference between the initial and final media due to the effective mass gradient is given by:

$$\Delta V = \frac{3}{2} k T \ln \left(\frac{m_i}{m_t} \right) \tag{21}$$

Inspection of the equation above shows that electrons will be accelerated toward the medium with the higher effective mass.

2.B.2. Tunneling: Single Step Barrier

The single step barrier is the building block for the most common kind of superlattice, the multiple step barrier (MSB), often referred to in the literature as the multiple quantum well (MQW). In the absence of an electric field, the potential is constant inside and outside the barrier, and simple analytical expressions are obtainable for the transmission coefficient. Even when there is an effective mass difference between the barrier and its surroundings, this only adds a small constant term to the potential in each region, and analytical expressions for T are still easily found. To illustrate the use of the transfer matrix in tunneling problems, the transmission coefficient is found below for the step barrier. This will provide a basis for comparison of tunneling through single and multiple barriers. (See Figure 5)

The total transfer matrix through the barrier is the product of the transfer matrices at each step:

$$M = M_1 \cdot M_2 \tag{22}$$

where M_1 is evaluated at $z = z_1$ and is:

$$M_1 = \frac{1}{2} \sqrt{\frac{m_1}{m_2}} \begin{pmatrix} \left(1 + \frac{k_2}{k_1}\right) e^{i(k_2 - k_1)z_1} & \left(1 - \frac{k_2}{k_1}\right) e^{-i(k_2 + k_1)z_1} \\ \left(1 - \frac{k_i}{k_1}\right) e^{i(k_2 + k_1)z_1} & \left(1 + \frac{k_2}{k_1}\right) e^{-i(k_2 - k_1)z_1} \end{pmatrix} \tag{23}$$

and:

$$k_1 = \frac{\sqrt{2m_1 E}}{\hbar} \qquad k_2 = \frac{\sqrt{2m_2 (E - V_0)}}{\hbar}$$

M_2 is evaluated at $z = z_2$:

$$M_2 = \frac{1}{2}\sqrt{\frac{m_2}{m_1}} \begin{pmatrix} \left(1 + \frac{k_1}{k_2}\right) e^{i(k_1 - k_2)z_2} & \left(1 - \frac{k_1}{k_2}\right) e^{-i(k_1 + k_2)z_2} \\ \left(1 - \frac{k_1}{k_2}\right) e^{i(k_1 + k_2)z_2} & \left(1 + \frac{k_1}{k_2}\right) e^{-i(k_1 - k_2)z_2} \end{pmatrix} \tag{24}$$

2.B.2.a. Single Step Barrier: E > V_0

Consider first the case where the incident energy E is greater than the barrier height, E > V_0. (Refer to Figure 5a) In this case k_1 and k_2 are both real and when M_1 and M_2 are multiplied, the matrix element M_{11} is:

$$M_{11} = \frac{1}{4} e^{ik_1 a} \left(4\cos^2 k_2 a - 2i \frac{\left(k_1^2 + k_2^2\right)}{k_1 k_2} \sin^2 k_2 a\right) \tag{25}$$

where a is equal to the barrier width (z_2-z_1), and $|M_{11}|$ is, after a little rearrangement:

$$M_{11} = \frac{4k_1 k_2^2 + \left(k_1^2 - k_2^2\right)^2 \sin^2 k_2 a}{4k_1^2 k_2^2} \tag{26}$$

The transmission coefficient T is thus $1/|M_{11}|$ or:

$$T = \left(1 + \frac{k_1^2 - k_2^2 \sin^2 k_2 a}{4k_1^2 k_2^2}\right)^{-1} \tag{27}$$

Inspection shows that T is at its maximum of 1 whenever $\sin(k_2 a)$ is zero, or when $k_2 a = n\pi$. This is resonance, in which standing waves exist in the region of the barrier. At resonance, an incident wave packet spends a comparatively long time in the vicinity of the barrier, even though its energy is greater than the barrier height.

T can be expressed explicitly as a function of incident energy E if the definitions of the wavevectors k_1 and k_2 are used in the expression above. At this point the effective masses should be retained in the expressions for the two wavevectors: if the effective masses are

different inside and outside the barrier, T(E) will differ from the standard expression which assumes that the mass is everywhere constant. The expression for T(E) which takes account of the effective mass variations is:

$$T = \left(1 + \frac{\left(E(m_1 - m_2) + m_2 V_o\right)^2 \sin^2\left(\frac{a}{\hbar}\sqrt{2m_2 (E - V_o)}\right)}{4m_1 m_2 E(E - V_o)}\right)^{-1} \quad (28)$$

Note that when the effective mass is equal throughout, this expression for T(E) becomes the standard formula:

$$T = \left(1 + \frac{V_o^2 \sin^2\left(\frac{a}{\hbar}\sqrt{2m_2 (E - V_o)}\right)}{4E (E - V_o)}\right)^{-1} \quad (29)$$

The difference between these two equations is worth noting. A term involving the incident energy and the difference between the two effective masses survives in the denominator of the first equation. This term changes the minimum values of the transmission coefficient relative to those in the constant mass case: the relative magnitudes of m_1 and m_2 determine whether the minima are raised or lowered. It is also evident that the oscillatory term in the denominator is a function of the effective mass inside the barrier, m_2.

In the constant effective mass expression, the energies at which the transmission coefficient is maximized are easily obtained by setting the argument of the sine equal to $n\pi$:

$$E = \frac{1}{2m_{eff}}\left(\frac{n\hbar\pi}{a}\right)^2 + V_o \quad (30)$$

Inspection shows that the first maximum in T occurs for E greater than the barrier height by $h\pi/2ma$. Successive maxima are scaled as n^2. However, when the masses inside and outside the barrier are different, the location of the transmission maxima are obtained by minimizing the denominator in equation 29. These maxima or resonance peaks will generally not occur at the same energies as in the constant-mass case. Effective mass variations therefore can significantly affect the transmission coefficient for single step barriers even when the incident energy is well above the barrier height.

2.B.2.b. Single Step Barrier: $E < V_0$

Tunneling may occur when the incident energy E is less than the barrier height V_0. (Refer to Figure 6b) In this case the wavevector k_2 is imaginary, and equal to:

$$k_2 = i \frac{\sqrt{2m_{eff}(V_o - E)}}{\hbar} = iK$$

Substituting $i\kappa$ for k_2 in equation 28, and using the definitions of k_1 and κ results in the expression for the tunneling transmission coefficient through the barrier:

$$T = \left(1 + \frac{\left(E(m_1 - m_2) + m_2 V_o\right)^2 \sinh^2\left(\frac{a}{\hbar}\sqrt{2m_2(V_o - E)}\right)}{4m_1 m_2 E(V_o - E)}\right) \quad (31)$$

Just as in the preceding case where $E > V_0$, the effective masses inside and outside the barrier have been retained. If the effective mass is constant, then the familiar expression for T(E) is retrieved:

$$T = \left(1 + \frac{V_o^2 \sinh^2\left(\frac{a}{\hbar}\sqrt{2m_{eff}(V_o - E)}\right)}{4E(V_o - E)}\right)^{-1} \quad (32)$$

Again, both the absolute values and the relative differences between the effective masses affect the transmission coefficient. In both expressions, T increases monotonically from zero, for incident energy of zero, to its maximum value (for energies less than the barrier height) when $E = V_0$. However, the rate at which T increases is a function of m_1 and m_2. The maximum value can be found by taking the limit in equation 32 as $(E - V_0)$ approaches zero:

$$T = \left(1 + \frac{m_1 a^2 V_o}{2\hbar^2}\right)^{-1} \quad (33)$$

It is interesting that the maximum value of T in the limit as E approaches V_0, is a function of the effective mass outside the barrier, and not the mass inside the barrier.

2.B.2.c. Single Step Barrier: Lim $E \rightarrow V_0$

It is worth examining what happens when the particle energy coincides exactly with the barrier height, a condition shown in Figure 7, and demonstrating that this does not result in any discontinuity in the transmission coefficient, since it is a frequent occurrence when an arbitrary potential is broken down into many small potential steps. This is the classical "turning point" of a particle in a potential. It is most easily treated by going back to the Schroedinger equation, and immediately using the fact that $E = V_0$. What results is the Laplace equation over the region of the barrier:

$$\frac{d^2\psi}{dz^2} = 0 \qquad 0 < z < a \tag{34}$$

The solutions to the Schroedinger equation outside the barrier are still the plane wave solutions described above. The wave functions inside and outside the barrier are then:

$$\psi = Ae^{ik_1 z} + Be^{-ik_1 z} \qquad z \leqslant 0 \tag{35a}$$

$$\psi = C + Dz \qquad 0 < z < a \tag{35b}$$

$$\psi = Fe^{ik_1 z} + Ge^{-ik_1 z} \qquad z \geqslant a \tag{35c}$$

The transfer matrix through the barrier is still given by:

$$\begin{pmatrix} A \\ B \end{pmatrix} = M_1 \cdot M_2 \cdot \begin{pmatrix} F \\ G \end{pmatrix} \tag{36}$$

where matching the wave functions and their first derivatives at $z = 0$ and $z = a$ gives the matrices M_1 and M_2:

$$M_1 = \frac{1}{2}\sqrt{\frac{m_1}{m_2}} \begin{pmatrix} e^{-ik_1 z_1} & \left(z_1 - \frac{i}{k_1}\right) e^{-ik_1 z_1} \\ e^{ik_1 z_1} & \left(z_1 + \frac{i}{k_1}\right) e^{ik_1 z_1} \end{pmatrix} \Bigg|_{z_1 = 0} \tag{37}$$

and:

$$M_2 = \frac{1}{2}\sqrt{\frac{m_2}{m_1}}\begin{pmatrix}(1-ik_1z_2)e^{ik_1z_2} & (1+ik_1z_2)e^{-ik_1z_2}\\ ik_1e^{ik_1z_2} & -ik_1e^{-ik_1z_2}\end{pmatrix}\Bigg|_{z_2=a} \tag{38}$$

From the product $M_1 M_2$, the overall transfer matrix element M_{11} is:

$$M_{11} = \frac{1}{2}\left((1-ik_1a)e^{ik_1a} + e^{-ik_1a}\right) \tag{39}$$

The transmission coefficient is $|M_{11}|^{-2}$ or:

$$T = \left(1+\frac{m_1 E a^2}{2\hbar^2}\right)^{-1} = \left(1+\frac{m_1 V_0 a^2}{2\hbar^2}\right)^{-1} \tag{40}$$

This is the same result obtained above, in the case where $E < V_0$, by taking the limit of T as E approaches V_0. There is no discontinuity in T when the incident energy happens to coincide with barrier height, and this applies as well when the barrier consists of many small steps of constant potential, V_i.

2.B.2.d. Tunneling Current Through Single Step Barrier

The tunneling current is easily found from the transmission coefficient whether the incident energy is above or below the barrier height. Recalling that the tunneling current is given by:

$$J = \frac{k_t}{k_i}\left(\frac{m_t}{m_i}\right) T$$

It is apparent that since the effective masses are the same on either side of the barrier, then so are the initial and final wavevectors. J is then just equal to the transmission coefficient. In a step barrier surrounded by media with different effective masses, the tunneling current would not take such a simple form, but would reflect the effects of the quasi-field caused by the net effective mass gradient.

2.B.3. Multiple Step Barriers

Just as the transmission coefficient through a single step barrier is calculated, one can perform the same calculation for an array of step barriers or superlattice. Tunneling through an array of step barriers is significantly different than for a single barrier. The most striking difference is that resonances are possible for energies below the barrier height, whereas the transmission coefficient through a single barrier can only have resonances when the incident energy is at least equal to the barrier height. If the MSB is symmetric with respect to the origin, the transmission coefficient at the resonances is equal to 1, as will be shown below, by using some of the general properties of the transfer matrix outlined in section 2.B.1.

The goal of tunneling calculations for MSB's is often to find the resonances and their Stark shift. It is possible to solve directly for the resonances when the MSB is not deformed by an external field, i.e., when there is even symmetry. When the symmetry is broken by a uniform field, and the Stark shift of the resonances and tunneling current density are desired, then a numerical solution by means of transfer matrices is useful. That problem will be dealt with in section 2.B.6; the solution for the zero-field case is given below for an MSB of N step barriers.

A typical MSB is shown in Figure 8. A total transfer matrix M for the MSB can be expressed as the matrix M_b for a single barrier of width a, multiplied by a phase factor accounting for transfer over the distance w between neighboring barriers, raised to the N^{th} power where N is the number of periods in the MSB:

$$M_t = \left(M_b \cdot \begin{pmatrix} e^{i k_o w} & 0 \\ 0 & e^{-i k_o w} \end{pmatrix} \right)^N \tag{41}$$

or:

$$M_t = {M_b}^N \begin{pmatrix} e^{i k_o w} & 0 \\ 0 & e^{-i k_o w} \end{pmatrix}^N \tag{42}$$

Sylvester's theorem (27) gives the Nth product of a square matrix as:

$$f(M_b) = (M_b)^N = \sum_{k=1}^{n} f(\lambda_k) \frac{\prod_{i \neq k} (M_b - \lambda_i I)}{\prod_{i \neq k} (\lambda_k - \lambda_i)} \tag{43}$$

where λ_i and λ_k are distinct eigenvalues of M_b. Representing M_b as:

$$M_b = \begin{pmatrix} A & C \\ D & B \end{pmatrix} \tag{44}$$

the eigenvalues are:

$$\lambda_{1,2} = (u \pm V) \tag{45}$$

where:

$$u = \frac{(A + B)}{2} \tag{46a}$$

$$V = \sqrt{\frac{(A - B)^2}{2} + CD} \tag{46b}$$

The element $(M_b{}^N)_{11}$ is then, by Sylvester's theorem:

$$(M_b{}^N)_{11} = \frac{(\lambda_1 - B)\ \lambda_1{}^N - (\lambda_2 - B)^N\ \lambda_2{}^N}{\lambda_2 - \lambda_1} \tag{47}$$

and the off-diagonal element $(M_b{}^N)_{12}$ is:

$$(M_b{}^N)_{12} = C\ \frac{\left(\lambda_1{}^N - \lambda_2{}^N\right)}{\lambda_1 - \lambda_2} \tag{48}$$

One can simplify these expressions by expanding $\lambda^N{}_{1,2}$ in binomial series and separating the even and odd powers into two series:

$$\lambda_{1,2} = (u + V)^N = \sum_{q=0}^{[N/2]} \binom{N}{2q} u^{N-2q}\, V^{2q} \pm V \sum_{q=1}^{[N+1]} \binom{N}{2q-1} u^{N-2q+1}\, V^{2q-2} \tag{49}$$

These expansions can be used in solving for the resonances of the MSB. It is more convenient to use the simpler expression for the off-diagonal element, instead of $(M_b{}^N)_{11}$.

Recall that the origin of the criterion for resonance is in the boundary condition on the wave:

$$\begin{pmatrix} A_j = 1 \\ B_j = 0 \end{pmatrix} = \begin{pmatrix} M_{t_{11}} & M_{t_{12}} \\ M_{t_{21}} & M_{t_{22}} \end{pmatrix} \begin{pmatrix} A_{last} = 1 \\ B_{last} = 0 \end{pmatrix}$$

At resonance the coefficient b is zero because there is no reflected wave. This implies not only that $(M_t)_{11}$ is 1, but also that $(M_t)_{12}$, and by symmetry, $(M_t)_{21}$ are zero. Then using equation 48 above for $(M_b{}^N)_{12}$ gives the resonance condition for the MSB in terms of the off-diagonal element:

$$M_{t_{12}} = 0 = (M_b{}^N)_{12} \begin{pmatrix} e^{ik_o N w} & 0 \\ 0 & e^{-ik_o N w} \end{pmatrix} \tag{50}$$

Hence:

$$(M_b{}^N)_{12} = 0 = C \frac{\lambda_1{}^N - \lambda_2{}^N}{\lambda_1 - \lambda_2} \tag{51}$$

Using the series expansions of equation 49 for $\lambda_1{}^N$ and $\lambda_2{}^N$ gives the resonance condition:

$$(M_b{}^N)_{12} = C \sum_{q=1}^{\frac{N+1}{2}} \binom{N}{2q-1} u^{N-2q+1} v^{2q-2} \tag{52}$$

The actual values of u and v are determined by the incident energy and the structure of the MSB.

As an example, consider the solution for the resonances of a three period MSB such as shown in Figure 9. The expression for $(M_b{}^N)_{12}$ is:

$$\left| (M_b{}^3)_{12} \right| = C \sum_{q=1}^{3} \binom{3}{2q-1} u^{4-2q} v^{2q-2} = 0 \tag{53}$$

and the resonances are found by solving:

$$\left| (M_b^3)_{12} \right| = C\,(3u^2 + V^2) = 0 \tag{54}$$

The fact that the determinant of M_b is equal to 1 can be used to put v in terms of u. Using a general expression for M_b gives:

$$\det(M_b) = \begin{vmatrix} A & C \\ D & B \end{vmatrix} = (AB - CD) = 1 \tag{55}$$

Recalling that:

$$u = \frac{(A+B)}{2} \qquad V = \sqrt{\frac{(A-B)^2}{2} + CD}$$

then:

$$\frac{(A+B)^2}{4} - \frac{(A-B)^2}{4} + CD = (AB - CD) = 1$$

or:

$$u^2 - V^2 = 1 \tag{56}$$

so that:

$$\left| (M_b^3)_{12} \right| = C(4u^2 - 1) = 0 \tag{57}$$

$$u = \pm \left(\frac{1}{2}\right) \tag{58}$$

In other words, there are two resonances given by u = 1/2 and u = -1/2. These are symmetrically spaced with respect to a single resonance in a single well between two such barriers. That single level is split by the coupling between wells.

This method can be applied whenever the MSB is symmetric with respect to the origin. The solution for the resonances, their Stark shift, and the tunneling current when the MSB is distorted by a uniform field is treated in a subsequent section.

2.B.4. Single step potential wells: zero external field

It is apparent that the transfer matrix method applies equally well to problems involving potential wells. Potential wells are taken in this study to be strictly below potential zero, or ground level,and a distinction is made between them and the kind of well which is formed between two potential step barriers.(See Figure 10) In the present work the terms "quantum well" and "multiple quantum well" (MQW) refer to structures below ground level. This use is adopted to avoid confusion,since the computation of bound states in a single finite well is different from that of the resonances formed between two finite step barriers. The use of the transfer matrix in finding the bound states of a particle in a quantum well, and the transmission coefficient of a particle overflying the well, is outlined below, for zero external field.

2.B.4.a. Single Quantum Well: E > 0 (Overflying the Well)

The treatment of a particle overflying a square potential well is very similar to the method already outlined for a step barrier. (Refer to Figure 11a) Given a well of width a, and depth $-V_0$, transfer matrices are found at each of its edges, and multiplied to find the overall transfer matrix M. The sole difference is that the wavevector in the region of the well, k_2, becomes:

$$k_2 = \frac{\sqrt{2m_2\,(E + V_o)}}{\hbar} \tag{59}$$

The wavevector k_1 outside the well is the same as for the step barrier. The transmission coefficient can be found by substituting k_2 above into the expression derived for the step barrier (equation 27). If the effective masses m_1 and m_2 inside and outside the well are retained, T is then:

$$T = \left(1 + \frac{\left(E(m_1 - m_2) - m_o V_o\right)^2 \sin^2\left(\frac{a}{\hbar}\sqrt{2m_2\,(E + V_o)}\right)}{4m_1 m_2 E\,(E + V_o)}\right)^{-1} \tag{60}$$

The only difference between this and equation 28 is in the algebraic sign of V_0. When the effective mass is constant everywhere, T becomes:

$$T = \left(1 + \frac{m_{eff} V_o^2 \sin^2\left(\frac{a}{\hbar}\sqrt{2m_{eff}\,(E + V_o)}\right)}{4E\,(E + V_o)}\right)^{-1} \tag{61}$$

This is also identical to equation 29 except for the sign of V_0. For a particle overflying a well, the transmission coefficient oscillates between a maximum of one and some minimum value, just as in the case of a particle overflying a potential barrier. Using equation 61 above with the fact that maxima occur when the argument of the sine is equal to $n\pi$, gives the maxima in T(E):

$$E = \frac{\hbar^2 n^2 \Pi^2}{2m_{eff} a^2} - \left| V_o \right| \tag{62}$$

The physical difference between overflying a well and a barrier, is that the particle travels faster over the well than in the surrounding regions, and more slowly over the barrier.

2.B.4.b. Single Quantum Well: $V_0 < E < 0$ (Bound States)

For a particle whose energy is between ground level and the bottom of the well, there is no transmission. The wave function decays exponentially into the surrounding media on both sides of the well, causing the energy of the particle inside the well to become quantized. The particle is said to be bound, and the eigenfunctions are bound states. (Refer to Figure 11b)

To find the bound state energy eigenvalues, the total transfer matrix is set up as for the particle overflying the well, only now the wavevectors outside and inside the well become:

$$k_1 = \frac{\sqrt{2m_1 (-E)}}{\hbar} \tag{63a}$$

$$k_2 = \frac{\sqrt{2m_2 \left| V_o - E \right|}}{\hbar} \tag{63b}$$

It is convenient to set $i\,k_1$ equal to κ. The total transfer matrix is then:

$$M_{well} = \begin{pmatrix} e^{ka} \frac{(k_2^2 - k^2)}{k_2 k} \sin k_2 a + 2 \cos k_2 a & M_{12} \\ M_{21} & M_{22} \end{pmatrix} \tag{64}$$

The eigenvalue condition follows from the constraint that the wave function be bounded on both sides of the well, and is that:

$$M_{11} = 0 \tag{65}$$

Thus the bound states inside the well are found by solving the equation:

$$e^{ka}\left(\frac{(k_2^2 - k^2)}{k_2 k}\sin k_2 a + 2\cos k_2 a\right) = 0 \tag{66}$$

This is a transcendental equation which can be solved semigraphically or by other numerical methods.

It is now apparent why the quantum well is much different than a well formed by a couple of step barriers. Transmission can always occur for any particle with energy below the barrier height in the latter case, provided the barriers are not extremely thick, so that there are no bound states for such a structure. At resonance the particle is equally likely to be found anywhere inside the well or out of it, and off resonance, the particle is reflected from the barriers to an extent given by the reflection coefficient R=(1 - T). No eigenvalue condition exists such as for the quantum well, since any energy is actually allowed to the particle.

2.B.5. Arbitrary potentials

Up to this point, constant step potentials have been considered. The transfer matrix method can be applied to potentials of arbitrary spatial variation, however. The formalism of the transfer matrix requires only that the potential V(z) be a real function of z. If the potential happens to be symmetric then the transfer matrix has some convenient symmetries, but a lack of symmetry does not hinder the general approach. In fact, even for asymmetric barriers the transmission and reflection coefficients are the same whether the particle approaches the barrier from the right or from the left (21).

In practice, when the potential V(z) is some arbitrary function of z, real but not even necessarily continuous, it can be approximated by steps which are piecewise constant, in the same manner as for numerical integration of a curve (Refer to Figure 12). Then the solutions to the Schroedinger equation in each interval are the simple plane waves. The functional forms of V(z) and the effective mass, $m_{eff}(z)$, are needed so that the wavevectors to the right and left of each step can be calculated. Then the transfer matrix at each step is calculated from equation 14, and the overall transfer matrix is found for the structure by multiplication, as in equation 15.

This method has already been used by Meijer and Van Roggen to calculate J-V curves for polymeric electronic devices (25,26). In such devices the electrode-polymer interfacial barriers and the applied electric field result in potentials which depart considerably from the simple

textbook step potentials discussed so far. The overall transfer matrices calculated for these structures yielded J-V characteristics in agreement with those which were experimentally observed.

2.B.6. Field effects: Constant Electric Field

A very important special case of an arbitrary potential is that due to a one-dimensional constant field. Such a potential is linear in the spatial coordinate:

$$V(z) = c F_{ap} z + V_o \tag{67}$$

where F is the field strength, V_0 is a constant potential offset, and c is a constant, which equals the electronic charge when F is the electric field strength. This potential also describes a constant gravitational field, where F is the acceleration due to gravity, g, and c is the mass of a particle in the field. (28-30)

Figure 13 shows a single quantum well and step barrier under a uniform electric field. Under such an electric field, the Schroedinger equation becomes:

$$\frac{-\hbar^2}{2 m_{eff}} \frac{d^2 \psi}{dz^2} - (V_o + c F_{ap} z) \psi = E\psi \tag{68}$$

The solutions of this equation yield the bound states of a quantum well, and the transmission coefficient for a step barrier or series of barriers in the presence of a constant field. The simple analytical solutions obtained in the preceding sections for zero field are no longer valid. The transfer matrix method can still be used, but the approach adopted depends on the geometry of the problem: a distinction must be made between a constant field of infinite extent and one which is "chopped" or restricted to a certain region. In the latter case, the transfer matrix method can be applied in a straightforward manner. In the former case, the transfer matrix method must be modified. The results depend as well on which set of boundary conditions are chosen.

The calculation of the Stark shift of the bound states in a single quantum well is described below. This example is chosen in order to illustrate the consequences of the form assumed by the applied field, whether it is uniform or localized. First, the solution for the unrestricted uniform field is outlined, assuming a uniform effective mass. Then it is explained how the solution must be modified when there is an effective mass jump at the well edges. Finally, the solution for a localized electric field is outlined.

2.B.6.a. Single Quantum Well in Unrestricted Uniform Electric Field

2.B.6.a.i. Constant Effective Mass $m_{eff} = m_0$

Let us first consider the fate of bound states of a single well in a uniform electric field. (Refer to Figure 14) Recall that the bound states of a finite potential well are easily found by setting the element M_{11} of the total transfer matrix to zero. This is the eigenvalue condition that follows from the requirement that the wave function be bounded on both sides of the well for energies below the top of the well. In that case the particle is localized in the well. Under a uniform electric field, however, true bound states no longer exist, because there is now the possibility that the particle can lower its energy by tunneling through the side of the well. There will still be energies, however, where the residence time of the particle in the well is long. These are close to the zero-field bound state energies, but are shifted by the field. The goal of this calculation is to find the quasi-bound states and their functional dependence on the applied field.

The criterion for quasi-bound states is not that the wave function must be bounded on either side of the well, but that its amplitude be maximized in the region of the well. The wave function on the downstream side of the well is composed of an incoming and outgoing part: quasi-bound states exist when the ratio of the incoming to the outgoing parts is maximized.

Refer to Figure 14 for the geometry of the well in an electric field. The Schroedinger equation in the regions in and around the well is:

$$\frac{-\hbar^2}{2\,m_{eff}}\frac{d^2\psi}{dz^2} - e\,F_{ap}\,z\,\psi = E\psi \qquad |z| > a \qquad (69a)$$

$$\frac{-\hbar^2}{2\,m_{eff}}\frac{d^2\psi}{dz^2} - (V_o + C\,F_{ap}z)\,\psi = E\,\psi \qquad |z| \leq a \qquad (69b)$$

Inside the well, the slanted potential can still be broken up into intervals of constant potential where the wave function is the sum of forward- and backward-propagating plane waves:

$$\psi_i = A_i\,e^{i\,k_i\,z} + B_i\,e^{-ik_i z}$$

The wave-vector in each interval, k_i, is easily calculated knowing the field and the coordinate at the edge of the interval:

$$k_i = \frac{\sqrt{2m_i\left(E - V(z_i)\right)}}{\hbar} \qquad (70)$$

The transfer matrix accumulated between the first and last intervals relates the coefficients of the wave functions:

$$\begin{pmatrix} B \\ C \end{pmatrix} = M_o \cdot M_1 \cdot M_2 \ldots M_f \begin{pmatrix} P \\ Q \end{pmatrix} \tag{71}$$

This matrix can now be used to relate the wave functions on either side of the well.

Outside the well, where $|z| > a$, because the field is uniform, the Schroedinger equation is most easily solved by a transformation of coordinate. A new coordinate, x, is defined which is a dimensionless length minus a dimensionless energy, or:

$$x = \left(\frac{2 m_{eff} \, e \, F_{ap}}{\hbar^2} \right)^{1/3} z + \frac{2 m_{eff} \, E}{(2 m_{eff} \, e \, F_{ap} \hbar)^{2/3}} \tag{72}$$

Inserting (-x) into equation 69a results in the Airy equation (31):

$$\frac{d^2 \psi}{d x^2} - x\psi = 0 \tag{73}$$

This has the general solution:

$$\psi = C \, Ai(-x) + D \, Bi(-x) \tag{74}$$

Figures 15 and 16 show the functions Ai(-x) and Bi(-x). Inspection of equation 73 for x shows that it is very large at small values of the field F. When this is the case, asymptotic forms of the Airy functions can be used (32):

$$Ai(x) \cong \frac{1}{2} \Pi^{-1/2} z^{-1/4} e^{-\zeta} \sum_0^\infty (-1)^k C_k \zeta^{-k} \qquad |\arg z| < \Pi \tag{75a}$$

$$Bi(x) \cong \Pi^{-1/2} z^{-1/4} e^{\zeta} \sum_0^\infty C_k \zeta^{-k} \qquad |\arg z| < \frac{\Pi}{3} \tag{75b}$$

where:

$$\zeta = \frac{2}{3} z^{2/3} \tag{76}$$

The requirement of a bounded wave function on the left side of the well means the wave function there consists of Ai(-x) alone:

$$\psi - = a\,Ai(-x) \tag{77}$$

On the right hand side of the well, the wave function is composed of both Ai(-x) and Bi(-x):

$$\psi^{+} = E\,Ai(-x) + F\,Bi(-x)$$

Referring again to Figures 15 and 16, shows that the component to be maximized to the right of the well for a quasi-bound state is Bi(-x). If Bi(-x) is maximized at the expense of Ai(-x), the amplitude of the wave function is peaked near the well. The problem of finding the quasi-bound states is a matter of searching for the values of the energy E at a given field strength which maximize the ratio F/E.

The ratio of the leftmost wave function to its derivative, at z = -a, gives the value of the wave vector there, k_0:

$$k_o = \left.\frac{Ai(-x)}{Ai'(-x)}\right|_{z=-a} \tag{78}$$

The transfer matrix M_0 can now be initialized at z = - a:

$$M_o = \frac{1}{2}\begin{pmatrix} \left(1+\frac{k_1}{k_o}\right) e^{i(k_1-k_o)a} & \left(1-\frac{k_1}{k_o}\right) e^{-i(k_1+k_o)a} \\ \left(1-\frac{k_1}{k_o}\right) e^{i(k_1+k_o)a} & \left(1+\frac{k_1}{k_o}\right) e^{-i(k_1-k_o)a} \end{pmatrix} \tag{79}$$

Now, matching the wave function and its derivative in the last interval of the well to that on the right at z = a allows the ratio of the incoming and outgoing waves, F/E, to be obtained in terms of the applied field:

$$P e^{ik_f a} + Q e^{-ik_f a} = E\,Ai(-x) + F\,Bi(-x)\Big|_{z=a} \tag{80a}$$

$$P_i k_f e^{ik_f a} - Q_i k_f e^{-ik_f a} = -\left(\frac{2m_{eff} e F_{ap}}{\hbar^2}\right)^{1/3} E\,Ai(-x) + F\,Bi(-x)\Big|_{z=a} \tag{80b}$$

Solving for the ratio F/E between the two equations above gives:

$$F/E = \frac{\frac{1}{Ai'(-x_2)}\left[\frac{1}{\gamma}\left(-\frac{P}{Q}e^{ik_f a} - ik_f e^{-ik_f a}\right) - \left(\frac{P}{Q}e^{ik_f a} + e^{-ik_f a}\right)\right]}{\frac{Bi'(-x_2)}{Ai'(-x_2)}\frac{1}{Ai(-x_2)}\left(\frac{P}{Q}e^{ik_f a} + e^{-ik_f a}\right) - \frac{Bi(-x_2)}{Ai(-x_2)}\frac{1}{A_i'(-x_2)\gamma}\left(-\frac{P}{Q}e^{ik_f a} + ik_f e^{-ik_f a}\right)} \quad (81)$$

where:

$$\gamma = \left(\frac{2 m_{eff} e F_{ap}}{\hbar^2}\right)^{1/3}$$

P/Q is determined by the total transfer matrix T, the coefficient of the leftmost wave function, A, and the wavevector at the left edge of the well, k_0:

$$\frac{P}{Q} = -\frac{T_{12} + T_{22} e^{2ik_1 a}\left(\frac{\gamma - ik_1 k_o}{\gamma + ik_1 k_o}\right)}{T_{11} + T_{21} e^{2ik_1 a}\left(\frac{\gamma - ik_i k_o}{\gamma + ik_1 k_o}\right)} \quad (82)$$

The expression above can be put in terms of these parameters by matching at z = -a. The wave vector just to the right of the left edge of the well is:

$$k_i = \frac{\sqrt{2 m_{eff}(E + V_o - |F_{ap} e a|)}}{\hbar} \quad (83)$$

and the wave vector just to the left of the right edge, at z = a, is:

$$k_f = \frac{\sqrt{2 m_{eff}(E + V_o + |F_{ap} e a|)}}{\hbar} \quad (84)$$

Inserting k_i and k_f into equation 81 and utilizing equation 78 for k_0 in the expression for P/Q (equation 82), will result in an expression for F/E explicitly in terms of the applied field F_{ap}, incident energy E, well geometry, and total transfer matrix T.

It is straightforward to write a computer program to calculate F/E from in equation 81. The ratio F/E can be plotted as a function of the energy for varying field strengths, and the quasi-bound state energy levels appear as the maxima in this ratio.

2.B.6.a.II. Non-Constant Effective Mass: Jump In m_{eff} at the Well Edges

In quantum wells formed of semiconductor heterojunctions, the effective mass can change sharply at the edges of the well. When this happens, the modified connection rules must be used when matching the plane waves to the Airy functions at the well edges. If the effective masses inside and outside the well (m_2 and m_1, respectively) are retained a new expression for P/Q results which differs from the one given in equation 82 only by a factor of $(m_2/m_1)^{1/2}$:

$$\frac{P}{Q} = -\sqrt{\frac{m_2}{m_1}}\left(\frac{T_{12} + T_{22}\, e^{2ik_1a}\left(\frac{\gamma - ik_1k_o}{\gamma + ik_1k_o}\right)}{T_{11} + T_{21}\, e^{2ik_1a}\left(\frac{\gamma - ik_1k_o}{\gamma + ik_1k_o}\right)}\right) \tag{85}$$

F/E is now found by inserting equation 85 into equation 81:

$$F/E = \frac{\frac{1}{Ai'(-x_2)}\left[\frac{1}{\gamma}\left(-\sqrt{\frac{m_2}{m_1}}\,\frac{P}{Q}\, e^{ik_fa} - ik_f e^{-ik_fa}\right) - \left(\sqrt{\frac{m_2}{m_1}}\,\frac{P}{Q}\, e^{ik_fa} + e^{-ik_fa}\right)\right]}{\frac{Bi'(-x_2)}{Ai'(-x_2)}\,\frac{1}{Ai(-x_2)}\left(\sqrt{\frac{m_2}{m_1}}\,\frac{P}{Q}\, e^{ik_fa} + e^{-ik_fa}\right) - \frac{Bi(-x_2)}{Ai(-x_2)}\,\frac{1}{Ai'(-x_2)}\,\frac{1}{\gamma}\left(-\sqrt{\frac{m_2}{m_1}}\,\frac{P}{Q}\, e^{ik_fa} + ik_f e^{-ik_fa}\right)} \tag{86}$$

It should be noted that the effective mass difference also makes its presence known in the values of k_0, k_i, and k_f. An effective mass jump at the edges of the well affects the number and energies of the calculated bound states in the well.

2.B.6.b. Single Quantum Well: Localized Electric Field

Figure 17 shows a single quantum well in a localized electric field. The field results in a linear potential restricted to the areas inside and just on either side of the well. Outside this region, the field is zero and the potential is constant. This configuration represents real physical situations better than the unrestricted uniform field picture: in real semiconductor quantum wells and superlattices, the structure is biased by means of cladding layers in ohmic contact with metals at constant potential. Outside the cladding, the field is ideally zero.

This is physically a different situation from the unrestricted uniform field case. There, as pointed out, no true bound states exist. When the field is localized around the well, however, bound and quasi-bound states may exist simultaneously. Whether or not they exist depends on the geometry of the well, the extent of the applied field, and the field strength. Figure 18 shows how either bound or quasi-bound states, or both, may arise. An obvious condition on the applied field, if true bound states are to exist, is that:

$$F \leqslant \frac{V_o}{a} \tag{87}$$

Field strengths higher than this allow only quasi-bound states.

The bound and quasi-bound states of the well, and their Stark shift, are easily found by means of transfer matrices. Here the environs of the well are surrounded by constant potential regions. The slanted regions around the well are broken into intervals (see Figure 19) over which, once again, the solutions to the Schroedinger equation are the plane waves. Then, as outlined in section 2.B.5, for arbitrary potentials, the overall transfer matrix is found by multiplication. The criterion for a bound state is that M_{11} be zero. For a quasi-bound state, M_{11} need only be minimized. To calculate the Stark shift of a level, M_{11} is calculated as a function of the applied field: the shift of the minimum under the field is the Stark shift of the level in question.

2.B.6.c. Multiple Step Barriers: Constant, Localized Electric Field

A solution for the transmission resonances of an MSB with N barriers, under zero external field, was outlined in a previous section. The solution was straightforward mainly because of the simple form of the zero-field Hamiltonian, and because of the right-left symmetry of the MSB. When a constant electric field is applied, that solution is no longer valid. The transfer matrix method is easily applied to calculating the Stark shift of the MSB's resonances, and hence the tunneling current-voltage curve, when a constant, localized electric field is applied. Figure 20 shows an N-barrier MSB, of overall length l, and barrier height V_0, under an applied field F_{ap} . The barrier widths are a, and the well widths, w. In each barrier and well region, the Schroedinger equation is given by:

$$\frac{-\hbar^2}{2m_b}\frac{d^2\psi}{dz^2} + (V_o - e F_{ap} z)\,\psi = E\,\psi \quad \text{(barrier)} \tag{88}$$

$$\frac{-\hbar^2}{2m_w}\frac{d^2\psi}{dz^2} - e F_{ap} z\,\psi = E\,\psi \quad \text{(well)} \tag{89}$$

Outside the MSB, the applied field is zero. The barrier and well regions of the I^{th} period are broken up into n_b and n_w intervals of constant potential, respectively. Within each interval, just as for the isolated well, the solutions to the Schroedinger equation are the backward- and forward-propagating plane waves:

$$\psi_{I,i,b,w} = A_{I,i,b,w}\, e^{ik_{I,i,b,w}z} + B_{I,i,b,w}\, e^{-ik_{I,i,b,w}z} \tag{90}$$

The potential drops at the steps are all the same size because the field is constant inside the MSB:

$$\Delta V_b = \frac{e F_{ap} a}{n_b} \quad (91a) \qquad \Delta V_b = \frac{e F_{ap} w}{n_w} \quad (91b)$$

The transfer matrix at each step in the I^{th} barrier or well is:

$$M_{I,i,b,w} = \frac{1}{2}\begin{pmatrix} \left(1 + \frac{k^+_{b,w}}{k^-_{b,w}}\right) e^{i\left(k^+_{b,w} - k^-_{b,w}\right) z_{I,i,b,w}} & \left(1 - \frac{k^+_{b,w}}{k^-_{b,w}}\right) e^{-i\left(k^+_{b,w} + k^-_{b,w}\right) z_{I,i,b,w}} \\ \left(1 - \frac{k^+_{b,w}}{k^-_{b,w}}\right) e^{+i\left(k^+_{b,w} + k^-_{b,w}\right) z_{I,i,b,w}} & \left(1 + \frac{k^+_{b,w}}{k^-_{b,w}}\right) e^{-i\left(k^+_{b,w} + k^-_{b,w}\right) z_{I,i,b,w}} \end{pmatrix} \tag{92}$$

where:

$$k^-_{b,w} = k_{I,i,b,w} = \frac{\sqrt{2m_{b,w}\,E - V(z_{I,i,b,w})}}{\hbar} \quad (93a) \qquad k^+_{b,w} = k_{I,i,b,w} = \frac{\sqrt{2m_{b,w}\,E - V(z_{I,i,b,w}) + \Delta V_{b,w}}}{\hbar} \quad (93b)$$

and m_b and m_w are the effective masses in the barriers.and wells There are $(n_{b,w} - 1)$ of these matrices in each region.

Transmission through the large steps at the right and left edges of the barriers is also handled by transfer matrices. The matrix through the left edge of the I^{th} barrier is:

$$M_{L,I} = \frac{1}{2}\sqrt{\frac{m_w}{m_b}}\begin{pmatrix} \left(1+\frac{k^+_{L,I}}{k^-_{L,I}}\right)e^{i\left(k^+_{L,I}-k^-_{L,I}\right)z_{L,I}} & \left(1-\frac{k^+_{L,I}}{k^-_{L,I}}\right)e^{-i\left(k^+_{L,I}+k^-_{L,I}\right)z_{L,I}} \\ \left(1-\frac{k^+_{L,I}}{k^-_{L,I}}\right)e^{+i\left(k^+_{L,I}+k^-_{L,I}\right)z_{L,I}} & \left(1+\frac{k^+_{L,I}}{k^-_{L,I}}\right)e^{-i\left(k^+_{L,I}+k^-_{L,I}\right)z_{L,I}} \end{pmatrix} \quad (94)$$

where:

$$z_{L,I} = (I-1)(a+w) \quad (95)$$

and:

$$k^+_{L,I} = \frac{\sqrt{2m_b\ E-(V_{L,I}+V_o)}}{\hbar} \quad (96a) \qquad k^-_{L,I} = \frac{\sqrt{2m_w\,(E-V_{L,I})}}{\hbar} \quad (96b)$$

with:

$$V_{L,I} = e\,F_{ap}\,(I-1)(a+w) \quad (97)$$

The transfer matrix through the right edge of the I^{th} barrier is:

$$M_{R,I} = \frac{1}{2}\sqrt{\frac{m_b}{m_w}}\begin{pmatrix} \left(1+\frac{k^+_{R,I}}{k^-_{R,I}}\right)e^{i\left(k^+_{R,I}-k^-_{R,I}\right)z_{R,I}} & \left(1-\frac{k^+_{R,I}}{k^-_{R,I}}\right)e^{-i\left(k^+_{R,I}-k^-_{R,I}\right)z_{R,I}} \\ \left(1-\frac{k^+_{R,I}}{k^-_{R,I}}\right)e^{+i\left(k^+_{R,I}+k^-_{R,I}\right)z_{R,I}} & \left(1+\frac{k^+_{R,I}}{k^-_{R,I}}\right)e^{-i\left(k^+_{R,I}+k^-_{R,I}\right)z_{R,I}} \end{pmatrix} \quad (98)$$

where:

$$z_{R,I} = I(a+w) - w \quad (99)$$

and:

$$k^+_{R,I} = \frac{\sqrt{2m_w\left(E-(V_{R,I}+V_o)\right)}}{\hbar} \quad (100a) \qquad k^-_{R,I} = \frac{\sqrt{2m_w\,(E-V_{R,I})}}{\hbar} \quad (100b)$$

with:

$$V_{R,I} = e\,F_{ap}\,(I(a+w)-w) \quad (101)$$

The overall transfer matrix is found, as usual, by multiplication. Then the transmission coefficient can be obtained as a function of both energy and applied field. This gives the Stark shift of the resonances.

Tunneling current-voltage curves are obtained using equation 20:

$$J(V_{ap}, E) = \frac{k_t}{k_i}\left(\frac{m_t}{m_i}\right) T(V_{ap}, E)$$

where $V_{ap} = -e F_{ap} l$, and E is treated as a parameter. In computing the J-V curve for an AlGaAs MSB, E can be taken as the Fermi energy in the n-cladding layer, typically a few thousandths of an eV. The effective masses m_t and m_i, are those of the n- and p-cladding layers. The wavevectors in these regions are k_t and k_i from above:

$$k_i = \frac{\sqrt{2m_i E}}{\hbar} \qquad (102a) \qquad k_t = \frac{\sqrt{2m_t (E - V_{ap})}}{\hbar} \qquad (102b)$$

It is easy to write a computer program which varies F_{ap} (or V_{ap}), and for a given MSB geometry, calculates the J-V curve. Comparison of the J-V curve with the T-E plots showing the Stark shift of the resonances, clarifies the role that resonant tunneling plays in conduction through these structures. This is discussed in detail in a subsequent section.

In AlGaAs MSB's, where the effective mass varies between the wells and barriers, the prefactors of the transfer matrices at barrier edges cancel when the matrices are multiplied. The effective mass difference does survive, however, in the wavevectors, and should not be neglected. The effective masses in both cladding layers may differ as well, and their ratio occurs in equation 20, which gives the tunneling current. The magnitude of the tunneling current, the location of the resonances, and hence the shape of the J-V curve, are all affected strongly by the effective masses used throughout, and care should be taken to use the appropriate values.

2.B.6.d. Sawtooth Barriers: Zero and Non-Zero External Electric Field

Tunneling calculations for sawtooth barriers of the kind shown in Figure 21, under zero external field, require solution of a Schroedinger equation for the which the Hamiltonian is:

$$\hat{H} = \frac{\hat{p}^2}{2m} + e\hat{F}_{eff}\hat{z} \qquad (103)$$

where:

$$e F_{eff} = (V_o/b) \tag{104}$$

is the slope of the barrier. This is effectively the same as the Hamiltonian for a step barrier or well under a constant, external electric field. The Schroedinger equation for the zero-field sawtooth barrier is:

$$-\frac{\hbar^2}{2 m_{eff}} \frac{d^2\psi}{dz^2} + e F_{eff} z\psi = E\psi \tag{105}$$

If an external, constant electric field is applied as well, another term, ($e F_{ap} z$), for the external field, is added to the Hamiltonian and the Schroedinger equation becomes:

$$-\frac{\hbar^2}{2m_{eff}} \frac{d^2\psi}{dz^2} + e\left(F_{eff} + F_{ap}\right) z\psi = E\psi \tag{106}$$

If the effective mass is not a function of z, a direct solution in terms of the Airy functions is possible in the same way it is carried out for a quantum well in a uniform field. Actual devices, however, are made from graded band-gap Al(x)Ga(1-x)As, and the effective mass is indeed dependent on z. By using the transfer matrix method, this complication of the Schroedinger equation is circumvented by approximating not just the potential, but the effective mass gradient as well, by a series of small steps of constant value.

Suppose there is an N-tooth sawtooth barrier for which the T-E and J-V curves are sought. Each barrier is divided into n intervals of width $\Delta z = b/n$, and for each of which the potential drop is given by:

$$\Delta V_j = \frac{\left(V_o + e F_{ap} b\right)}{n} \tag{107}$$

The solution to the Schroedinger equation in each interval is, as usual:

$$\psi_{l,j}(z) = A_{l,j} e^{i k_{l,j} z} + B_{l,j} e^{-i k_{l,i} z} \tag{108}$$

where:

$$k_{l,i} = \frac{\sqrt{2m_{eff}\,(j\,\Delta z)\,\left(E - (V_o/b + e\,F_{ap})(l\,b + (j-1)\,\Delta z)\right)}}{\hbar} \tag{109}$$

The transfer matrix at each step is:

$$M_{l,i} = \frac{1}{2}\sqrt{\frac{m_{eff}\,(z_i)}{m_{eff}\,(z_{j+1})}} \begin{pmatrix} \left(1 + \frac{k_{l,j+1}}{k_{l,i}}\right) e^{i(k_{l,j+1} - k_{l,j})\,z_{l,j}} & \left(1 - \frac{k_{l,j+1}}{k_{l,j}}\right) e^{-i(k_{l,j+1} + k_{l,j})\,z_{l,j}} \\ \left(1 - \frac{k_{l,j+1}}{k_{l,j}}\right) e^{i(k_{l,j+1} + k_{l,j})z_{l,j}} & \left(1 + \frac{k_{l,j+1}}{k_{l,j}}\right) e^{-i(k_{i,j+1} - k_j)z_j} \end{pmatrix} \tag{110}$$

where:

$$k_{l,j+1} = \frac{\sqrt{2m_{eff}\,(z_i + \Delta z)\,\left(E - (V_o/b + e\,F_{ap})\,z_{l,j}\right)}}{\hbar} \tag{111}$$

and:

$$z_{l,j} = (l\,b + j\,\Delta z) \tag{112}$$

The transfer matrix through the right-most edge of the I^{th} sawtooth handles a potential drop of V_0, the peak barrier height:

$$M_i = \frac{1}{2}\sqrt{\frac{m_l^+}{m_l^-}} \begin{pmatrix} \left(1 + \frac{k_l^+}{k_l^-}\right) e^{i(k_l^+ - k_l^-)\,z_l} & \left(1 - \frac{k_l^+}{k_l^-}\right) e^{-i(k_l^+ + k_l^-)\,z_l} \\ \left(1 - \frac{k_l^+}{k_l^-}\right) e^{i(k_l^+ + k_l^-)z_l} & \left(1 - \frac{k_l^+}{k_l^-}\right) e^{-i(k_l^+ - k_l^-)\,z} \end{pmatrix} \tag{113}$$

where:

$$k_l^+ = \frac{\sqrt{2m_l^+(E - V_l^+)}}{\hbar} \tag{114a}$$

$$k_l^- = \frac{\sqrt{2m_l^-(E - V_l^-)}}{\hbar} \tag{114b}$$

and:

$$V_l^- = (V_o + e\,F_{ap}\,z_l) \tag{115a}$$

$$V_l^+ = e\,F_{ap}\,z_l \tag{115b}$$

$$Z_l = l\,b \tag{116}$$

$$m_l^- = m_{eff}\,(l\,b) = m_{max} \tag{117a}$$

$$m_l^+ = m_{eff}\,(0) = m_{min} \tag{117b}$$

The transmission coefficient and tunneling current are computed from the element M_{11} of the overall transfer matrix exactly as for the MSB described in the previous section. Assuming that the effective mass is graded in some manner over the barrier width, when the multiplication of all the transfer matrices is carried out, the prefactors containing the ratio of the effective masses to the right and left of each step, do not cancel as they did for the MSB with alternating layers. This is a consequence of the asymmetry of the sawtooth barrier. In AlGaAs sawtooth barriers, the triangular shape is accomplished by linear aluminum concentration grading. The attendant gradation of the effective mass must be accounted for by considering the functional dependence of $m_{eff}(z)$ at each step when the transfer matrices are computed. This is because the effective mass has a strong effect on the number and energy levels of the resonances supported by the structure, just as in the MSB and quantum well.

The AlGaAs multiple sawtooth barrier which finds application as an avalanche photo-diode is operated under high reverse bias. This means that the applied field is of opposite sign to the effective field caused by the band-gap grading in each layer. As the applied field is raised, at some value it will exceed the band-gap grading and the sawtooth will become a staircase structure. (Refer to Figure 21) The value of the applied field where this occurs is:

$$F_{staircase} = -\frac{V_o}{e\,b} \tag{118}$$

At this point there are no longer any barriers through which to tunnel. It is expected that the transition from sawtooth to staircase should be reflected by a change in the character of the J-V characteristic. In this respect a multiple sawtooth barrier is much different than a multiple step barrier.

2.C. Al(x)Ga(1-x)As Heterostructures

2.C.1. Properties of Al(x)Ga(1-x)As

Superlattices of quantum wells and barriers, in real semiconductor materials such as Al(x)Ga(1-x)As, are made possible by the conduction and valence band discontinuities occurring at interfaces of materials with different band structures. In Al(x)Ga(1-x)As, the energy band structure depends on the aluminum content, x. By combining layers of differing Al content, it is possible to adjust the band-gap on either side of the interface and in that way to tailor the

conduction and valence band discontinuities. These discontinuities are what form the barriers to electron and hole transport through the superlattice. In tunneling calculations for Al(x)Ga(1-x)As superlattices, it is thus necessary to know the relationships between composition, energy band structure, and band alignment at heterojunctions.

Carrier transport through a superlattice is also dependent on the carrier effective mass at every point in the structure. The effective mass in semiconductors is generally a function of the energy band structure, and in Al(x)Ga(1-x)As it is therefore dependent on x. Tunneling calculations in Al(x)Ga(1-x)As thus also require some knowledge of the relationship between composition, band structure and effective mass.

In this study, only tunneling of electrons between direct conduction bands is considered. The information used in these calculations is: the direct conduction band alignment at GaAs-Al(x)Ga(1-x)As heterojunctions, and the electron effective mass in the direct conduction band minimum, as a function of x. The effect of non-parabolicity of the bands on the effective mass of electrons at high energy, for instance, when the electron encounters a step in a staircase superlattice, is neglected. The effective mass is assumed scalar.

In the sections below, there is a brief discussion of the energy band structures of GaAs, AlAs, and Al(x)Ga(1-x)As, covering only the properties needed to perform tunneling calculations for Al(x)Ga(1-x)As superlattices in the effective mass approximation.

2.C.1.a. GaAs Energy Band Structure and Effective Masses

Pure GaAs is a direct-gap material: its conduction and valence band extrema occur at the Brillouin zone center. Figure 22 shows the <100> and <111> energy band diagram for GaAs (33). The two lowest-energy conduction bands are shown: Γ_{1c}, and X_{1c}, the direct and indirect bands, respectively. Also shown are the three highest-energy valence bands: Γ_{1v} and Γ_{2v}, heavy and light-hole bands, respectively, and a third, Γ_{3v}, split off by 0.36 eV from the other two by spin-orbit coupling.

The direct band-gap, at the zone center, is 1.44 eV. The indirect X_{1c} minimum is 0.38 eV above the direct minimum. In thermal equilibrium, free carriers are found only in the lowest conduction band minima, although scattering of electrons by strong electric fields can excite them into X_{1c}. (29) This effect has been neglected in this study. Density-of-states effective masses for electrons and holes in GaAs have been determined (18), and are used throughout the present study: this is quite appropriate for the Γ_{1c} band in GaAs, for which the constant E(k) surface near the band minimum is spherical, and hence, for which the effective mass is actually scalar. (For the hole bands Γ_{1v} and Γ_{2v}, this is a less satisfactory approximation, since these bands are non-parabolic and anisotropic.) The electron effective mass m_Γ at Γ_{1c} is 0.0636 ±0.002 (at 290 K); for

electrons in X_{1c}, m_X is estimated as 0.39. The heavy-hole effective mass in Γ_{1v} is approximately 0.68.

2.C.1.b. AlAs Energy Band Structure and Effective Masses

Figure 23b (34) shows the <100> energy band structure of pure AlAs: inspection of this diagram shows that AlAs is an indirect-gap material, unlike GaAs. As Figure 23 shows, however, the symmetry of the conduction and valence bands is similar in the two materials. The indirect band-gap in AlAs is 2.2 eV; the band gap at the zone center is 2.9 eV. The energy separation of Γ_{1c} and X_{1c} is 0.877 eV. As in GaAs, there are two degenerate valence bands with maxima at the zone center.

The density-of-states effective masses for AlAs have been determined as follows: in X_{1c}, m_X is 0.37, in Γ_{1c} m_Γ is reported as 0.128 to 0.15, depending on the method of calculation. (18) The heavy-hole mass in Γ_{1v} is estimated as 0.85.

2.C.1.c. Al(x)Ga(1-x)As Energy Band Structure and Effective Masses as a Function of x

In the mixed crystal Al(x)Ga(1-x)As, the band structure and effective masses depend strongly on the aluminum concentration x. Since the pure compounds AlAs and GaAs are indirect and direct gap materials, respectively, there is naturally an aluminum concentration at which the Al(x)Ga(1-x)As changes from one type of material to the other.

Figure 24 shows how the energy gap in Al(x)Ga(1-x)As depends on x at room temperature (19). The band-gap at Γ_{1c} increases with x, from 1.43 eV in pure GaAs, to 2.9 eV in pure AlAs. The experimentally measured band-gap at Γ_{1c} is (18):

$$E_o = 1.424 + 1.266\,x + 0.26\,x^2 \qquad (119)$$

The quadratic term is relatively small compared to the linear term in x, hence E_0 is roughly linearly dependent on x. The gap at X_{1c} increases less rapidly with x, and intersects the Γ_{1c} curve at a band-gap of 1.96 eV, when x is approximately 0.4. The band-edge separation between X_{1c} and Γ_{1c} has been reported as (18):

$$\Delta = 0.380 - 0.892\,x - 0.365\,x^2 \qquad (120)$$

For x greater than 0.4, Al(x)Ga(1-x)As is an indirect-gap material. In fact, although the X_{1c} - Γ_{1c} crossover occurs at x = 0.4, Figure 25 (18) shows that already half of the conduction electrons are in the X_{1c} minimum when x is only 0.3. This is because, even though the X_{1c} minimum is still at higher energy than that of Γ_{1c}, the density of states is a factor of 45 greater at X_{1c} (18). This means that for GaAs-Al(x)Ga(1-x)As heterojunctions where x is greater than 0.4, direct-indirect band tunneling plays a dominant role in carrier transport across the interface. Since the calculations presented here address only direct-direct band tunneling, treatment of GaAs-Al(x)Ga(1-x)As heterojunctions is restricted to compositions with $x < 0.4$.

The density-of-states effective masses for Al(x)Ga(1-x)As, obtained by linear interpolation with x (18), gives the following relation for m_X, the effective mass of electrons in X_{1c}:

$$m_x = 0.39\,(1 - x) + 0.37\,x \tag{121}$$

For m_Γ in Γ_{1c}, the experimentally measured band-gap E_0 was used to find the spin-orbit splitting of the mixed crystal; m_Γ is estimated using this information as (18):

$$m_\Gamma = 0.0636 + 0.0552\,x + 0.0092\,x^2 \tag{122}$$

This is the relationship used throughout this work for the electron effective mass in Al(x)Ga(1-x)As: the effective mass m_Γ ranges from 0.0636 in pure GaAs, to 0.0872 in Al(0.4)Ga(0.6)As. For sawtooth barriers in Al(x)Ga(1-x)As, the linear grading of Al results in approximately linear band-edge grading. Inspection of equation 119 for the band-gap as a function of x, however, shows that there is a slight bowing, indicated by the small quadratic term. Likewise, the linear aluminum grading results in a parabolic z-dependence of the effective mass m in the sawtooth barrier, reflected by the small quadratic term in equation above. The bowing of the band-gap was neglected, but the parabolic term in the effective mass was taken account of in these tunneling calculations for AlGaAs sawtooth superlattices.

2.C.1.d. Band Alignments at GaAs-Al(x)Ga(1-x)As Heterojunctions

The phenomenon giving rise to barriers to electron and hole transport through semiconductor superlattices, is the misalignment of conduction and valence band edges when materials with different band structures are brought into contact. The theoretical and experimental determination of these band misalignments in heterojunctions is difficult and, for GaAs-Al(x)Ga(1-x)As interfaces, is still not completely settled (13,35-40). In this study, the average values of the

best available measurements were used for the Γ_{1c} band-edge alignments. These are represented in Figure 26 (courtesy of R. C. Miller, ATT-Bell Labs) showing ΔE_c as a function of x. Note the shift to the indirect minimum at x = 0.4, where ΔE_c is 0.33 eV. Up to this point the ratio of the band-edge misalignments, ΔE_c:ΔE_v, is approximately 60:40. The 0.33 eV direct conduction band-edge misalignment at x = 0.4, is the largest attainable in GaAs-Al(x)Ga(1-x)As heterojunctions, before interband tunneling takes over. This may be a practical limitation on the efficiency of electron impact ionization in AlGaAs staircase avalanche photodiodes, since the probability of impact ionization at an interface is directly related to the magnitude of ΔE_c there (3).

2.C.2. Some Previous Tunneling Calculations In AlGaAs Heterostructures: Tunneling In Multiple Step Barriers, Stark Shift of Bound and Quasi-Bound States In Single Quantum Wells

In the section below, some previous solutions to two important problems are outlined. Both problems are relevant to the problem of tunneling in graded band-gap superlattices.

The first work to be discussed consists of tunneling calculations by Esaki and Tsu (11) for multiple step barriers formed by GaAs-Al(0.5)Ga(0.5)As heterojunctions. They obtained the transmission coefficient T(E), and the tunneling current J(V), for a small number of barriers. The approach they adopted is very similar to the transfer matrix method used in this study. Their results for step barriers are qualitatively somewhat similar to those expected for a sawtooth array of the same barrier height, composition, and roughly the same spacing. For these reasons, the results of Esaki and Tsu for MSB's were reproduced by the method used in this study in order to verify its accuracy, since there are no prior tunneling calculations for sawtooth superlattices with which to compare.

The second work to be discussed is a calculation by Austin and Jaros (41), of the Stark shift of quasi-bound states in a single GaAs-Al(0.5)Ga(0.5)As quantum well, in an unrestricted uniform electric field. This work is reviewed primarily to show how the spatial extent of the applied field affects the calculated Stark shift. This is relevant to tunneling calculations for sawtooth superlattices, since practical devices will be operated by applying an electric field that is confined to the superlattice between two metal contacts. Assumption of an unrestricted uniform field will lead to the wrong functional dependence of the Stark shift. In the present work, the results of Austin and Jaros for a single quantum well in a uniform field, are reproduced by means of the hybrid Airy function-transfer matrix method detailed in section 2.B.6.a. above. Then, the same calculation is repeated for the well in a localized electric field. The results, which show the consequences of the geometry of the electric field for the calculated Stark shift, are presented in a later section.

2.C.2.a. Esaki - Tsu Tunneling Calculations for the Multiple Step Barrier

Esaki and Tsu (11) performed tunneling calculations for conduction electrons in two, three, and five barrier GaAs-Al(0.5)Ga(0.5)As MSB's. The barrier heights were taken as 0.5 eV. (The data in Figure 26 giving ΔE_c as a function of x, would have set the direct conduction band misalignment at 0.4 eV at x = 0.5, instead of 0.5 eV) The barriers were 2 nm wide and 5 nm apart. (See Figure 27) Working within the effective mass approximation, they do not cite the values used for the effective masses in the well and barrier layers, nor do they quote a source. It is likely that the values they used were close to those calculated by means of equation 122 for the Γ_{1c} effective mass: 0.0636 in pure GaAs, and 0.0935 in Al(0.5)Ga(0.5)As. These are the values used in reproducing their results. In calculating the J-V curves for these MSB's, Esaki and Tsu postulated a constant electric field distributed over the length l of the superlattice. They use a transfer matrix method which is outlined below.

The total energy E for an electron in this one dimensional superlattice is the sum of longitudinal (in the direction of the superlattice) and transverse parts:

$$E = E_\ell + \frac{\hbar^2 k^2}{2m_\Gamma} \tag{123}$$

and likewise the wave function is:

$$\psi = \psi_t \, \psi_\ell \tag{124}$$

For an N period superlattice, the wave functions immediately to the left and right of the superlattice are:

$$\psi_L = \psi_t \left(e^{i k_L z} + R\, e^{-i k_L z} \right) \tag{125a}$$

$$\psi_R = T \psi_t \, e^{i k_R z} \tag{125b}$$

R and T are the reflection and transmission coefficients for the structure. They are obtained from a product of the transfer matrices at each barrier:

$$\begin{pmatrix} T \\ O \end{pmatrix} = M_1 \cdot M_2 \cdot \ldots \cdot M_p \cdot \ldots \cdot M_N \begin{pmatrix} I \\ R \end{pmatrix} \tag{126}$$

where M_p is obtained by matching ψ_p and ψ'_p at each interface:

$$M_p = \frac{1}{4}\begin{pmatrix} e^{ik_{p+2}d_{p+2}} & e^{ik_{p+2}d_{p+2}} \\ e^{-ik_{p+2}d_{p+2}} & -e^{-ik_{p+2}d_{p+2}} \end{pmatrix}\begin{pmatrix} e^{k_{p+1}d_{p+1}} & e^{-k_{p+1}d_{p+1}} \\ -i\left(\frac{k_{p+1}}{k_{p+2}}\right)e^{k_{p+1}d_{p+1}} & -\left(\frac{k_{p+1}}{k_{p+2}}\right)e^{k_{p+1}d_{p+1}} \end{pmatrix}\begin{pmatrix} 1+i\left(\frac{k_p}{k_{p+1}}\right) & 1-i\left(\frac{k_p}{k_{p+1}}\right) \\ 1-i\left(\frac{k_p}{k_{p+1}}\right) & 1+i\left(\frac{k_p}{k_{p+1}}\right) \end{pmatrix} \quad (127)$$

and where:

$$k_p = \frac{\sqrt{2m_{\Gamma,p}(V_p - E)}}{\hbar} \quad (128)$$

V_p and $m_{\Gamma,p}$ are the potential and the effective mass in the p^{th} layer of the superlattice. This transfer matrix gives the same results as the transfer matrix defined in section 2.B.6, however, the identification of the coefficients of the wave functions as in equation 125 above results immediately in the expressions below for the transmission and reflection coefficients:

$$R = -\frac{M_{12}}{M_{22}} \quad (129a) \qquad T = M_{11} - M_{12} \cdot \frac{M_{21}}{M_{22}} \quad (129b)$$

This is the expression for T(E) that the authors use.

In calculating the J-V curves for the MSB, they neglect the potential gradient within each layer, and take account only of the potential difference between the centers of each layer. (Refer to Figure 27) This is an approximation which, because of the small dimensions involved, is probably acceptable.

The expression below is used to calculate the tunneling current:

$$J = \frac{e}{4\pi^3\hbar}\int_0^\infty dk_\ell \int_0^\infty dk_t \left[f(E) - f(E')\right] T^* T \frac{\partial E_\ell}{\partial k_\ell} \quad (130)$$

where f(E) is the Fermi distribution function and:

$$f(E) = \left(e^{(E_\ell - E_f)/kT} + 1\right)^{-1} \quad (131a)$$

$$f(E') = \left(e^{\left(E_\ell - (E_f - eV)\right)/kT} + 1 \right)^{-1} \qquad (131b)$$

The Fermi level, E_f, is taken as 0.005 eV for GaAs with n = $10^{17}/cm^3$. An integration of equation 130 over the transverse direction using the Fermi functions in equation 131, gives:

$$J = \frac{e m_\Gamma kT}{2\pi^2 \hbar^3} \int_0^{E_f} T^* T \ln \left(\frac{1 + e^{(E_f - E_\ell)/kT}}{1 + e^{(E_f - E_\ell - eV)/kT}} dE_\ell \right) \qquad (132)$$

For small values of T, J is reduced to:

$$J = \frac{e m_\Gamma}{2\pi^2 \hbar^3} \int_0^{E_f} (E_f - E_\ell)\, T^* T\, dE_\ell \qquad V \geq E_f \qquad (133a)$$

$$J = \frac{e m_\Gamma}{2\pi^2 \hbar^3} \left(V \int_0^{E_f - V} T^* T\, dE_\ell + \int_{E_f - V}^{E_f} (E_f - E_\ell)\, T^* T\, dE_\ell \right) \qquad V < E_f \qquad (133b)$$

In this manner the contribution of all electrons within about ±kT of the Fermi level of the cladding layer, is integrated into the total tunneling current.

2.C.2.b. Stark Shift of Quasi-Bound States In GaAs-Al(0.5)Ga(0.5)As Single Quantum Well

Austin and Jaros present an exact numerical calculation of the Stark shift of the quasi-bound states in a single quantum well. The well they consider is one which they find supports a single bound state at zero field strength. The well is 3 nm wide, 0.4 eV deep, and is formed between two GaAs-Al(0.5)Ga(0.5)As heterojunctions. The authors work within the effective mass approximation, taking the effective mass of the conduction electrons to be 0.067 inside and outside the well, and neglecting the discontinuity at the edges. They find the Stark shift for both electrons and holes, but only the results for electrons are discussed here.

The approach adopted is similar to the hybrid transfer matrix - Airy function solution outlined in a previous section. The Hamiltonian used is:

$$\hat{H} = \frac{\hat{p}^2}{2m_{eff}} - e\hat{F}_{ap}\hat{z} + \hat{V}_o \qquad (134)$$

for a uniform field F_{ap}. The Schroedinger equation is then given by equations 69a and 69b:

$$-\frac{\hbar^2}{2m_\Gamma}\frac{d^2\psi}{dz^2} - eF_{ap}z\psi = E\psi \qquad |z| > a \tag{69a}$$

$$-\frac{\hbar^2}{2m_\Gamma}\frac{d^2\psi}{dz^2} - (V_o + eF_{ap}z)\psi = E\psi \qquad |z| \leq a \tag{69b}$$

where, as formerly, a is the well width and V_0 its depth. The solutions to the Schroedinger equation in each region are:

$$\psi^- = aAi(-x^-) \qquad z < -a \tag{135a}$$

$$\psi_w = CAi(-x_w) + DBi(-x_w) \qquad |z| \leq a \tag{135b}$$

$$\psi^+ = EAi(-x^+) + FBi(-x^+) \qquad z > a \tag{135c}$$

where:

$$x^- = x^+ = \left(\frac{2m_\Gamma eF_{ap}}{\hbar^2}\right)^{1/3} z + \frac{2m_\Gamma E}{\left(2m_\Gamma eF_{ap}\hbar\right)^{2/3}} \qquad |z| > a \tag{136a}$$

$$x_w = \left(\frac{2m_\Gamma eF_{ap}}{\hbar^2}\right)^{1/3} z + \frac{2m_\Gamma (E + V_o)}{\left(2m_\Gamma eF_{ap}\hbar\right)^{2/3}} \qquad |z| \leq a \tag{136b}$$

The authors match these wave functions and their first derivatives at both edges of the well, obtaining the coefficients of each of the components. They state that resonances, or quasi-bound states, are characterized by an abrupt increase of π in the phase ϕ in the equation:

$$\tan\varphi = \left(\frac{F}{E}\right) \tag{137}$$

This is another way of stating that the ratio of the downstream wave function components, Bi(-x) : Ai(-x), must be maximized for a quasi-bound state. By varying the applied field F_{ap}, calculating the ratio F/E, and searching for shifts of π, they obtain the quasi-bound state Stark shift. They find a Stark shift with quadratic dependence on the field, for field strengths between 100 and 500 kV/cm. Their results agree with those previously obtained by means of variational calculations. (42,43)

The authors neglect the effective mass difference inside and outside the well. Outside the well, using equation 92 and x = 0.5, m_{eff} is 0.0935, almost 50% higher than the value inside

the well. Neglecting this difference leads to an error in the calculated energy level of the resonances. This is discussed in greater detail in a later section, where their results are compared with those obtained in this study.

3. RESULTS AND DISCUSSION

3.A. Scope

3.A.1. Description of Work

The aim of this work is to gain an understanding of the tunneling properties of electrons in graded band-gap AlGaAs sawtooth superlattices. All computations are carried out by means of the transfer matrices described in the theory section, working entirely within the effective mass approximation. T-E and J-V curves are here presented for these sawtooth structures.

In order to put these results in the context of previous work on conventional step barrier superlattices, tunneling calculations for some other simple structures are also presented. Transfer matrix tunneling calculations for single and multiple step barriers under constant external electric fields are reported. The effects of the external field on the resonances supported by these structures are discussed, and J-V curves are presented for the MSB. In particular, results obtained here for Al(0.5)Ga(0.5)As-GaAs MSB's are compared to those obtained by Esaki and Tsu (ref) for identical structures. This is done to demonstrate the accuracy of the computational method used here.

Bound and quasi-bound states of Al(0.5)Ga(0.5)As-GaAs single quantum wells are calculated, along with their Stark shift under constant electric fields. These calculations are done for the two configurations of uniform and localized field, in order to illustrate that, which of the above is chosen will determine whether the calculated Stark shift is quadratic or linear. These results are compared with those obtained by Austin and Jaros (ref) for an identical quantum well under uniform fields, again by way of validation of the present work.

Finally, tunneling calculations for sawtooth barriers and superlattices are reported. The properties of sawtooth and step barriers are compared, and similarities between MSB's and sawtooth superlattices are pointed out. Throughout, particular emphasis is placed on the consequences of the effective mass variations in all the structures studied here, and need to use modified wavefunction connection rules at interfaces where the effective mass makes a discontinuous change.

3.A.2. Approach

All computations are carried out by means of the matrix methods described in the preceding theory section. VAX Fortran computer programs computing the T-E and J-V curves for all step and sawtooth barriers and arrays, and the bound and quasi-bound states and Stark shifts

for single quantum wells, are found in Appendix A, along with descriptions of the operation of each program. All programs involving variations in the effective mass use the modified connection rules described in section 2.A.

3.B. Single Step Barrier

Tunneling calculations for single step barriers are done in the programs ZIGGURAT and ZIGGEFFMASS. The former assumes a constant effective mass equal everywhere to m_0, while the latter models Al(x)Ga(1-x)As-Al(y)Ga(1-y)As step barriers, accepting the aluminum concentrations x and y as inputs, and calculating m_{eff} inside and outside the barrier from equation 122. Both programs accept the zero-field barrier height V_0 and width a, and the use of ZIGGEFFMASS requires choosing V_0 to agree with ΔE_c given in Figure 26 as a function of x and y at the interfaces. The applied field F_{ap} enters as a parameter: each run of the program then produces a file of T versus E, for a given value of F_{ap}, which can be plotted. Both programs model the barrier in a localized field restricted to the barrier.

3.B.1. Single Step Barrier: Zero external field

Consider a single GaAs-Al(0.4)Ga(0.6)As step barrier 10 nm wide. The barrier height V_0 must be 0.33 eV, according to Figure 26. The effective mass inside the barrier is 0.0872, while outside it is 0.0636. The T-E curve for this barrier is shown in Figure 28, where the energy ranges from 0.5 to 1.5 times the barrier height. The first transmission maximum occurs at 0.372 eV, well above the barrier height: this curve is described by equation 28 for $E > V_0$, and by equation 31 for $E < V_0$.

To see the strong influence the effective mass can have on the T-E curve of step barriers, refer to Figure 29, which shows the curve for a barrier of identical height and width as the one above, but with constant effective mass equal to m_0. The first maximum occurs at 0.334 eV, only slightly above the barrier height, and five more closely-spaced peaks follow. This curve is described by equations 29 and 32, above and below V_0, respectively. Equation 30 gives the energies of the maxima in this case.

Further differences between the two barriers are evident in Figure 30, where their T-E curves are overlapped. The effective masses m_1 and m_2, and their relative difference, $(m_1 - m_2)$, entering into equations 28 and 31, result in higher transmission minima throughout the range, in broadened resonances shifted to higher energies, and in lower-frequency transmission oscillations. The latter is the dominant effect, and is caused by the effective mass inside the

barrier, m_2, appearing in the argument of the sine, being a great deal smaller than m_0. The elevated minima however, reflect the effective mass difference (m_1 - m_2), which is negative and makes the denominator in equation 28 smaller. Figure 30b shows this: the T-E curve for a step barrier with constant $m_{eff} = m_2$, is superposed on Figure 28. The two curves agree except in the absolute values of the transmission coefficient, which are highest when the mass difference (m_1 - m_2) is retained. In AlGaAs step barriers, this difference is always negative; hence the minima are always higher than those where the effective mass is taken as constant.

3.B.2. Single Step Barrier: Non-Zero Field

In considering the effects of a constant electric field on the transmission properties of single step barriers, it is easiest to start with the constant mass case ($m_{eff} = m_0$), and then show how the effective mass further alters the picture when dealing with AlGaAs. Unlike the zero-field case, there is no analytical expression for T(E) for a step barrier under a constant field.

T-E curves for the 10 nm, 0.33 eV high barrier were obtained, using the program ZIGGURAT, for applied field strengths F_{ap}, of 2 and 5×10^{-2} eV/nm. These are shown together with that of the zero-field barrier, in Figure 31. The field deforms the barrier to a thinner, triangular shape, and this facilitates tunneling at energies below V_0. In fact, resonance peaks occur at approximately 0.297 and 0.320 eV for $F_{ap} = 2\times10^{-2}$ eV/nm, and at 0.255 and 0.300 eV for $F_{ap} = 5\times10^{-2}$ eV/nm. This is a major effect of the applied field, since resonance maxima below the top of the barrier are not possible when there is no external field, as equations 31 and 32 show.

The broadening of the peaks evident in Figure 31, is a consequence of the tapered thickness of the barrier: for E greater than the lower edge of the barrier, there is no longer a single barrier width to serve as the resonance criterion:

$$\sin k_2 a = n\Pi \qquad (138a)$$

Instead, there is a spread in the wavelength over which some kind of resonance can take place, because the width of the barrier varies. The field not only broadens the peaks, but causes them to be more widely spaced for the same reason.

Another striking effect of the field is to lower the contrast between the resonance peaks and valleys. For any non-zero field, the peaks no longer reach 1, and the minima are raised with respect the zero-field barrier. The transmission curve asymptotically approaches 1 at infinite energy. As Figure 31 shows, increasing the field strength washes out the contrast of the peaks and valleys, and slows the approach to the maximum value of 1, while increasing the amount of tunneling below V_0.

When the 10 nm Al(0.6)Ga(0.4)As-GaAs step barrier is subjected to a constant electric field, effective mass variations further change the T-E curves. T-E curves generated by ZIGGEFFMASS for F_{ap} = 2 and 5×10^{-2} eV/nm are found in Figure 32, along with the zero-field curve. The increasing electric field has an even more pronounced effect on the transmission through the GaAs-Al(0.4)Ga(0.6)As step barrier, than it had when $m_{eff} = m_0$ throughout. The same trends are evident in much greater force: the peaks are broadened and shifted to lower energies, and their contrast is much reduced, relative to the zero-field case.

Figure 33 compares the T-E curves of the constant mass and Al(0.4)Ga(0.6)As barriers. Figures 33a and 33b give the T-E curves for $F_{ap} = 2\times10^{-2}$ and 5×10^{-2} eV/nm, respectively. Most of the structure in the T-E curves of the constant mass barrier is obliterated by the smaller effective mass of the Al(0.4)Ga(0.6)As barrier. Field-assisted tunneling is more probable through the Al(0.4)Ga(0.6)As barrier at all energies, at $F_{ap} = 5\times10^{-2}$ eV/nm. At $F_{ap} = 2\times10^{-2}$ eV/nm, this effect is less pronounced, but transmission minima for the Al(0.4)Ga(0.6)As are still higher than those of the constant mass barrier.

Field-assisted tunneling calculations for AlGaAs step barriers should thus certainly use at least the correct average effective mass, and optimally, the effective masses appropriate to the barrier and adjacent layers. The former will result at least in the correct peak locations,although the absolute values of the transmission coefficient will be somewhat in error, away from the resonance maxima. Simply using the free electronic mass throughout will lead to gross error in the T-E curves obtained at all field strengths.

3.C. Single Quantum Well: Bound States and Stark Shift

In this section, the bound states of AlGaAs single quantum wells (SQW's) and their Stark shift in a constant electric field, are obtained by means of transfer matrices. First, the zero-field solution for the bound states is given: the role of the effective mass in determining the energy eigenvalues of the SQW is described. The programs for the zero-field SQW bound states are WELL and ALGAASWELL. Both programs accept values for the well width a and depth V_0, and produce files of the total transfer matrix element M_{11} as a function of the energy E below the top of the well, which is taken as zero. Minima in M_{11} indicate the bound states of the well. The program WELL assumes a constant effective mass $m_{eff} = m_0$ everywhere inside and outside the well. The program ALGAASWELL, however, models SQW's formed by Al(x)Ga(1-x)As- Al(y)Ga(1-y)As heterojunctions, and, just as the program ZIGGEFFMASS does, requires the x and y values in order to calculate the effective masses inside and outside the well. V_0 must be chosen in accordance with $\Delta E_c(x,y)$ read from Figure 26.

The Stark shift of the energy eigenvalues of AlGaAs SQW's is obtained for constant electric fields localized to an area surrounding the well, and also for unrestricted uniform fields. This is done in order to show that, which of the two configurations is used, will determine whether the Stark shift is linearly or quadratically dependent on the field strength.

The localized-field Stark shift is calculated in the program STARKMASS. This program models a 3nm wide Al(0.5)Ga(0.5)As well under the field as shown in Figure 18c. This is identical to the SQW studied by Austin and Jaros (41). The extent of the field is such that level of the plateau downstream of the well is at the same level as the lowest potential in the well. This makes sure that bound states in the well can tunnel out under a non-zero field. This allows a direct comparison with the results for the unrestricted uniform field, where all bound states under any field are susceptible to tunneling. In other respects, this program works identically to ALGAASWELL, except that the applied field F_{ap} enters as a parameter. Each run of the program results in field-shifted minima in M_{11}. Plotting the minimum M_{11} as a function of F_{ap} then gives the Stark shift.

The program AIRYWELL is used to calculate the Stark shift of a 3nm GaAs-Al(0.5)Ga(0.5)As SQW, under uniform electric fields. This program accepts the applied field as a parameter, and calculates the ratio (F/E) (of the inbound to outgoing wavefunction components downstream of the well), as a function of the energy E below the top of the well. Maxima of |F/E| indicate the bound state energy levels. Each run of the program gives these Stark-shifted levels at a given field. These levels are plotted as function of the field strength.

3.C.1. Single Quantum Well: Zero-Field

The program ALGAASWELL gives the spectrum for a GaAs-Al(0.5)Ga(0.5)As SQW, 3nm wide and according to Figure 26, 0.4eV deep. This is shown in Figure 34, where the total transfer matrix element M_{11} is plotted as a function of of E. This well supports a single bound state at -0.197 eV. This is in agreement with the results of others (ref) who first determined that these well dimensions, along with an effective mass of 0.0636, result in a single level. There is also rough agreement with an approximate calculation of the number and level of bound states, using equations 66b and 66c. These predict a single level at -0.211 eV.

The discrepancy between these values is a consequence of neglecting the effective mass difference between the well and the adjacent layers. The program ALGAASWELL uses the appropriate values of 0.0636 outside, and 0.0935 inside the well. If instead, an effective mass of 0.0636 is used throughout, then a single bound state at -0.217 eV is obtained. This is in excellent agreement with an easily derived equation for the energy of the ground state of a finite quantum well (44):

$$E \simeq V_o - \frac{m_{eff}{}^a}{2\hbar^2} V_o^2 \qquad (138b)$$

Figure 35 shows the M_{11} versus E curves overlapped for these two treatments of this well: the bound state level is strongly affected by how the variation of m_{eff} at the well edges is handled. This illustrates the risk involved in applying standard formulae to semiconductor heterostructures. Most, if not all, of these take no account of the effective mass variations at interfaces, and this will impair the accuracy of the results obtained.

To illustrate further how profoundly the effective mass influences the bound states of the well, calculations for an SQW 3nm wide and 0.4 eV deep, but with the mass constant and equal to m_0, were repeated in the program WELL. The results are shown in Figure 36. Instead of a single level there are four, and this is in agreement with the equation below giving the number of bound states of a finite quantum well (44):

$$N > \frac{\sqrt{2\, m_{eff}\, V_o\, a^2}}{\pi\hbar} > N - 1 \qquad (139)$$

Inspection of this equation shows that the number of levels that a well can trap is proportional to the square root of the mass of the particle in the well. Since m_0 is approximately sixteen times as great as m_{eff} in GaAs, there are four times as many trapped states in this well. Again it is apparent that the appropriate effective masses must be used in calculations intented to model real semiconductor heterostructures, potential wells in this instance.

3.C.2. Single Quantum Well: Stark Effect

When an electric field is applied to a single quantum well such as the one described above, the bound states shift to lower energies inside the well. The magnitude and field-strength dependence of this energy shift depend on whether the field is localized or unrestricted.

3.C.2.a. Single Quantum Well: Stark Effect Under Localized Field

First, the Stark shift for the 3nm Al(0.5)Ga(0.5)As single quantum well in a localized field is calculated. In order to make a direct comparison with the work of Austin and Jaros and others (41-

43) the effective mass is taken as 0.0636 everywhere, neglecting the discontinuity at the well edges. It was shown above that this results in an error in the determination of the bound state energy. It has no effect on the functional dependence of the Stark shift, however. In the program STARKMASS the total transfer matrix element M_{11} is computed as a function of the energy and field strength. These data are plotted in Figure 37; the field strengths range between 0 and 5×10^{-2} eV/nm. The bound states, just as for zero field, are the minima in M_{11}. It is easy to see the shift of the bound state energies to deeper in the well as the field increases.

When these shifts are referred to the zero-field bound state energy of -0.217eV with the differences plotted in Figure 38 as a function of the field strength, it is clear that the Stark shift is linear. This effect is either explicitly described in the work of others, for instance, Schwartz in his study of AlGaAs MSB's (17), or is implied in the results of still others. Esaki and Tsu (11) for example, report J-V characteristics for MSB's, which, interpreted in the light of T-E curves for the same structure, indicate a linear Stark shift of the resonances. (This is described in detail in the following section). Here, the Stark shift of an isolated well is calculated. The common feature of the isolated well and the MSB's studied in the works referred to above, is that the field is localized around the structure in question.

3.C.2.b. Single Quantum Well: Stark Effect Under Uniform Field

Now the same isolated Al(0.5)Ga(0.5)As well in a uniform, unrestricted electric field is considered. The program AIRYWELL computes the ratio F/E of the well as a function of energy and applied field strength. Figure 39 shows F/E versus E for several field strengths between 1×10^{-2} and 5×10^{-2} eV/nm. The peaks in F/E, analogously to the minima in M_{11}, indicate the bound states. The shift in the location of the bound state is again to values deeper in the well, but this time the shift is obviously not linear.

Figure 40 shows the bound state energy levels plotted as a function of the field strength. A polynomial least-squares fit to the data results in a quadratic Stark shift:

$$E_w = -221.85 - 0.9217\, F_{ap}^2 \qquad (140)$$

The energy shift with field strength is plotted in Figure 41 along with the same data for an identical well reported by Austin and Jaros. Fairly good agreement exists between the two sets of data. A larger shift is obtained by the present means, however, and the source of the discrepancy is uncertain.

The Stark shifts obtained from the localized and unrestricted fields applied to the well are plotted together in Figure 42. The linear shift for the localized field is much larger at a given field strength than the quadratic shift. In fact, the magnitude of the linear Stark shift is calculated assuming that the geometric origin is centered at the left hand edge of the well. Comparing the linear Stark shift with the product of the field strength and the well half-width, shows that the Stark shift is entirely made up of the lowering of the potential in the center of the well, under the field. This is also observed when the Stark shift of the resonances of MSB's subjected to local fields is calculated. The linear shift under localized fields appears actually to be just the shift in the base of the well. For MSB's and isolated quantum wells alike, the virtual state is then still the result of resonance of the wave off the sides of the well, only the wavevector is referred to the bottom of the well, which is now shifted lower by the field.

The Stark shift under unrestricted fields is in agreement with the results of others (41-43). It is reported, however, that under stronger electric fields, (i.e. greater than about 1×10^{-1} eV/nm) it departs from its quadratic dependence on the field. This regime is not explored in the present study.

In any case, it is clear that calculations of the Stark shift of the resonances in actual semiconductor heterostructures should probably be made by assuming that the electric field will be localized to the structure. The consequences of assuming an unrestricted field are that the wrong functional dependence and magnitude will result. For this reason, the field-assisted tunneling calculations for AlGaAs sawtooth superlattices, to be described below, are all performed assuming localized fields.

3.D. Multiple Step Barriers

Tunneling calculations for multiple step barriers are presented in this section. The transmission coefficient is computed as a function of incident energy, just as for the single step barrier, under zero external electric field. In addition, the tunneling current as a function of applied voltage is calculated.

The tunneling calculations for AlGaAs MSB's are performed in the programs ALMSB and JVALMSB. ALMSB computes the transmission coefficient for an MSB of an arbitrary number, N, of periods, where a period is composed of a barrier and the well to the right of it. The applied electic field may be varied as a parameter, so that T-E plots parametric in F_{ap} may be generated for a given MSB. The program is similar to ZIGGEFFMASS, used for single AlGaAs step barriers, except for the fact that the total transfer matrix is accumulated through several barriers instead of one.

JVALMSB computes the tunneling current as a function of the applied voltage, creating data files from which J-V curves are made. It is a derivative program of ALMSB, differing only in the use of a single incident energy of 0.005 eV, roughly equal to the Fermi energy in bulk GaAs. The applied voltage is in this case the independent variable.

Both of these programs have analogues which compute the transmission coefficients and tunneling currents through ideal structures where the effective mass is constant and equal to m_0. These are the programs MSB and JVMSB, respectively. Except for using a single, constant effective mass throughout, they are identical to ALMSB and JVALMSB.

In the text below, first the T-E and J-V data are reported for 2, 3, and 5 barrier GaAs-Al(0.5)Ga(0.5)As MSB's. These are the same structures studied by Esaki and Tsu (11): the results of the present study are described and compared with theirs. The correlation of the transmission resonances with features in the J-V characteristic is discussed.

Then, the same calculations are repeated for GaAs-Al(0.4)Ga(0.6)As MSB's of the same dimensions and number of periods. This is done to provide a basis for comparison with the GaAs-Al(0.4)Ga(0.6)As sawtooth tunneling calculations in the final section.

Results of tunneling calculations for ideal, $m_{eff} = m_0$, MSB's are presented as well, in order to show once again the strong influence the effective mass has upon the resonances of a quantum heterostructure.

3.D.1. GaAs-Al(0.5)Ga(0.5)As MSB's: Comparison with Results of Esaki and Tsu

3.D.1.a. GaAs-Al(0.5)Ga(0.5)As MSB: Transmission Coefficient versus Energy

The MSB's for which Esaki and Tsu did tunneling calculations consisted of 2, 3, and 5 step barriers 2 nm wide and 5nm apart, and 0.5 eV high. These are the dimensions used in this study.The barrier height of 0.5 eV is not an accurate representation of Ec for this composition. A value of 0.4 eV, which was used in the bound state calculations for the quantum well, is more appropriate, according to Figure 26. The barrier height of 0.5 eV is used in the tunneling calculations presented here, however, for purposes of comparison.

The transmission coefficients calculated in the program MSB, are plotted as a function of energy in Figure 43a, b and c, for 2, 3 and 5 barriers respectively. Below the barrier height in each case, there are two sets of resonances. The two-barrier MSB has a single resonance at 0.12 eV and another, much broader, one at 0.43 eV.

As pointed out in section 2.B.3, the occurance of resonances below the barrier height (under zero field) is impossible in tunneling through a single step barrier. When two or more barriers are involved, resonance of the wave with the wells between them is possible at energies much below their height, and that is what is giving rise to the resonances seen in Figure 43. Furthermore, each resonance peak reaches 1. As demonstrated in section 2.B.3, this is characteristic of superlattices with even spatial symmetry, and these MSB's have this symmetry. When it is broken by applying an electric field, the peaks no longer reach 1.

The three- and five-barrier MSB's have resonances which are split by coupling between the two and four wells, respectively, formed by the barriers. The T-E curves for the two- and five-barrier MSB's are shown on the same scale in Figure 44. There are four resonances distributed around the each single peak belonging to the two-barrier structure; two at higher, and two at lower energy. The off-resonance transmission coefficient is several orders of magnitude lower at most energies for the five-barrier MSB due to the greater difficulty of tunneling through three more barriers.

The T-E curves calculated by Esaki and Tsu for each of the structures, are found in Figure 45. These are in good qualitative agreement with those shown Figure 43, however, the resonances are now centered at 0.08 eV and at 0.32 ev, instead of 0.12 eV and 0.43 eV. The source of this discrepancy is unknown, however, the location of the resonances is very sensitive to the values of the effective mass that are used in these calculations. It is likely that the authors used somewhat different values than those used in this work; since they do not cite their values, this is unresolved. Agreement is good enough to conclude, however, that the method used in this study is valid.

3.D.1.b. Tunneling Current versus Applied Voltage

The tunneling current as a function of the applied voltage is calculated for these GaAs-Al(0.5)Ga(0.5)As MSB's in the program JVALMSB. The incident energy is 0.005 eV, that is, the Fermi level in n-doped GaAs where n = $10^{17}/cm^3$. The applied voltage ranges between zero and 2 volts. This range is sufficient to show how the resonances of these MSB's influence their J-V characteristics.

In Figure 46 are found the J-V curves for the two- and three-barrier MSB's. The curve for the two-barrier MSB is particularly simple because there is only one well in the structure. There is a current peak at approximately 0.23 V, and another broader one at 0.86 V. On the high-voltage sides of these peaks are regions of negative differential resistance. These features are consequences of the resonances supported by the MSB, and are manifestations of resonant tunneling. There is a current peak at 0.23 V because half of this voltage is dropped at the center

of the MSB, and this shifts the lowest resonance, located 0.12 eV above the bottom of the well, to coincide roughly with the incident energy E = 0.005 eV. When this happens then resonant tunneling through the first barrier is highly probable, and there is a corresponding peak in the J-V characteristic. As the voltage is increased and the resonance is shifted below the incident energy level, resonant tunneling declines, giving rise to the region of negative differential resistance. The broad current peak at 0.86 V is likewise caused by the coincidence of the similarly broad resonance at 0.43 eV, with the incident energy; in other words, when the voltage dropped at the center of the MSB is 0.43 eV.

It is worth pointing out, that these features of the J-V curve indicate unambiguously that the Stark shift of the MSB resonances is linear in the applied voltage or field strength. Also implied, is the fact that the shift, under localized fields, is simply caused by a shifted baseline or reference level. This is observed by others; for instance, by Schwartz (17), who reports a linear Stark shift in the resonances of AlGaAs MSB's, when calculating the resonances by means of a very similar transfer matrix technique. It appears likely, however, that if these calculations were to be repeated for MSB's subjected to uniform fields, the Stark shift of the resonances would not be linear, analogously to the behavior of bound states in single quantum wells.

The J-V curves obtained by Esaki and Tsu are shown in Figure 47. Comparison with Figure 46 shows good agreement with the J-V curves calculated in the present study. This is a significant validation of the transfer matrix method used here. The curves of Esaki and Tsu show sharper peaks and deeper minima, however. This may be caused by two things. One is that they did not use a single incident energy, but integrated, according to equations 133a and b, the contribution of conduction electrons within about +/- kT of the Fermi energy. Another is that they neglected the voltage gradients inside the barriers and wells, taking account only of the drop between the centers of each. Although this is not a bad approximation for the barriers, which are only 2 nm wide, it may be less satisfactory for the 5 nm well regions.

3.D.2. GaAs-Al(0.4)Ga(0.6)As MSB's and the Influence of the Effective Mass

The resonances of the step barriers and the bound states of the single quantum wells discussed in the preceding sections, proved to be strongly influenced by the values of the effective mass used in calculating them. That the effective mass is similarly important to the outcome of tunneling calculations for MSB's, is shown by the T-E curve calculated for a two-barrier MSB, identical in geometry to the Esaki-Tsu GaAs-Al(0.5)Ga(0.5) As MSB, but with an effective mass m_{eff} which is constant, and equal to m_0. These calculations are done in the program MSB. Figure 48 shows this T-E curve and the one belonging to the two-barrier GaAs-Al(0.5)Ga(0.5)As

MSB for which the proper effective masses are used. There is quite a significant difference between the two. Instead of two resonances, there are now five below the barrier height. The transmission coefficient is also lower by several orders of magnitude at most energies away from resonance. Analogously to quantum wells, the number of resonances that an MSB can support is proportional to the effective mass of the particle interacting with it. Similarly, the values of transmission minima through a single step barrier are a function of the difference between the effective masses inside and outside the barrier, and it appears that this is also the case for MSB's.

The data in Figure 48 above, illustrate the consequences of using a grossly wrong effective mass in tunneling calculations for MSB's. Suppose instead that the electronic effective mass of pure GaAs, $m_{eff} = 0.0636$, is used throughout, neglecting the change to $m_{eff} = 0.0935$ inside the barriers. This is the approximation frequently made in the calculations of the bound states of single AlGaAs quantum wells, for instance in the work of Austin and Jaros and others (41-43). It has already been shown that this strongly affects the location of the bound state in a single GaAs-Al(0.5)Ga(0.5)As quantum well.

Figure 49a shows the T-E curves for two MSB's: one of them the two-barrier Esaki-Tsu MSB using the correct effective masses, and the other of the same geometry, but using $m_{eff} = 0.0636$ everywhere inside and outside the barriers. The resonances in the latter case are more widely spaced and slightly broader than those of the realistically modelled MSB, with the lowest resonance shifted down to 0.10 eV, and the higher one to approximately 0.82 eV. The off-resonance transmission coefficient is also higher throughout, because the average effective mass is lower.

Figure 49b shows the resulting J-V curves for the above two structures. The current peaks follow the same trends as the resonances of the T-E curves. When the effective mass is taken as 0.0636 everywhere, the low- voltage current peak is shifted to 0.20 V from 0.23 V. The tunneling current is approximately half an order of magnitude higher at all voltages, following the behavior of the transmission coefficient, and the current peaks are broadened in the same manner as the resonances in the T-E curve.

The T-E and J-V curves of Figure 49 show that it is necessary to take careful account of the variations in effective mass in MSB's for accurate determination of the resonances. The MSB's used to illustrate this, however, are somewhat unrealistic, because the barrier heights are not correct for the assumed aluminum concentrations. These MSB's served mainly as a basis for comparison with the results of Esaki and Tsu. Tunneling calculations for GaAs-Al(0.4)Ga(0.6)As MSB's are now discussed. These are layer compositions for which the maximum direct conduction band edge discontinuity, and hence, the largest possible barrier height, is 0.33 eV. Single step barriers of the same composition were discussed in section 3.B. above. The discussion to follow on such MSB's is aimed at providing a basis for comparison with sawtooth barriers which have this

as the composition at the end of each layer. Results of tunneling calculations for these sawtooth superlattices are found in the next section.

The T-E and J-V curves are calculated in the programs ALMSB and JVALMSB for GaAs-Al(0.4)Ga(0.6)As MSB's. These MSB's have two and five barriers, 2nm wide and 5 nm apart (i.e., with the same number, width and spacing as the Esaki-Tsu MSB's just dealt with), and barrier heights of 0.33 eV. These curves for the two-barrier MSB are presented in Figure 50a and b, respectively. Shown together with them, for the purpose of comparison, are the T-E and J-V curves for the two-barrier GaAs-Al(0.5)Ga(0.5)As MSB's.

In Figure 50a, the upper T-E curve belongs to the GaAs-Al(0.4)Ga(0.6)As MSB. The resonances are shifted slightly to lower energies, and are broadened: the lowest resonance occurs at roughly 0.09 eV, and the upper one at 0.37 eV. The off-resonance transmission coefficient is also raised by at least an order of magnitude. In this case, these differences are the result not just of changing the value of the effective mass inside the barrier, (and hence also the average value for the MSB), but also of the fact that the barrier height is lower, at 0.33 eV instead of 0.5 eV. The lower average effective mass and the lower barrier height both contribute to greater probability of tunneling through this structure than in the Esaki- Tsu MSB.

In Figure 50b, again the upper curve belongs to the GaAs-Al(0.4)Ga(0.6)As MSB. The features of this simple J-V curve follow from the T-E curve: there is a current peak at approximately 0.18 V, or at twice the energy of the lowest resonance, and another very broad one around 0.75 eV. The tunneling current is generally one half to one order of magnitude higher throughout than for the GaAs-Al(0.5)Ga(0.5)As MSB.

3.E. Sawtooth Superlattices

In this final section, the results of tunneling calculations for sawtooth barrier superlattices are presented. The transmission coefficient as a function of incident energy, and the tunneling current as a function of the applied voltage are computed, and the results are compared with those obtained for step barriers.

The transmission coefficient is calculated by the matrix method outlined in section 2.B.6.d., in the programs SAWTOOTH and ALSTAIR. These programs are found in Appendix A along with a description of their operation. Both programs accept the number of barriers, N, and assume right triangles, accepting their base and altitude. The applied electric field enters as a parameter. Data files of the transmission coefficient versus the incident energy are created and used to make T-E plots parametric in the applied field. The program SAWTOOTH assumes a constant effective mass equal to m_0, the free electronic mass. The program ALSTAIR models

graded band-gap Al(x)Ga(1-x)As superlattices, and accepts the maximum and minimum aluminum concentrations within each barrier, assuming a linear concentration variation. The effective mass at each point in the barrier is calculated by means of equation 122. The modified connection rules taking account of the effective mass variation at each step are used in this program.

The tunneling current is calculated as a function of the applied voltage in the programs JVSAWTOOTH and JVALSTAIR. These programs are derivatives of SAWTOOTH and ALSTAIR, respectively. Instead of the incident energy, the applied voltage is the independent variable. An incident energy of E = 0.005 eV is used just as for the MSB's of the preceding section. Data files of the tunneling current versus applied voltage are used to construct J-V plots.

Below, results of tunneling calculations for single sawtooth barriers are first discussed and are compared with those already obtained for single square step barriers, in section 3.B. The effects of external electric fields and the effective mass are discussed. Then, tunneling calculations for multiple sawtooth barriers are presented, and compared to those for similar multiple step barriers, in particular the MSB's studied by Esaki and Tsu (11).

3.E.1. Single Sawtooth Barriers

3.E.1.a. Single Sawtooth Barrier In Zero External Field

There is no analytical solution for the transmission coefficient through a sawtooth barrier, hence transfer matrices are especially well suited for this problem. It is interesting to compare the results of tunneling calculations for sawtooth barriers with those of step barriers, and to see what are the effects of the graded barrier height. Recall that in section 3.B., the transmission coefficient for 10 nm wide, 0.33 eV step barriers was calculated. The T-E curves obtained showed resonances above the barrier height: under zero field these occurred whenever the barrier width was an integral number of half wavelengths. The character of these curves was strongly influenced by the average effective mass as well as the difference in mass inside and outside the barrier. The behavior of waves encountering sawtooth barriers might be expected to be similar. The transmission coefficient for a 10nm wide, 0.33 eV sawtooth barrier with effective mass constant and equal to m_0, is shown in Figure 51a, along with the T-E curve from Figure 28 for a step barrier of the same dimensions and effective mass. There is a striking absence of resonances in the T-E data of the sawtooth barrier. Tunneling is much more likely through the sawtooth barrier, for energies well below the peak barrier height and the maximum value of 1 is approached monotonically. By way of contrast, the transmission coefficient through the step barrier is extremely small until just above the barrier height, where it rises steeply to 1, and then oscillates strongly.

The smooth shape of the transmission curve for the sawtooth can be thought of as resulting from the lack of a resonance condition such as exists in square step barriers. In fact a similar effect has already been encountered in step barriers under external, constant electric fields. There, the field effectively tapers the upper part of the barrier: the stronger the field, the broader the resonances and the lower the contrast between peaks and valleys. The approach to the maximum value of 1 is also more gradual as the field strength increases. The grade in a sawtooth barrier is analytically indistinguishable from the grade in a step barrier induced by an externally imposed electric field, so the similarity of their T-E data is not terribly surprising.

Figure 51b shows the T-E data obtained for a single GaAs-Al(0.4)Ga(0.6)As sawtooth barrier, 10 nm wide and 0.33 eV high. The effective mass in this barrier is graded parabolically from 0.0636 to 0.0871 at the peak. The curve for this barrier is superposed on that of a 10nm wide GaAs-Al(0.6)Ga(0.6)As step barrier. The same qualitative differences observed between the T-E data of the constant m_{eff}, step and sawtooth barriers in Figure 51a, are also present in Figure 51b. Considerably more tunneling takes place at all energies below the barrier height in the sawtooth, and there is a similar lack of resonances.

In fact, as Figure 52 shows, tunneling through sawtooth barriers appears to be much less susceptible to the influence of the effective mass than is tunneling in step barriers. In Figure 52 the T-E curves of the constant mass, $m_{eff} = m_0$ and the GaAs-Al(0.4)Ga(0.6)As sawtooth barriers are plotted together. The two curves are quite similar. Just as observed in step barriers, the lower average effective mass enhances tunneling at all energies. The transmission coefficient is 0.5 at 0.25 eV in the GaAs-Al(0.6)Ga(0.6)As sawtooth, only reaching this value at 0.33 in the constant mass sawtooth. The similarity between the two curves is otherwise much stronger than between T-E curves belonging to comparable step barriers (Refer to Figure 30a).

3.E.1.b. Single Sawtooth Barriers under Constant, Localized Electric Fields

Field-assisted tunneling through sawtooth barriers is expected to differ somewhat from that through step barriers. If the field is constant, it results in an additional linear potential in the region of the sawtooth. This potential just adds to the already existing one, and as pointed out above, is not analytically different from it. This is different from imposing such a field on a step barrier, since that results in a situation that is analytically different from the zero-field case. For this reason it is expected that the effects of the field on tunneling through sawtooth barriers should be less radical than when dealing with step barriers.

In this study, the applied field is taken as constant and opposing the gradient of the sawtooth itself. This is illustrated in Figure 2. As the field strength is increased to the value of the

sawtooth potential gradient, the barrier changes to a staircase potential. When this happens, tunneling no longer occurs, since there is no longer a barrier to tunnel through. The transmission coefficient must always be greater than zero for such a potential. Again, this is unlike field-assisted tunneling through step barriers, where no matter how great the field strength, a barrier to tunneling always exists.

Field-assisted tunneling calculations for 10 nm, 0.33 eV sawtooth barriers are done for field strengths of 0.02 and 0.05 eV/nm. (These are same values used in the field-assisted tunneling calculations for the 10 nm, 0.33 eV step barriers.) Calculations are done for both $m_{eff} = m_0$, and for the GaAs- Al(0.4)Ga(0.6)As sawtooth. The resulting T-E curves are shown for all field strengths in Figure 53. As the field strength is increased, the transmission coefficient also increases at all energies, but the approach to 1 is slowed. Note that the T-E curves for F = 0.05 eV/nm are of a different character than those obtained at 0.02 eV/nm: T is greater than zero for all energies in the former case. Figure 54 shows the deformation of the sawtooth barrier under the applied field. At F = 0.05 eV/nm, the structure is a staircase, not a sawtooth. This transition occurs at a field strength of 0.033 eV/nm. At field strengths less than this, tunneling can still occur, and, for the constant mass sawtooth, the T-E curves have an inflection point, at energies equal to the peak height of the sawtooth, where the value of the transmission coefficient is 0.5. For the GaAs-Al(0.4)Ga(0.6)As sawtooth, these inflection points are shifted to lower energies.

An interesting feature of the curves in Figure 53, is that as the field strength increases, the difference between the T-E curves of the GaAs- Al(0.4)Ga(0.6)As and the constant mass sawtooth barriers becomes less significant. The curves obtained at F = 0.05 eV/nm in fact are practically identical. The reason for this is not apparent. This trend was not evident in the step barriers studied here, although it might have been, in the limit of very high fields, which was not adressed in this study.

Overall, it appears that single sawtooth barriers differ from step barriers in a few respects. One is that, because of the sawtooth's graded thickness, transmission resonances are almost totally supressed. This is a consequence of the lack of a resonance condition such as exists in step barriers. Another is that the interaction of the incident wave with the sawtooth barrier changes character at field strengths sufficient to deform the barrier into a staircase structure. Finally, for reasons that are not clear, the influence of the effective mass is very much less pronounced, and tends to become still less important as the field strength is raised. In the next section, the same issues will be adressed for multiple sawtooth barriers.

3.E.2. Multiple Sawtooth Barriers

Recalling that resonances below the barrier height and equal to one were possible in superlattices of step barriers, one expects to observe a similar phenomenon in sawtooth superlattices. The resonance peaks, however, are anticipated to be broader than those in MSB's, because instead of square wells there are now triangular ones. Triangular barrier shapes result in suppressed and broadened transmission resonances as was observed in single sawtooth barriers and step barriers under external fields. Thus any resonance peaks found in sawtooth superlattices are expected to be broader than those in similar MSB's of the same composition.

In Figure 55, the transmission coefficient as a function of energy is plotted for a two-barrier sawtooth superlattice, with bases equal to 4.5 nm, peak heights of 0.5 eV, and m_{eff} taken as constant and equal to m_0. Compare this with the same data for a two-barrier MSB, with 2nm wide bases, 5nm apart, barrier heights of 0.5 eV, and m_{eff} equal to m_0, found in Figure 48. There are indeed resonances in the transmission coefficient of the sawtooth superlattice, but they are fewer in number than those of the MSB. Instead of five, there are only two occurring below the barrier height of 0.5 eV. The upper resonances are considerably broader than those of the MSB. Finally, the value of the transmission coefficient is higher, away from the resonances, than in the MSB, except at the lowest energies, where the thickness of the sawtooth and the step barriers is the same. These discrepancies between the two curves in Figure 55 are explained by the difference in shape of the sawtooth and step barriers.

In Figure 56, the T-E data for two-barrier sawtooth superlattices with differing effective masses are plotted. The data shown are for the same geometry as above, with Figure 56a showing the transmission coefficient for $m_{eff} = m_0$, and Figure 56b showing that of a superlattice with the composition in each barrier graded from pure GaAs to Al(0.5)Ga(0.5)As. The effective mass is thus graded from 0.0636 to 0.0935 in each sawtooth. Comparing Figures 56a and b shows that the effective mass variation eliminates two of the resonances occurring below the barrier height. This is most likely a result of simultaneous shifting and broadening of the resonances. A single, very broad resonance at approximately 0.31 eV persists, however.

It appears that in Al(x)Ga(1-x)As sawtooth superlattices, the effective mass variations have a rather more pronounced effect on tunneling than in single sawtooth barriers. As Figure 53 illustrated, the T-E curves obtained for single sawteeth were quite insensitive to the values used for the mass. This is evidently not the case for tunneling through multiple sawtooth barriers.

3.E.2.a. GaAs-Al(0.5)Ga(0.5)As Sawtooth Superlattices: Comparison with Similar MSB's (Esaki-Tsu)

Comparison is made in this section between GaAs-Al(0.5)Ga(0.5)As step and sawtooth superlattices. Since the tunneling properties of such MSB's are well understood, and calculations

have been done for them here and elsewhere, they provide a convenient basis for comparison with sawtooth superlattices.

The transmission coefficient is calculated for two- and five-barrier sawtooth superlattices, with bases of 4.5 nm, heights of 0.5 eV, and with composition graded from GaAs to Al(0.5)Ga(0.5)As. These dimensions result in the same number of periods and overall length for sawtooth superlattices, as for MSB's with 2nm wide barriers 5nm apart. The transmission resonances and consequent tunneling current-voltage characteristics should thus be somewhat similar.

The T-E curves for the two-barrier step and sawtooth superlattices are shown in Figure 57. Instead of the two resonances supported by the MSB, the sawtooth superlattice has only a single very broad one around 0.31 eV. The effective mass gradient, as well as the barrier gradient, likely contribute to the breadth of this resonance.

The T-E curves for the five-barrier GaAs-Al(0.5)Ga(0.5)As sawtooth superlattice and MSB are found in Figure 58. The MSB supports two sets of resonances below the barrier height, each resonance split by coupling into four peaks. These are centered around 0.12 and 0.43 eV. The sawtooth superlattice, however, has only a single set of resonances. These are likewise four in number and are centered around the two-barrier resonance at 0.31 eV. These four resonances are much broader than those of the MSB. The transmission coefficient is higher for the sawtooth barrier down to an energy of approximately 0.22 ev, below which energy the sawteeth are thicker than the step barriers.

The J-V curves for the two-barrier structures are found in Figure 59. These curves are both calculated assuming an electric field localized to the superlattice. Note that there is a qualitative similarity between the two curves: a low-voltage current peak, followed by an area of negative differential resistance (NDR), then another broader peak at higher voltage, also followed by a regime of NDR. The current peaks of the sawtooth J-V curve are naturally broader than those of the MSB, since the resonances are very broad. The appearance of regions of NDR in sawtooth superlattices means that they may find novel applications in electronics, just as MSB's have (6).

It was shown earlier that the features of the J-V characteristic of this MSB were explained by resonant tunneling between the incident energy level (0.005 eV), and the resonances shifted downward by the applied field. The fact that the voltage peaks occur at twice the resonance energy levels, implied a linear shift of the resonances under the field.

Comparison of the J-V characteristic of the sawtooth superlattice with its T-E curve, however, indicates a different behavior under the field. There is a current peak at about 0.47 volts, and another at roughly 1.3 volts. Neither of these would result from a resonance at 0.35 eV shifted linearly downward with the applied field. It appears that for sawtooth superlattices, as the applied field strength is raised, new resonances form in the triangular wells, which may, at certain

values of the field, coincide with the incident energy of 0.005. In other words, the Stark effect in sawtooth superlattices is more complicated than in MSB's. This is a consequence of the way the sawtooth deforms under external fields. As the field strength is raised, the shape of the well between the barriers changes; in particular, the slope of the leftmost edges decreases. This is unlike the behavior of MSB's under uniform fields, as Figure 3 shows.

Figure 60 shows the shape of this sawtooth superlattice under applied voltages of zero, 0.47, and 1.3 V. At 0.47 V, there is still a small barrier to tunneling, but at 1.3 V the structure is a staircase and no tunneling is occurring. At 0.47 V, a shallow state is still probably trapped between the barriers, from which resonant tunneling can take place.

Figure 61 shows the T-E curve for this sawtooth superlattice under an an applied field strength of 0.052 eV: this corresponds to an applied voltage of 0.47 V. A slope change is evident at approximately 0.03 eV; another at around 0.35 eV. A shallow bound state may be hinted at by the knee in the curve at 0.03 eV. If such a state does exist, however, it must necessarily be difficult to resolve in the T-E data, since its energy level must be close to zero (i.e.to the incident energy level of 0.005 eV).

The peak at 1.3 V is a bit more puzzling, since no trapped states exist at such a high field. As earlier observed in single step barriers, however, there can still be pronounced resonances at energies well above the barrier height. This may explain the broad peak and region of NDR at around 1.3 V.

3.E.2.b. GaAs-Al(0.4)Ga(0.6)As Sawtooth Superlattices

The preceding section explored the similarities between sawtooth superlattices and multiple step barriers. It focused on GaAs-Al(0.5)Ga(0.5)As superlattices mainly because of the abundance of existing data on MSB's of that composition with which comparisons could be made. Al(x)Ga(1-x)As is an indirect gap material for aluminum concentrations greater than approximately 0.4 mole fraction,however,and only tunneling between direct conduction bands is considered in this work. Hence this final section will focus on GaAs-Al(0.4)Ga(0.6)As sawtooth superlattices, as this is the composition giving the greatest direct conduction band discontinuity of about 0.33 eV.

The transmission coefficient of a two-barrier sawtooth superlattice, with 4.5 nm bases and peak heights of 0.33 eV, is shown as a function of energy in Figure 62. Superposed is the T-E curve of a similar GaAs-Al(0.5)Ga(0.5)As MSB. As might be expected, the curves are qualitatively very similar. The resonance in the Al(0.4)Ga(0.6)As data is shifted to approximately 0.23 eV, however, compared to 0.31 eV for the GaAs-Al(0.5)Ga(0.5)As MSB. Off resonance, the transmission coefficient is also higher throughout the range. These changes are consequences

of the lower average effective mass throughout each barrier, as well as of the lower barrier height, in GaAs-Al(0.4)Ga(0.6)As.

The tunneling current as a function of the applied voltage in the two- barrier superlattices is shown in Figure 64. Again, a strong qualitative resemblance between the two curves is observed. The tunneling current is greater in the Al(0.4)Ga(0.6)As superlattice by about two orders of magnitude, and this naturally follows from the higher transmission coefficient observed in Figure 62. A low-voltage current peak at roughly 0.35 V, followed by a region of negative differential resistance is evident in the Al(0.4)Ga(0.6)As curve. As was the case for the Al(0.5)Ga(0.5)As sawtooth superlattice, the location of this peak implies a more complicated change in the resonances under applied fields than in MSB's. Certainly the shift is not a simple linear function of the field strength.

4. CONCLUSION

A transfer matrix method has been applied to quantum mechanical tunneling calculations in GaAs-Al(x)Ga(1-x)As semiconductor heterostructures. The focus of this work was a novel type of heterostructure in which the band gap is graded linearly, giving rise to a sawtooth superlattice. Tunneling calculations for such a structure are presented here for the first time. In addition, tunneling calculations were performed for conventional step barrier heterostructures. The Stark shift of the bound and quasi-bound states of single finite quantum wells was calculated as well. Some conclusions are:

1. The Stark shift of bound states in single quantum wells can be obtained by the transfer matrix method used here. The extent of the applied field, however, determines the functional dependence of the Stark shift. If the field is restricted to an area near the well, the Stark shift is linear in the field. If the field is infinite in extent, the shift is quadratic. The extent of the field must be considered in tunneling calculations for sawtooth and step barrier superlattices as well.

2. The tunneling properties of step and sawtooth superlattices show some strong qualitative similarities. Both structures can exhibit resonant tunneling, as evidenced by correlation of transmission resonances with peaks in the current-voltage curves. However, the shift of the resonances is linear in the field in step barrier superlattices, while in sawtooth superlattices the shift is not a simple function of the field. This is because the two kinds of structure deform differently under uniform fields. The sawtooth deforms into a staircase under a high enough field strength, and tunneling no longer occurs since the barriers are eradicated. Step barriers always present some barrier to tunneling no matter how strong the field.

3. The effective mass variations encountered in semiconductor heterostructures should not be neglected. The conventional wave function boundary conditions at interfaces must be modified to conserve probability current density when the mass is discontinuous. The range of effective mass in the GaAs-Al(x)Ga(1-x)As heterostructures studied here was found to have a significant effect on the outcome of calculations.

a. The number and level of the bound states in single quantum wells is strongly affected by average effective mass, and by the discontinuity at well edges. Neglecting the average effective mass results in a gross error in the number of levels, while ignoring discontinuities at the well edges results in a significant change in their energy.

b. The use of the correct effective masses in single and multiple step and sawtooth barriers is also important ,as the number and energy of transmission resonances is a function of the average effective mass and the discontinuities at interfaces .In sawtooth superlattices the parabolic effective mass gradient within each layer should be taken account of.

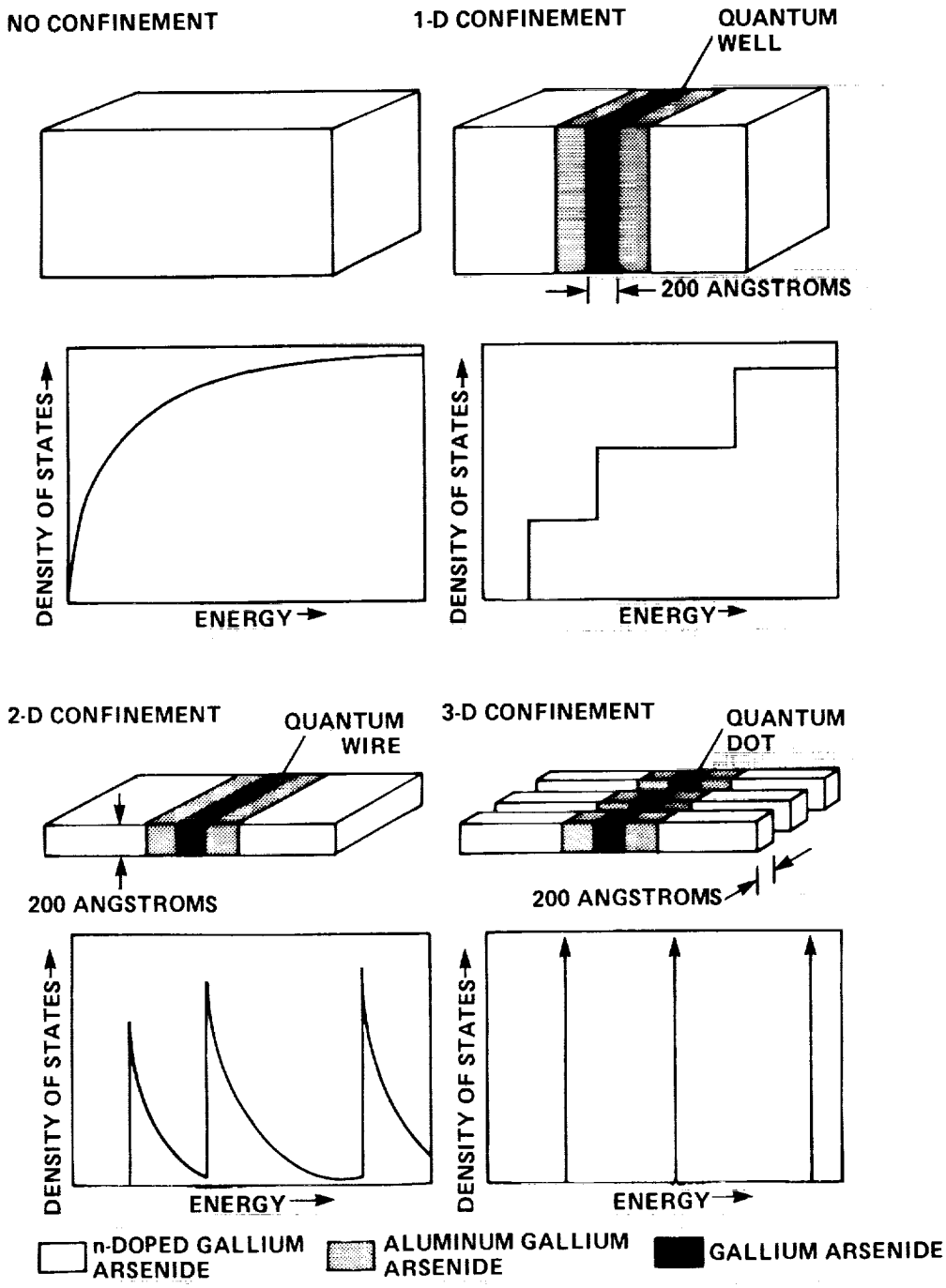

1. Quantum Confinement and Resultant Quantization of Energy Eigenvalues (1)

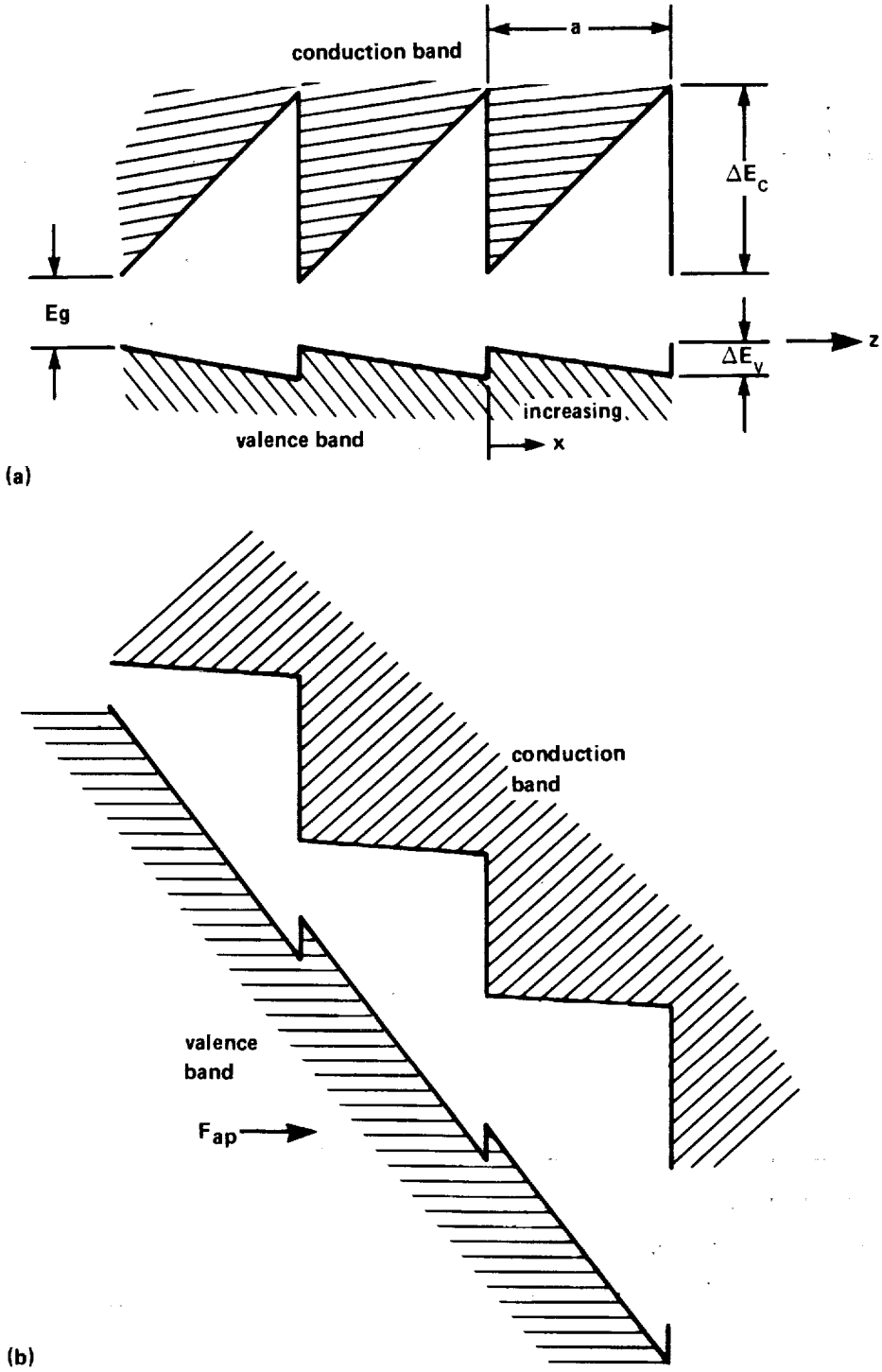

2. Sawtooth Superlattice with and without Strong External Reverse Bias

a. Zero-field sawtooth superlattice

b. Strong external reverse bias F_{ap}, resulting in staircase superlattice.

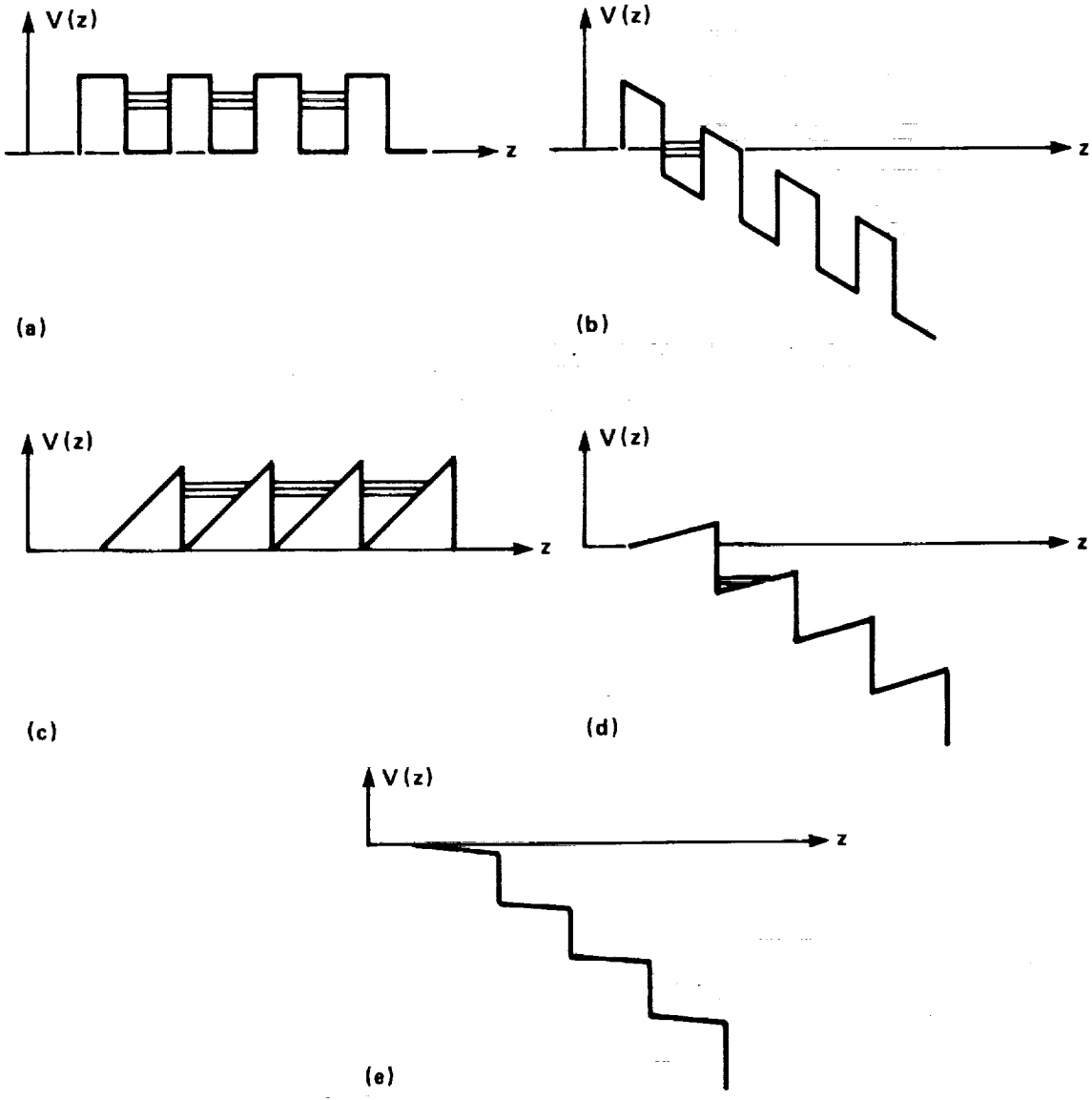

3. Step- and Sawtooth-Barrier Superlattices under Reverse Bias

a. Step-barrier superlattice under zero external field. Virtual states are shown;

b. Step-barriers under strong reverse bias. Virtual states can still exist;

c. Sawtooth-barrier superlattice under zero field. Virtual states are formed as in the case of step-barrier superlattices;

d. Sawtooth-barrier superlattice under moderate reverse bias. The applied voltage is less than the sum of the barrier heights, and virtual, or quasi- bound, states can still be formed,

e.Sawtooth-barrier superlattice under strong reverse bias. Structure is actually a staircase and quasi-bound states no longer are possible, although resonances still occur.

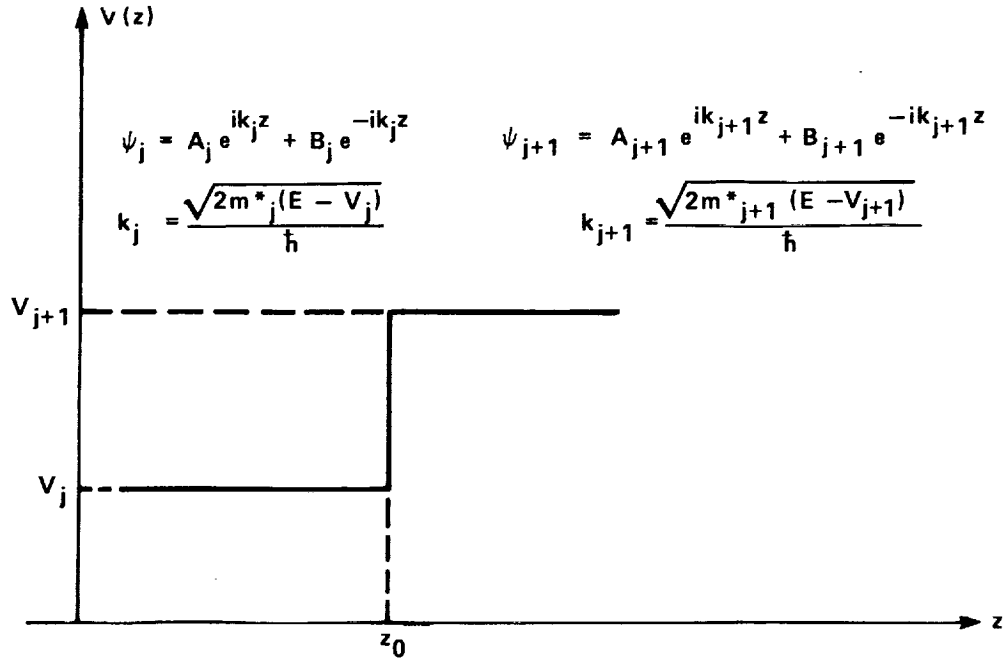

$$\begin{pmatrix} A_j \\ B_j \end{pmatrix} = \begin{pmatrix} M_{11} & M_{12} \\ M_{21} & M_{22} \end{pmatrix} \begin{pmatrix} A_{j+1} \\ B_{j+1} \end{pmatrix}$$

4. Transfer Matrix at a Potential Step

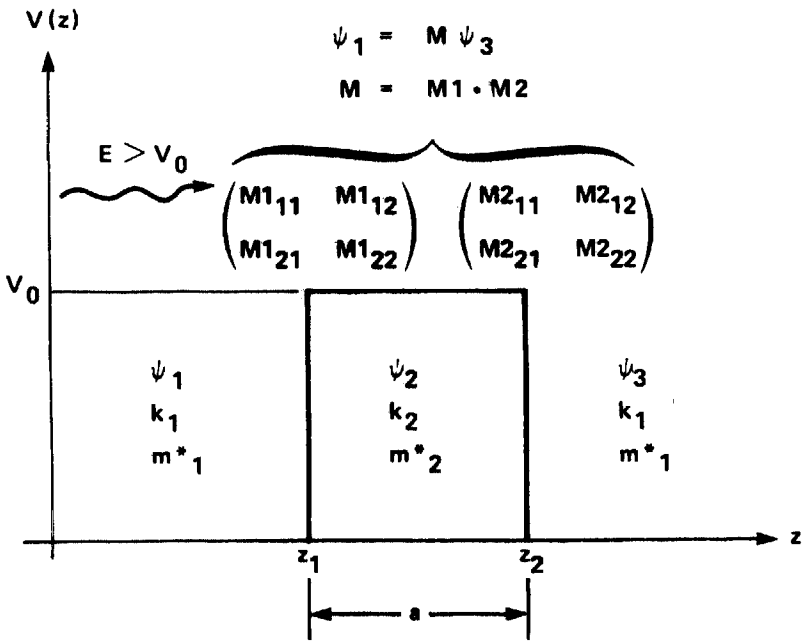

a) $m^*_1 = m^*_2 = m^*$:

$$T = \left(1 + \frac{V_0^2 \sin^2\left(a/\hbar\sqrt{2m^*(E - V_0)}\right)}{4E(E - V_0)}\right)^{-1}$$

b) $m^*_1 \neq m^*_2$:

$$T = \left(1 + \frac{\left(E(m^*_1 - m^*_2) + m^*_2 V_0\right)^2 \sin^2\left(a/\hbar\sqrt{2m^*_2(E - V_0)}\right)}{4m^*_1 m^*_2 E(E - V_0)}\right)^{-1}$$

5. Transfer Matrix for a Single Step Barrier: $E > V_0$

a. Transmission coefficient for uniform effective mass;

b. Transmission coefficient for different effective masses inside and outside the barrier.

a) $m^*_1 = m^*_2 = m^*$

$$T = \left(1 + \frac{V_0^2 \sinh^2\left(a/\hbar\sqrt{2m^*(V_0 - E)}\right)}{4E(V_0 - E)}\right)^{-1}$$

b) $m^*_1 \neq m^*_2$

$$T = \left(1 + \frac{\left(E(m^*_1 - m^*_2) + m^*_2 V_0\right)^2 \sinh^2\left(a/\hbar\sqrt{2m^*_2(V_0 - E)}\right)}{4m^*_1 m^*_2 E(V_0 - E)}\right)^{-1}$$

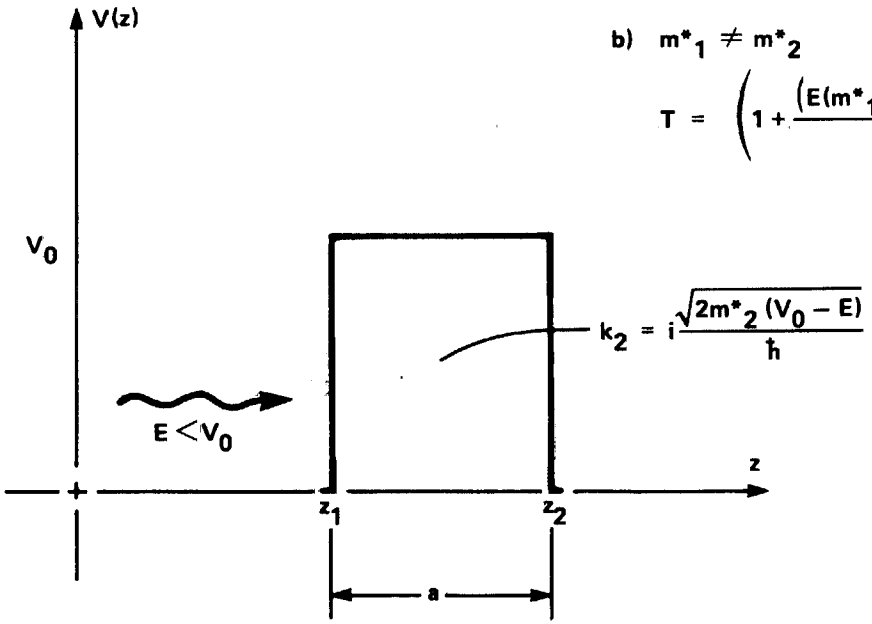

6. Tunneling In a Single Step Barrier: $E < V_0$

a. Transmission coefficient for uniform effective masses;

b. Transmission coefficient for different effective masses inside and outside the barrier.

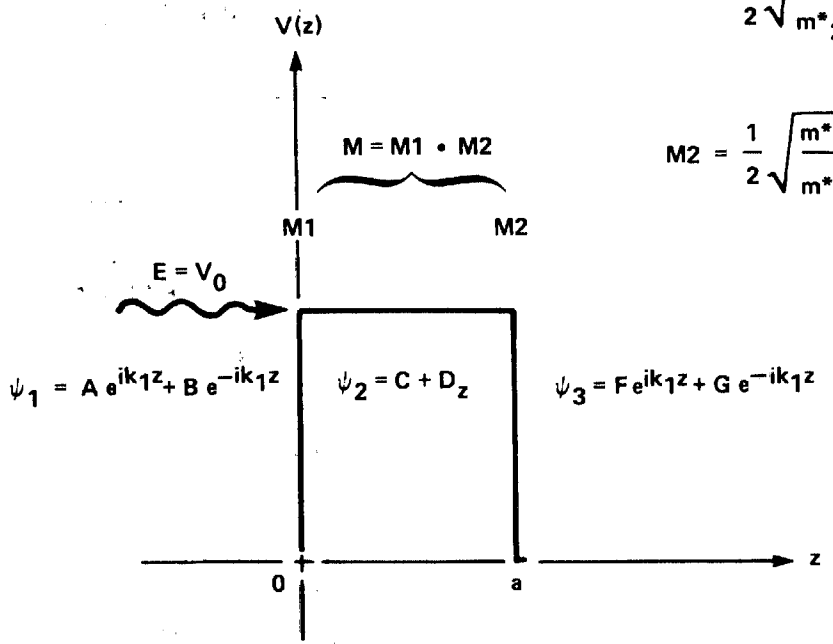

$$M1 = \frac{1}{2}\sqrt{\frac{m^*_1}{m^*_2}} \begin{pmatrix} 1 & (-i/k_1) \\ 1 & (i/k_1) \end{pmatrix}$$

$$M2 = \frac{1}{2}\sqrt{\frac{m^*_2}{m^*_1}} \begin{pmatrix} (1 - k_1 a)\, e^{ik_1 z} & (1 + ik_1 a)\, e^{-ik_1 a} \\ i k_1 e^{ik_1 a} & -i k_1 e^{-e\, k_1 a} \end{pmatrix}$$

$$T = \left(1 + \frac{m^*_1 V_0 a^2}{2\hbar^2}\right)^{-1}$$

7. Transfer Matrix for a Single Step Barrier: $E = V_0$.

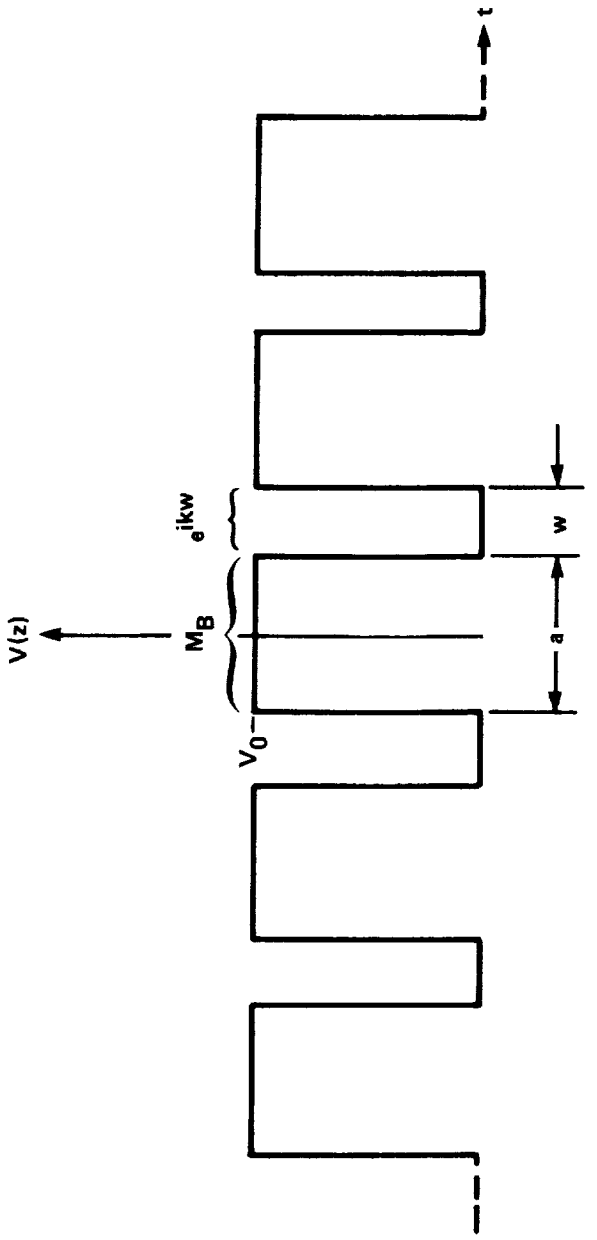

8. Multiple Step Barrier (MSB): N periods.

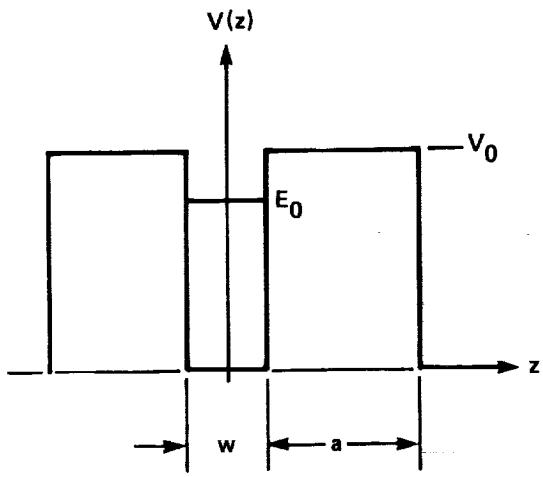

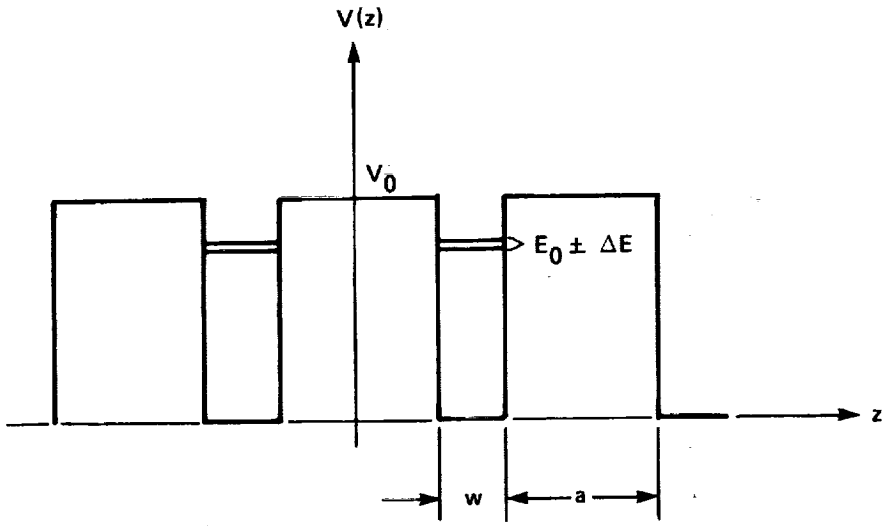

9. Multiple Step Barrier with Three Periods

The single resonance at E_0 is split into two levels at $E_0 \pm \Delta E$ by coupling between the two wells.

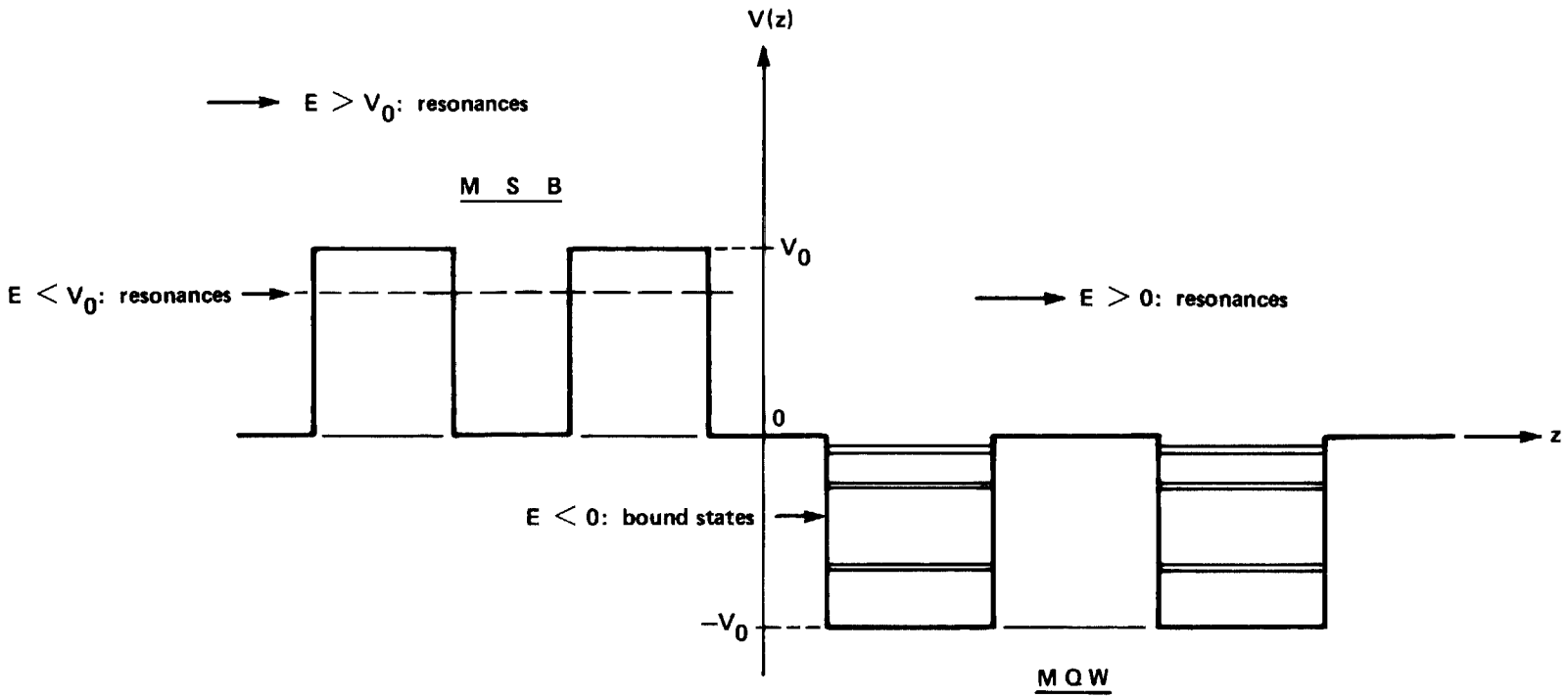

10. The Difference Between Multiple Step Barriers and Multiple Quantum Wells (MQW).

For energies E below the top of the barriers or well, respectively, MSB's can have only virtual, or quasi-bound, states, while MQW's can have true bound states. Both types of heterostructure can support resonances for E greater than the barrier or well height.

a) For $E > 0$:

$m^*_1 = m^*_2 = m^*$:

$$T = \left(1 + \frac{m^* V_0^2 \sin^2\left(a/\hbar\sqrt{2m^*(E+V_0)}\right)}{4E(E+V_0)}\right)^{-1}$$

$m_1^* \neq m_2^*$

$$T = \left(1 + \frac{\left(E(m_1^* - m_2^*) - m_2^* V_0\right)^2 \sin^2\left(a/\hbar\sqrt{2m_2^*(E+V_0)}\right)}{4m_1^* m_2^* E(E+V_0)}\right)^{-1}$$

b) For $E < 0$:

Criterion for bound states

$$e^{\kappa a}\left(\frac{(k_2^2 - K^2)}{k_2 K}\sin k_2 a + 2\cos k_2 a\right) = 0$$

$$k_2 = \frac{\sqrt{2m^*_2 |V_0 - E|}}{\hbar} \quad K = \frac{-\sqrt{2m_1^* E}}{\hbar}$$

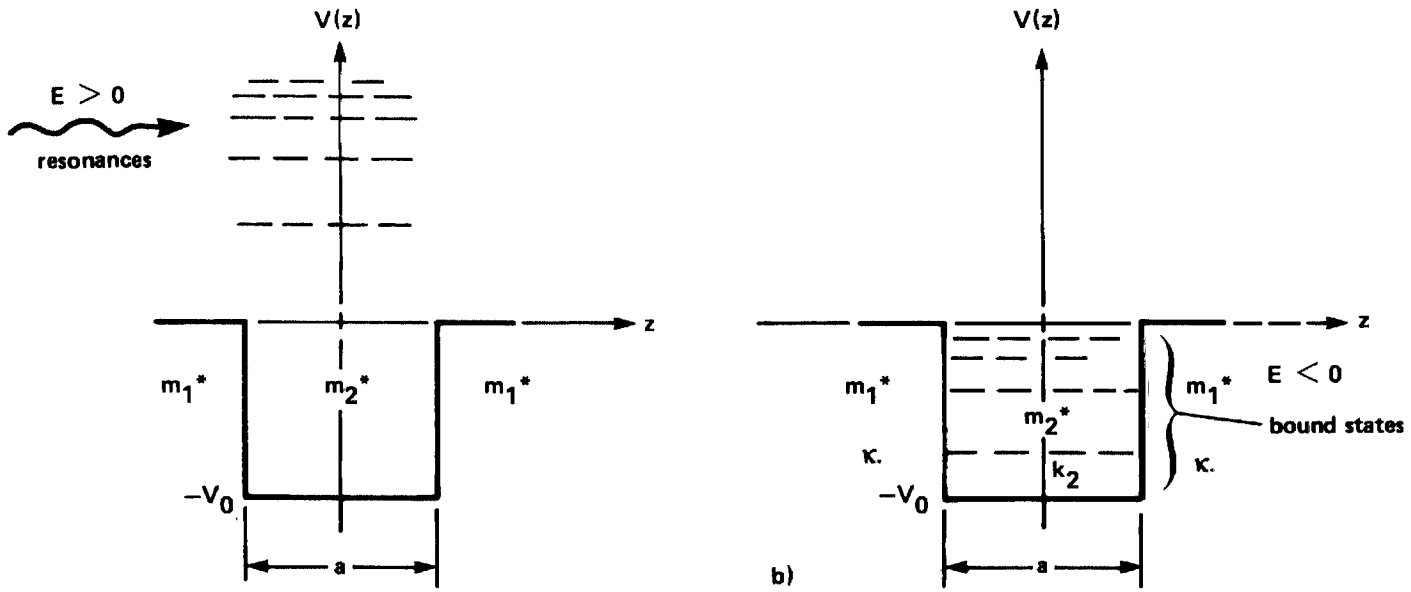

11. Bound States and Resonances of a Single Quantum Well.

a. $E > 0$: Transmission coefficients for uniform and varying effective masses. Resonances in T;

b. $E < 0$: Criterion for bound states. Eigenvalue condition on M_{11} gives bound states.

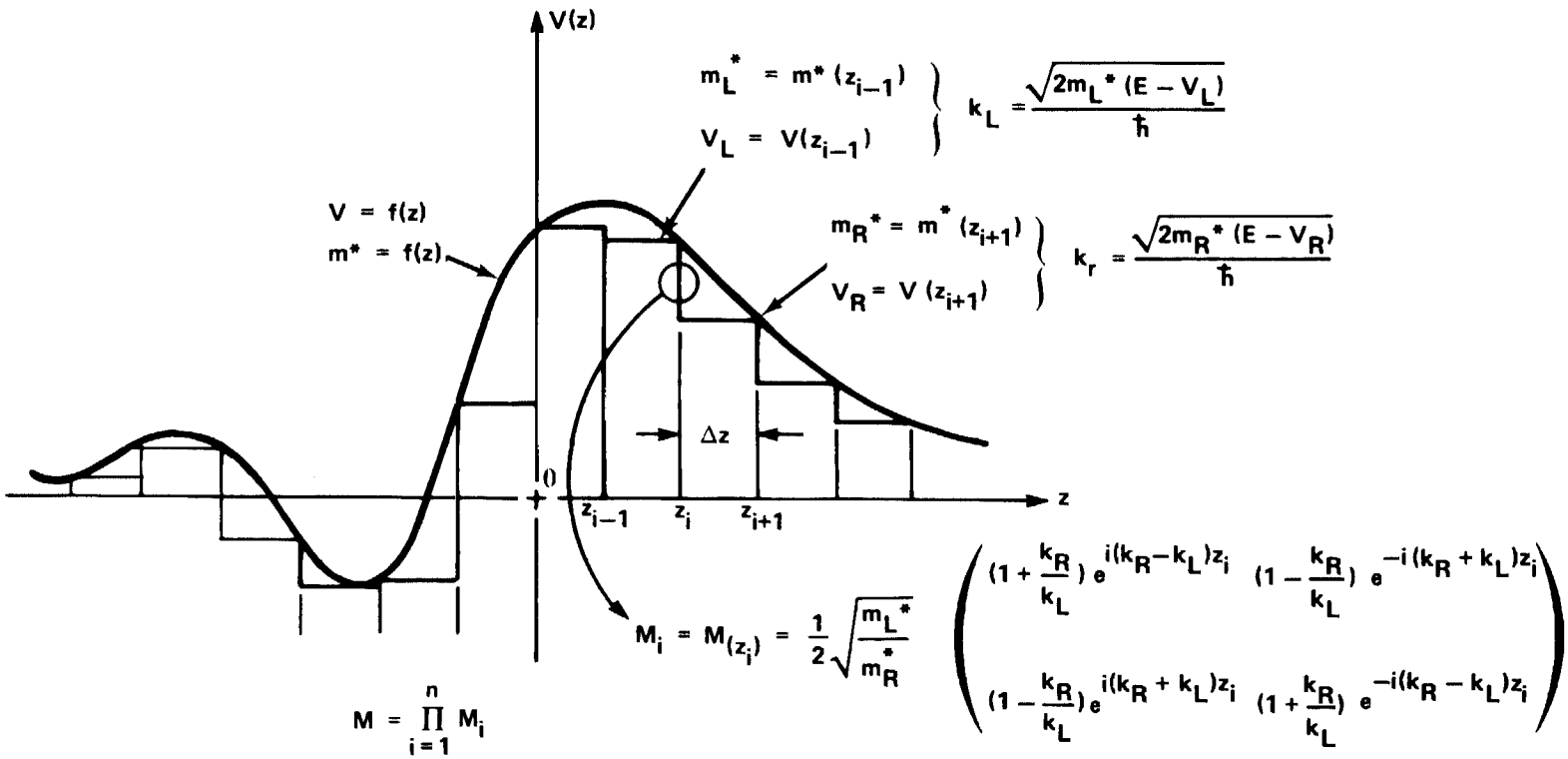

12. Transfer Matrix Method Applied to Arbitrary, Real Potential V(z).

The potential is broken into intervals Δz wide. Transfer matrices M_i at each step are multiplied to give overall transfer matrix M.

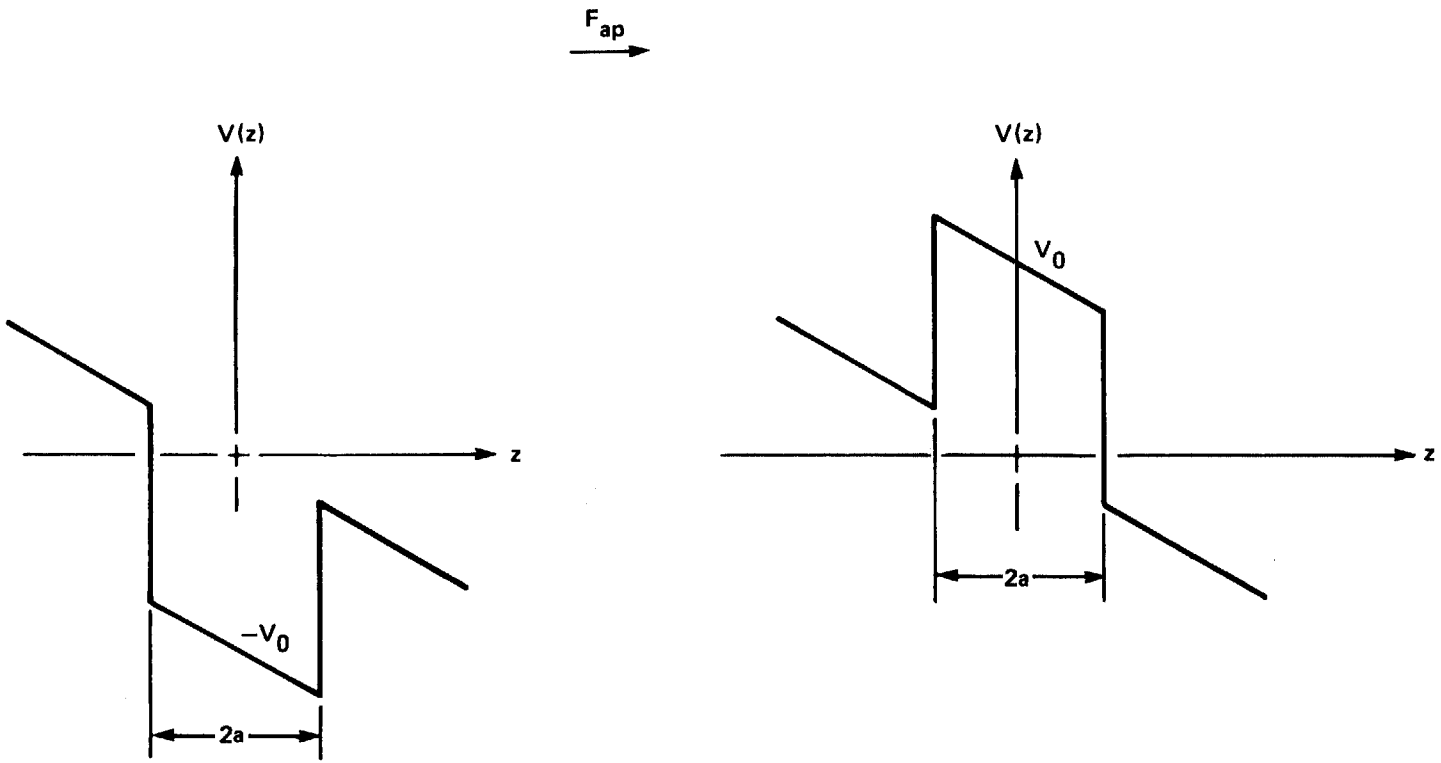

V(z): $-V_0 - F_{ap}\, e\, z$ $\quad |z| < 0$

V(z): $-F_{ap}\, e\, z$ $\quad |z| \geqslant a$

V(z): $V_0 - F_{ap}\, e\, z$ $\quad |z| < a$

V(z): $-F_{ap}\, e\, z$ $\quad |z| \geqslant a$

13. Single Quantum Well and Barrier In Uniform Electric Field F_{ap}

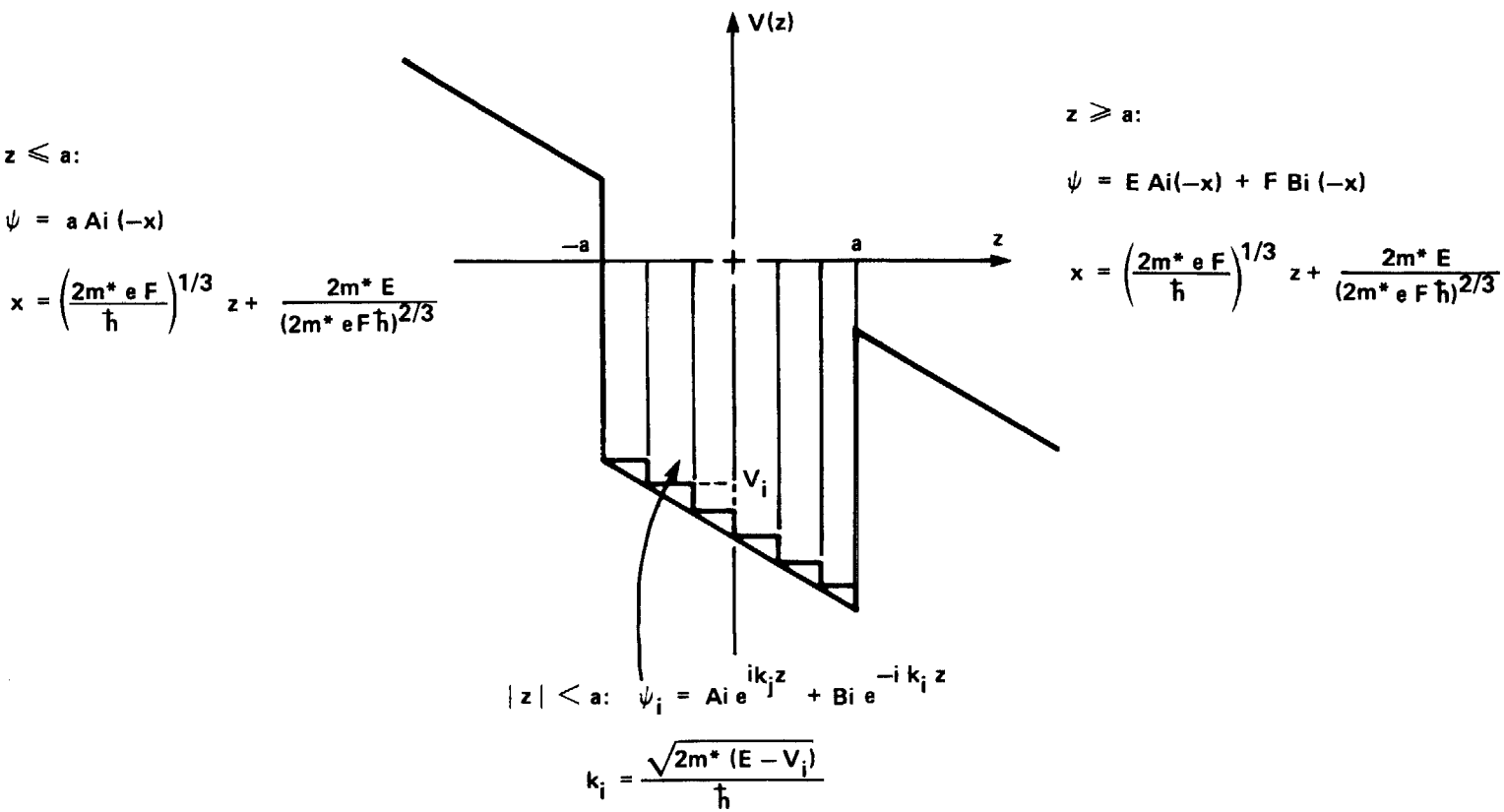

14. Transfer Matrix Method Applied to Finding Bound States of a Single Quantum Well in Uniform Electric Field F_{ap}.

The region inside the well is divided into intervals where plane-wave transfer matrices are calculated. In the regions outside the well, the solutions of the Schroedinger equation are the Airy functions.

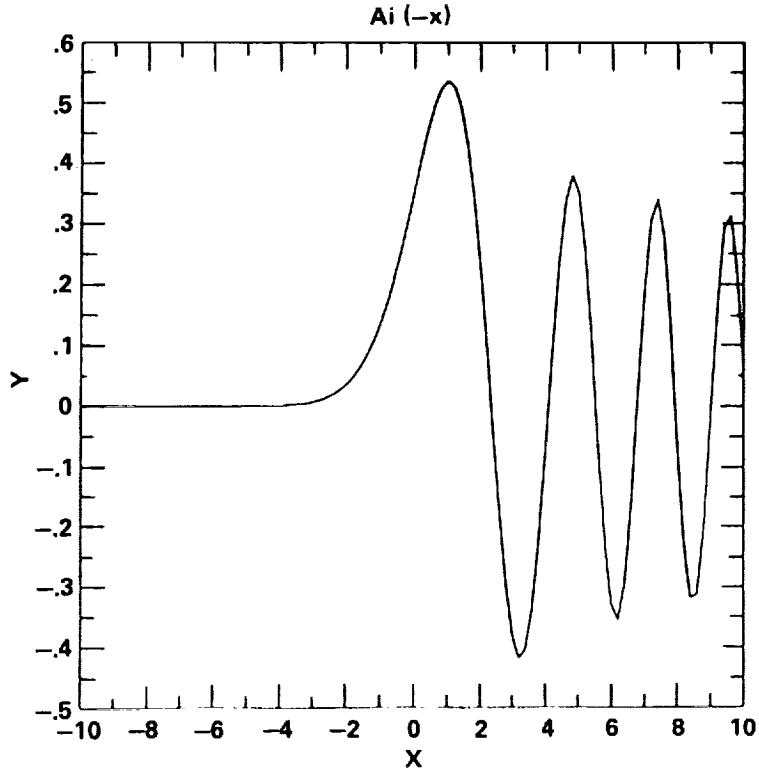

a)

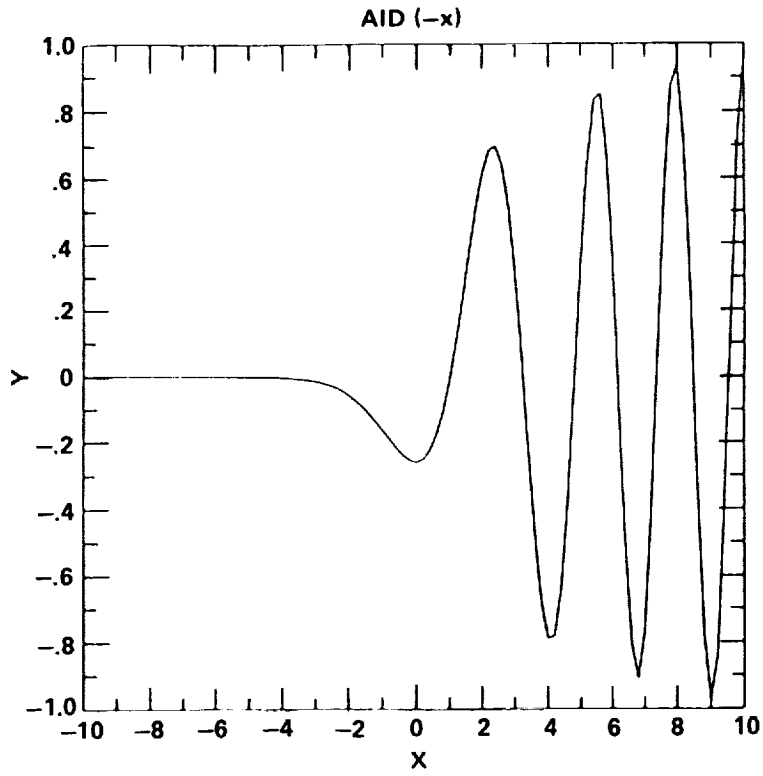

b)

15. The Airy Function and Derivative with Negative Argument.

a. Ai(-x)

b. Ai'(-x)

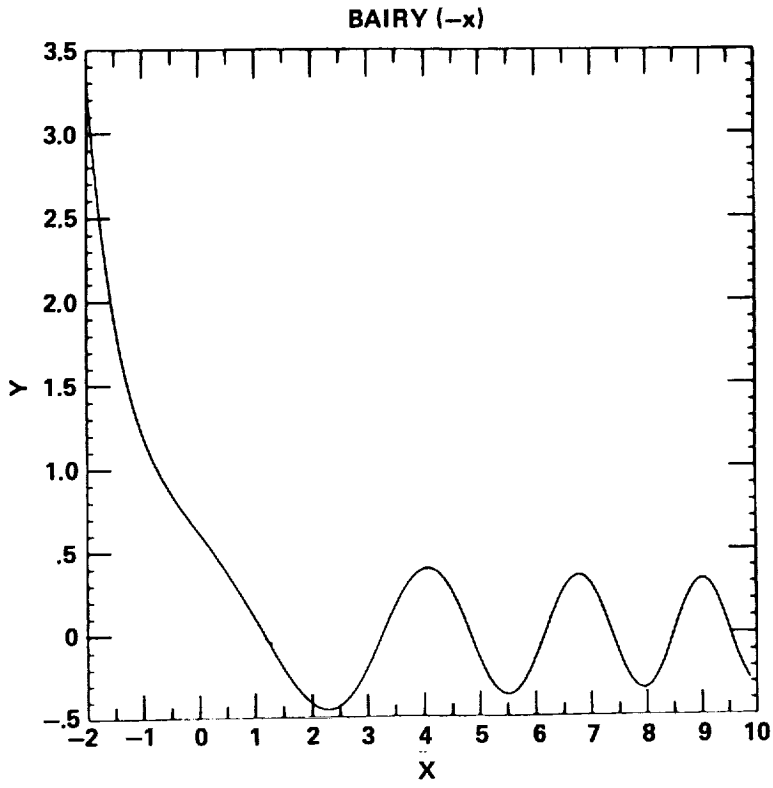

a)

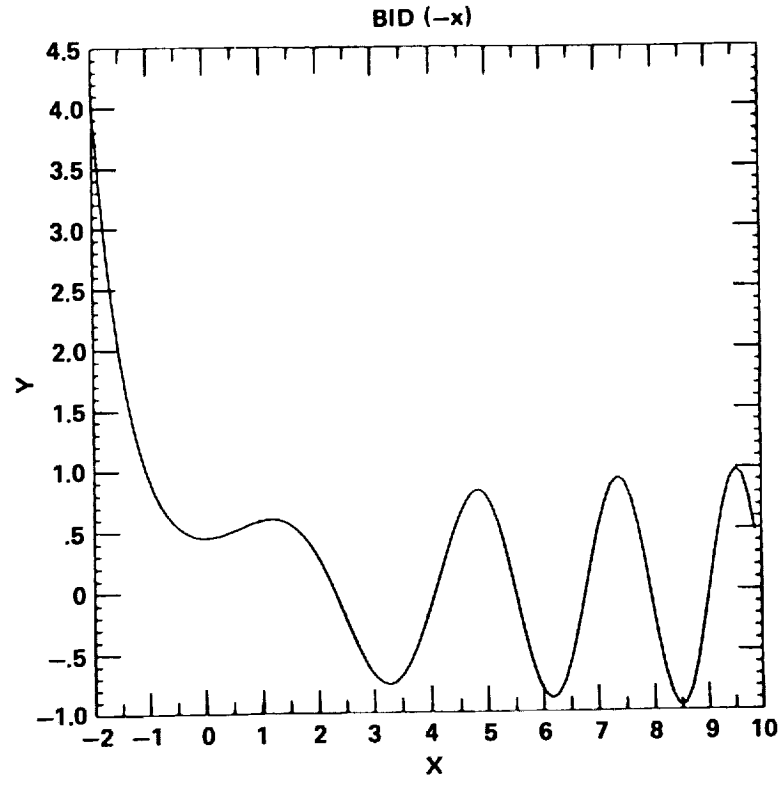

b)

16. The Bairy Function and Derivative with Negative Argument.

a. Bi(-x)

b. Bi'(-x)

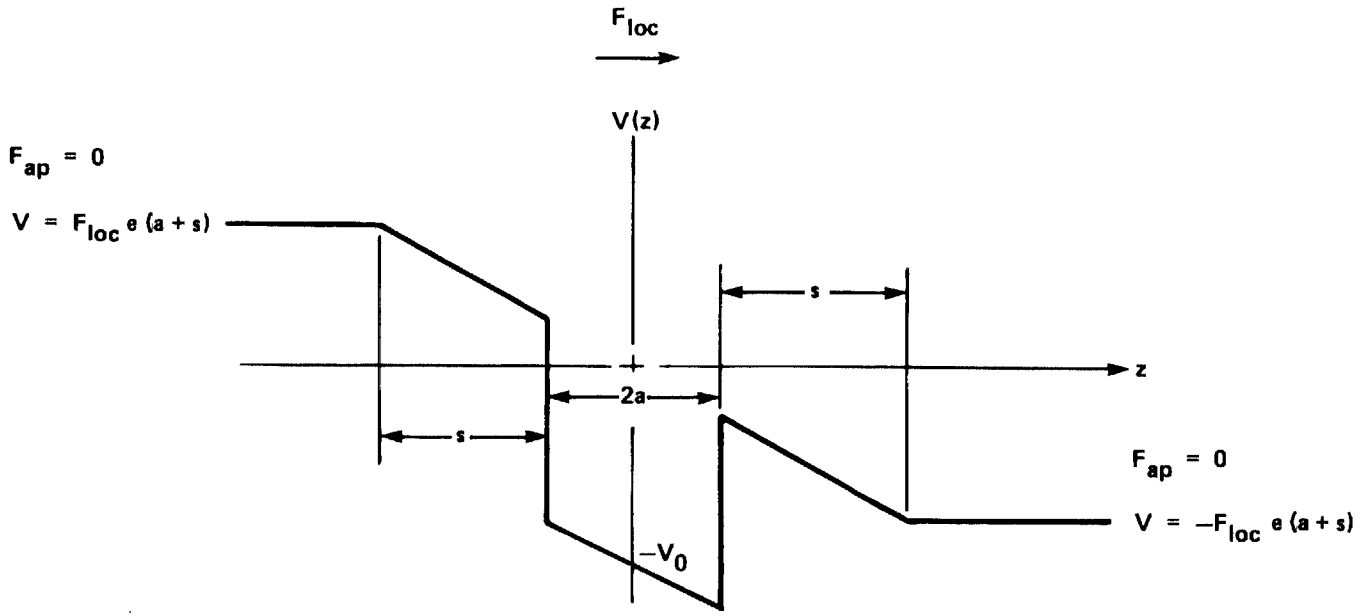

$$F_{ap} = F_{loc} \qquad |z| < 2(a + s)$$

$$F_{ap} = 0 \qquad |z| \geqslant 2(a + s)$$

17. Single Quantum Well in a Localized Electric Field.
The applied field is zero far from the well.

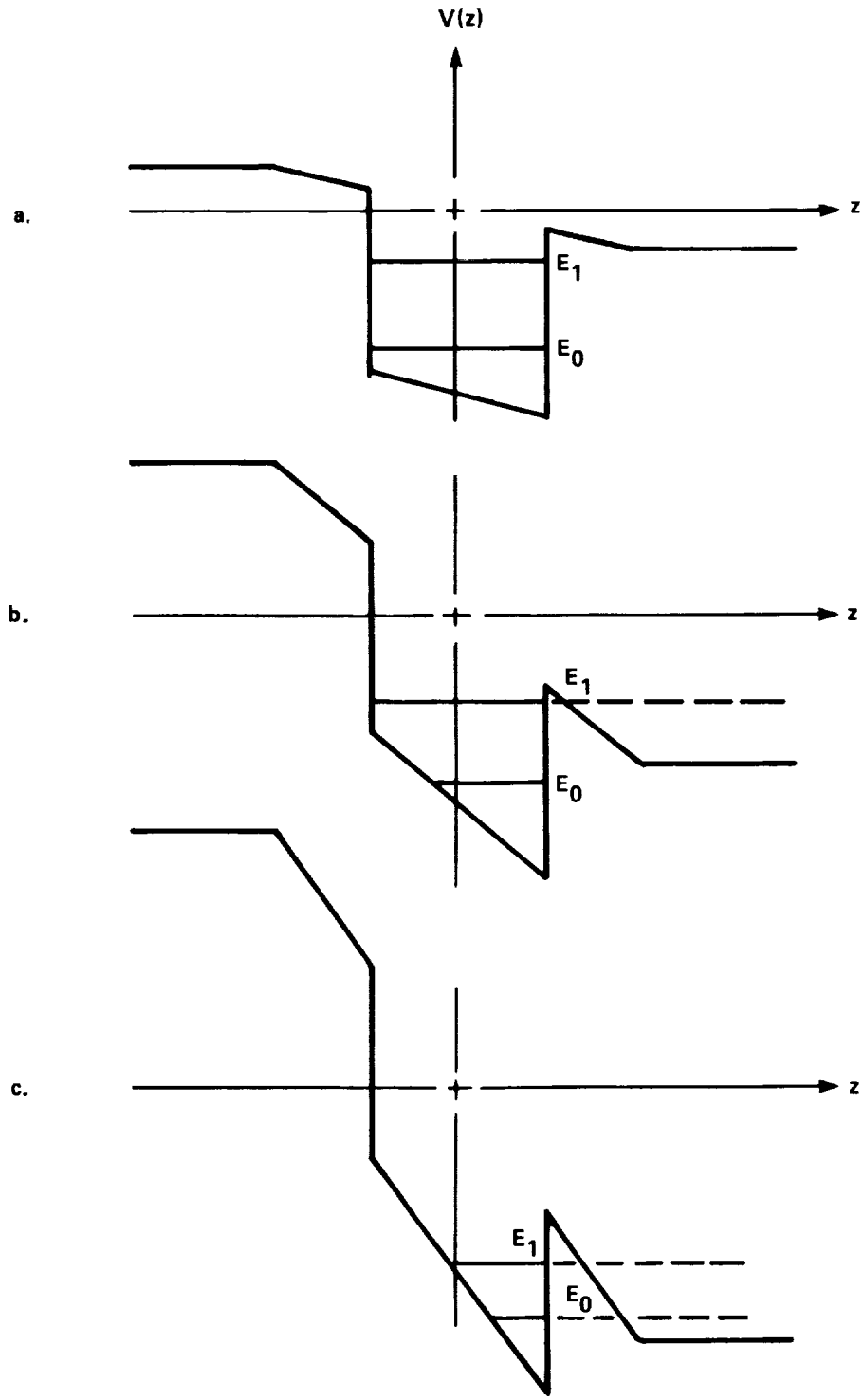

18. Deformation of a Single Quantum Well in a Localized Electric Field.
The applied field shifts the bound and quasi-bound levels to lower energy.
a. Low field strength, with true bound states at E_0 and E_1;
b. Moderate field strength, with one true bound state at $E_0 - \Delta$, and a quasi-bound state at $E_1 - \Delta$;
c. High field strength, only quasi-bound states remain.

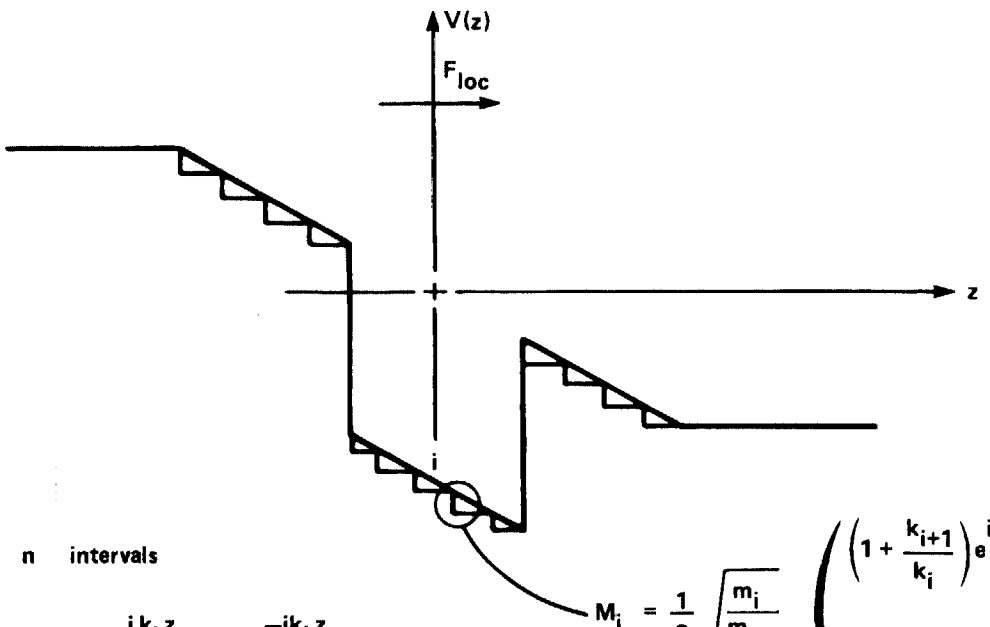

n intervals

$$\psi_i = A_i e^{i k_i z} + B_i e^{-i k_i z}$$

$$M_i = \frac{1}{2}\sqrt{\frac{m_i}{m_{i+1}}} \begin{pmatrix} \left(1 + \frac{k_{i+1}}{k_i}\right) e^{i(k_{i+1} - k_i)z_i} & \left(1 - \frac{k_{i+1}}{k_i}\right) e^{-i(k_{i+1} + k_i)z_i} \\ \left(1 - \frac{k_{i+1}}{k_i}\right) e^{i(k_{i+1} + k_i)z_i} & \left(1 + \frac{k_{i+1}}{k_i}\right) e^{-i(k_{i+1} - k_i)z_i} \end{pmatrix}$$

$$M = \prod_{i=1}^{n} M_i$$

19. Transfer Matrix Method Applied to Single Quantum Well in Localized Field. The well and a small surrounding area over which the field extends are broken into intervals. At each step a transfer matrix M_i is calculated; the overall transfer matrix M is the product of all the M_i.

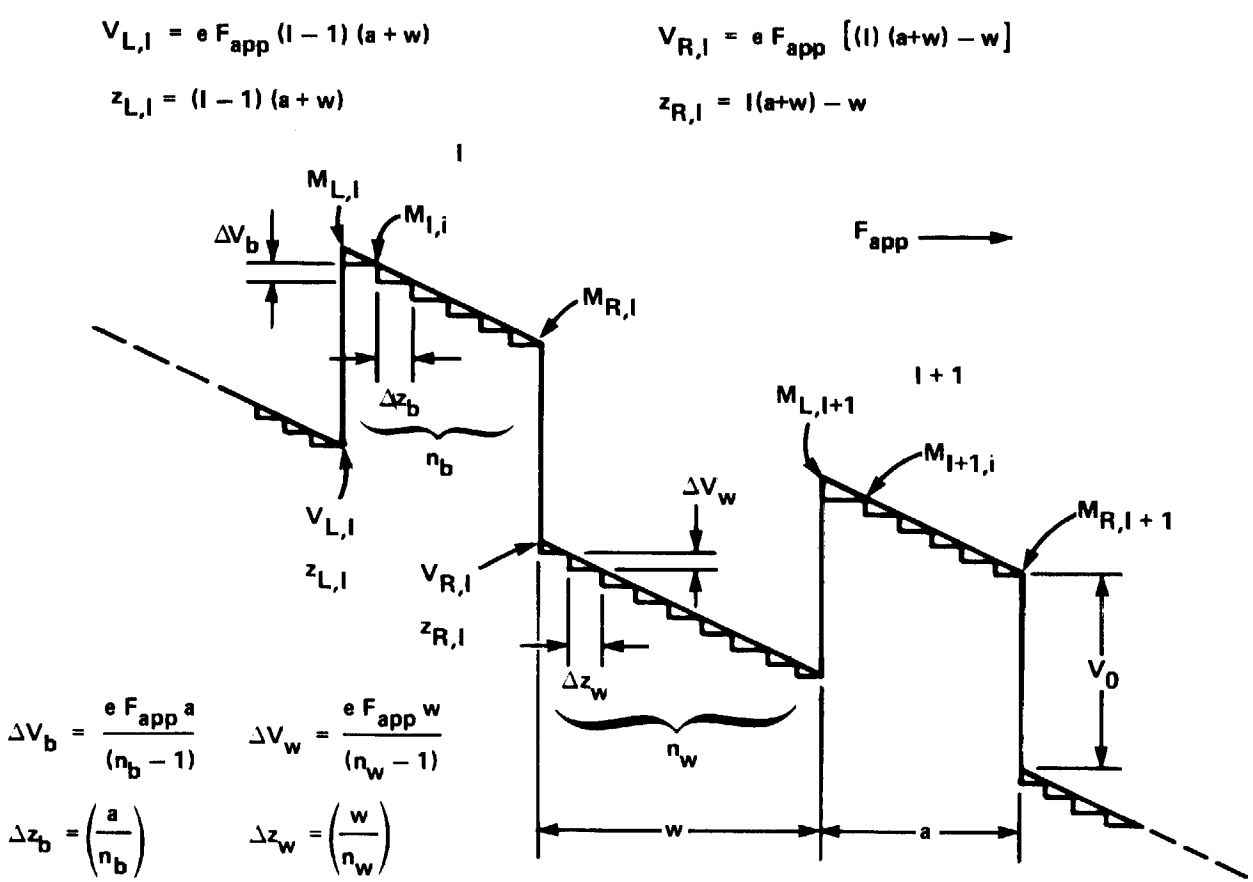

20. Transfer Matrix Method Applied to Multiple Step Barrier with N Periods in an External, Localized Electric Field F_{ap}.

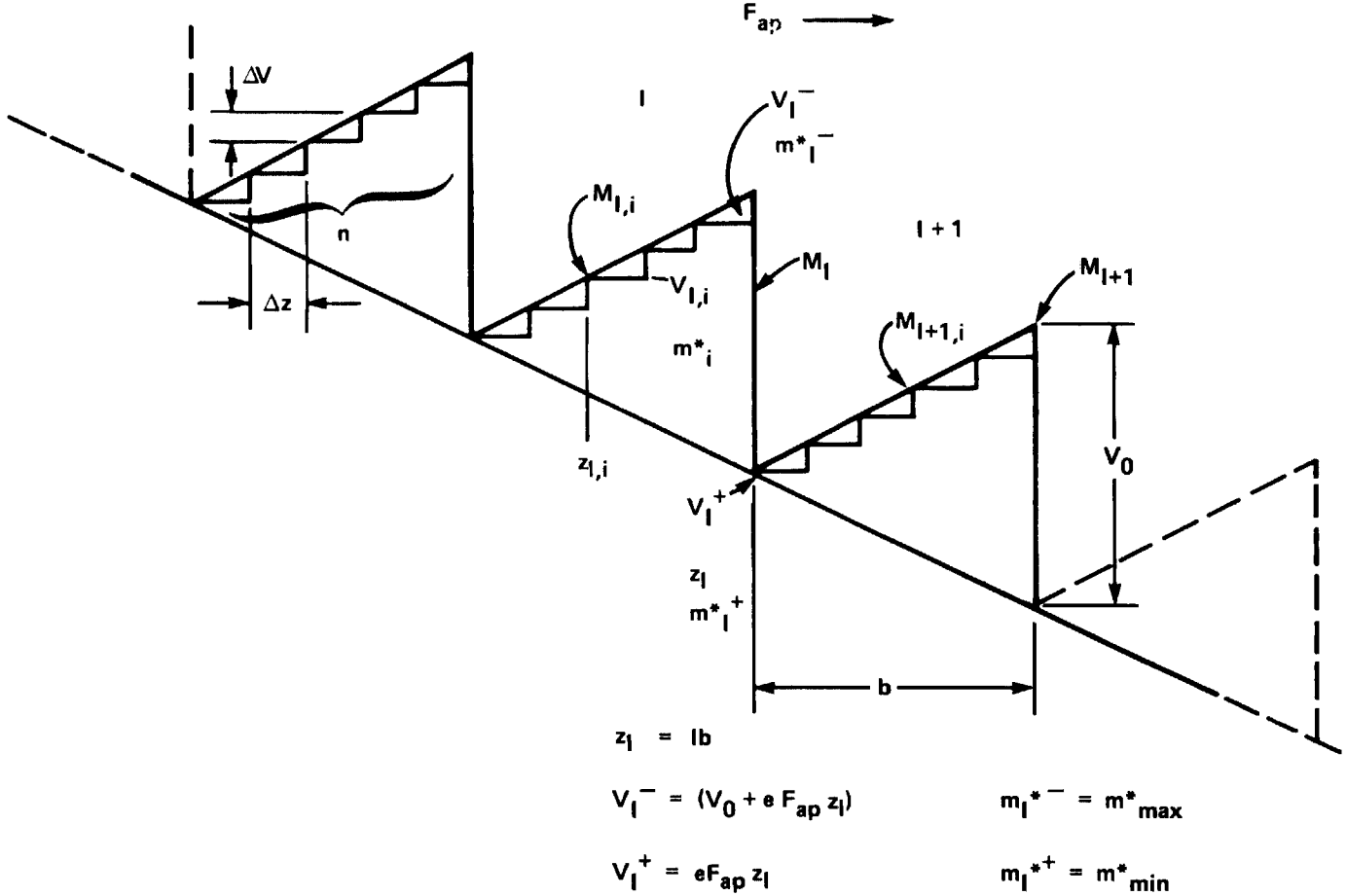

21. Transfer Matrix Method Applied to Sawtooth Superlattice with N Periods in an External, Localized Electric Field F_{ap}.

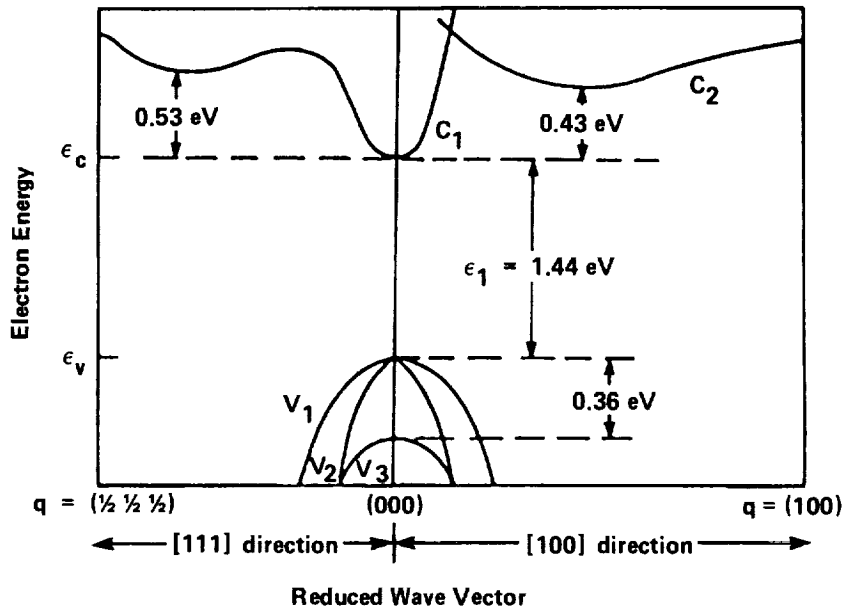

22. Energy Band Structure of Pure GaAs (<100> and <111> directions) (33).

i)

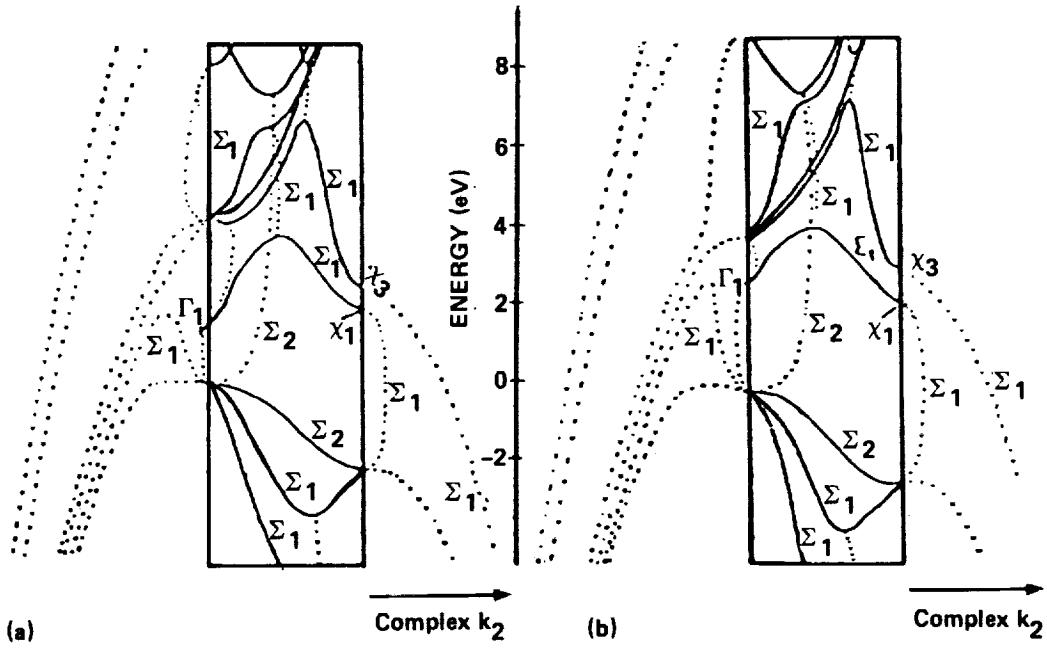

ii)

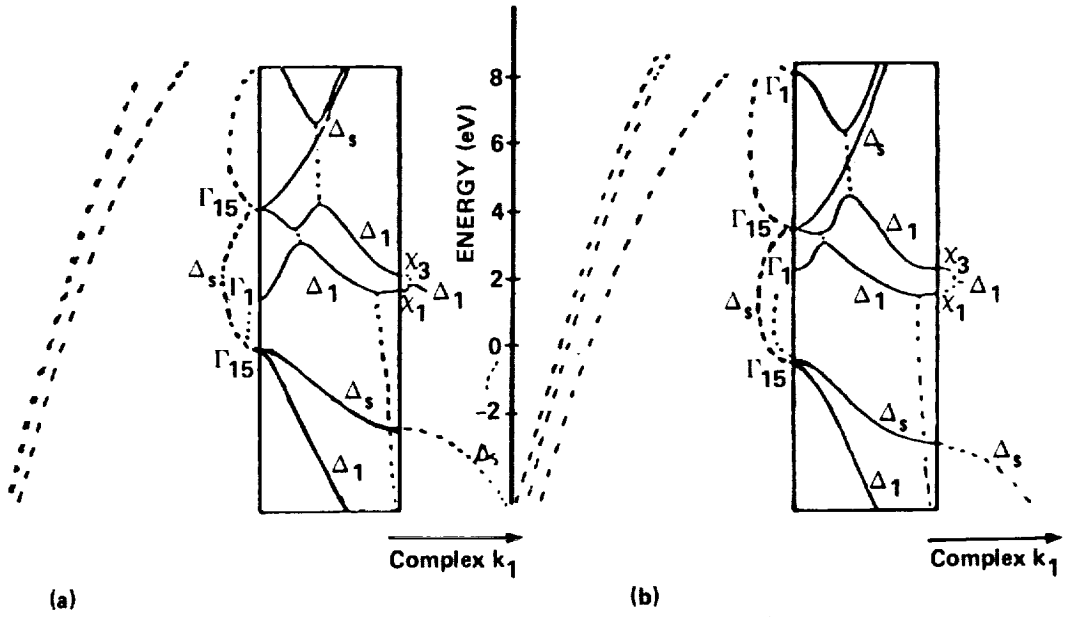

23. Complex Energy Band Structures of pure GaAs and AlAs (34)

i. (110) interface: a. GaAs b. AlAs;

ii. (100) interface: a. GaAs b. AlAs.

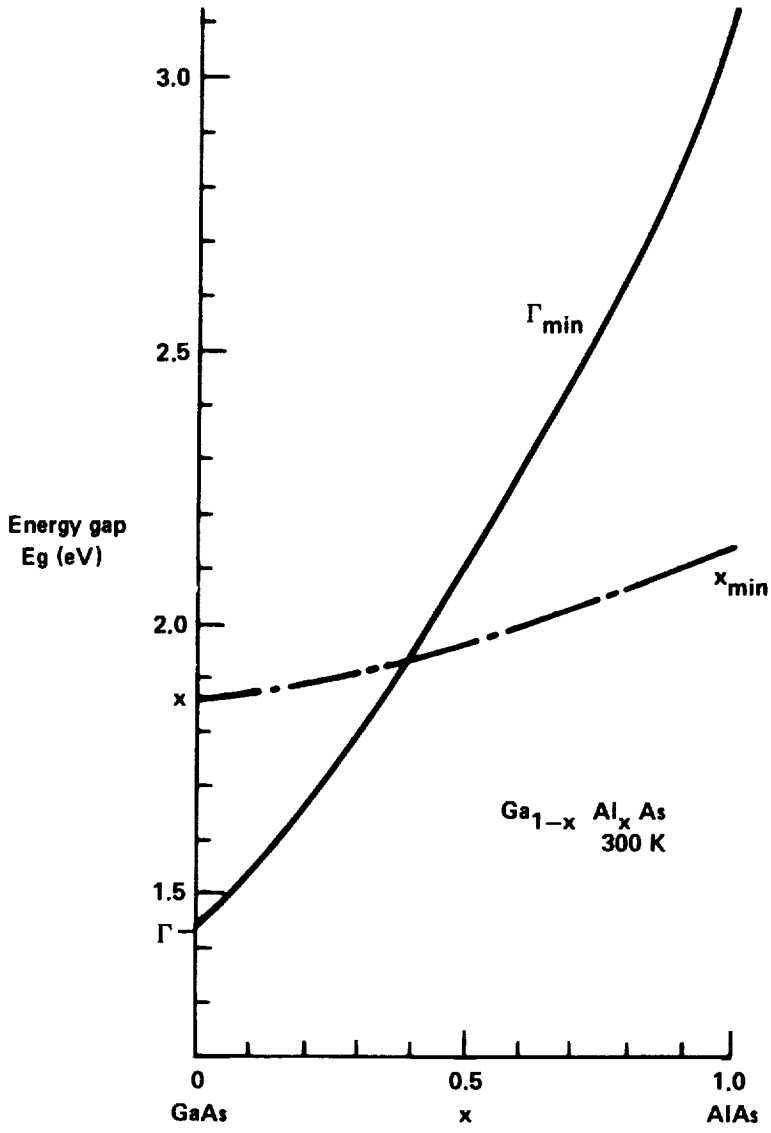

24. Energy Gap in Al(x)Ga(1-x)As as a Function of AlAs Mole Fraction x (19). The x-dependence of the direct conduction band Γ_{1c} is shown by the solid line; that of the indirect gap X_{1c} by the dashed line. The direct and indirect minima are equal at x = 0.37.

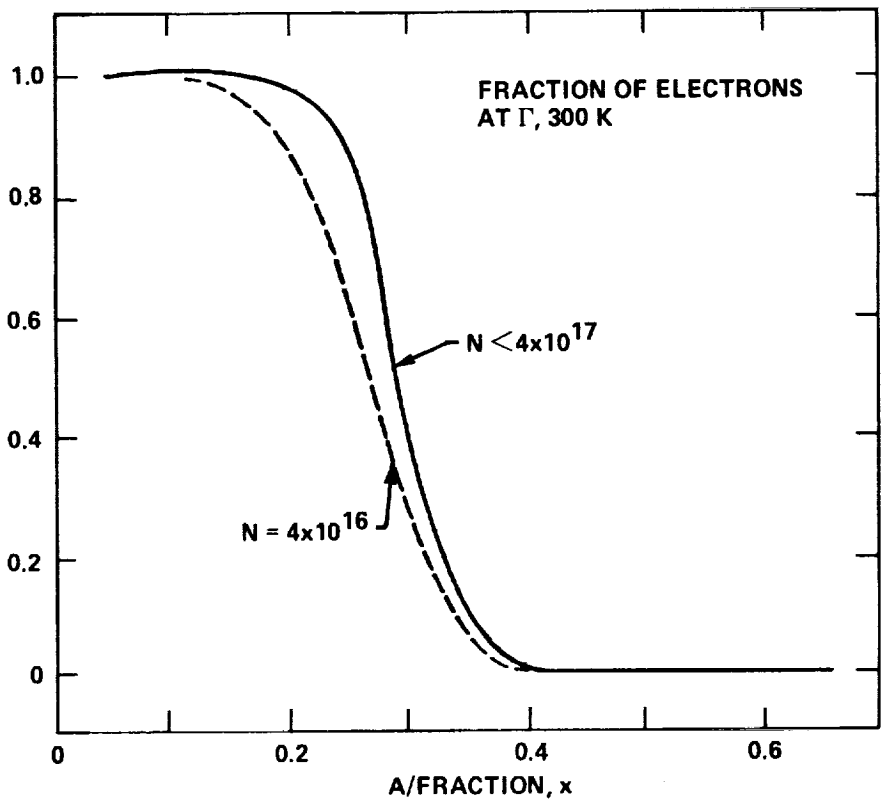

25. The Fraction of Conduction Electrons in Γ_{1c} of Al(x)Ga(1-x)As as a Function of AlAs Mole Fraction x.(18)

Data are taken at 300 K. Dotted line is for degenerate case with N = 4×10^{17} cm^{-3} ; solid line is for nondegenerate case with N = 4×10^{16} cm^{-3}.

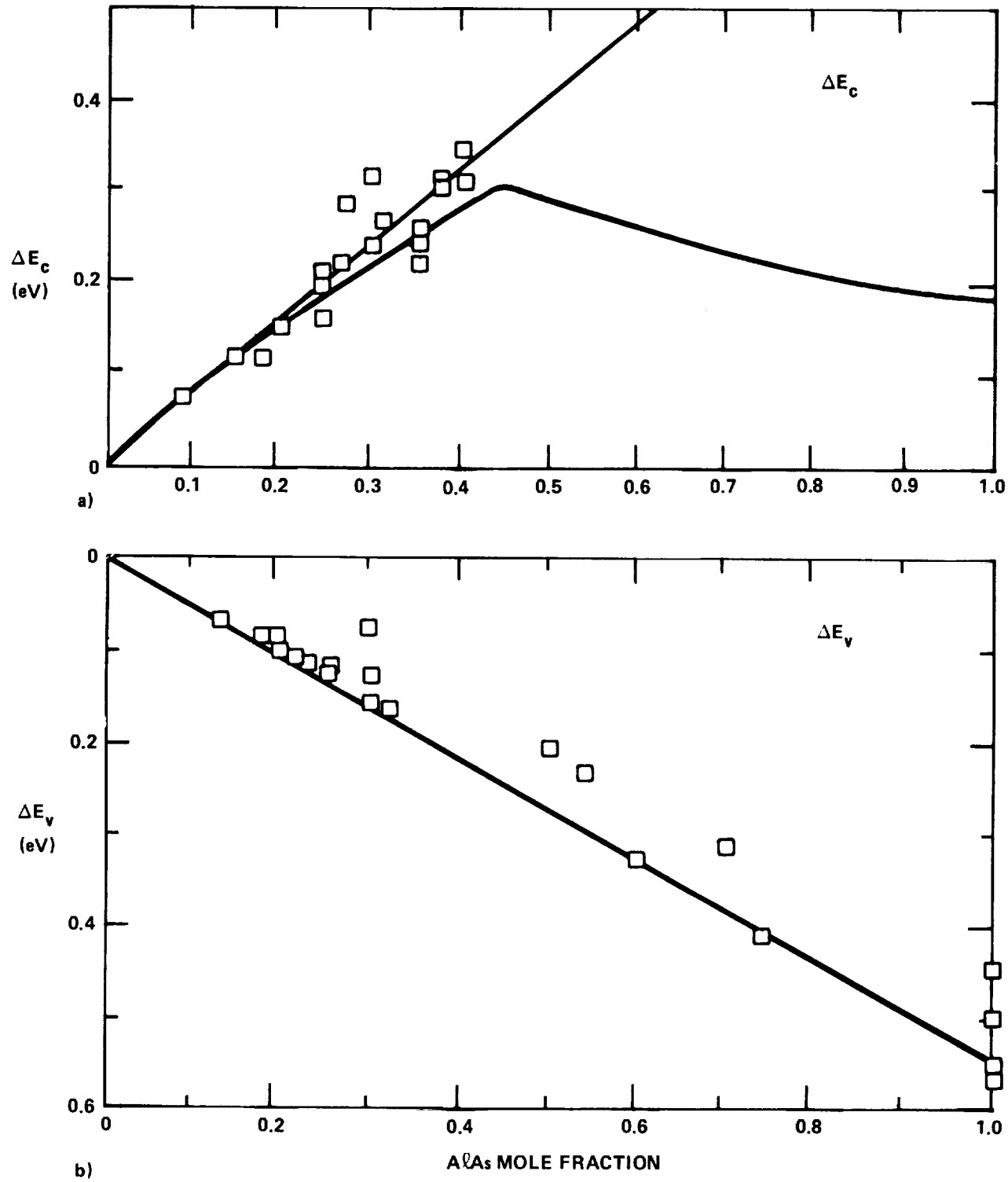

26. **Band-Edge Alignments at GaAs-Al(x)Ga(1-x)As Heterojunctions (R. Miller, ATT-Bell Laboratories).**

a. ΔE_C, conduction band misalignment;

b. ΔE_V, valence band misalignment.

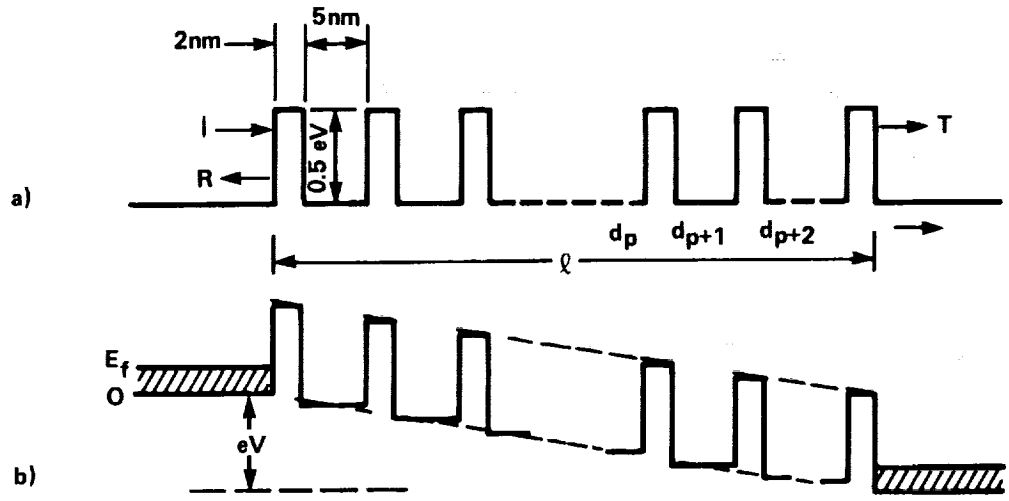

27. Esaki-Tsu Multiple Step Barrier Geometry (11)

a. Zero applied electric field;

b. Applied field strength F = F_{ap} over the length l of the MSB.

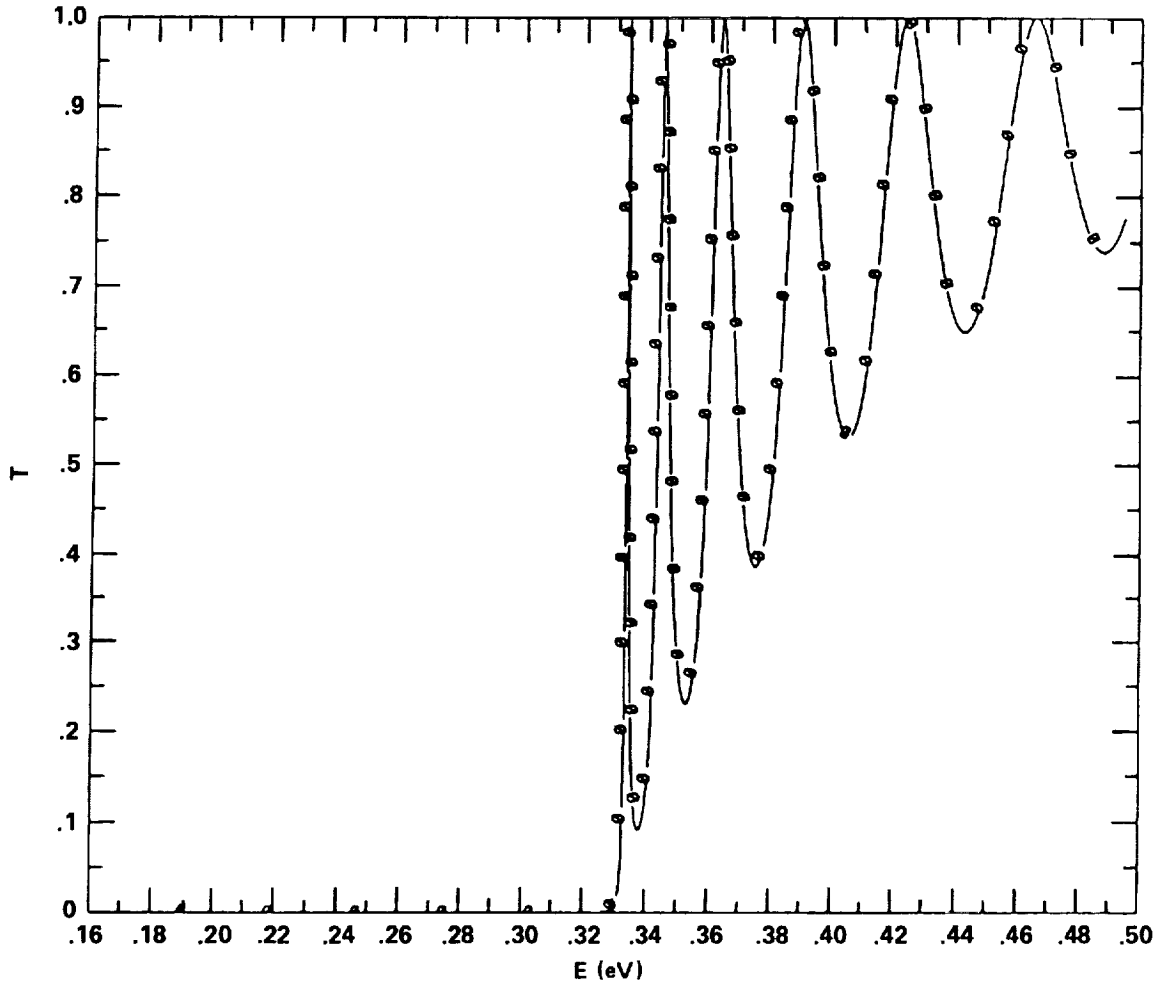

28. T-E Data for Single Step Barrier.

Barrier is 10 nm wide, 0.33 eV high. Effective mass is uniform and equal to free electronic mass m_0.

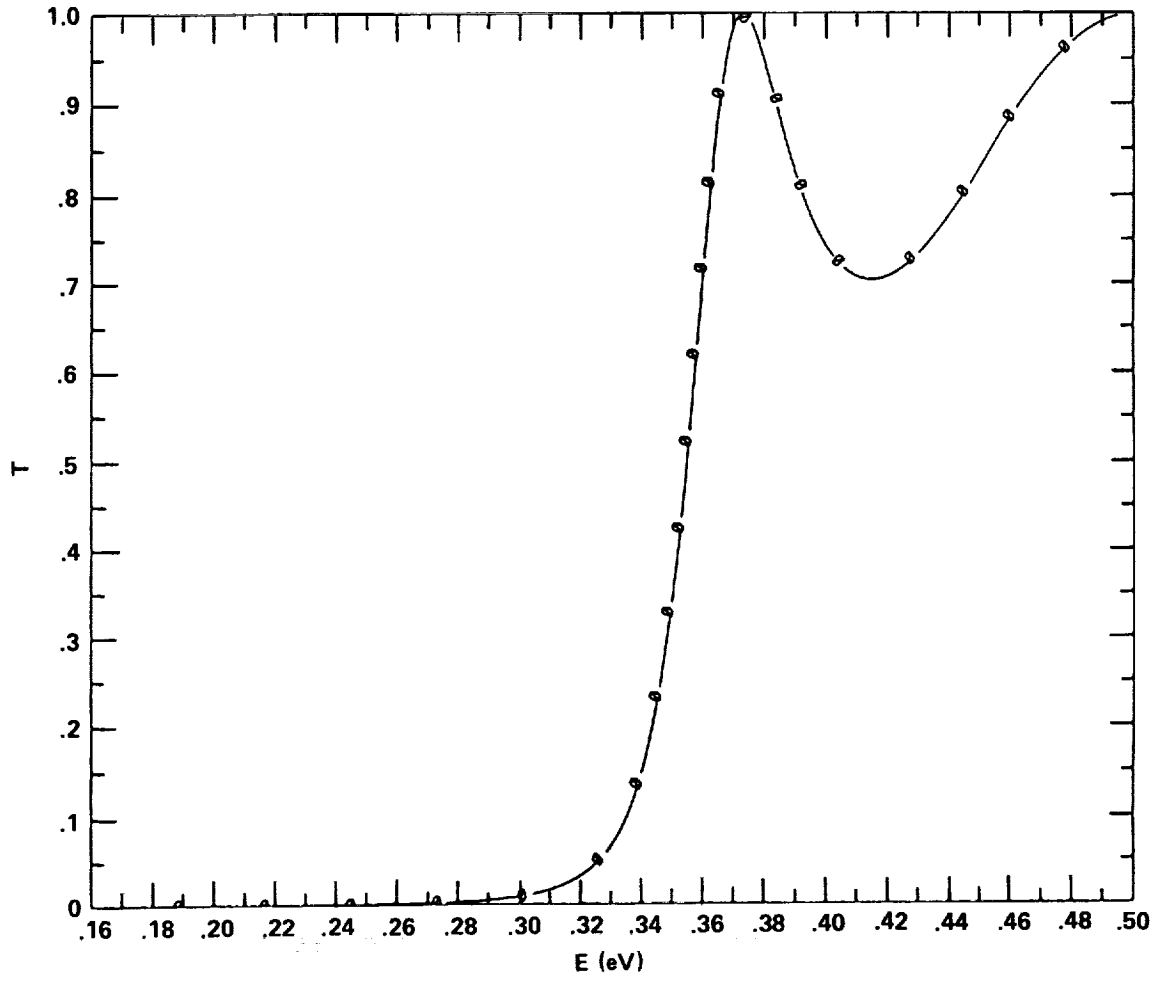

29. T-E Data for Single GaAs-Al(0.4)Ga(0.6)As Step Barrier.

Barrier is 10 nm wide and 0.33eV high. Effective mass is m_{in} = 0.0871 inside the barrier, m_{out} = 0.0636 outside.

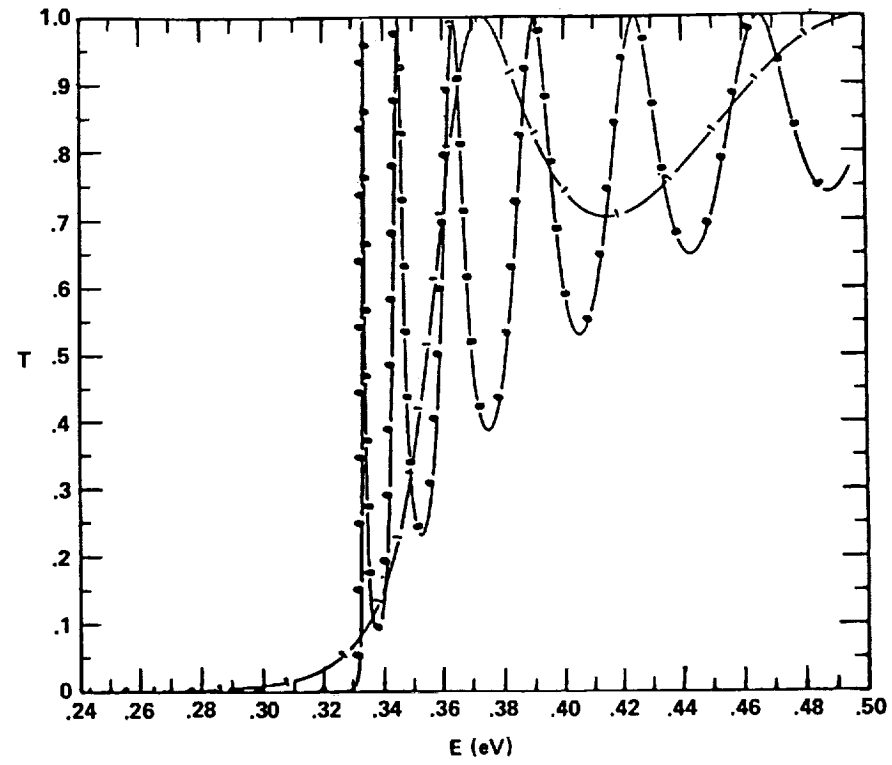

(a)

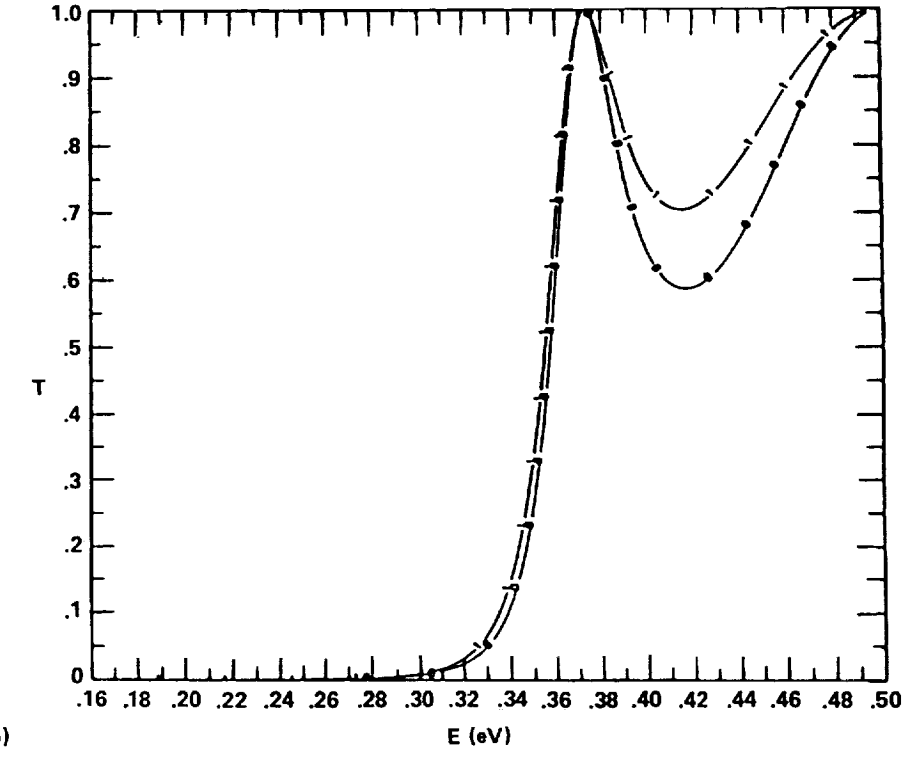

(b)

30. T-E Data for Single Step Barriers 10nm Wide and 0.33 eV High.

a. Superposed T-E curves for GaAs-Al(0.4)Ga(0.6)As barrier, and barrier with uniform effective mass $m_{eff} = m_0$ everywhere. Curve 1: GaAs-Al(0.4)Ga(0.6)As, $m_{in} = 0.0871$, $m_{out} = 0.0636$; Curve 0: $m_{eff} = m_0$;

b. Superposed T-E curves for GaAs-Al(0.4)Ga(0.6)As barrier, and barrier with uniform effective mass $m_{eff} = 0.0636$ everywhere. Curve 0: GaAs-Al(0.4)Ga(0.6)As; Curve 1: $m_{eff} = 0.0636$.

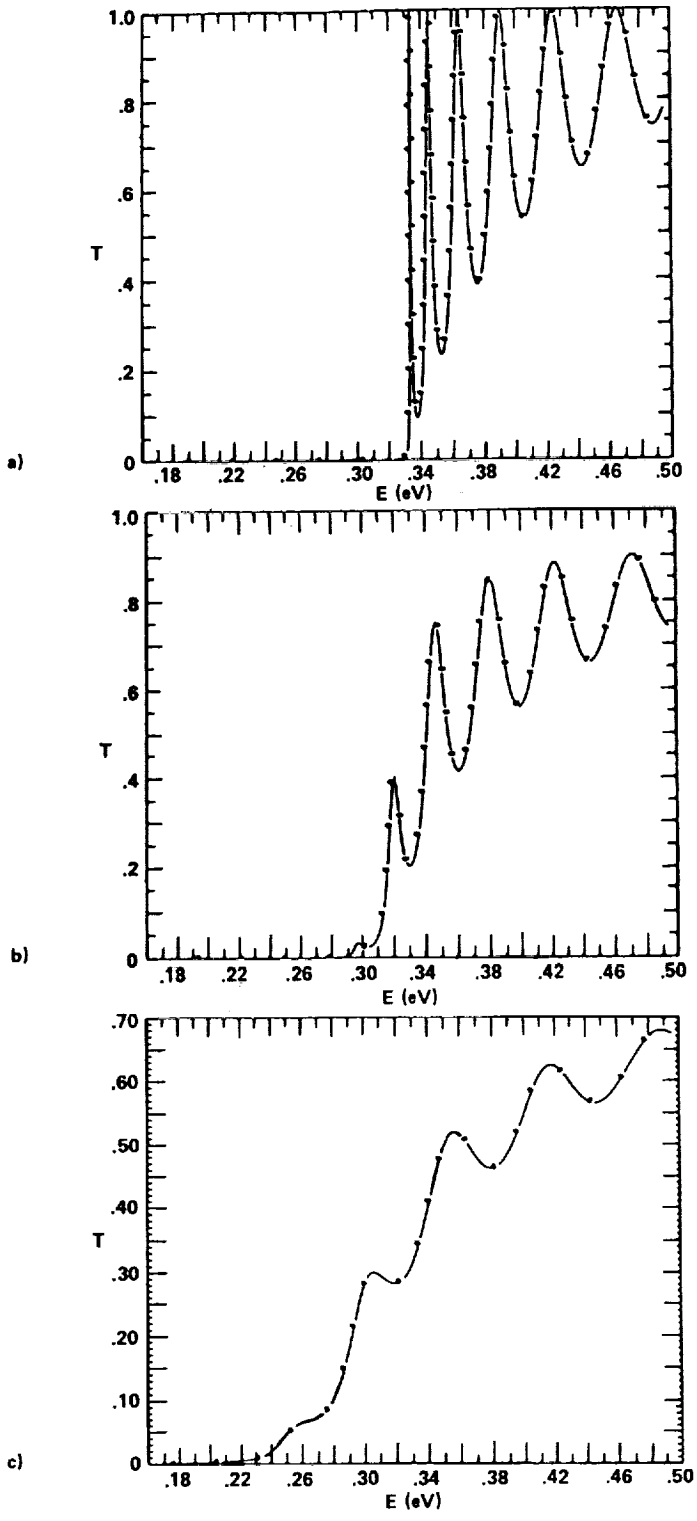

31. Effects of Applied Electric Field on Transmission Coefficient of Single Step Barrier.

Barrier is 10 nm wide, 0.33 eV high. Effective mass = m_0 everywhere.

a. $F_{ap} = 0$;

b. $F_{ap} = 2 \times 10^{-2}$ eV/nm;

c. $F_{ap} = 5 \times 10^{-2}$ eV/nm.

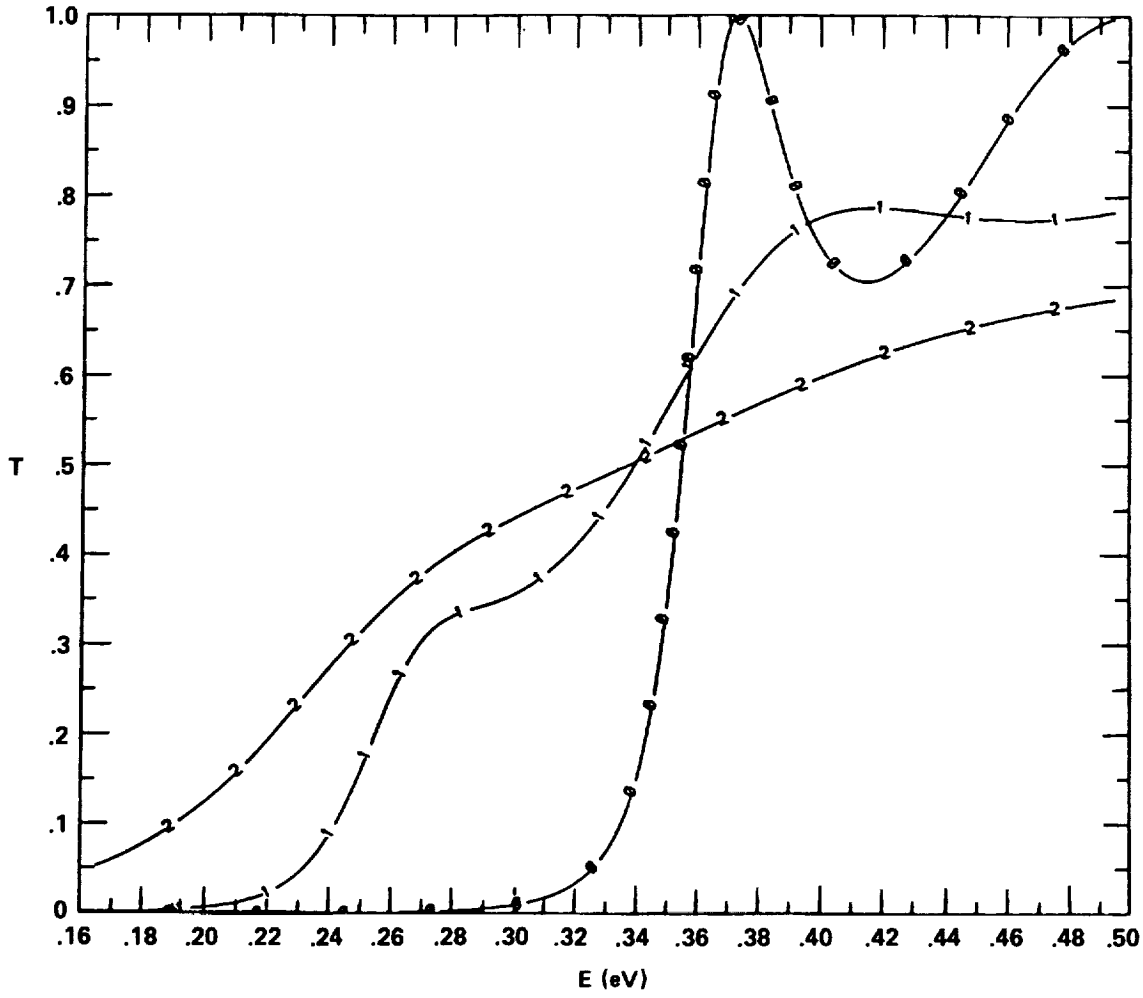

32. Effects of Applied Electric Field on Transmission Coefficient of Single GaAs-Al(0.4)Ga(0.6)As Step Barrier.

Barrier is 10 nm wide, 0.33 eV high. Inside the barrier m_{eff} = 0.0871, outside the barrier m_{eff} = 0.0636. Curve 0: $F_{ap} = 0$; Curve 1: $F_{ap} = 2 \times 10^{-2}$ eV/nm; Curve 2: $F_{ap} = 5 \times 10^{-2}$ eV/nm.

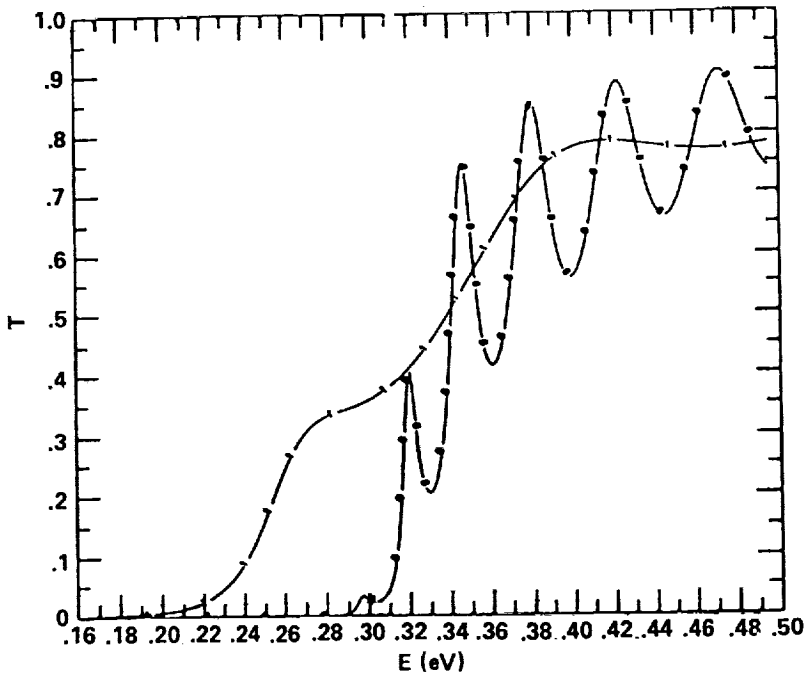

a)

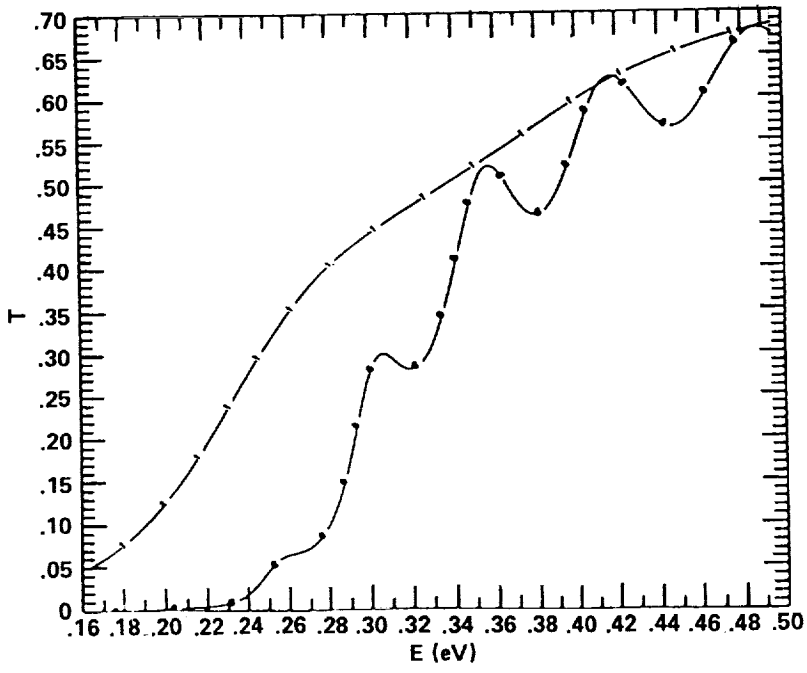

b)

33. Applied Field and Effective Mass Effects on Transmission Coefficient of Single Step Barriers.

Barriers are 10nm wide, 0.33 eV high. The two curves in each figure are for a barrier with uniform effective mass $m_{eff} = m_0$, and a GaAs-Al(0.4)Ga(0.6)As barrier: Curve 0: $m_{eff} = m_0$; Curve 1: $m_{in} = 0.0871$, $m_{out} = 0.0636$.

a. Applied field $F_{ap} = 2 \times 10^{-2}$ eV/nm;

b. Applied field $F_{ap} = 5 \times 10^{-2}$ eV/nm.

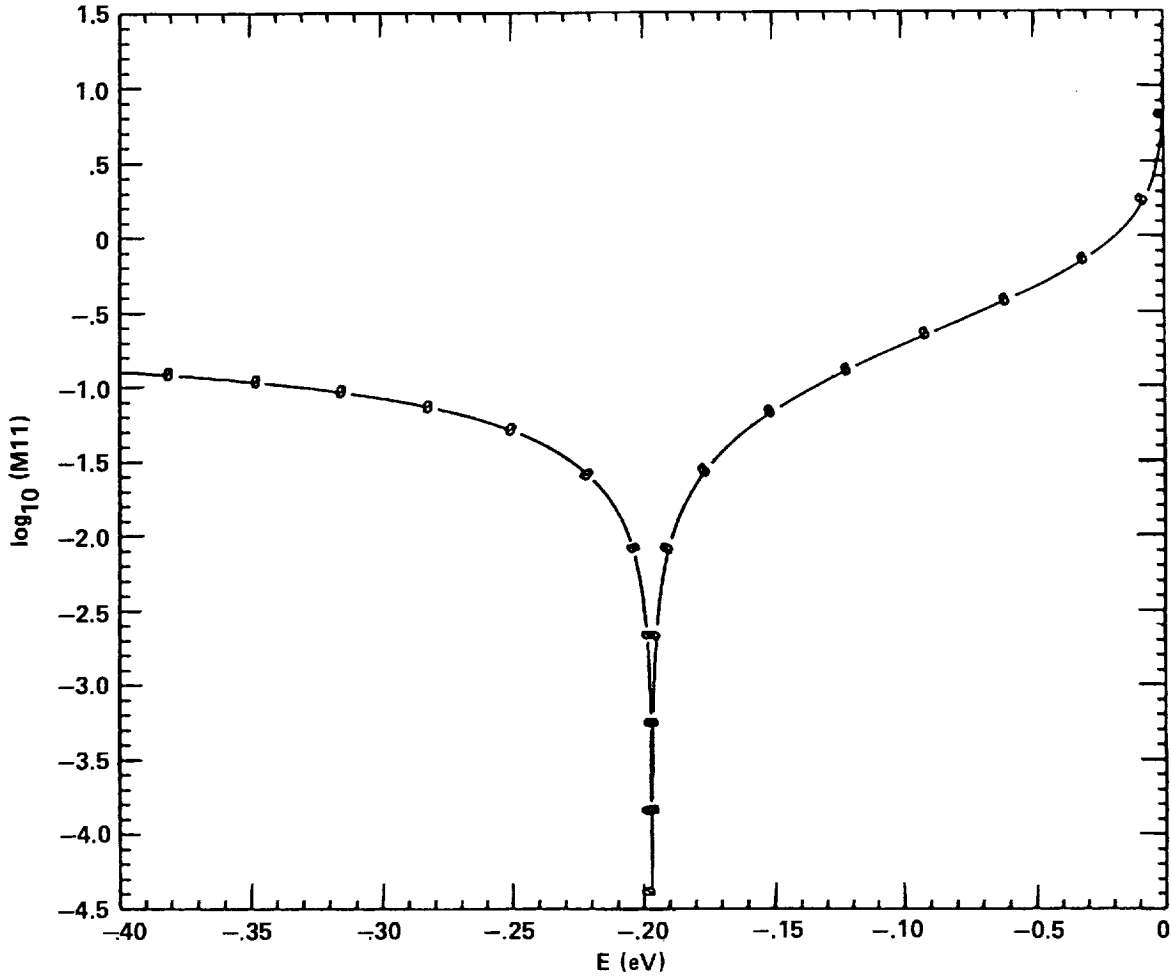

34. Total Transfer Matrix Element M_{11} for Single GaAs-Al(0.5)Ga(0.5)As Quantum Well: Bound State.

Well is 3 nm wide, 0.4 eV deep. This calculation took account of the effective mass variation at the well edges: the effective masses inside and outside the well are m_{in} = 0.094, m_{out} = 0.0636. The minimum of M_{11} gives a bound state energy of -0.197 eV below the top of the well.

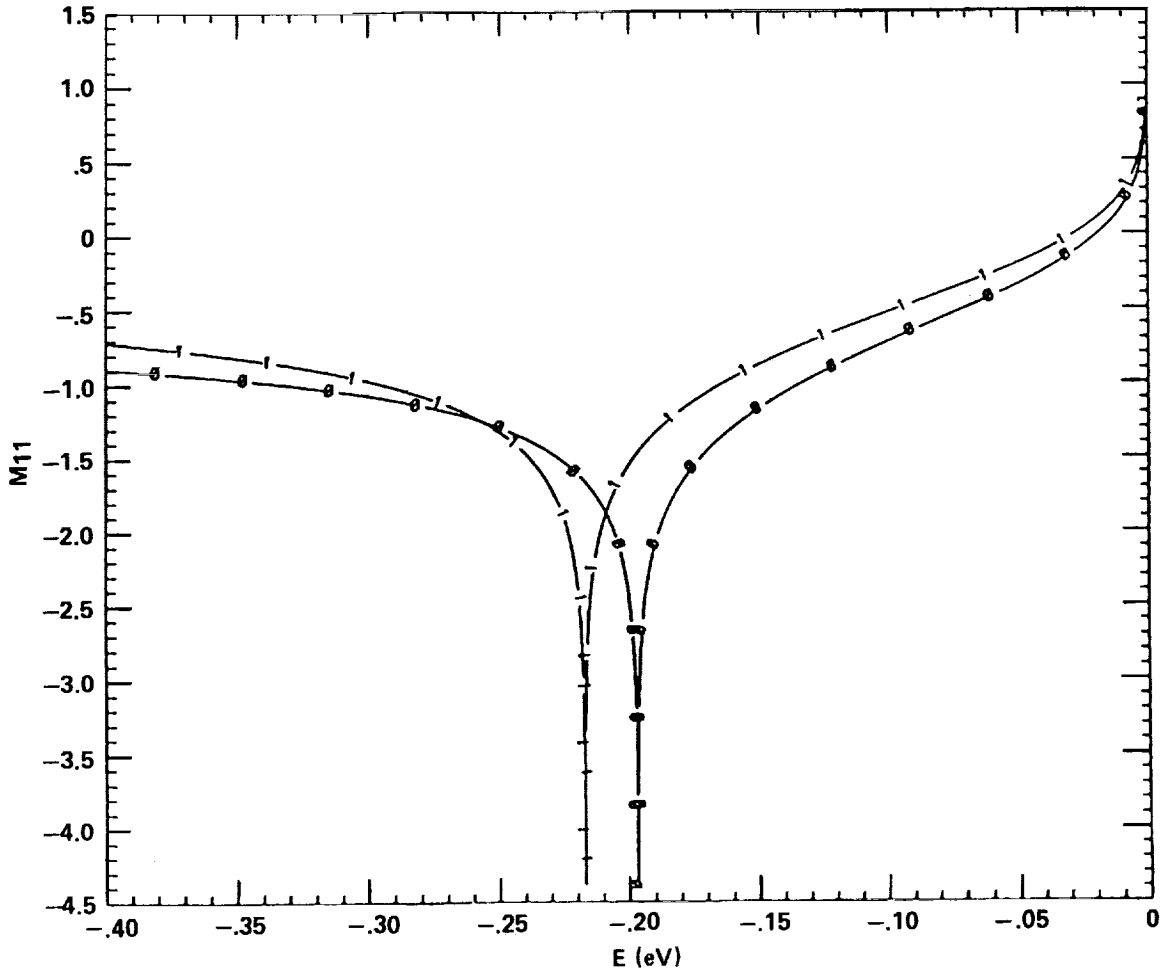

35. Bound State Energy as a Function of the Effective Mass Inside Well.

Well is the same as that of Figure 34. The effective mass, however, is taken in this calculation as 0.0636 inside and outside the well. The new bound state energy is -0.217 eV below the top of the well, instead of -0.197 eV.

Curve 0: Effective mass = 0.0636 everywhere. E_0 = -0.217 eV.

Curve 1: Effective mass = 0.094 inside the well, 0.0636 outside the well.E_0 = -0.197 eV.

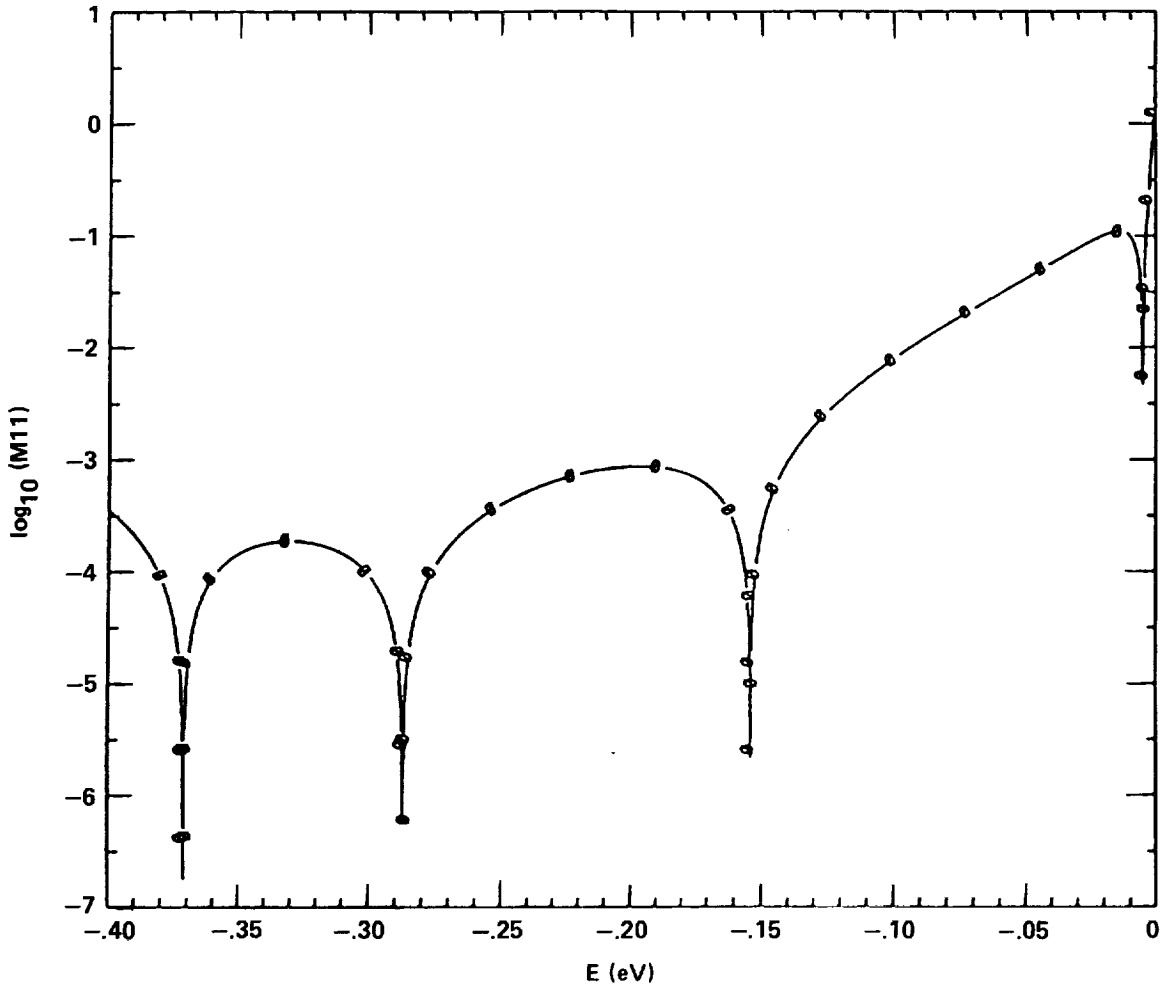

36. Bound States In Single Quantum Well.

Well is 3nm wide, 0.4 eV deep. Effective mass is uniform and equal to m_0. The minima in M_{11} correspond to bound states. Using the free-electronic mass results in four bound states, in agreement with Equation 139.

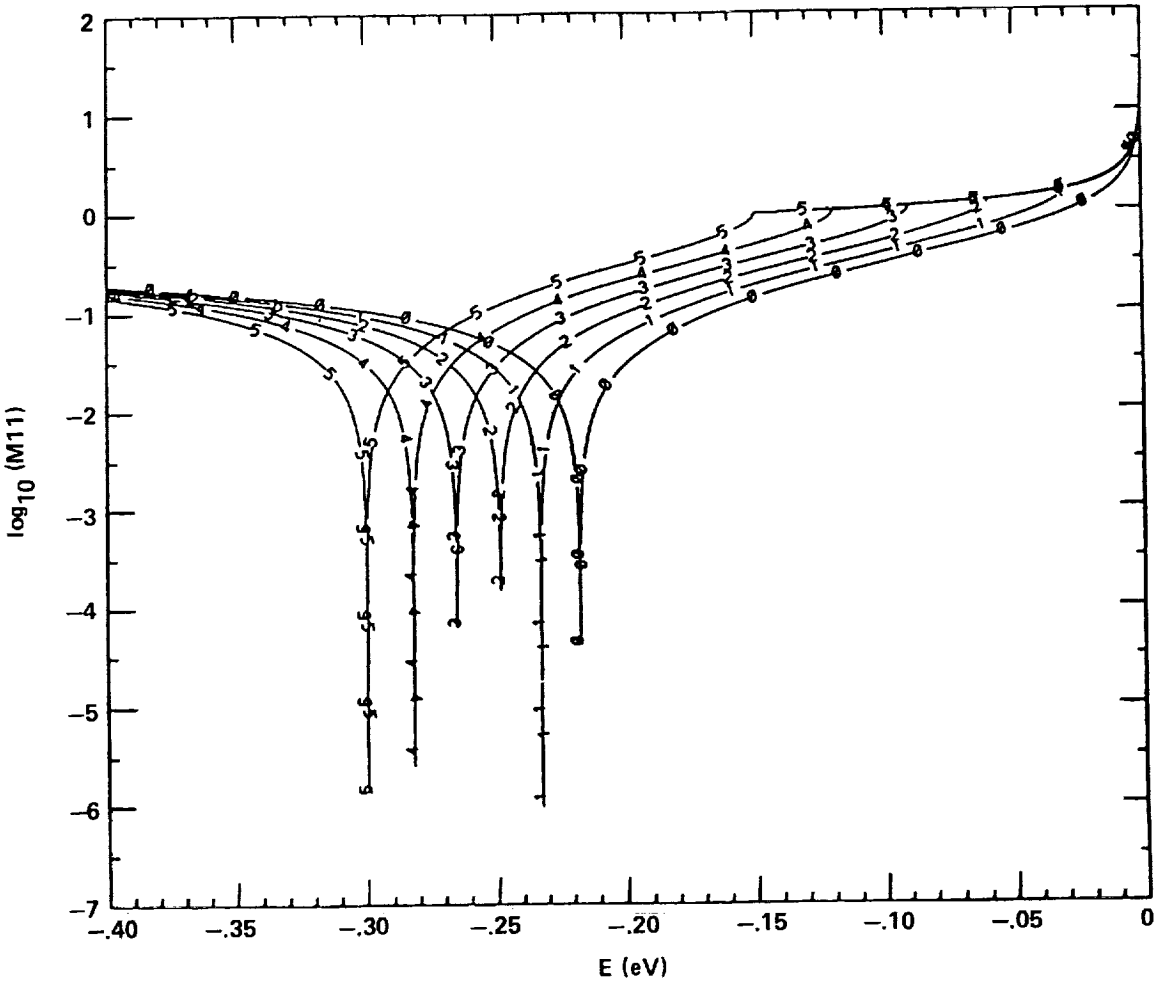

37. Total Transfer Matrix Element M_{11} as a Function of Localized Field Strength. Data are for single GaAs-Al(0.5)Ga(0.5)As quantum well, 3 nm wide and 0.4 eV deep. Effective mass taken as 0.0636 everywhere. Each curve corresponds to a different field strength. Minima shift to energies deeper in the well as the field strength is increased.

Curve 0: $F_{ap} = 0$; Curve 1: $F_{ap} = 1 \times 10^{-2}$ eV/nm; Curve 2: $F_{ap} = 2 \times 10^{-2}$ eV/nm;

Curve 3: $F_{ap} = 3 \times 10^{-2}$ eV/nm; Curve 4: $F_{ap} = 4 \times 10^{-2}$ eV/nm;

Curve 5: $F_{ap} = 5 \times 10^{-2}$ eV/nm.

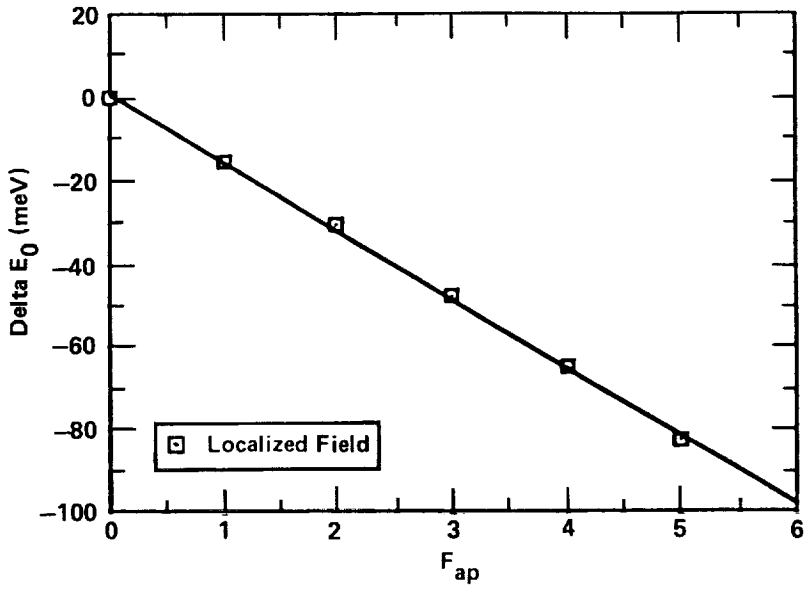

38. Stark Shift of Bound State Energy Level under Localized Field.

Data are for single GaAs-Al(0.5)Ga(0.5)As quantum well, 3 nm wide and 0.4 eV deep. Effective mass taken as 0.0636 everywhere. In this figure the Stark shift (referred to the zero-field bound state energy) is plotted as a function of the applied field strength. The Stark shift is linear in the field strength.

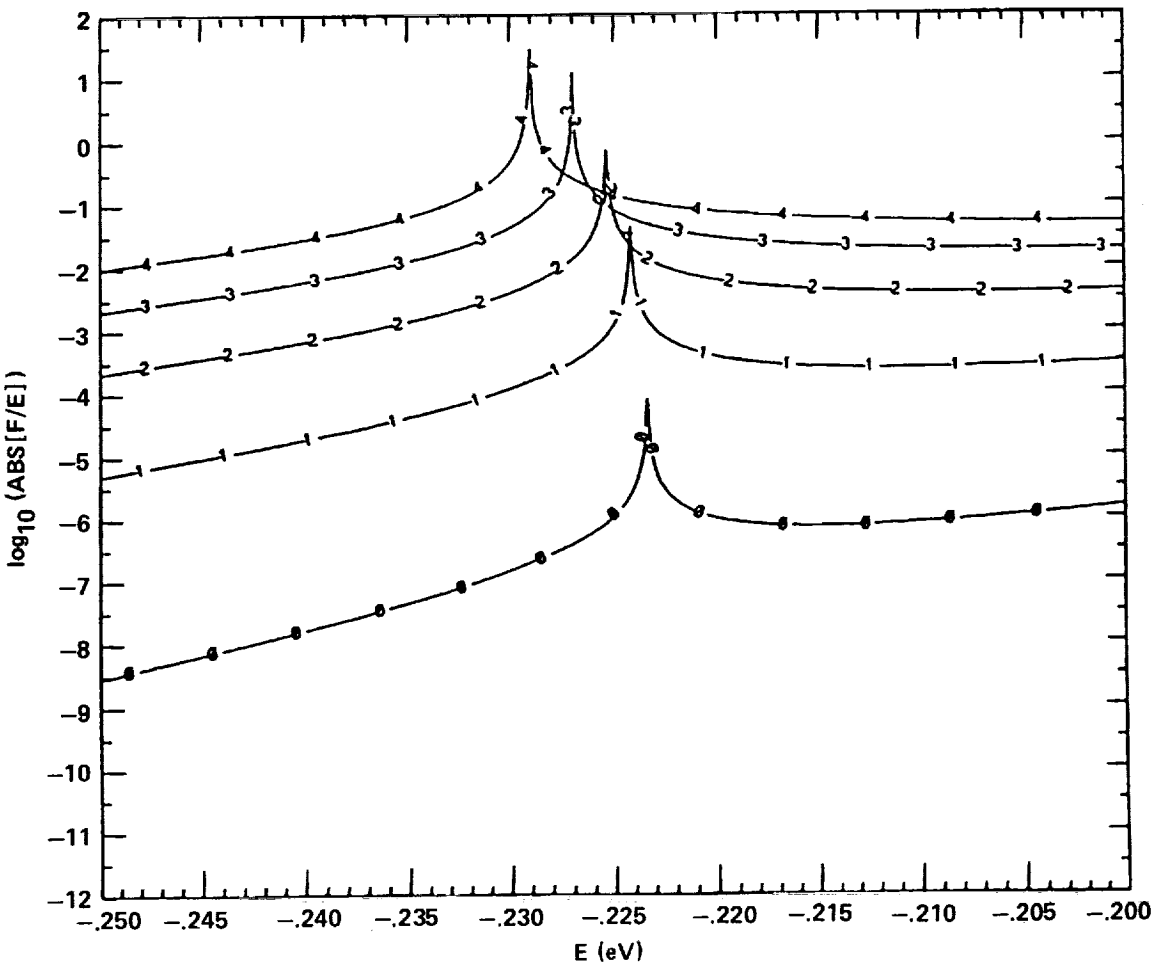

39. The Ratio (F/E) as a Function of Energy and Applied Field Strength.

Data are for single GaAs-Al(0.5)Ga(0.5)As quantum well, 3 nm wide and 0.4 eV deep. Effective mass taken as 0.0636 everywhere; field is uniform and unrestricted. Each curve is for a different field strength; the maxima in the data correspond to quasi-bound states of the quantum well. Maxima shift to energies deeper in the well as the field strength increases.

Curve 0: F_{ap} = 1.0 $\times 10^{-2}$ eV/nm; Curve 1: F_{ap} = 1.5 $\times 10^{-2}$ eV/nm;

Curve 2: F_{ap} = 2.0 $\times 10^{-2}$ eV/nm; Curve 3: F_{ap} = 2.5 $\times 10^{-2}$ eV/nm; and

Curve 4: F_{ap} = 3.0 $\times 10^{-2}$ eV/nm.

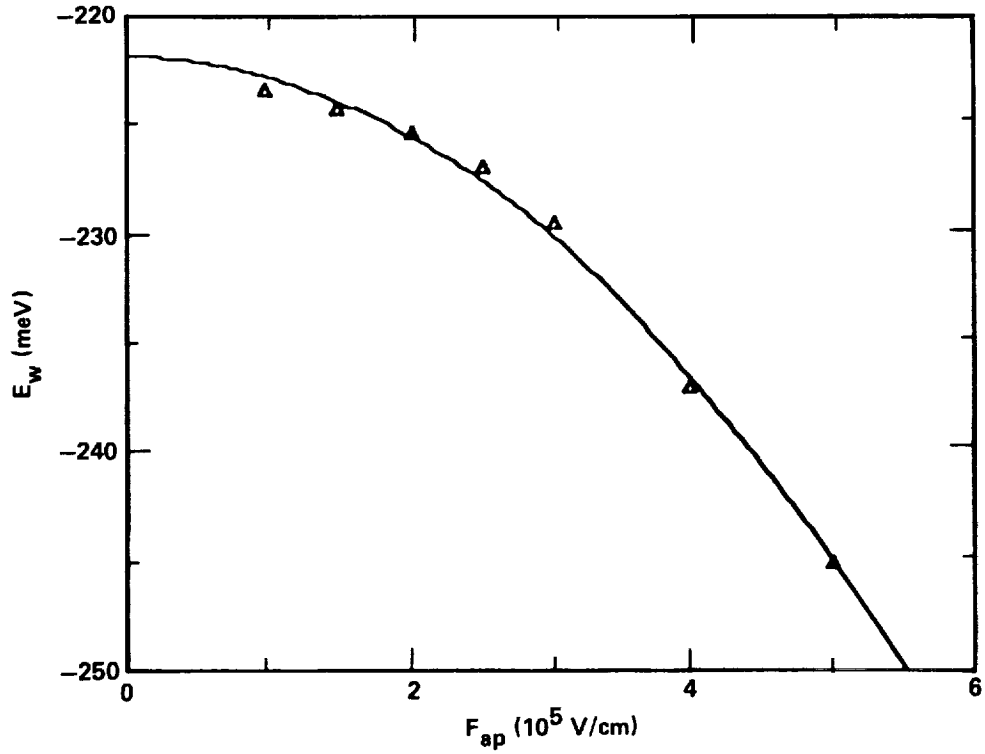

40. Stark Shift of Bound State Energy Level Under Uniform, Unrestricted Field. From Figure 39, the energy levels of the maxima in (F/E) are plotted as function of the applied field strength. The bound state energies are quadratically dependent on the applied field strength.

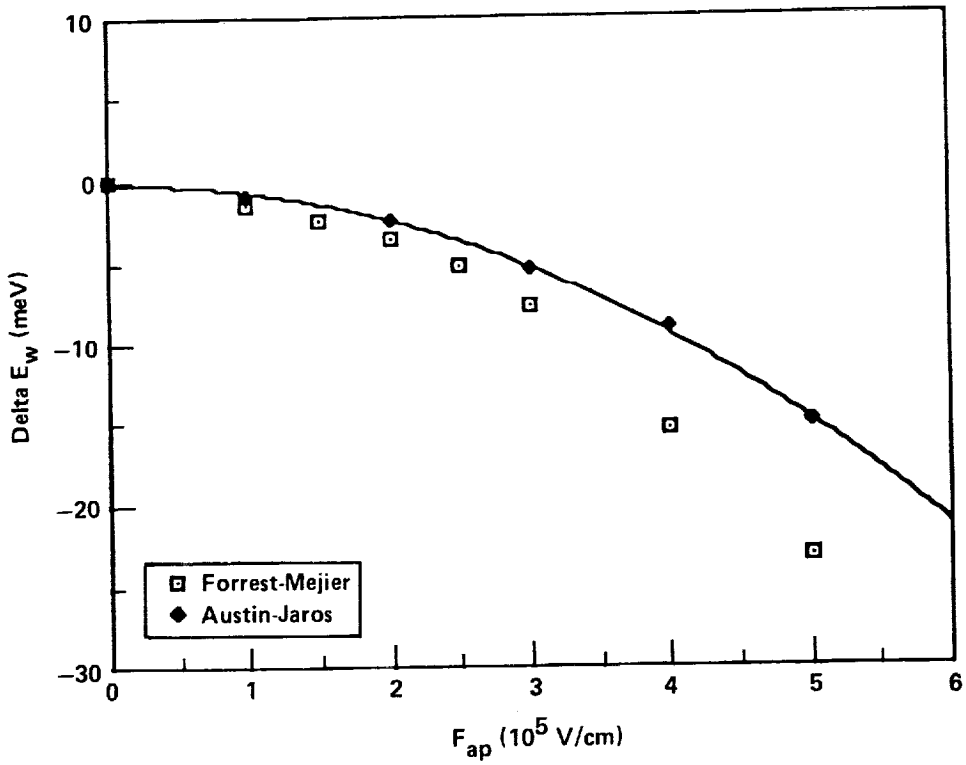

41. Stark Shift of Bound State Energy Levels Under Uniform, Unrestricted Field. From Figure 40, the Stark shift relative to the zero-field level is plotted as a function of the applied field strength. Also shown are the data of Austin and Jaros (41) for an identical quantum well.

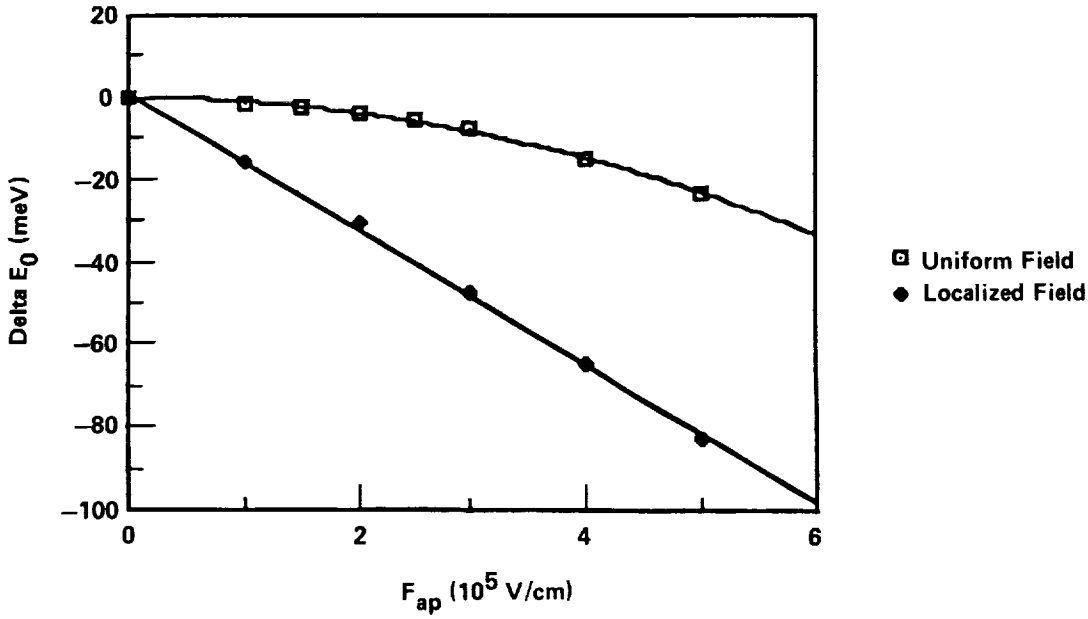

42. Stark Shifts under Localized and Unrestricted Uniform Fields Compared. From Figures 38 and 41, the Stark shifts calculated for a 3nm, 0.4 eV Al(0.5)Ga(0.5)As quantum well are plotted together.

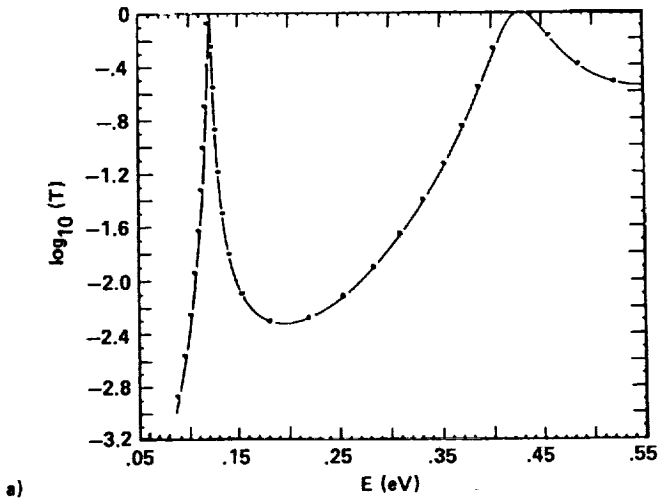

a)

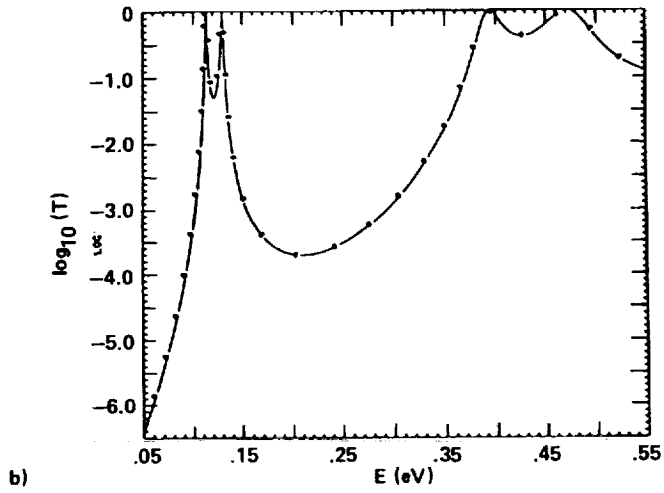

b)

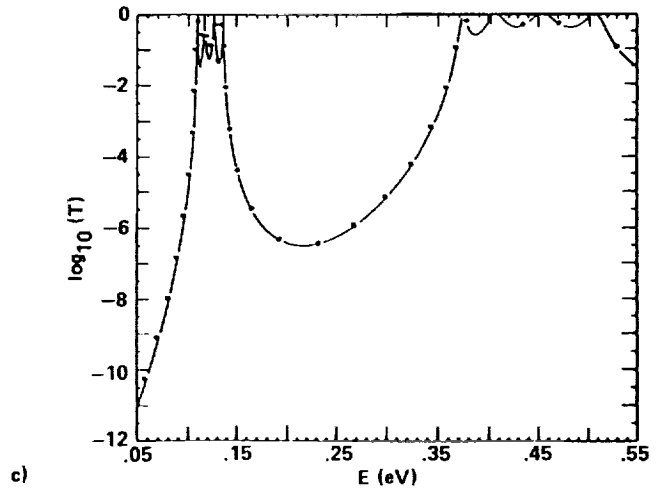

c)

43. T-E Curves for Two-, Three-, and Five-Barrier GaAs-Al(0.5)Ga(0.5)As Multiple Step Barriers.

These are the results of transfer matrix calculations for step barrier superlattices identical to those of Esaki and Tsu (11). Barriers are 2 nm wide, 5 nm apart, and 0.5 eV high. Effective mass in the barriers is m_{in} = 0.094, between the barriers m_{out} = 0.0636. Modified connection rules are used. Figures a, b, and c are for two, three and five barriers, respectively.

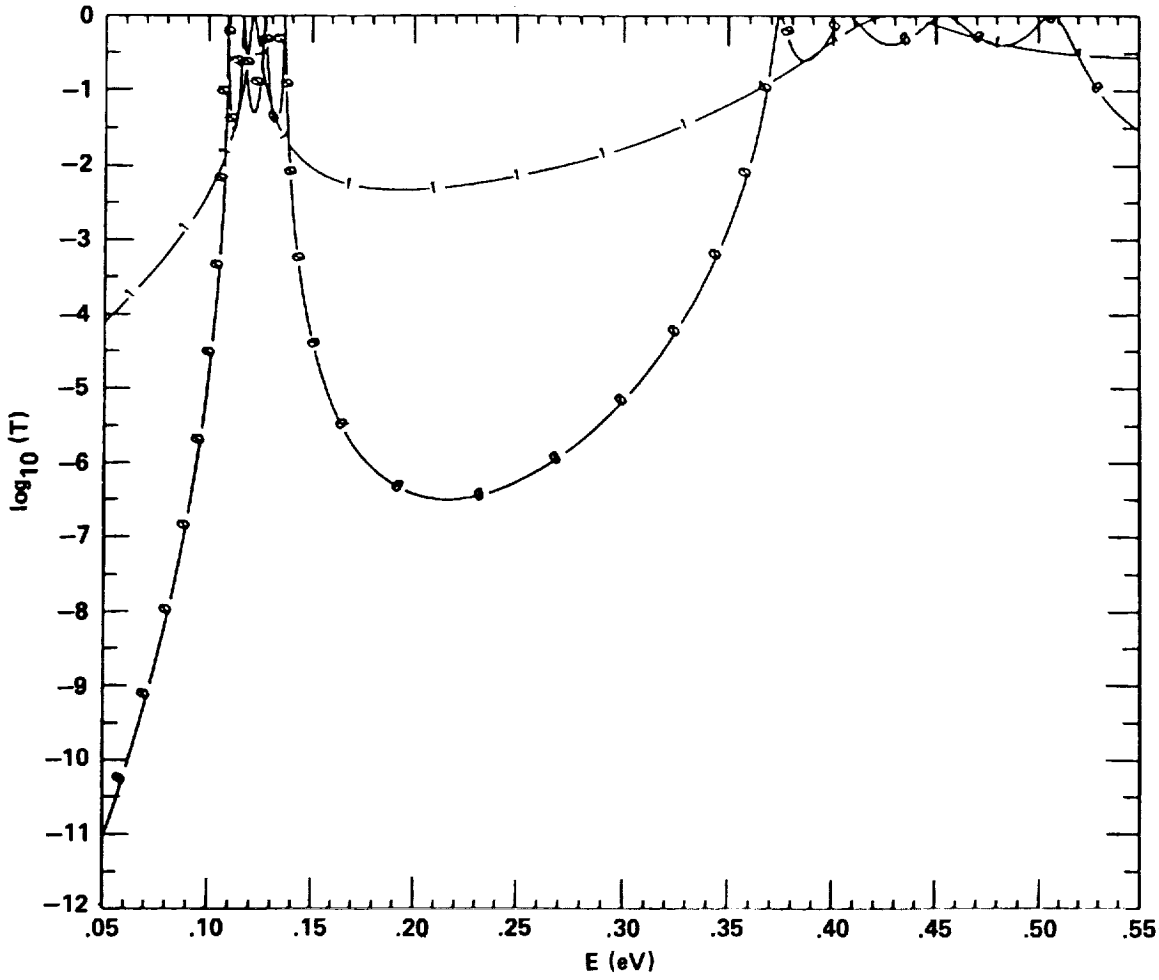

44. T-E curves for Two- and Five- Barrier Esaki-Tsu Type MSB's

The T-E curves from Figure 43 for two and five barriers superposed. Note the splitting of single resonances into four, caused by coupling between wells.

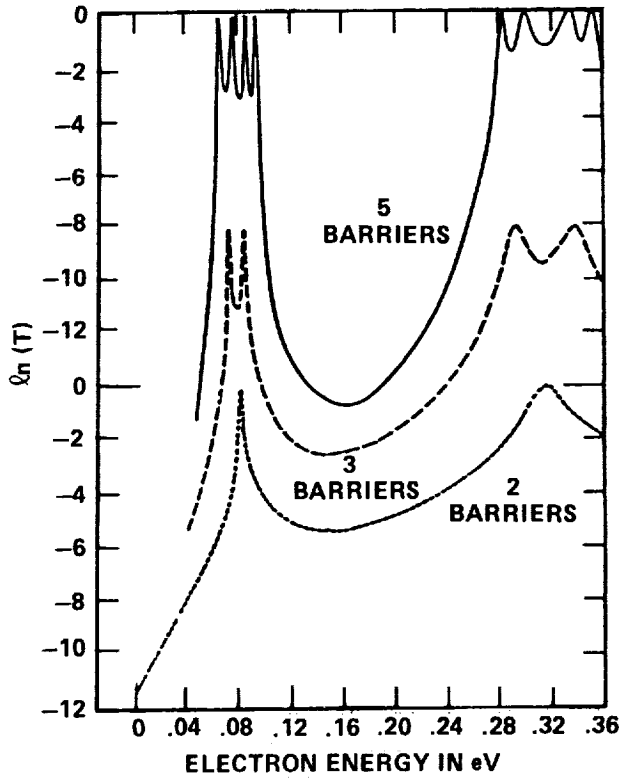

45. T-E Curves for Two-, Three-, and Five-Barrier MSB's Calculated By Esaki and Tsu (11).

Note the close agreement between these curves and those of Figure 43.

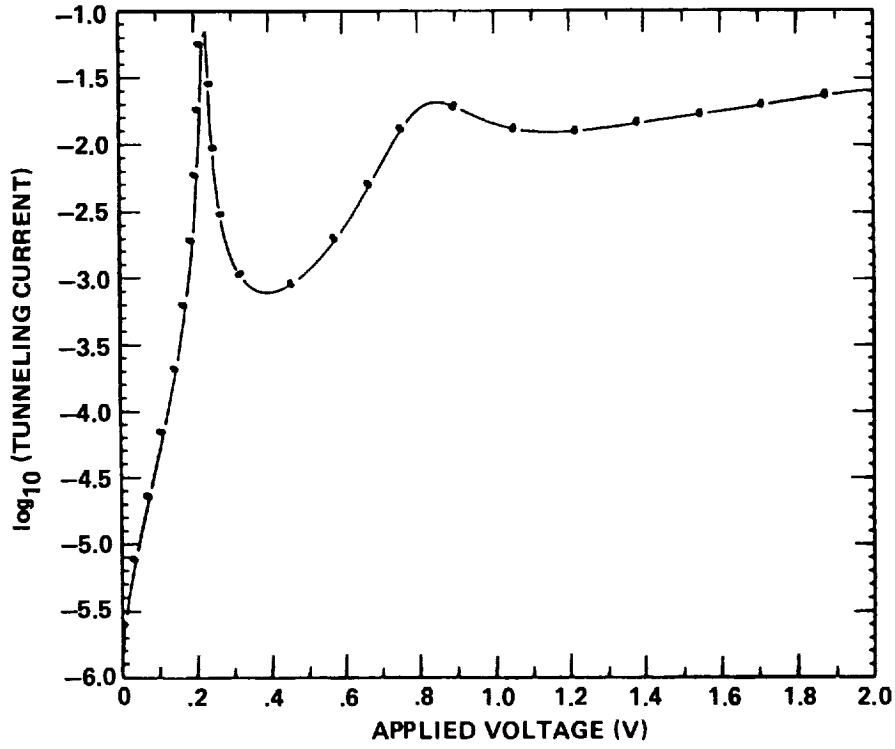

a)

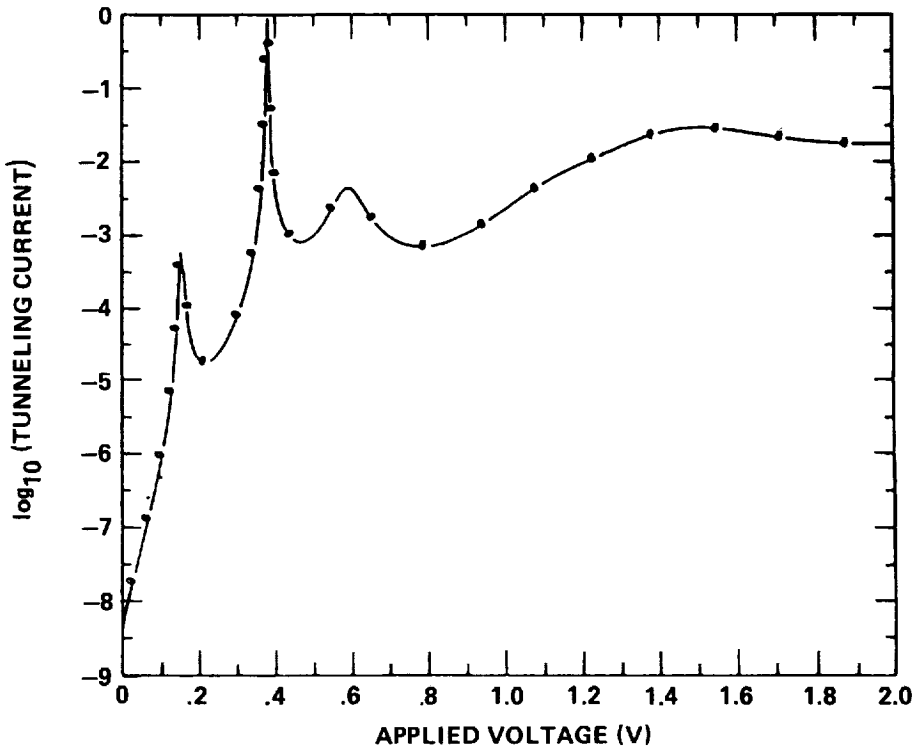

b)

46. J-V Curves for Two- and Three-Barrier GaAs-Al(0.5)Ga(0.5)As MSB's

These curves are calculated for the same MSB's whose T-E curves appear in Figure 43.

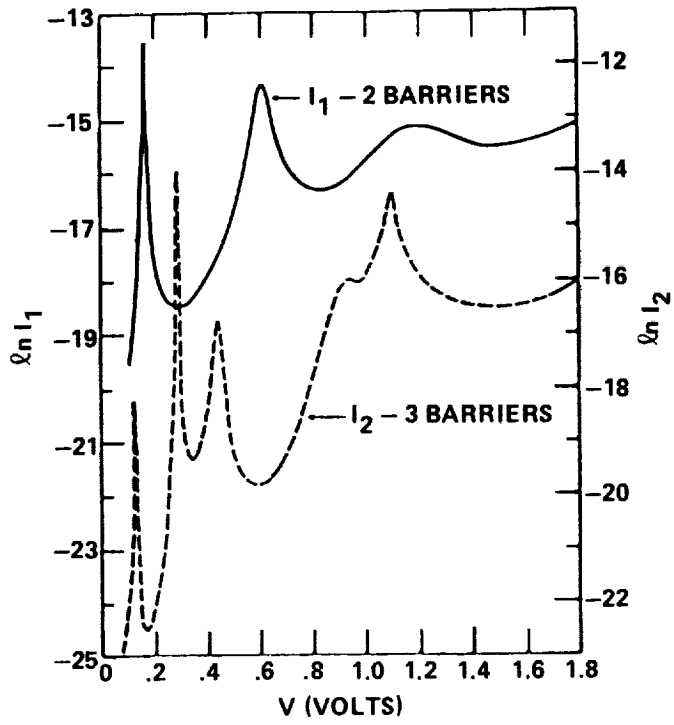

47. J-V Curves for Two- and Three-Barrier MSB's Calculated by Esaki and Tsu (11).

Note the agreement between these curves and those of Figure 46.

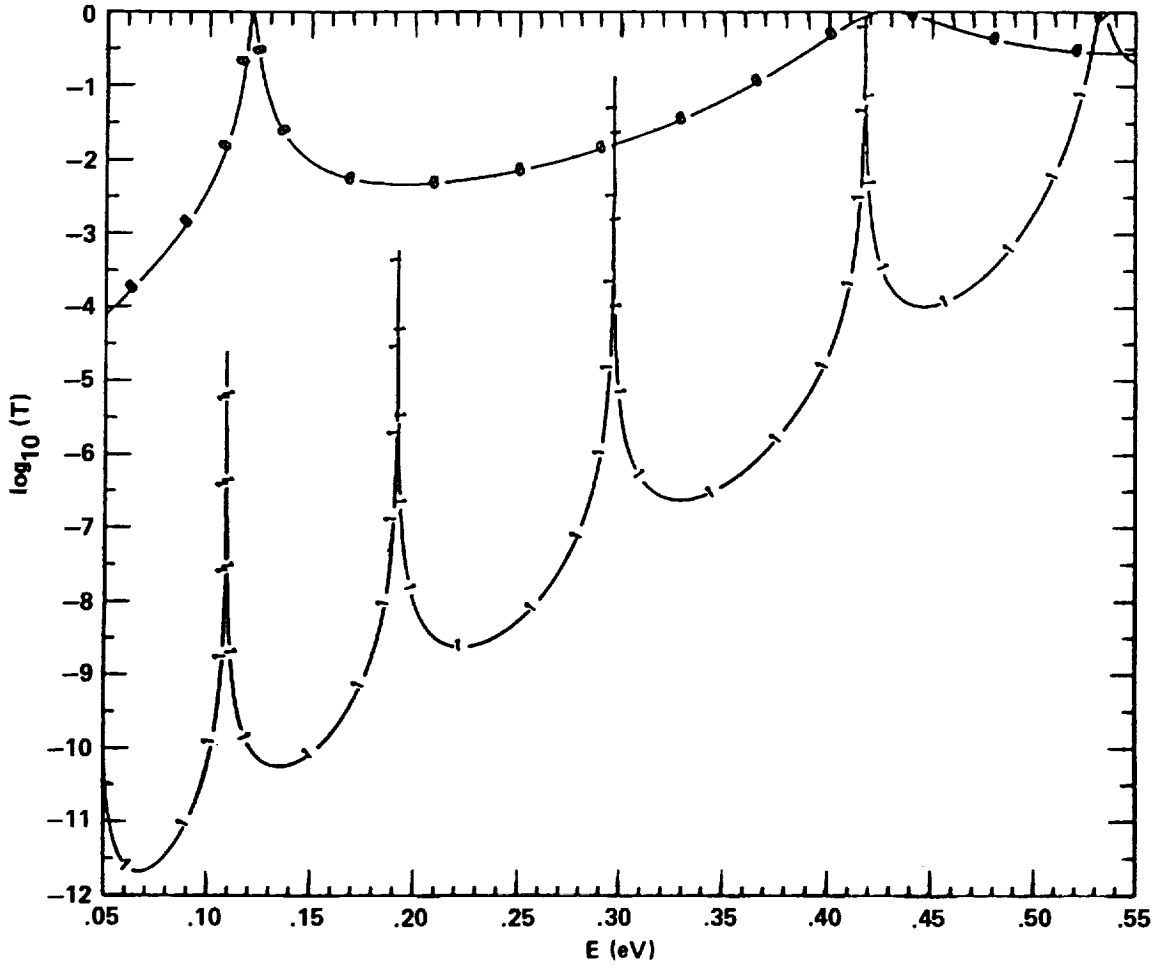

48. T-E Curves of Two-Barrier MSB's: Influence of Effective Mass.

Both curves are for two-barrier MSB's with barriers 2 nm wide,5 nm apart, and 0.5 eV high. Curve 0 is for GaAs-Al(0.5)Ga(0.5)As MSB with effective mass variations taken into account, and Curve 1 is for MSB with effective mass uniform and equal to mo.

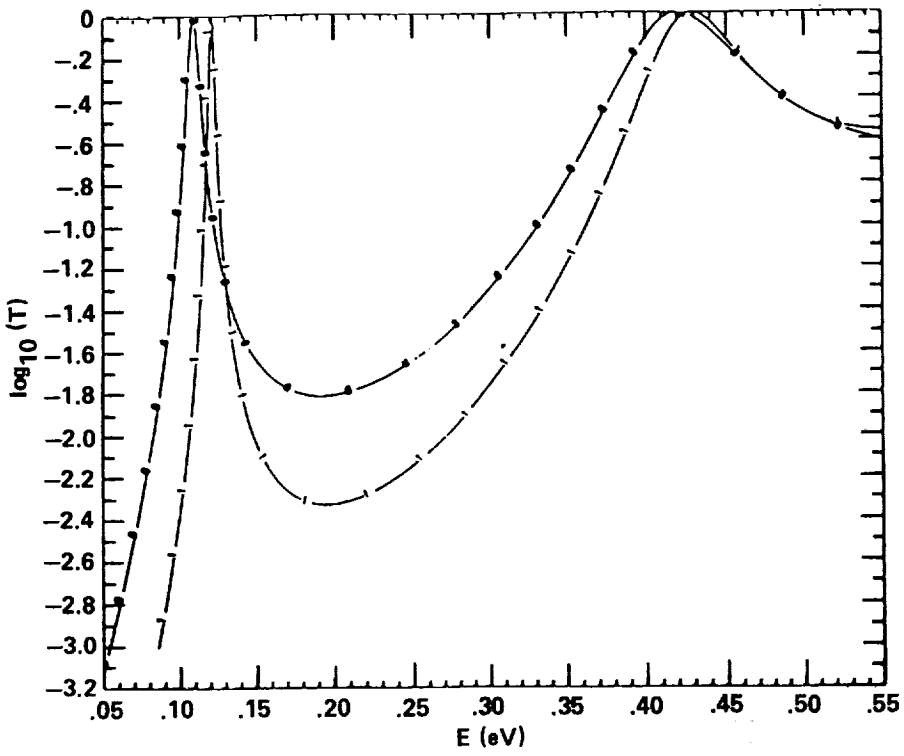

a)

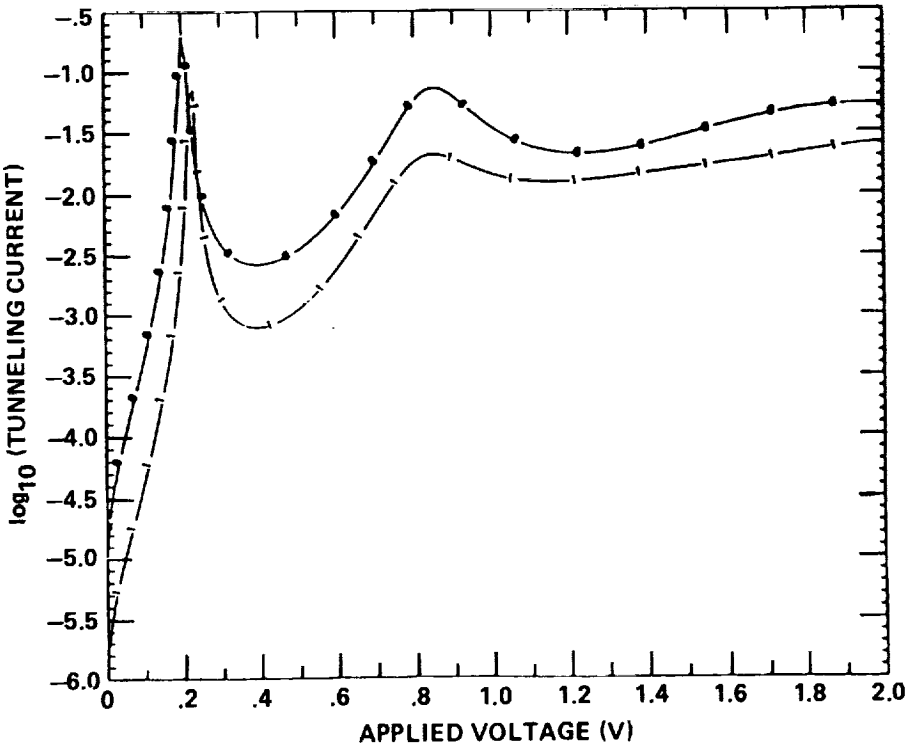

b)

49. T-E and J-V Curves of Two-Barrier MSB's: Effect of Neglecting the Effective Mass Step at Heterojunctions.

Data are for GaAs-Al(0.5)Ga(0.5)As Esaki-Tsu-type MSB's. Figures a and b are T-E and J-V curves respectively. In Curve 0, the effective mass is taken as uniform and equal to 0.0636. In Curve 1, the effective mass is 0.094 inside the barriers, and 0.0636 in the wells.

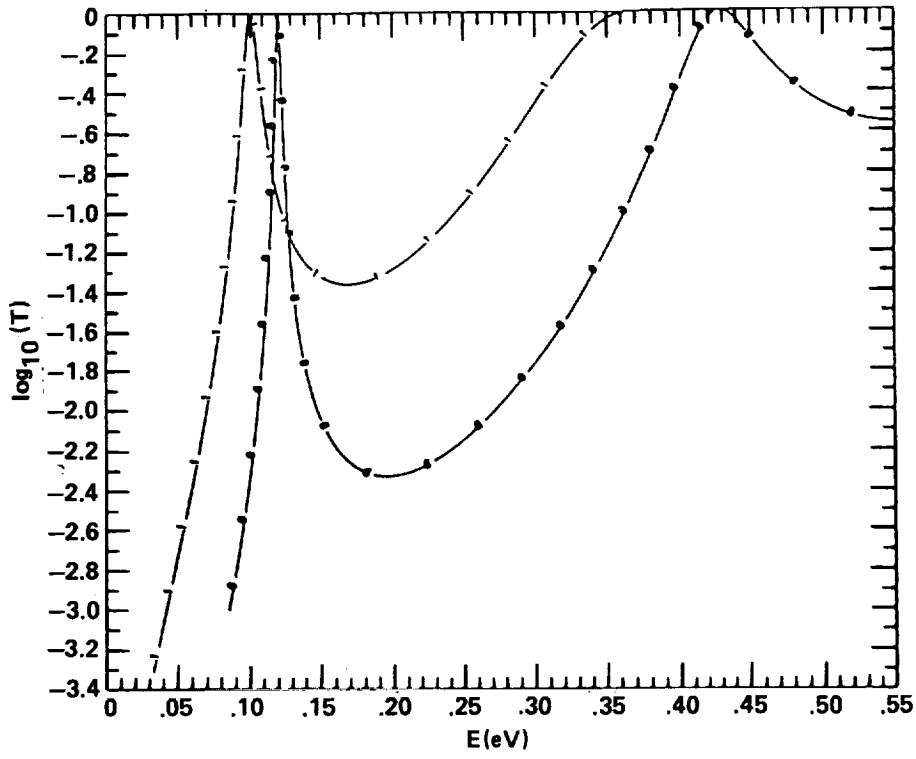

a)

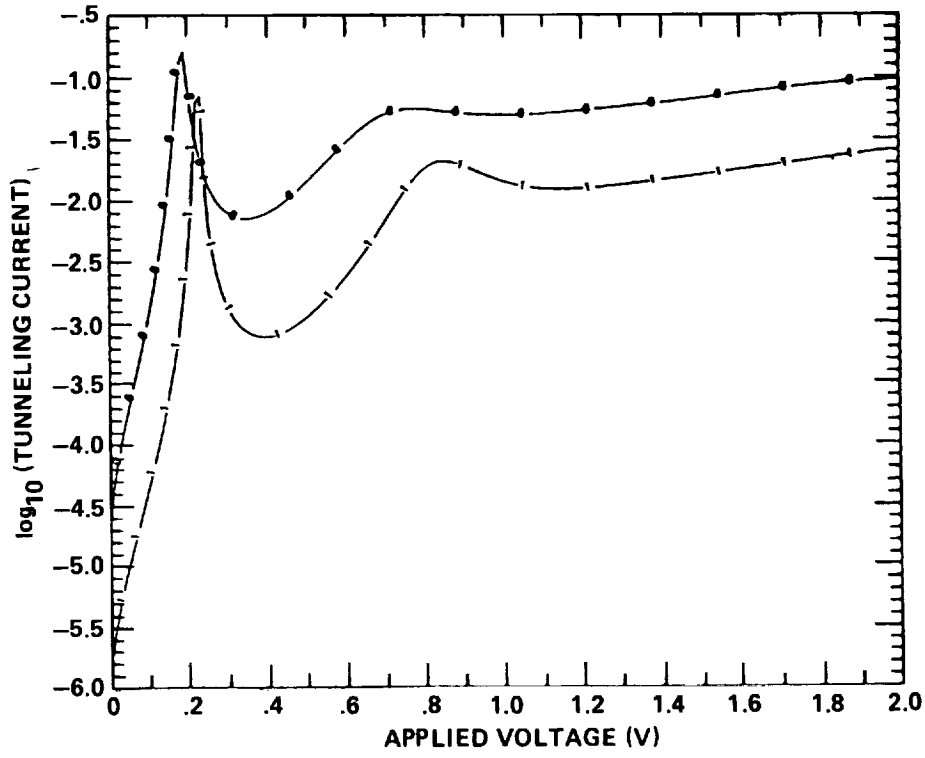

b)

50. T-E and J-V Curves for GaAs-Al(0.4)Ga(0.6)As and GaAs-Al(0.5)Ga(0.5)As Two-Barrier MSB's: Effects of Composition

Data are for MSB's with barriers 2 nm wide, 5 nm apart. Figures a and b are T-E and J-V curves respectively. Curve 0 is for GaAs-Al(0.4)Ga(0.6)As. Curve 1 is GaAs-Al(0.5)Ga(0.5)As.

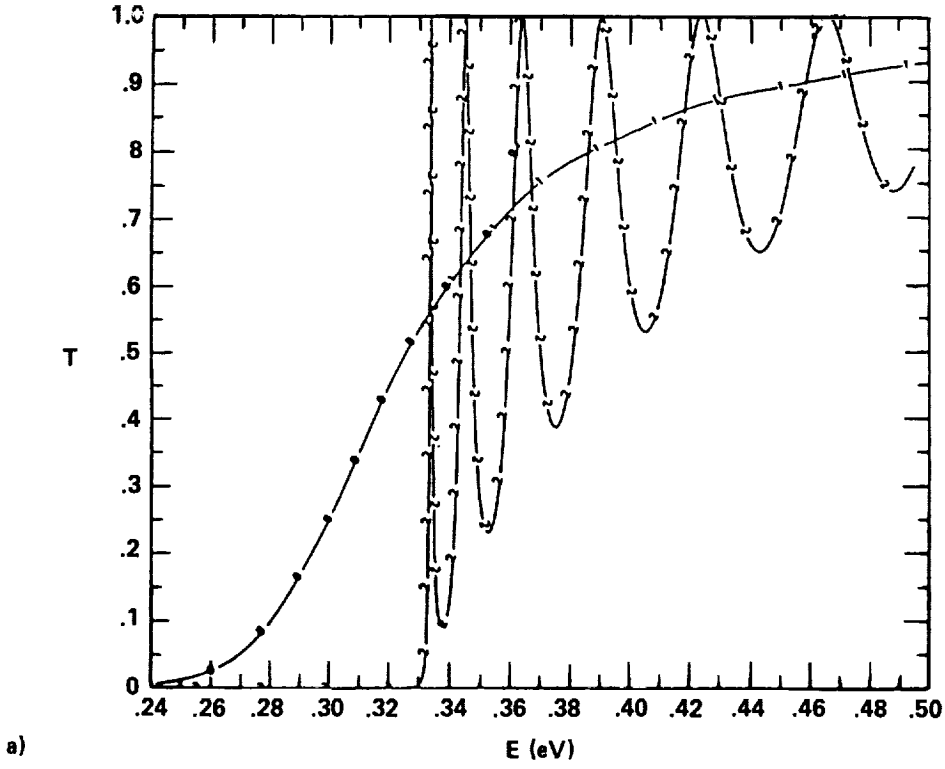

a)

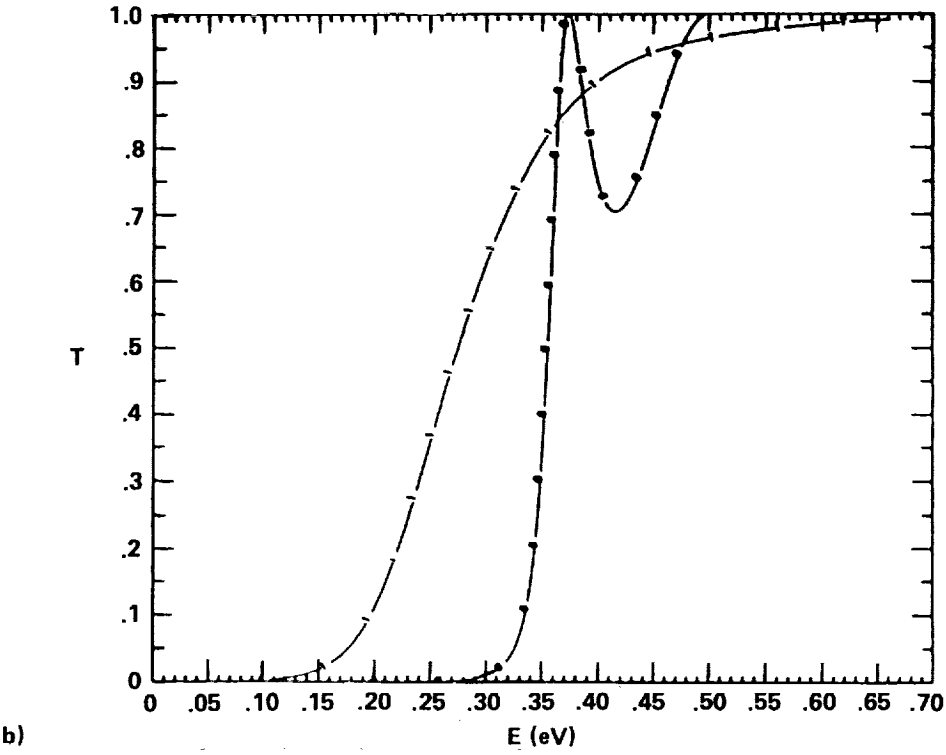

b)

51. T-E Curves for Sawtooth and Step Barriers Compared.

Sawtooth barrier is 10 nm wide at the base, step barrier is 10 nm wide. Both are 0.33 eV high.

Figure a. Effective mass is uniform and equal to m_0. Curve 1 is for the sawtooth, Curve 2 is for the step barrier.

Figure b. Barriers are made of GaAs-Al(0.4)Ga(0.6)As. Effective mass is 0.0636 in GaAs, 0.0871 in Al(0.4)Ga(0.6)As. Curve 0 is for step barrier, Curve 1 is for the sawtooth.

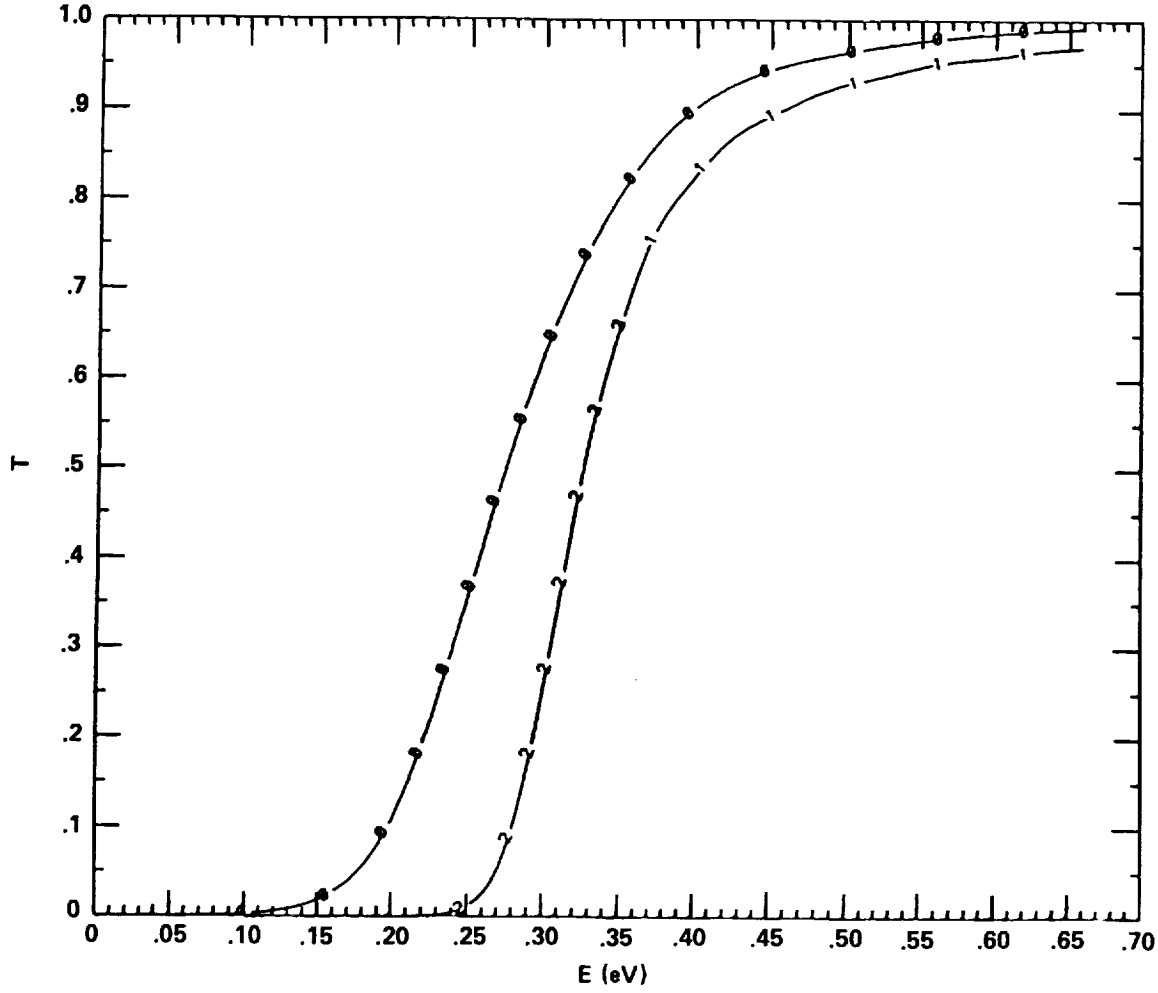

52. T-E Curves for GaAs-Al(0.4)Ga(0.6)As Sawtooth Barriers: Influence of the Effective Mass.

Both barriers are 10 nm wide at the base and are 0.33 eV high. Curve 0 is for GaAs-Al(0.4)Ga(0.6)As with effective mass variations taken account of, and Curve 1 is for effective mass uniform and equal to m_0. Note the similarity between the two curves, as opposed to the same data for step barriers.

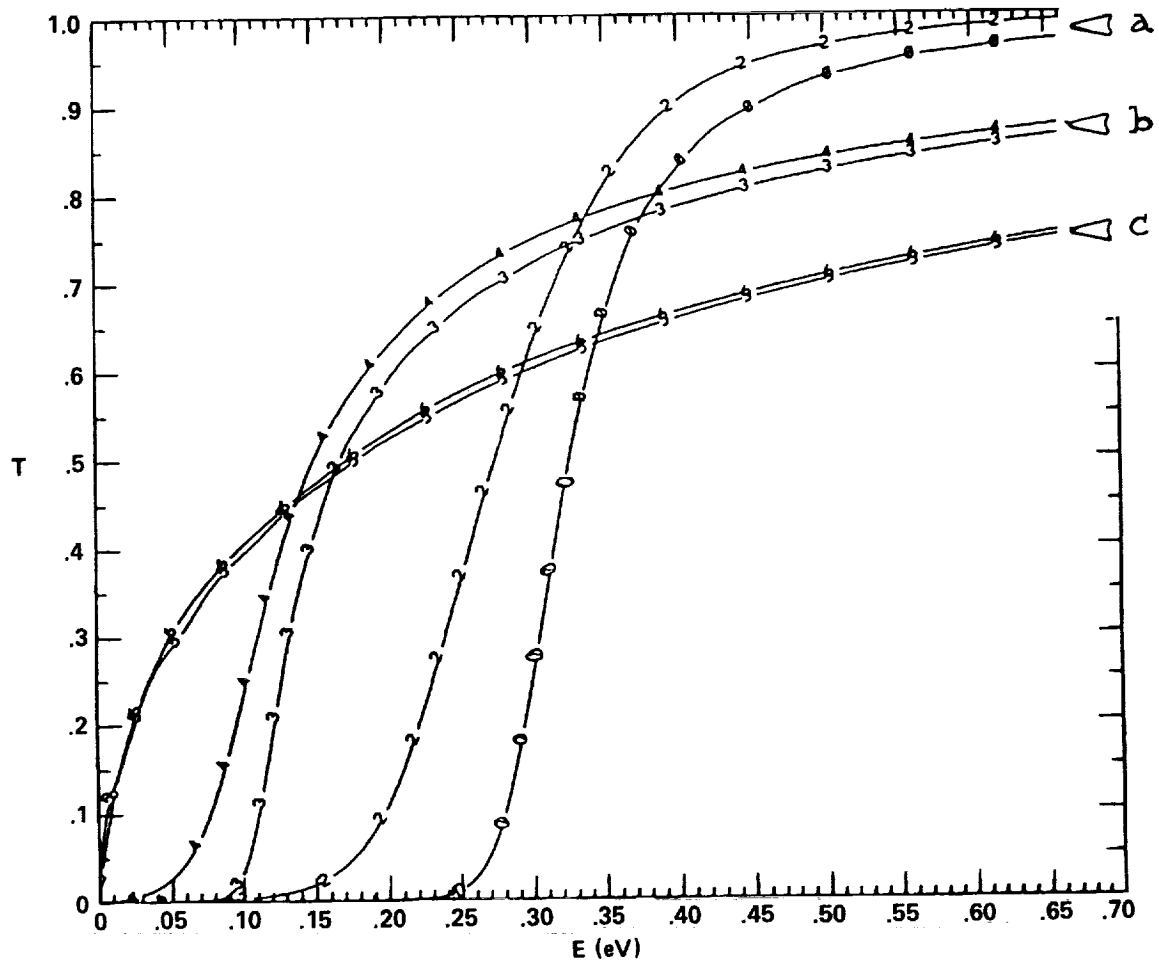

53. T-E Curves for Sawtooth Single Step Barriers: Influence of Effective Mass and Applied Electric Field Strength.

All data is for barriers 10 nm wide at the base and 0.33 eV high. Curve 0: F_{ap} = 0, m_{eff} = m_0. Curve 2: F_{ap} = 0, GaAs-Al(0.4)Ga(0.6)As Curve 3: F_{ap} = 0.02 eV/nm, m_{eff} = mo. Curve 4: F_{ap} = 0.02 eV/nm, GaAs-Al(0.4)Ga(0.6)As Curve 5: F_{ap} = 0.05 eV/nm, m_{eff} = m_0. Curve 6: F_{ap} = 0.05 eV/nm, GaAs-Al(0.4)Ga(0.6)As

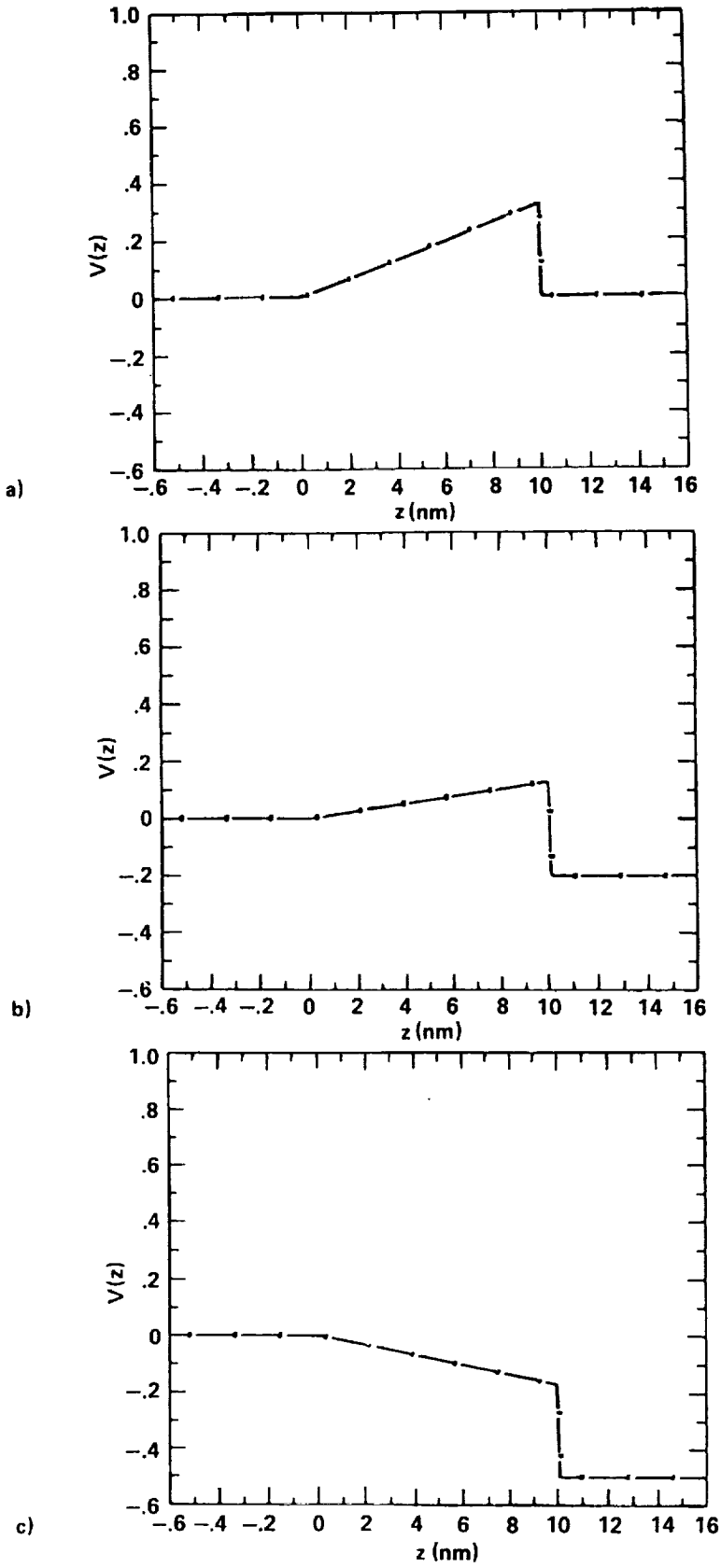

54. Deformation of Single Sawtooth Barrier under Applied Electric Field. The shape of the barrier under F_{ap} = 0, 0.02, and 0.05 eV/nm is shown in Figures a, b, and c, respectively. At F_{ap} = 0.05 eV/nm the barrier is actually a staircase.

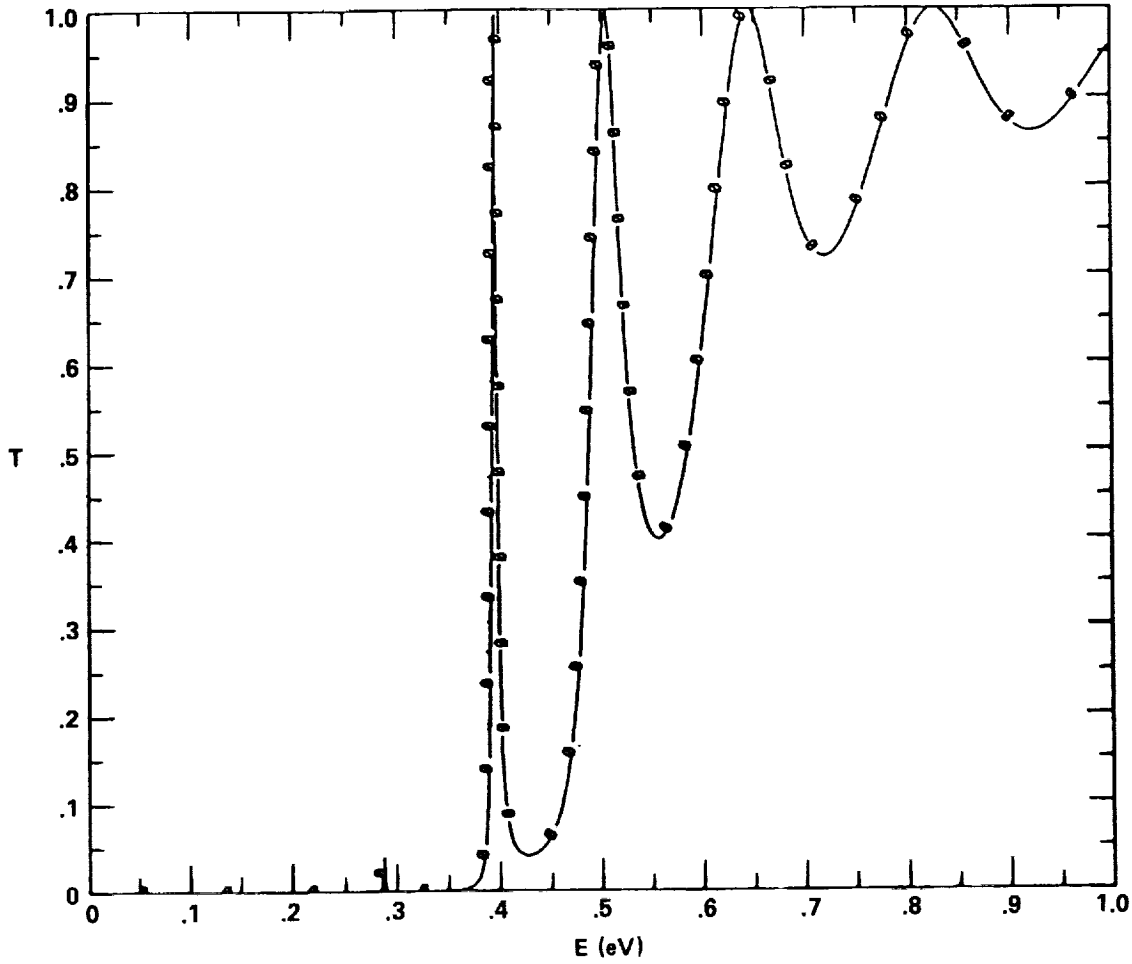

55. T-E Curve for Two-Barrier Sawtooth Superlattice

Bases are 4.5 nm wide, heights are 0.5 eV. Effective mass is uniform and equal to m_0.

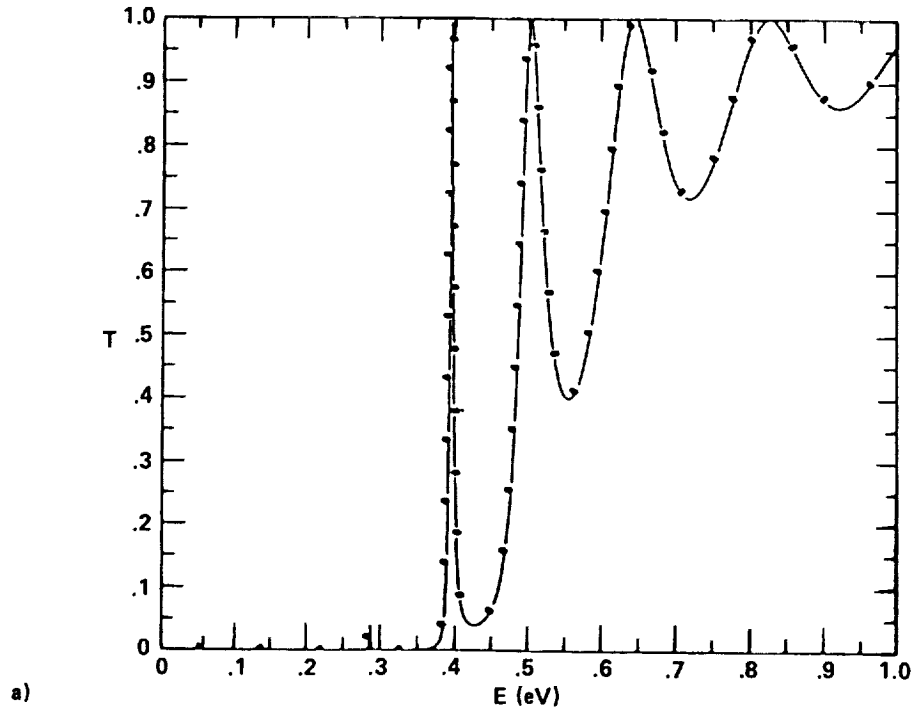

a)

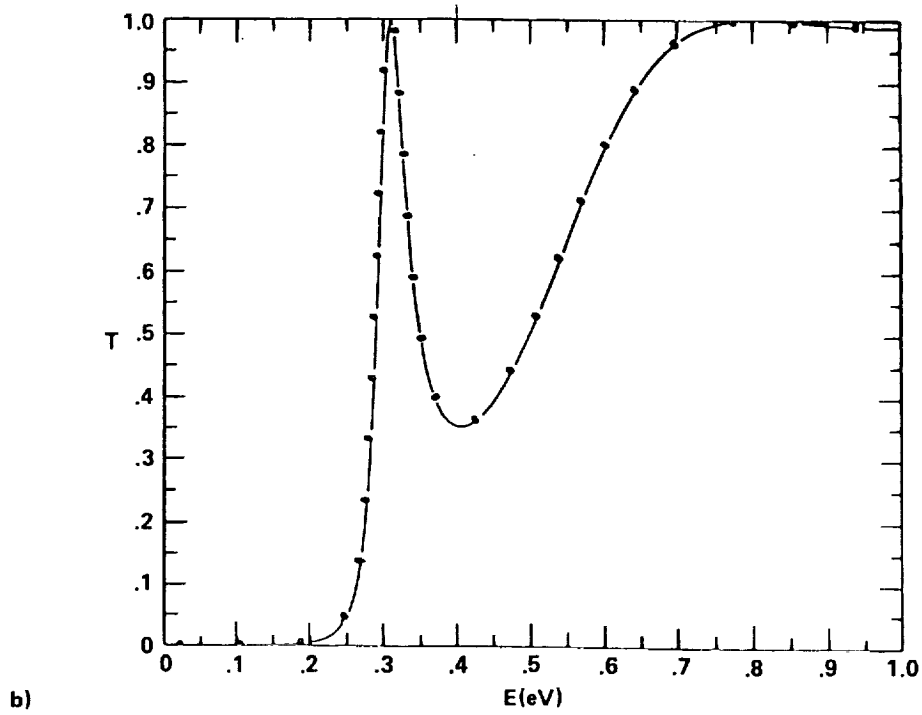

b)

56. T-E Curves for Two-Barrier Sawtooth Superlattices: Influence of Effective Mass.

Bases are 4.5 nm wide, heights are 0.5 eV. Figure a is for $m_{eff} = m_0$, Figure b is for GaAs-Al(0.5)Ga(0.5)As superlattice.

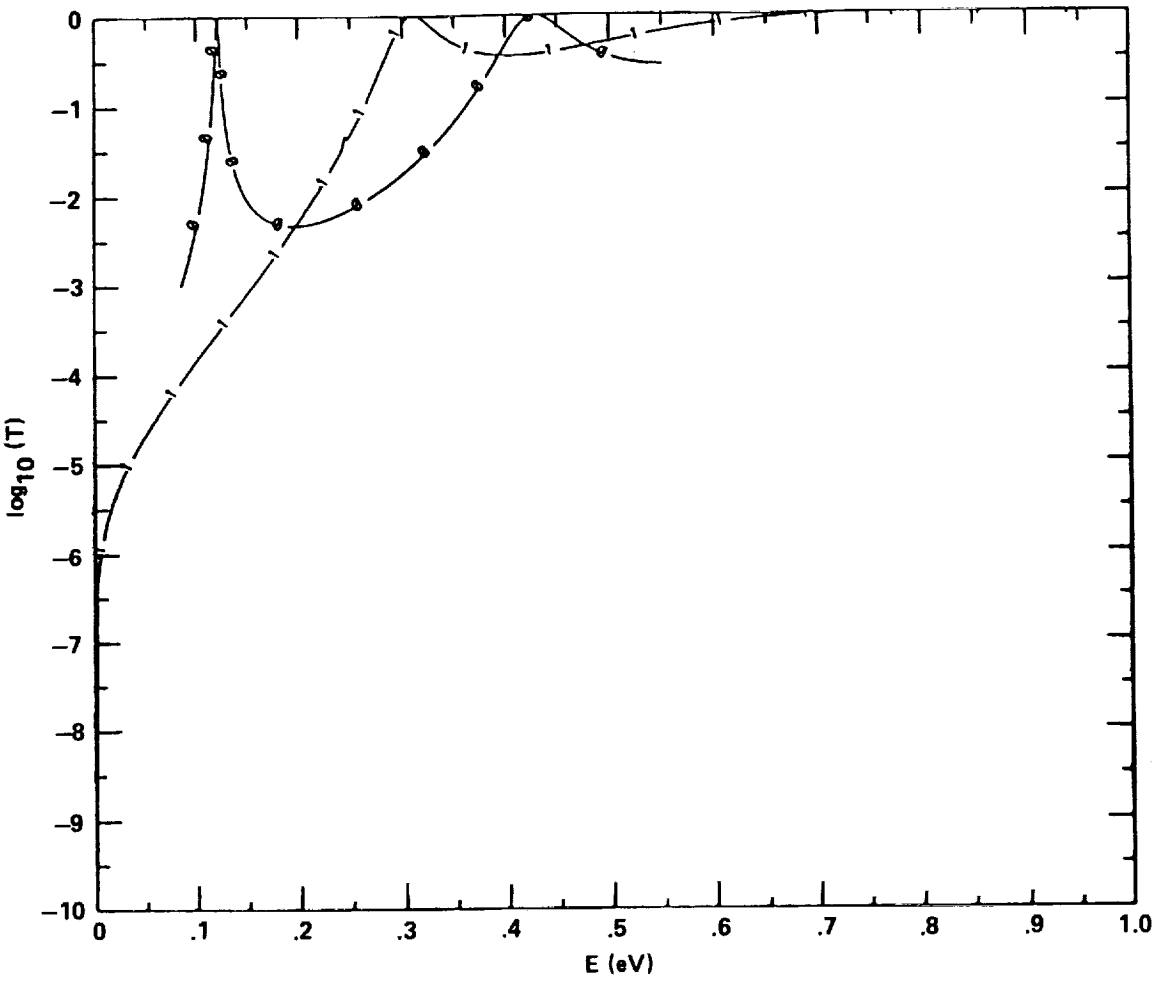

57. T-E Curves for Sawtooth and Step Two-Barrier GaAs-Al(0.5)Ga(0.5)As Superlattices.

Curve 0: MSB with barriers 2 wide, 5 nm apart, and 0.5 eV high

Curve 1: Sawtooth superlattice with 4.5 nm wide bases.

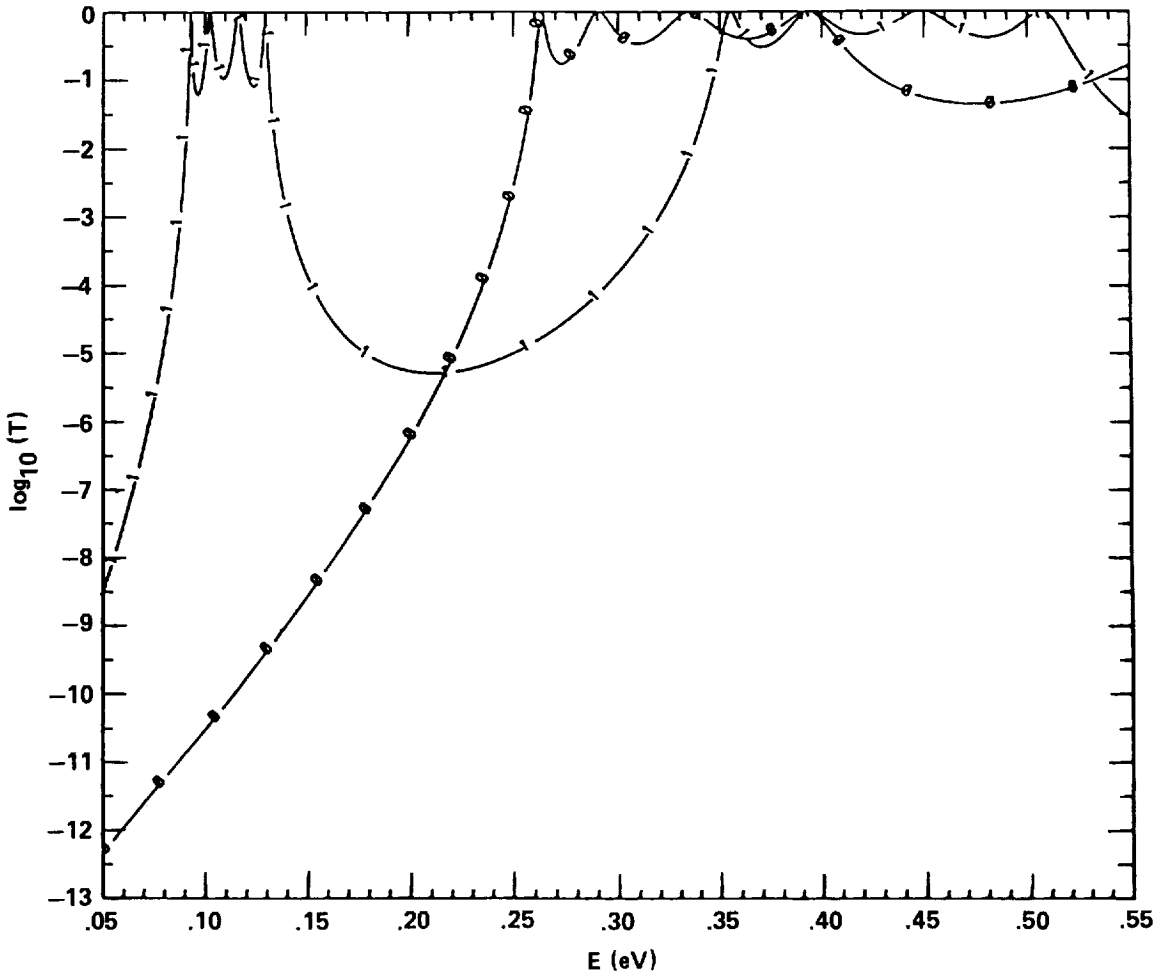

58. T-E Curves for Sawtooth and Step Five-Barrier GaAs-Al(0.5)Ga(0.5)As Superlattices.

Curve 0: Sawtooth superlattice with 4.5 nm wide bases.

Curve 1: MSB with barriers 2 wide, 5 nm apart, and 0.5 eV high

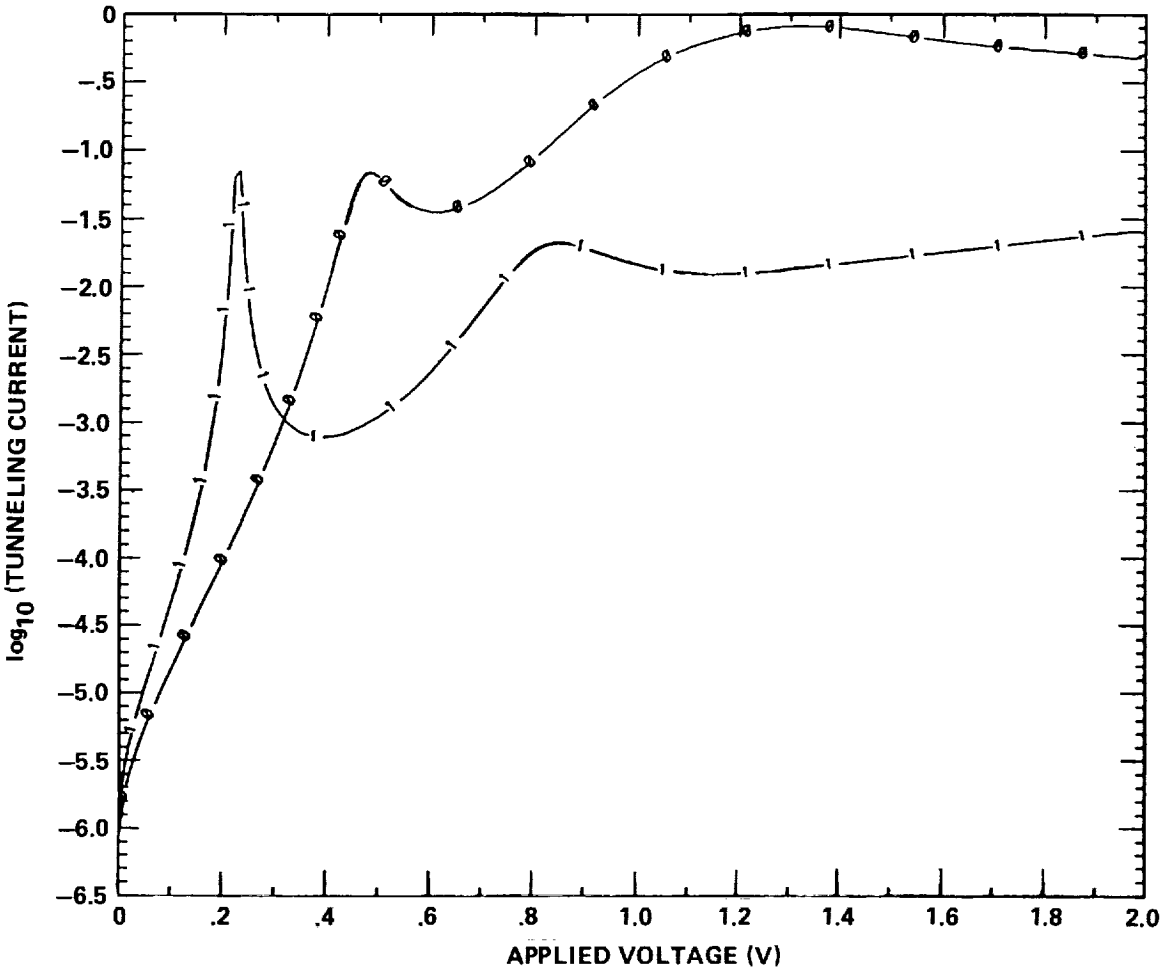

59. J-V Curves for Two-Barrier GaAs-Al(0.5)Ga(0.5)As Sawtooth and Step Superlattices.

Curve 0: Sawtooth superlattice with 4.5 nm bases, 0.5 eV high

Curve 1: MSB with barriers 2 nm wide, 5 nm apart, 0.5 eV high

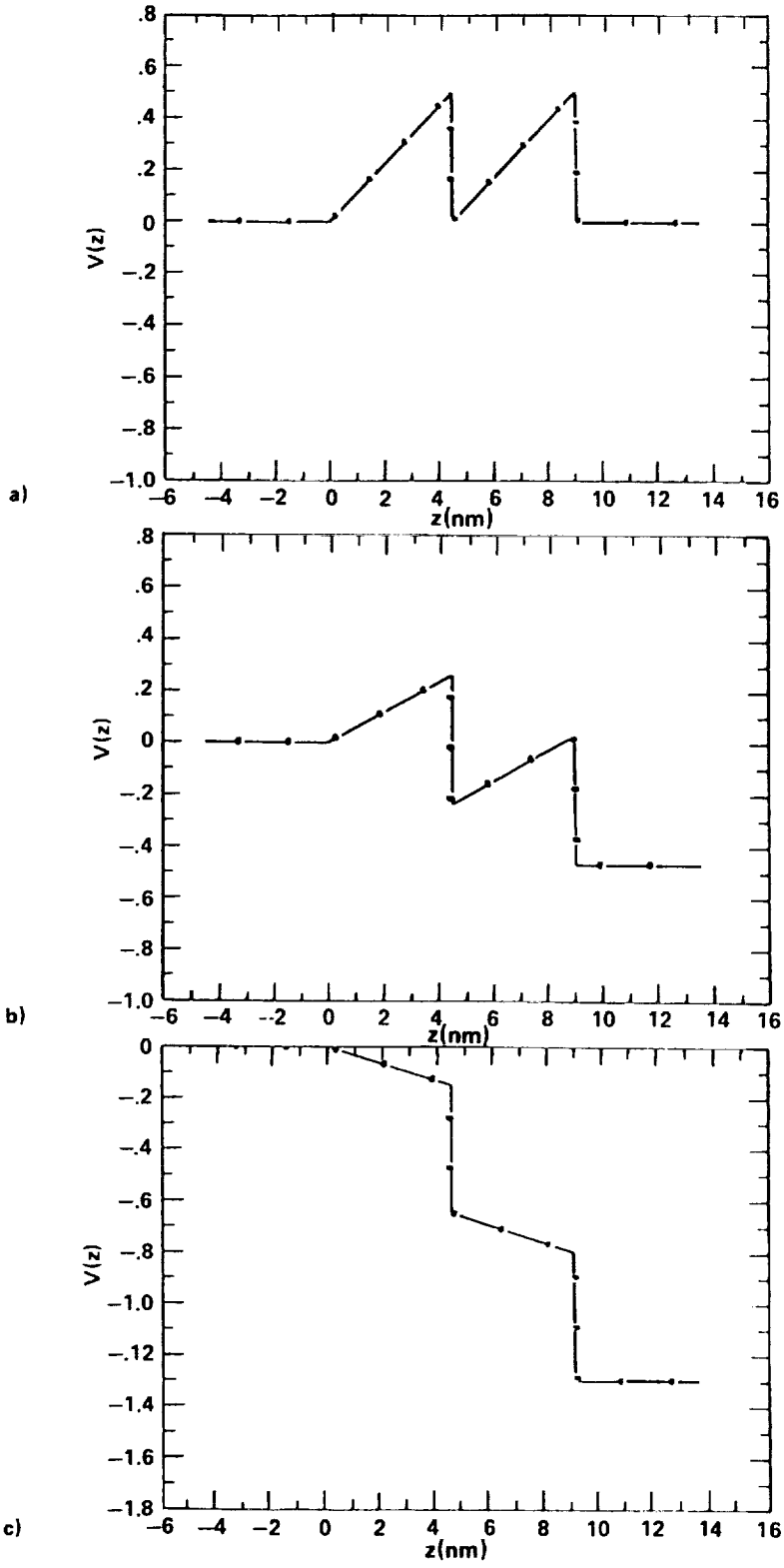

60. Deformation of Two-Barrier Sawtooth Superlattice under Applied Electric Field.

In Figures a, b, and c the applied field strength F_{ap} is 0, 0.02 and 0.05 eV/nm, respectively. At F_{ap} = 0.05 eV/nm the structure is a staircase.

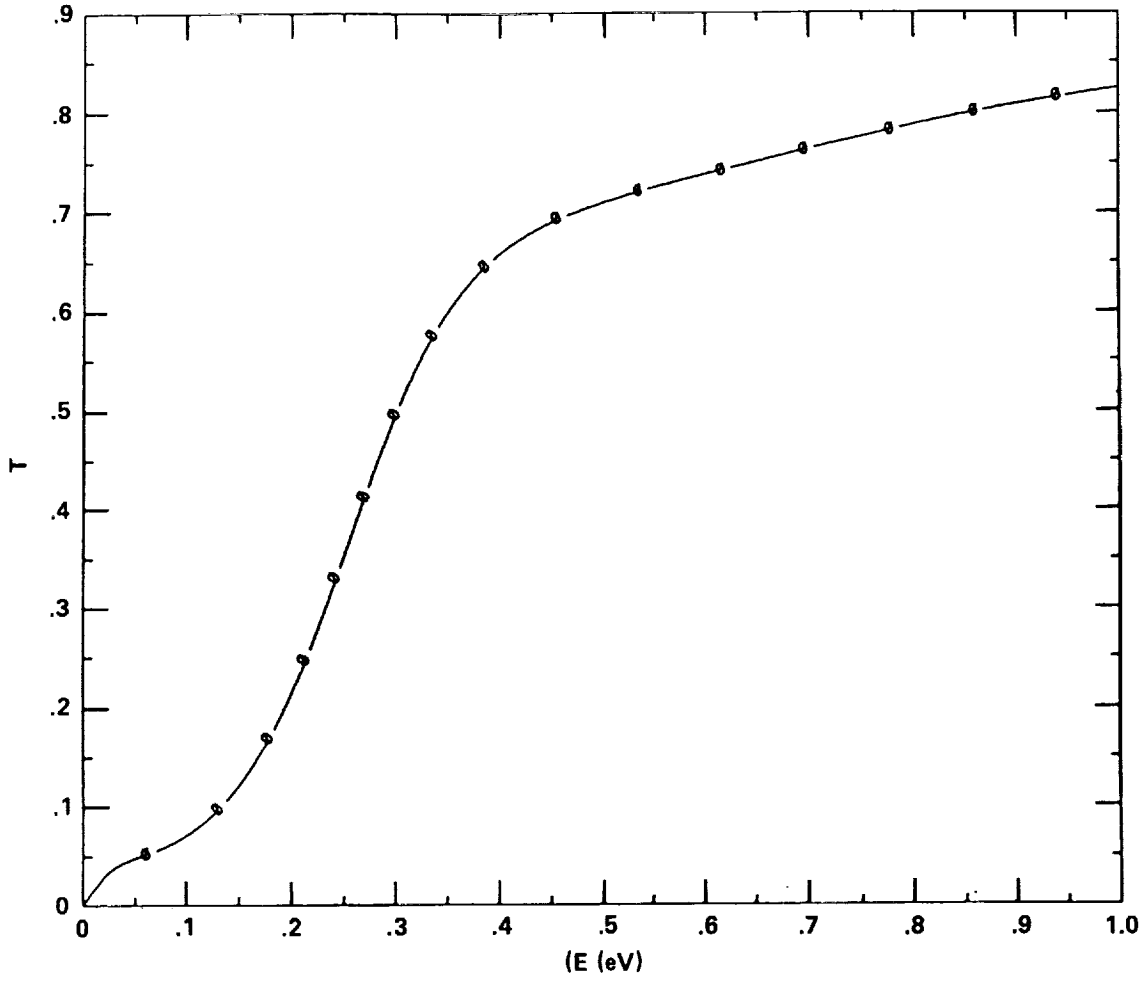

61. T-E Curve for Two-Barrier GaAs-Al(0.5)Ga(0.5)As Superlattice

Bases are 4.5 nm wide, heights are 0.5 eV. The applied field strength is 0.052 eV/nm (applied voltage = 0.47 V).

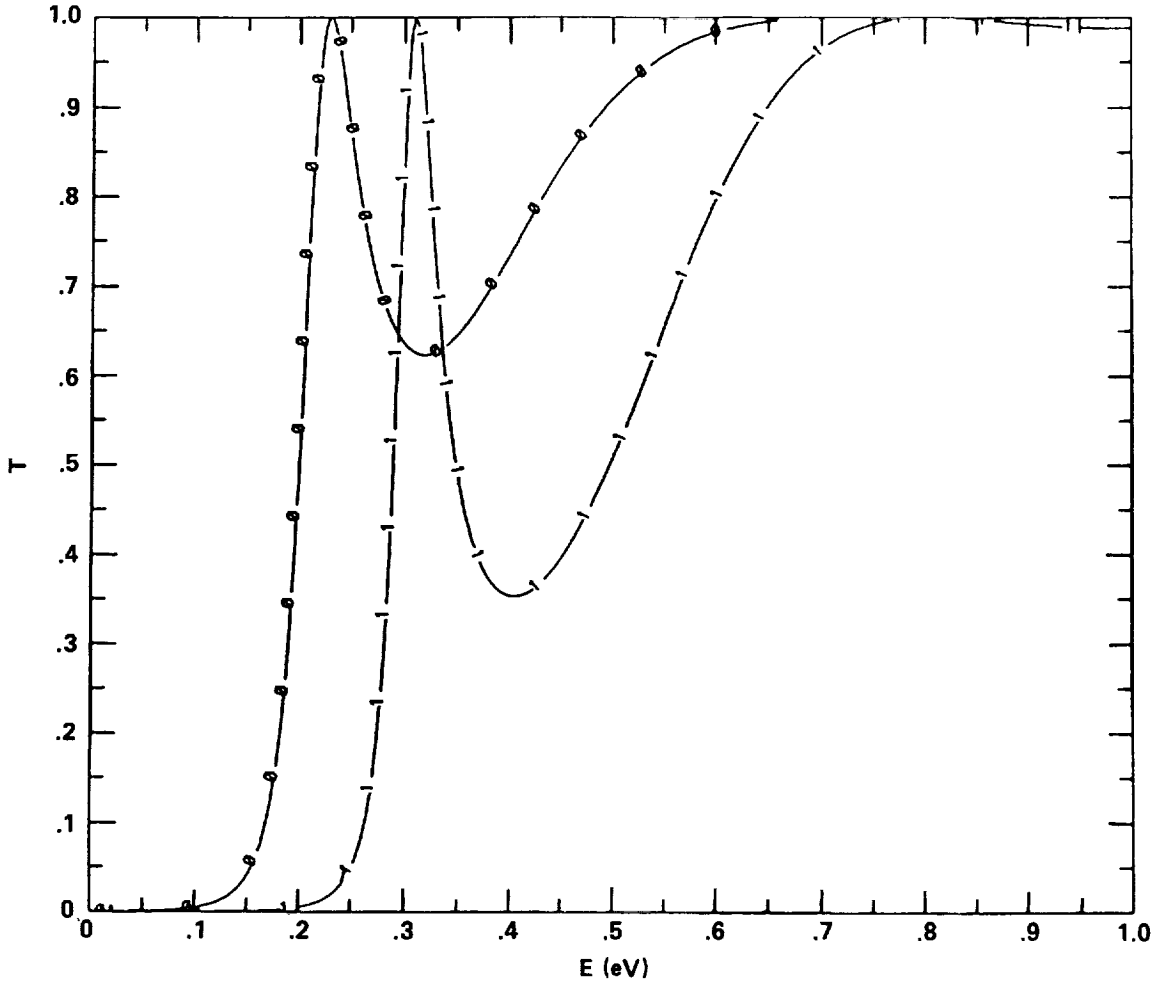

62. T-E Curves for Two-Barrier Sawtooth Superlattices: Effects of Composition. Data for GaAs-Al(0.4)Ga(0.6)As and GaAs-Al(0.5)Ga(0.5)As superlattices are shown in Curves 0 and 1 respectively. Bases are 4.5 nm wide.

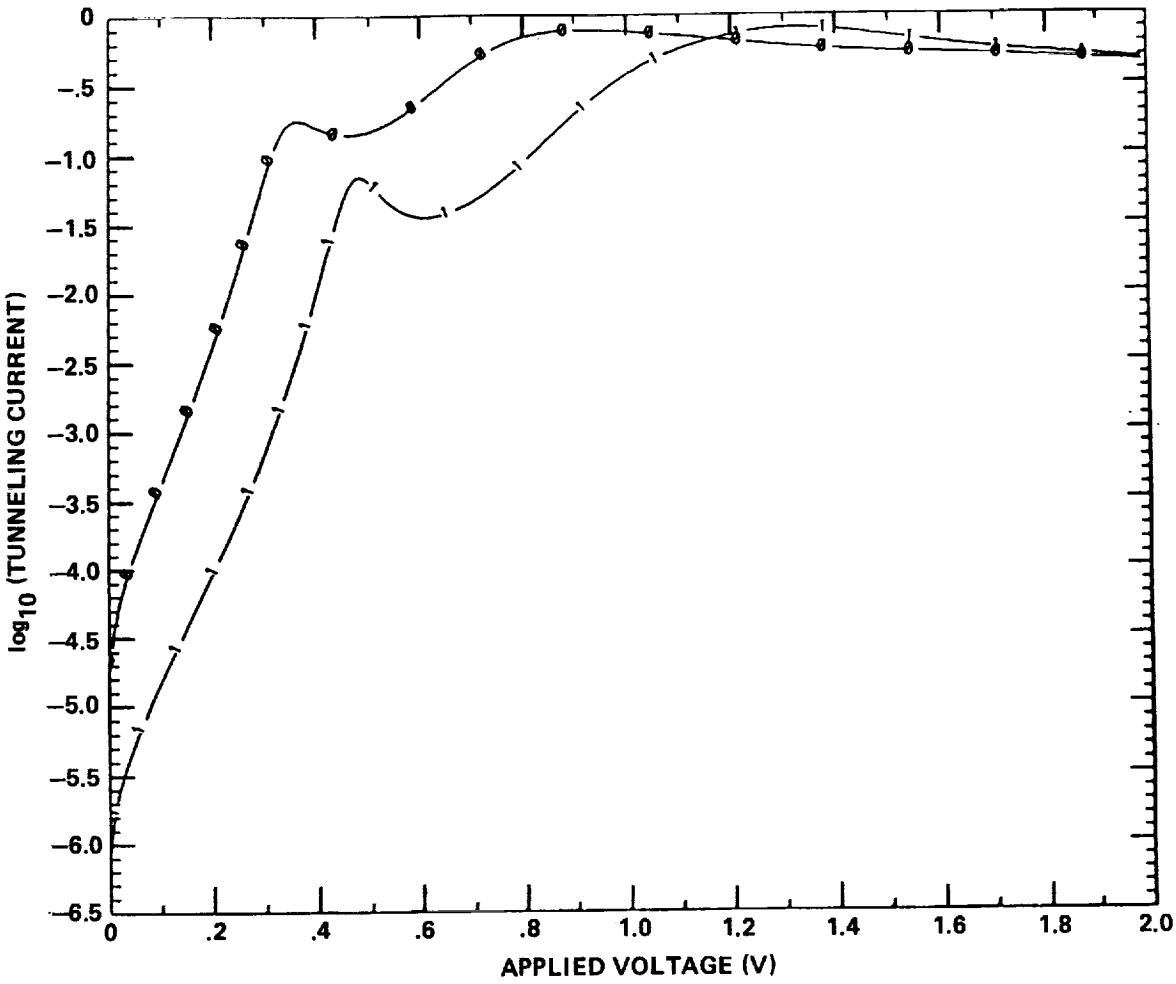

63. J-V Curves for Two-Barrier Sawtooth Superlattices: Effects of Composition. Data for GaAs-Al(0.4)Ga(0.6)As and GaAs-Al(0.5)Ga(0.5)As superlattices are shown in Curves 0 and 1, respectively. Bases are 4.5 nm wide.

APPENDIX

The tunneling calculations of the present study use the programs in this appendix. All of the programs are based on the transfer matrix method described in Section 2.B.; their structure actually differs very little from program to program. These programs are written in VAX FORTRAN, and are compiled using the G_FLOAT option, which allows computations involving numbers roughly as large as 10^{308}. This proves necessary in programs calculating resonance spectra and tunneling current voltage curves for superlattices longer than 10 nm or so.

The transmission resonance programs are: ZIGGURAT; ZIGGEFFMASS; MSB; ALMSB; SAWTOOTH, and ALSTAIR. To calculate transmission resonance spectra, the incident energy is varied in small steps in a do-loop. The shape of the potential is determined from input parameters of barrier composition, number, height and width, and from the applied electric field strength. The potential is divided into many small steps of constant potential and effective mass. The transfer matrix, denoted by T in the code, is initialized as the unit matrix. In the main program, the position z_i, wave numbers k_i and k_{i+1}, and effective masses m_i and m_{i+1}, are calculated at each step. These values are passed to a subroutine, EFFMASSTEP (or STPTRN if the effective mass is taken as uniform and equal to m_0), where the transfer matrix at the step is computed, multiplied by the product of the transfer matrices at all preceding steps, and the accumulated T is returned to the main program. After this has been done at each step in the superlattice, the total accumulated transfer matrix element T_{11} is used to calculate the transmission coefficient (equation 18). This value is deposited with the corresponding incident energy E in an output file from which T-E plots are made.

Tunneling current-voltage programs are: JVMSB, JVALMSB, JVSAWTOOTH, and JVALSTAIR. To calculate J-V curves, a single incident energy is chosen, 0.005 eV in this study. The applied voltage over the structure is varied within a do-loop in steps of 0.01 V, from 2 V to zero. Inside the do-loop, the operation of the program is very similar to that of the T-E programs: the potential shape is calculated from input parameters and divided into steps, the transfer matrix calculated at each step, inside the subroutines EFFMASSTEP or STPTRN, and the accumulated transfer matrix returned to the main program. After the last step, the tunneling current is calculated from T_{11} according to equation 20, and deposited with the corresponding value of V in an output file for plotting.

The program WELL is used to calculate the bound states in a single quantum well where the effective mass is uniform and equal to m_0. The programs for calculating the bound states in single GaAs-$Al_xGa_{(1-x)}As$ quantum wells are ALGAASWELL and STARKMASS. WELL and ALGAASWELL are used to calculate the bound states under zero applied field, while STARKMASS is used to find the Stark shift of those states under non-zero, localized electric

fields. These programs are almost identical to those used to calculate T-E curves for step barriers. The differences are that the energies are negative, i.e. $V_0<E<0$; then $|\log_{10}(T_{11})|$ (where T_{11} is from the total transfer matrix accumulated inside and outside the well) is simply deposited with it's corresponding energy in an output file.

To calculate the Stark shift in a GaAs-$Al_xGa_{(1-x)}As$ quantum well under an extended electric field, the program AIRYWELL is used. In this program the Airy function solutions of the Schroedinger equation inside and outside the well are calculated from the input values of the well width and depth and applied field strength. The values of x, the argument of the Airy functions, defined by equation 72, are calculated at the well edges. The Airy functions are obtained from the IMSL, Incorporated, special function library SFUN/LIBRARY. Matching wavefunctions and derivatives at the well edges gives the wavefunction coefficients to the left of (C and D) and inside (P and Q) the well. From these and from R, S, T and U, the ratios of Airy functions evaluated at the well edges, the components F and E are calculated from the relation:

$$F/E = (C/D * (S-P) + T - Q) / (U * (C/D * P + Q) - R * (C/D * S + T))$$

This is equivalent to equation 86 in the text. This calculation is done inside a do-loop which varies the energy in steps equal to 0.001 times the zero-field well depth plus the applied voltage across the well. Then $|\log_{10}(F/E)|$ and the corresponding value of energy are stored in an array. In this program an NCAR graphics subroutine is used to obtain plots from the data array.

```
      SUBROUTINE  STPTRN ( E, VL, VR, FK, Z, T1)
C
C     This subroutine computes the accumulated transfer matrix TR
C     through a potential step, where the wavenumber changes from AKL
C     on the left, to AKR on the right, at position Z.
C
      IMPLICIT REAL*8 (A-H, O-Z)
      DIMENSION T1(4), T2(4), TR(4), EX(4)
      COMPLEX*16 AKL, AKR, T1, T2, TR, EX
      PSILON = 10E-7
      DIFFL = (E - VL)
      DIFFR = (E - VR)
      IF (ABS(DIFFL) .LT. PSILON) DIFFL = SIGN(PSILON,DIFFL)
      IF (ABS(DIFFR) .LT. PSILON) DIFFR = SIGN(PSILON,DIFFR)
      AKL = FK*DIFFL
      AKL = SQRT(AKL)
      AKR = FK*DIFFR
      AKR = SQRT(AKR)
      EX(1) = (0,1.0) * (AKR - AKL) * Z
      EX(2) = (0, -1.0) * (AKR - AKL) * Z
      EX(3) = (0, -1.0) * (AKR + AKL) * Z
      EX(4) = (0,1.0) * (AKR + AKL) * Z
      T2(1) = 0.5 * (1 + AKR/AKL) * EXP(EX(1))
      T2(2) = 0.5 * (1 + AKR/AKL) * EXP(EX(2))
      T2(3) = 0.5 * (1 - AKR/AKL) * EXP(EX(3))
      T2(4) = 0.5 * (1 - AKR/AKL) * EXP(EX(4))
      TR(1) = T1(1)*T2(1) + T1(3)*T2(4)
      TR(2) = T1(4)*T2(3) + T1(2)*T2(2)
      TR(3) = T1(1)*T2(3) + T1(3)*T2(2)
      TR(4) = T1(4)*T2(1) + T1(2)*T2(4)
      T1(1) = TR(1)
      T1(2) = TR(2)
      T1(3) = TR(3)
      T1(4) = TR(4)
400   RETURN
      END
```

```
      SUBROUTINE EFFMASSTEP ( E, VL, VR, ML, MR, FK, Z, T1)
C
C     This subroutine computes the accumulated transfer matrix TR
C     through a potential step, where the wavenumber changes from AKL
C     on the left, to AKR on the right, at position Z.
C
      IMPLICIT REAL*8 (A-H, O-Z)
      DIMENSION T1(4), T2(4), TR(4), EX(4)
      COMPLEX*16 AKL, AKR, T1, T2, TR, EX
      REAL*8  ML, MR
      PSILON = 10E-7
      DIFFL = (E - VL)
      DIFFR = (E - VR)
      IF (ABS(DIFFL) .LT. PSILON) DIFFL = SIGN(PSILON,DIFFL)
      IF (ABS(DIFFR) .LT. PSILON) DIFFR = SIGN(PSILON,DIFFR)
      AKL = FK * ML * DIFFL
      AKL = SQRT(AKL)
      AKR = FK * MR * DIFFR
      AKR = SQRT(AKR)
      EX(1) = (0,1.0) * (AKR - AKL) * Z
      EX(2) = (0, -1.0) * (AKR - AKL) * Z
      EX(3) = (0, -1.0) * (AKR + AKL) * Z
      EX(4) = (0,1.0) * (AKR + AKL) * Z
      RAT = ML / MR
      RAT = SQRT(RAT)
      T2(1) = 0.5 * RAT * (1 + AKR/AKL) * EXP(EX(1))
      T2(2) = 0.5 * RAT * (1 + AKR/AKL) * EXP(EX(2))
      T2(3) = 0.5 * RAT * (1 - AKR/AKL) * EXP(EX(3))
      T2(4) = 0.5 * RAT * (1 - AKR/AKL) * EXP(EX(4))
      TR(1) = T1(1)*T2(1) + T1(3)*T2(4)
      TR(2) = T1(4)*T2(3) + T1(2)*T2(2)
      TR(3) = T1(1)*T2(3) + T1(3)*T2(2)
      TR(4) = T1(4)*T2(1) + T1(2)*T2(4)
      T1(1) = TR(1)
      T1(2) = TR(2)
      T1(3) = TR(3)
      T1(4) = TR(4)
400   RETURN
      END
```

```
                        PROGRAM ZIGGURAT
C       This program finds the transmission coefficient T for an
C       incident plane wave of energy E on an asymmetric step potential
C       where the potential gradient (V1-V2) is broken into a series of
C       any desired number of steps NST. The initial and final
C       potential values V0 and VF are arbitrary.
C
C
        IMPLICIT REAL*8 (A-H,O-Z)
        DIMENSION T1(4)
        COMPLEX*16 T1
        FK = 26.2451
        PRINT*, 'ENTER V1 IN eV (V1 is the barrier height)'
        READ*, V1
        PRINT*, 'ENTER TOTAL BARRIER WIDTH BW IN nm'
        READ*, BW
        PRINT*, 'ENTER THE APPLIED FIELD STRENGTH F IN eV/nm'
        READ*, F
        PRINT*, 'ENTER DESIRED NUMBER OF STEPS NST'
        READ*, NST
        Z0 = 0
        V0 = 0
        DLTAV = F * BW
        V2 = V1 - DLTAV
        VF = V0 - DLTAV
        DLTAV = DLTAV / NST
        DLTAZ = BW / NST
        TYPE*, DLTAZ
        PRINT 10, 'E(eV)', 'T'
10      FORMAT ( //,1X, A7, 1X, A5, 1X, / 1X, 20('=') )
        OPEN (UNIT = 16, FILE = 'ZIGGURAT.DAT', STATUS = 'NEW')
C
C       Here starts the energy loop
C
        DO 20 NE = 1, 2000
          EDIV = V1 / 2000
          Z = Z0
          E = 1.5 * V1 - (NE * EDIV)
          T1(1) = ( 1.0, 0.0 )
          T1(2) = ( 1.0, 0.0 )
          T1(3) = ( 0.0, 0.0 )
          T1(4) = ( 0.0, 0.0 )
          CALL STPTRN(E,V0,V1,FK,Z,T1)
c
c       This takes care of the leading edge of the barrier.Now a loop
c       inside the barrier will handle the potential drop V1-V2.
c
           IF (DLTAV .EQ. 0) THEN
             Z = Z0 + BW
             VL = V2
             VR = VF
             CALL STPTRN(E,VL,VR,FK,Z,T1)
             GO TO 29
           END IF
           DO I = 1, (NST - 1)
            Z = Z + DLTAZ
            VL = V1 - (I - 1) * DLTAV
            VR = VL - DLTAV
```

```
            CALL STPTRN(E,VL,VR,FK,Z,T1)
           END DO
C
c          Now the transfer matrix through the trailing edge of the barrier
c          is found and multiplied by the accumulated T-matrix.
c
28          VL = VR
            VR = VF
            CALL STPTRN(E,VL,VR,FK,Z,T1)
C
C            the control passes to statement 29 from the block IF
C            above which handles the case of zero-field
C
29          T = ABS(T1(1))**2
            T = 1.0 / T
            PRINT 30, E,T
30          FORMAT (F7.2,E12.3)
            WRITE (16,300) E, T
300         FORMAT (2E15.7)
20          CONTINUE
21          END
```

```
                        PROGRAM ZIGGEFFMASS
C
C       This program finds the transmission coefficient T for an
C       incident plane wave of energy E on an asymmetric step potential
C       where the potential gradient (V1-V2) is broken into a series of
C       any desired number of steps NST. The applied field F is
C       arbitrary and determines the barrier shape. The effective mass
C       takes an abrupt jump at the edges of the barrier from mx to my,
C       determined by the aluminum contents x and y put in by the
C       operator. This program has the output file ZIGGEFFMASS.DAT.
C
C
        IMPLICIT REAL*8 (A-H,O-Z)
        REAL*8 M1, M2
        DIMENSION T1(4)
        COMPLEX*16 T1
        FK = 26.2451
        PRINT*, 'ENTER BARRIER HEIGHT V1 IN eV'
        READ*, V1
        PRINT*, 'ENTER THE APPLIED FIELD STRENGTH F IN eV/nm'
        READ*, F
        PRINT*, 'ENTER TOTAL BARRIER WIDTH BW IN nm'
        READ*, BW
        PRINT*, 'ENTER DESIRED NUMBER OF STEPS NST'
        READ*, NST
        PRINT*,'ENTER Al CONTENT X OF NARROW GAP MATERIAL'
        READ*, X
        PRINT*,'ENTER Al CONTENT Y OF WIDE GAP MATERIAL'
        READ*, Y
        Z0 = 0
        V0 = 0
        VAP = F * BW
        V2 = V1 - VAP
        VF = V0 - VAP
        M1 = 0.0636 + 0.0552 * X + 0.0092 * X**2
        M2 = 0.0636 + 0.0552 * Y + 0.0092 * Y**2
        PRINT*, 'THIS FIELD RESULTS IN V2=',V2,'AND VF=',VF
        DLTAV = (V1 - V2)
        IF (NST.EQ.1) GO TO 6
        DLTAV = DLTAV/(NST-1)
6       TYPE*, DLTAV
        DLTAZ = BW/NST
        TYPE*, DLTAZ
        OPEN (UNIT = 18, FILE = 'ZIGGEFFMASS.DAT', STATUS = 'NEW')
        PRINT 10, 'E(eV)', 'T'
10      FORMAT ( //,1X, A7, 1X, A5, 1X, / 1X, 20('=') )
C
C       Here starts the energy loop
C
        DO 20 NE = 1, 2000
          EDIV = V1/2000
          Z = Z0
          E = 1.5 * V1 - (NE * EDIV)
          T1(1) = ( 1.0, 0.0 )
          T1(2) = ( 1.0, 0.0 )
          T1(3) = ( 0.0, 0.0 )
          T1(4) = ( 0.0, 0.0 )
          CALL EFFMASSTEP(E,V0,V1,M1,M2,FK,Z,T1)
```

```
            Z = Z + DLTAZ
c
c         This takes care of the leading edge of the barrier.Now a loop
c         inside the barrier will handle the potential drop V1-V2.
c
              IF (DLTAV .EQ. 0) THEN
                Z = Z0 + BW
                VL = V2
                VR = VF
                CALL EFFMASSTEP(E,VL,VR,M2,M1,FK,Z,T1)
                GO TO 29
              END IF
              DO 25 VI = V1,V2+DLTAV,-(DLTAV)
               VL = VI
               VR = VI - DLTAV
               CALL EFFMASSTEP(E,V1,VR,M2,M2,FK,Z,T1)
               Z = Z + DLTAZ
25             CONTINUE
c
c          Now the transfer matrix through the trailing edge of the barrier
c          is found and multiplied by the accumulated T-matrix.
c
28          VL = V2
            VR = VF
            CALL EFFMASSTEP(E,VL,VR,M2,M1,FK,Z,T1)
C
C            the control passes to statement 29 from the block IF
C            above which handles the case of zero-field
C
29          T = ABS(T1(1))**2
            T = 1.0/T
            PRINT 30, E,T
30          FORMAT (F7.2,E12.3)
            WRITE (18,300) E, T
300         FORMAT (2E15.6)
20          CONTINUE
21          END
```

```
                        PROGRAM  MSB
C       The program ALMSB finds the transmission coefficient T as
C       a function of incident plane wave energy E for multiple
C       step potential barriers of height V1, width BW, separation
C       DSEP, and total number NTEETH for AlGaAs-GaAs. Applied field
C       F = 0. Effective mass varies in wells and barriers. Data are
C       written into output file MSB.DAT
C
        IMPLICIT REAL*8 (A-H,O-Z)
        DIMENSION T1(4)
        COMPLEX*16 T1
        FK = 26.2451
        V0 = 0.0
        Z0 = 0.0
        PRINT*, 'ENTER BARRIER HEIGHT V1 IN eV'
        READ*, V1
        PRINT*, 'ENTER BARRIER WIDTH, BW, AND SEPARATION DSEP IN nm.'
        READ*, BW, DSEP
        PRINT*, 'HOW MANY BARRIERS ARE THERE ? (NTEETH)'
        READ*, NTEETH
        PRINT 10,'E(eV)','T'
10      FORMAT (//,1X,A7,1X,A5,1X,/,1X,20('='))
        OPEN ( UNIT = 11, FILE = 'ALMSB.DAT', STATUS ='NEW')
        DO 20 NE = 1,10000
          EDIV = V1 / 10000
          Z = Z0
          E = (1.10 * V1) - ( NE * EDIV)
          T1(1) = (1.0,0.0)
          T1(2) = (1.0,0.0)
          T1(3) = (0.0,0.0)
          T1(4) = (0.0,0.0)
          PERIOD = BW + DSEP
          DO 30 NST = 1, NTEETH
            CALL STPTRN(E,V0,V1,FK,Z,T1)
            Z = Z + BW
            CALL STPTRN(E,V1,V0,FK,Z,T1)
            Z = NST * PERIOD + Z0
30        CONTINUE
C
C         END TEETH LOOP
C
          T = ABS(T1(1))**2
          T = 1.0/T
          T = LOG10(T)
          WRITE (11,300) E,T
300       FORMAT (2E15.7)
          PRINT 35, E, T
35        FORMAT ( 2E12.3 )
20      CONTINUE
C
C       END OF E-LOOP
C
        END
```

```
                        PROGRAM  ALMSB
C       The program ALMSB finds the transmission coefficient T as
C       a function of incident plane wave energy E for multiple
C       step potential barriers of height V1, width BW, separation
C       DSEP, and total number NTEETH for AlGaAs-GaAs. Applied field
C       F = 0. Effective mass varies in wells and barriers.
C
        IMPLICIT REAL*8 (A-H,O-Z)
        REAL*8 MX, MY
        DIMENSION T1(4)
        COMPLEX*16 T1
        FK = 26.2451
        V0 = 0.0
        Z0 = 0.0
        PRINT*, 'ENTER BARRIER HEIGHT V1 IN eV'
        READ*, V1
        PRINT*, 'ENTER BARRIER WIDTH, BW, AND SEPARATION DSEP IN nm.'
        READ*, BW, DSEP
        PRINT*, 'HOW MANY BARRIERS ARE THERE ? (NTEETH)'
        READ*, NTEETH
        PRINT*,'Al CONCENTRATION IN BARRIERS, X,?'
        READ*, X
        PRINT*,'Al CONCENTRATION IN WELLS, Y,?'
        READ*, Y
        MX = 0.0636 + 0.0552 * X + (0.0092 * X**2)
        MY = 0.0636 + 0.0552 * Y + (0.0092 * Y**2)
        PRINT 10,'E(eV)','T'
10      FORMAT (//,1X,A7,1X,A5,1X,/,1X,20('='))
        OPEN ( UNIT = 11, FILE = 'ALMSB.DAT', STATUS ='NEW')
        DO 20 NE = 1,10000
          EDIV = V1/10000
          Z = Z0
          E = (1.10 * V1) - ( NE * EDIV)
          T1(1) = (1.0,0.0)
          T1(2) = (1.0,0.0)
          T1(3) = (0.0,0.0)
          T1(4) = (0.0,0.0)
          PERIOD = BW + DSEP
          DO 30 NST = 1, NTEETH
            CALL EFFMASSTEP(E,V0,V1,MY,MX,FK,Z,T1)
            Z = Z + BW
            CALL EFFMASSTEP(E,V1,V0,MX,MY,FK,Z,T1)
            Z = NST * PERIOD + Z0
30        CONTINUE
C
C       END TEETH LOOP
          T = ABS(T1(1))**2
          T = 1.0/T
          T = LOG10(T)
          WRITE (11,300) E,T
300       FORMAT (2E15.7)
          PRINT 35, E, T
35        FORMAT ( 2E12.3 )
20      CONTINUE
C
C       END OF E-LOOP
        END
```

```
                        PROGRAM SAWTOOTH
c
c
c       This program calculates the quantum mechanical transmission
c       coefficient through a series of sawtooth potential barriers
c       under an applied electic field resulting in a voltage drop
c       over the length of the entire barrier of VAP. This program
c       uses the subroutine STPTRN. A data file of T versus E is
c       generated in the output file SAWTOOTH.DAT.
c
c
        IMPLICIT REAL*8 (A-H, O-Z)
        DIMENSION T1(4)
        COMPLEX*16 T1
        FK = 26.2451
        Z00 = 0
        V00 = 0
        PRINT*, 'HOW MANY SAWTEETH, AND HOW WIDE ARE THEIR BASES IN nm ?'
        READ*, NTH, BSE
        PRINT*, 'HOW HIGH IS THE TRAILING EDGE OF EACH TOOTH (eV)?'
        READ*, V10
        EDIV = V10 / 2000
        PRINT*,'ENTER THE APPLIED FIELD IN eV/nm'
        READ*, F
        VAP = F * BSE * NTH
        IF (VAP .EQ. V10) VAP = (VAP + EDIV / 2)
        NST = 50 + NINT(ABS((-(VAP / NTH) + V10) / 0.01))
        DLTAZ = BSE / NST
        DLTAV = (-(VAP / NTH) + V10) / NST
        PRINT 10, 'E(eV)', 'T'
10      FORMAT (//, 1X, A7, 1X, A5, 1X, /, 1X, 20('='))
        OPEN(UNIT = 55, FILE = 'SAWTOOTH.DAT', STATUS = 'NEW')
        DO NE = 1, 2000
          E = 1.10 * V10 -  (NE * EDIV)
          T1(1) = (1.0,0.0)
          T1(2) = (1.0,0.0)
          T1(3) = (0.0,0.0)
          T1(4) = (0.0,0.0)
          DO NT = 1, NTH
            V0 = V00 - (VAP / NTH) * (NT - 1)
            Z = Z00 + (NT - 1) * BSE
            DO I = 1, NST
              VL = V0 + (I - 1) * DLTAV
              VR = VL + DLTAV
              CALL STPTRN(E, VL, VR, FK, Z, T1)
              Z = Z + DLTAZ
            END DO
            VL = VR
            VR = V00 - (VAP / NTH) * NT
            CALL STPTRN(E, VL, VR, FK, Z, T1)
          END DO
          T = ABS(T1(1))**2
          T = (1.0 / T)
          T = LOG10(T)
          PRINT 100, E, T
100       FORMAT (F7.2, E12.4)
          WRITE (55,200) E,T
200       FORMAT (2E15.8)
```

```
END DO
END
```

```
                        PROGRAM ALSTAIR
c
c
c       This program calculates the quantum mechanical transmission
c       coefficient through a series of sawtooth potential barriers
c       under an applied electic field resulting in a voltage drop
c       over the length of the entire barrier of VAP. This program
c       uses the subroutine EFFMASSTEP. It takes into
c       account the changes in effective mass of the electron in each
c       layer in the superlattice structure. it is intended for use
c       in the alas-gaas system. (compare to esaki-tsu)
c
c
        IMPLICIT REAL*8 (A-H, O-Z)
        DIMENSION T1(4)
        COMPLEX*16 T1
        REAL*8 MMIN,MMAX,ML,MR
        FK = 26.2451
        V00 = 0
        Z00 = 0
        PRINT*, 'HOW MANY SAWTEETH, AND HOW WIDE ARE THEIR BASES IN nm ?'
        READ*, NTH, BSE
        PRINT*, 'HOW HIGH IS THE TRAILING EDGE OF EACH TOOTH (eV)?'
        READ*, V10
        EDIV = V10 / 2000
        PRINT*, 'WHAT IS THE APPLIED FIELD F? (IN eV/nm)'
        READ*, F
        VAP = F * BSE * NTH
        IF (VAP .EQ. V10) VAP = (VAP + EDIV / 2)
        NST = 50 + NINT(ABS((-(VAP / NTH) + V10)/0.01))
        DLTAZ = BSE / NST
        DLTAV = (-(VAP / NTH) + V10) / NST
        PRINT*,'WHAT IS THE MAX Al CONCENTRATION'
        PRINT*, 'ANYWHERE IN THE STRUCTURE?'
        READ*, XMAX
        MMAX = 0.0636 + 0.0552 * XMAX + (0.0092 * XMAX**2)
        PRINT*,'WHAT IS THE MIN Al CONCENTRATION'
        PRINT*, 'ANYWHERE IN THE STRUCTURE?'
        READ*, XMIN
        MMIN = 0.0636 + 0.0552 * XMIN + (0.0092 * XMIN**2)
        DLTAAL = (XMAX - XMIN) / NST
        PRINT 10, 'E(eV)', 'LOG10(T)'
10      FORMAT (//, 1X, A7, 1X, A15, 1X, /, 1X, 24('='))
        OPEN (UNIT = 59, FILE = 'ALSTAIR.DAT', STATUS = 'NEW')
        DO NE = 1, 2000
          E = 1.1 * V10 - NE * EDIV
          T1(1) = (1.0,0.0)
          T1(2) = (1.0,0.0)
          T1(3) = (0.0,0.0)
          T1(4) = (0.0,0.0)
          DO NT = 1, NTH
            V0 = V00 - (VAP / NTH) * (NT - 1)
            Z = Z00 + (NT - 1) * BSE
            DO I = 1, NST
              VL = V0 + (I - 1) * DLTAV
              VR = VL + DLTAV
              XL = XMIN + (I - 1) * DLTAAL
              ML = 0.0636 + 0.0552 * XL + (0.0092 * XL**2)
```

```
            XR = XL + DLTAAL
            MR = 0.0636 + 0.0552 * XR + (0.0092 * XR**2)
            CALL EFFMASSTEP( E, VL, VR, ML, MR, FK, Z, T1)
            Z = Z + DLTAZ
          END DO
          Z = Z00 + NT * BSE
          VL = VR
          VR = V00 - (VAP / NTH) * NT
          CALL EFFMASSTEP(E, VL, VR, MMAX, MMIN, FK, Z, T1)
        END DO
        T = ABS(T1(1))**2
        T = (1.0 / T)
        T = LOG10(T)
        PRINT 100, E, T
100     FORMAT (F7.3, E12.4)
        WRITE (59,200) E, T
200     FORMAT (2E15.8)
      END DO
      END
```

```
                        PROGRAM JVMSB
C
C
C     This program calculates the quantum mechanical tunneling current
C     through a series of step potential barriers under an applied
C     electric field resulting in a voltage drop of VAP over the length
C     of the array. It assumes uniform effective mass of mo throughout
C     the structure.Data files of LOG10(Tunneling current) v.s. applied
C     voltage are written into the output file is JVMSB.DAT
C
C
      IMPLICIT REAL*8 (A-H, O-Z)
      DIMENSION T1(4)
      COMPLEX*16 T1, AKI, AKT
      FK = 26.2451
      V00 = 0.0
      Z0 = 0.0
      E = 0.005
      PRINT*,'ENTER THE NUMBER OF BARRIERS'
      READ*, NBAR
      PRINT*,'ENTER THE BARRIER HEIGHTS (eV), WIDTHS (nm),
     + AND SEPARATIONS (nm)'
      READ*, V10, BW, DSEP
      NPER = (NBAR - 1)
      PER = BW + DSEP
      PRINT 10, 'VAP(eV)', 'LOG10(TUNCUR)'
10    FORMAT ( //,A9,1X,A15,1X,/ 1X,24('~'))
      OPEN (UNIT = 89, FILE = 'JVMSB.DAT', STATUS = 'NEW')
C
C   Here's the voltage loop
C
      DO NV = 1, 200
        VDIV = 0.01
        VAP = 2.0 - NV * VDIV
        F = VAP / (NPER * PER + BW)
        NST = 25 + IDNINT(F * BW / 0.001)
        NWST = NST * (DSEP / BW)
        DLTAV = (F * BW) / NST
        DLTAZ = BW / NST
        WDLTAV = (F * DSEP) / NWST
        WDLTAZ = DSEP / NWST
        T1(1) = (1.0,0.0)
        T1(2) = (1.0,0.0)
        T1(3) = (0.0,0.0)
        T1(4) = (0.0,0.0)
C
C    Here's the period loop
C
        DO N = 1, NPER
          Z = Z0 + (N - 1) * PER
          VL = V00 - F * (N - 1) * PER
          VR = V10 - F * (N - 1) * PER
          CALL STPTRN(E, VL, VR, FK, Z, T1)
C
C    Here's the top edge of the barrier loop
C
          DO I = 1, (NST - 1)
```

```
            Z = Z + DLTAZ
            VL = V10 - (F * (N - 1) * PER) - (I - 1) * DLTAV
            VR = VL - DLTAV
            CALL STPTRN(E, VL, VR, FK, Z, T1)
          END DO
C
C     Here's the trailing edge of the barrier
C
          Z = Z0 + ((N - 1) * PER) + BW
          VL = V10 - F * ((N - 1) * PER + BW) + DLTAV
          VR = V00 - F * ((N - 1) * PER + BW)
          CALL STPTRN(E, VL, VR, FK, Z, T1)
C
C     Here's the well loop
C
          DO J = 1, (NWST - 1)
            Z = Z + WDLTAZ
            VL = V00 - F * ((N - 1) * PER + BW) - (J - 1) * WDLTAV
            VR = VL - WDLTAV
            CALL STPTRN(E, VL, VR, FK, Z, T1)
          END DO
        END DO
C
C     The following are the computations for the last barrier
C
        Z = NPER * PER
        VL = VR
        VR = V10 - (F * NPER * PER)
        CALL STPTRN(E, VL, VR, FK, Z, T1)
        DO M = 1, (NST - 1)
          Z = Z + DLTAZ
          VL = V10 - (F * NPER * PER) - (M - 1) * DLTAV
          VR = VL - DLTAV
          CALL STPTRN(E, VL, VR, FK, Z, T1)
        END DO
        Z = NPER * PER + BW
        VL = V10 - F * ((NPER * PER) + BW) + DLTAV
        VR = V00 - F * ((NPER * PER) + BW)
        CALL STPTRN(E, VL, VR, FK, Z, T1)
C
C     This takes care of all the barriers
C
        AKI = FK * E
        AKI = SQRT(AKI)
        AKT = FK * (E - VR)
        AKT = SQRT(AKT)
        T = ABS(T1(1))**2
        T = 1.0 / T
        TUNCUR = (AKT / AKI) * T
        TUNCUR = LOG10(TUNCUR)
        PRINT 20, VAP, TUNCUR
20      FORMAT ( F7.3, E12.4)
        WRITE (89,30) VAP, TUNCUR
30      FORMAT (2E15.8)
      END DO
      END
```

```
                              PROGRAM JVALMSB
C
C
C     This program calculates the quantum mechanical tunneling current
C     through a series of step potential barriers under an applied
C     electric field resulting in a voltage drop of VAP over the
C     length of the array.
C     This program uses the subroutine EFFMASSTEP. It is intended for
C     use with GaAs-Al(x)Ga(1-x)As superlattices, taking account of the
C     effective mass of the electron in each layer of the superlattice.
C     Data files of LOG10(Tunneling current) vs. applied voltage are
C     written into the output file JVALMSB.DAT
C
C
      IMPLICIT REAL*8 (A-H, O-Z)
      REAL*8 MX, MY, MI, MT
      DIMENSION T1(4)
      COMPLEX*16 T1, AKI, AKT
      FK = 26.2451
      V00 = 0.0
      Z0 = 0.0
      E = 0.005
      PRINT*,'ENTER THE NUMBER OF BARRIERS'
      READ*, NBAR
      PRINT*,'ENTER THE BARRIER HEIGHTS (eV), WIDTHS (nm)
     + AND SEPARATIONS (nm)'
      READ*, V10, BW, DSEP
      PRINT*,'Remember, the Al concentration in the barrier is
     + higher than in the well!!!!'
      PRINT*,'WHAT IS THE Al CONCENTRATION IN THE BARRIER, XMAX?'
      READ*, XMAX
      PRINT*,'WHAT IS THE Al CONCENTRATION IN THE WELL, XMIN?'
      READ*, XMIN
      MX = 0.0636 + 0.0552 * X + 0.0092 * X**2
      MY = 0.0636 + 0.0552 * Y + 0.0092 * Y**2
      MI = MY
      MT = MY
      NPER = (NBAR - 1)
      PER = BW + DSEP
      PRINT 10, 'VAP(eV)', 'LOG10(TUNCUR)'
10    FORMAT ( //,A9,1X,A15,1X,/ 1X,24('~'))
      OPEN (UNIT = 86, FILE = 'JVALMSB.DAT', STATUS = 'NEW')
C
C   Here's the voltage loop
C
      DO NV = 1, 200
        VDIV = 0.01
        VAP = 2.0 - NV * VDIV
        F = VAP / (NPER * PER + BW)
        NST = 25 + IDNINT(F * BW / 0.001)
        NWST = NST * (DSEP / BW)
        DLTAV = (F * BW) / NST
        DLTAZ = BW / NST
        WDLTAV = (F * DSEP) / NWST
        WDLTAZ = DSEP / NWST
        T1(1) = (1.0,0.0)
        T1(2) = (1.0,0.0)
```

```
      T1(3) = (0.0,0.0)
      T1(4) = (0.0,0.0)
C
C     Here's the period loop
C
      DO N = 1, NPER
        Z = Z0 + (N - 1) * PER
        VL = V00 - F * (N - 1) * PER
        VR = V10 - F * (N - 1) * PER
        CALL EFFMASSTEP(E, VL, VR, MY, MX, FK, Z, T1)
C
C     Here's the top edge of the barrier loop
C
        DO I = 1, (NST - 1)
          Z = Z + DLTAZ
          VL = V10 - (F * (N - 1) * PER) - (I - 1) * DLTAV
          VR = VL - DLTAV
          CALL EFFMASSTEP(E, VL, VR, MX, MX, FK, Z, T1)
        END DO
C
C     Here's the trailing edge of the barrier
C
        Z = Z0 + ((N - 1) * PER) + BW
        VL = V10 - F * ((N - 1) * PER + BW) + DLTAV
        VR = V00 - F * ((N - 1) * PER + BW)
        CALL EFFMASSTEP(E, VL, VR, MX, MY, FK, Z, T1)
C
C     Here's the well loop
C
        DO J = 1, (NWST - 1)
          Z = Z + WDLTAZ
          VL = V00 - F * ((N - 1) * PER + BW) - (J - 1) * WDLTAV
          VR = VL - WDLTAV
          CALL EFFMASSTEP(E, VL, VR, MY, MY, FK, Z, T1)
        END DO
      END DO
C
C     The following are the computations for the last barrier
C
      Z = NPER * PER
      VL = VR
      VR = V10 - (F * NPER * PER)
      CALL EFFMASSTEP(E, VL, VR, MY, MX, FK, Z, T1)
      DO M = 1, (NST - 1)
        Z = Z + DLTAZ
        VL = V10 - (F * NPER * PER) - (M - 1) * DLTAV
        VR = VL - DLTAV
        CALL EFFMASSTEP(E, VL, VR, MX, MX, FK, Z, T1)
      END DO
      Z = NPER * PER + BW
      VL = V10 - F * ((NPER * PER) + BW) + DLTAV
      VR = V00 - F * ((NPER * PER) + BW)
      CALL EFFMASSTEP(E, VL, VR, MX, MY, FK, Z, T1)
C
C     This takes care of all the barriers
C
      AKI = FK * MI * E
      AKI = SQRT(AKI)
```

```
        AKT = FK * MT * (E - VR)
        AKT = SQRT(AKT)
        T = ABS(T1(1))**2
        T = 1.0 / T
        TUNCUR = (AKT / AKI) * (MI / MT) * T
        TUNCUR = LOG10(TUNCUR)
        PRINT 20, VAP, TUNCUR
20      FORMAT ( F7.3, E12.4)
        WRITE (86,30) VAP, TUNCUR
30      FORMAT (2E15.8)
      END DO
      END
```

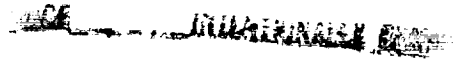

```
                        PROGRAM JVSAWTOOTH
C
C
C       This program calculates the quantum mechanical tunneling
C       current through a series of sawtooth potential barriers
C       under an applied voltage VAP. It uses the subroutine STPTRN.
C       Data files of LOG10(tunneling current) versus applied voltage
C       VAP are created under the filename JVSAWTOOTH.DAT
C
C
        IMPLICIT REAL*8 (A-H, O-Z)
        DIMENSION T1(4)
        COMPLEX*16 T1, AKI, AKT
        FK = 26.2451
        V00 = 0
        Z00 = 0
        E = 0.005
        PRINT*, 'HOW MANY SAWTEETH, AND HOW WIDE ARE THEIR BASES IN nm ?'
        READ*, NTH, BSE
        PRINT*, 'HOW HIGH IS THE TRAILING EDGE OF EACH TOOTH (eV)?'
        READ*, V10
C
C       THIS TAKES CARE OF THE INPUT STATEMENTS
C
        PRINT 10, 'VAP (V)', 'LOG10(TUNCUR)'
10      FORMAT (//, 1X, A9, 1X, A15, 1X, /, 1X, 24('~'))
        OPEN(UNIT = 51, FILE = 'JVSAWTOOTH.DAT', STATUS = 'NEW')
        DO NV = 1, 200
          VDIV = 0.01
          VAP = 2.0 - VDIV * NV
          IF (VAP .EQ. V10) VAP = VAP + VDIV / 2
          NST = 25 + NINT(ABS((-(VAP / NTH) + V10) / 0.001))
          DLTAZ = BSE / NST
          DLTAV = (-(VAP / NTH) + V10) / NST
          T1(1) = (1.0,0.0)
          T1(2) = (1.0,0.0)
          T1(3) = (0.0,0.0)
          T1(4) = (0.0,0.0)
          DO NT = 1, NTH
            V0 = V00 - (VAP / NTH) * (NT - 1)
            Z = Z00 + (NT - 1) * BSE
            DO I = 1, NST
              VL = V0 + (I - 1) * DLTAV
              VR = VL + DLTAV
              CALL STPTRN(E, VL, VR, FK, Z, T1)
              Z = Z + DLTAZ
            END DO
            Z = Z00 + NT * BSE
            VL = VR
            VR = V00 - (VAP / NTH) * NT
            CALL STPTRN(E, VL, VR, FK, Z, T1)
          END DO
          AKI = FK * E
          AKI = SQRT(AKI)
          AKT = FK * (E - VR)
          AKT = SQRT(AKT)
          T = ABS(T1(1))**2
          T = (1.0 / T)
```

```
          TUNCUR = (AKT / AKI) * T
          TUNCUR = LOG10(TUNCUR)
          PRINT 100, VAP, TUNCUR
100       FORMAT (F7.3, E12.4)
          WRITE (51,200) VAP,TUNCUR
200       FORMAT (2E15.8)
        END DO
        END
```

```
                        PROGRAM JVALSTAIR
C
C
c       This program calculates the quantum mechanical tunneling
c       current through a series of sawtooth potential barriers
c       under an applied electic field resulting in a voltage drop
c       over the length of the entire barrier of vap. This program
c       uses the subroutine EFFMASSTEP. It takes into
c       account the changes in effective mass of the electron in each
c       layer in the superlattice structure. It is intended for use
c       on GaAs-Al(x)Ga(1-x)As sawtooth superlattices.
c       Data files of LOG10(tunneling current) versus applied voltage
c       VAP are in output file JVALSTAIR.DAT
c
        IMPLICIT REAL*8 (A-H, O-Z)
        REAL*8 M1,M2,ML,MR,MI,MT
        DIMENSION T1(4)
        COMPLEX*16 T1, AKI, AKT
        FK = 26.2451
        V00 = 0
        Z00 = 0
        E = 0.005
        PRINT*, 'HOW MANY SAWTEETH, AND HOW WIDE ARE THEIR BASES IN nm ?'
        READ*, NTH, BSE
        PRINT*, 'HOW HIGH IS THE TRAILING EDGE OF EACH TOOTH (eV)?'
        READ*, V10
        PRINT*,'WHAT IS THE MAX Al CONCENTRATION'
        PRINT*, 'ANYWHERE IN THE STRUCTURE?'
        READ*, XMAX
        PRINT*,'WHAT IS THE MIN Al CONCENTRATION'
        PRINT*, 'ANYWHERE IN THE STRUCTURE?'
        READ*, XMIN
        M1 = 0.0636 + (0.0552 * XMAX) + (0.0092 * XMAX**2)
        M2 = 0.0636 + (0.0552 * XMIN) + (0.0092 * XMIN**2)
        MI = M2
        MT = M2
        PRINT 10, 'VAP(eV)', 'LOG10(TUNCUR)'
10      FORMAT (//, 1X, A9, 1X, A15, 1X, /, 1X, 24('='))
        OPEN (UNIT = 60, FILE = 'JVALSTAIR.DAT', STATUS = 'NEW')
        DO NV = 1, 200
          VDIV = 0.01
          VAP = 2.0 - VDIV * NV
          IF (VAP .EQ. V10) VAP = (VAP + VDIV / 2)
          NST = 25 + NINT(ABS((-(VAP / NTH) + V10)/0.001))
          DLTAZ = BSE / NST
          DLTAV = (-(VAP / NTH) + V10) / NST
          DLTAAL = (XMAX - XMIN) / NST
          T1(1) = (1.0,0.0)
          T1(2) = (1.0,0.0)
          T1(3) = (0.0,0.0)
          T1(4) = (0.0,0.0)
          DO NT = 1, NTH
            V0 = V00 - (VAP / NTH) * (NT - 1)
            Z = Z00 + (NT - 1) * BSE
            DO I = 1, NST
              VL = V0 + (I - 1) * DLTAV
              VR = VL + DLTAV
              XL = XMIN + (I - 1) * DLTAAL
```

```
            ML = 0.0636 + 0.0552 * XL + (0.0092 * XL**2)
            XR = XL + DLTAAL
            MR = 0.0636 + 0.0552 * XR + (0.0092 * XR**2)
            CALL EFFMASSTEP( E, VL, VR, ML, MR, FK, Z, T1)
            Z = Z + DLTAZ
          END DO
          Z = Z00 + NT * BSE
          VL = VR
          VR = V00 - (VAP / NTH) * NT
          CALL EFFMASSTEP(E, VL, VR, MR, M2, FK, Z, T1)
        END DO
        AKI = FK * MI * E
        AKI = SQRT(AKI)
        AKT = FK * MT * (E - VR)
        AKT = SQRT(AKT)
        T = ABS(T1(1))**2
        T = (1.0 / T)
        TUNCUR = (AKT / AKI) * (MI / MT) * T
        TUNCUR = LOG10(TUNCUR)
        PRINT 100, VAP, TUNCUR
100     FORMAT (F7.3, E12.4)
        WRITE (60,200) VAP, TUNCUR
200     FORMAT (2E15.8)
      END DO
      END
```

```
                              PROGRAM WELL
C
C       This program finds the total transfer matrix element M11
C       for a single quantum well of depth V1 and width a, as a
C       function of the energy below the top of the well. A constant
C       effective mass m* = mo is assumed. Data files of LOG10(M11)
C       versus E are generated.
C
        IMPLICIT REAL*8 (a-h,o-z)
        REAL*8 M11
        DIMENSION T1(4)
        COMPLEX*16 T1
        FK = 26.2451
        Z0 = 0
        V0 = 0
        PRINT*, 'ENTER WELL DEPTH V1 IN eV (ENTER ABS VALUE)'
        READ*, V1
        PRINT*, 'ENTER WELL WIDTH, a,  IN NANOMETERS'
        READ*, A
        OPEN (UNIT = 80, FILE = 'WELL', STATUS = 'NEW')
        PRINT 10,'E(eV)','LOG10(M11)'
10      FORMAT (//,1X,A7,1X,A11,1X,/,1X,24('='))
        V1 = -V1
        EDIV = V1 / 2000
        DO 20 NE = 1,2000
          E =  NE * EDIV
          Z = Z0
          T1(1) = (1.0,0.0)
          T1(2) = (1.0,0.0)
          T1(3) = (0.0,0.0)
          T1(4) = (0.0,0.0)
          CALL STPTRN(E,V0,V1,FK,Z,T1)
          Z = Z + A
          CALL STPTRN(E,V1,V0,FK,Z,T1)
          M11 = ABS(T1(1))
          M11 = LOG10(M11)
          WRITE (80,300) E, M11
300       FORMAT (2E15.6)
          PRINT 35, E, M11
35        FORMAT (F7.2, E12.3)
20      CONTINUE
C
C       END OF E-LOOP
C
        END
```

```
                        PROGRAM ALGAASWELL
C
C       This program calculates the total transfer matrix element
C       M11 for a single Al(x)Ga(1-x)As-Al(y)Ga(1-y)As quantum well
C       of depth V1 and width a, as a function of the energy below the
C       top of the well. The input well depth must be in accord with
C       the values used for x and y, where x and y are the aluminum
C       concentrations outside and inside the well,respectively. Data
C       files of LOG10(M11) versus E are generated.
C
        IMPLICIT REAL*8 (A-H,O-Z)
        REAL*8 M1, M2, M11
        DIMENSION T1(4)
        COMPLEX*16 T1
        FK = 26.2451
        Z0 = 0
        V0 = 0
        PRINT*, 'ENTER WELL DEPTH V1 IN eV (ENTER ABS VALUE)'
        READ*, V1
        PRINT*, 'ENTER WELL WIDTH, a, IN NANOMETERS'
        READ*, A
        PRINT*, 'ENTER MIN AL CONTENT, y, (IN THE WELL)'
        READ*, XMIN
        PRINT*,'ENTER MAX AL CONTENT, x, (OUTSIDE THE WELL)'
        READ*, XMAX
        M1 = 0.0636 + (0.0552 * XMAX) + (0.0092 * XMAX**2)
        M2 = 0.0636 + (0.0552 * XMIN) + (0.0092 * XMIN**2)
        OPEN (UNIT = 73, FILE = 'ALGAASWELL', STATUS = 'NEW')
        PRINT 10,'E(eV)','LOG10(M11)'
10      FORMAT (//,1X,A7,1X,A11,1X,/,1X,24('='))
        V1 = -V1
        EDIV = V1 / 2000
        DO 20 NE = 1,2000
          E =  NE * EDIV
          Z = Z0
          T1(1) = (1.0,0.0)
          T1(2) = (1.0,0.0)
          T1(3) = (0.0,0.0)
          T1(4) = (0.0,0.0)
          CALL EFFMASSTEP(E,V0,V1,M1,M2,FK,Z,T1)
          Z = Z + A
          CALL EFFMASSTEP(E,V1,V0,M2,M1,FK,Z,T1)
          M11 = ABS(T1(1))
          M11 = LOG10(M11)
          WRITE (73,300) E,M11
300       FORMAT (2E15.6)
          PRINT 35, E, M11
35        FORMAT (F7.2, E12.3)
20      CONTINUE
C
C       END OF E-LOOP
C
        END
```

```
                        PROGRAM STARKMASS
C
C       This program calculates the total transfer matrix element
C       M11 in a single Al(x)Ga(1-x)As-Al(y)Ga(1-y)As quantum well,
C       of depth V1 and width a as a function of the energy below the
C       top of the well and the applied field F. This program assumes
C       the applied field is restricted to the area of the well.
C       The input value of V1 must be compatible with the values of
C       x and y, the aluminum concentrations outside and inside the
C       well, respectively. 75 intervals are used. A data file of
C       LOG10(M11) versus E is generated.
C
C
        IMPLICIT REAL*8 (A-H,O-Z)
        REAL*8 M1, M2, M11
        DIMENSION T1(4)
        COMPLEX*16 T1
        FK = 26.2451
        Z0 = 0
        V0 = 0
        NST = 75
        PRINT*, 'ENTER WELL DEPTH |V1| IN eV'
        READ*, V1
        PRINT*, 'ENTER WELL WIDTH a IN nm'
        READ*, A
        PRINT*, 'ENTER THE APPLIED FIELD STRENGTH F IN eV/nm'
        READ*, F
        PRINT*,'ENTER Al CONTENT x OUTSIDE WELL'
        READ*, XMAX
        PRINT*,'ENTER Al CONTENT y INSIDE WELL'
        READ*, XMIN
        M1 = 0.0636 + 0.0552 * XMAX + (0.0092 * XMAX**2)
        M2 = 0.0636 + 0.0552 * XMIN + (0.0092 * XMIN**2)
        V1 = -V1
        VAP = F * A
        V2 = V1 - VAP
        VF = V0 - VAP
        DLTAV = ABS(V1 - V2)
        DLTAV = DLTAV/(NST)
        DLTAZ = A/NST
        OPEN (UNIT = 13, FILE = 'STARKMASS.DAT', STATUS = 'NEW')
        PRINT 10, 'E(eV)', 'M11'
10      FORMAT ( //,1X, A7, 1X, A11, 1X, / 1X, 24('=') )
C
C       Here starts the energy loop
C
        EDIV = V1/2000
        DO 20 NE = 1, 2000
          E = (NE * EDIV)
          Z = Z0
          T1(1) = ( 1.0, 0.0 )
          T1(2) = ( 1.0, 0.0 )
          T1(3) = ( 0.0, 0.0 )
          T1(4) = ( 0.0, 0.0 )
          CALL EFFMASSTEP(E,V0,V1,M1,M2,FK,Z,T1)
           IF (DLTAV .EQ. 0) THEN
             Z = Z0 + A
             VL = V2
```

```
              VR = VF
              CALL EFFMASSTEP(E,VL,VR,M2,M1,FK,Z,T1)
              GO TO 29
             END IF
             DO I = 1, (NST - 1)
              Z = Z + DLTAZ
              VL = V1 - (I - 1) * DLTAV
              VR = VL - DLTAV
              CALL EFFMASSTEP(E,V1,VR,M2,M2,FK,Z,T1)
             END DO
28           VL = V2
             VR = VF
             Z = Z0 + A
             CALL EFFMASSTEP(E,VL,VR,M2,M1,FK,Z,T1)
C
C             the control passes to statement 29 from the block IF
C             above which handles the case of zero-field
C
29           M11 = ABS(T1(1))
             M11 = LOG10(M11)
             PRINT 30, E,M11
30           FORMAT (F7.3,E12.3)
             WRITE (13,300) E, M11
300          FORMAT (2E15.7)
20         CONTINUE
C
C          END OF E-LOOP
C
21           END
```

```
                        PROGRAM AIRYWELL
C
C    THIS PROGRAM CALCULATES THE RATIO OF COEFFICIENTS OF THE WAVE
C    FUNCTION ON THE DOWNSTREAM SIDE OF A SINGLE QUANTUM WELL, (F/E),
C    AS A FUNCTION OF INCIDENT ENERGY AND APPLIED ELECTRIC FIELD.
C    A PLOT IS THEN GENERATED GIVING THIS RATIO VERSUS ENERGY. WHERE-
C    EVER THE RATIO IS MAXIMIZED, A VIRTUAL STATE EXISTS. THIS PROGRAM
C    ASSUMES A GaAs-Al(0.5)Ga(0.5)As 3 nm WIDE WELL, 0.5 eV DEEP, WITH
C    CONSTANT EFFECTIVE MASS m* = 0.0636.
C
C
      DIMENSION EARR(1000), RARR(1000)
      W = 1.5
      V0 = 0.4
      PRINT*,'WHAT APPLIED FIELD STRENGTH IN V/nm?'
      READ*, FAPP
      EMAX = FAPP * W
      EMIN = -V0 - FAPP * W
      FAPP = FAPP * 1.0E9
C
C  OPEN GKS
      CALL GOPKS (6,1)
C  OPEN THE WORKSTATION
      CALL GOPWK (1,2,1)
C  ACTIVATE THE WORKSTATION
      CALL GACWK (1)
C
      DO I = 1, 1000
        A = 1.2103E-3
        B = 1.2147E6
        EARR(I) = EMIN + (I/1000.0) * (EMAX - EMIN)
        X1NEG = A*(-W)* FAPP**(1./3.) + B*EARR(I)/FAPP**(2./3.)
        X1POS = A*(-W)*FAPP**(1./3.) + B*(EARR(I) + V0)/FAPP**(2./3.)
        X2NEG = A*(W)*FAPP**(1./3.) + B*(EARR(I) + V0)/FAPP**(2./3.)
        X2POS = A*(W)*FAPP**(1./3.) + B*EARR(I)/FAPP**(2./3.)
        C = AI(-X1NEG)*BID(-X1POS) - AID(-X1NEG)*BI(-X1POS)
        D = AI(-X1POS)*AID(-X1NEG) - AID(-X1POS)*AI(-X1NEG)
        P = AI(-X2NEG)/AI(-X2POS)
        Q = BI(-X2NEG)/AI(-X2POS)
        R = BI(-X2POS)/AI(-X2POS)
        S = AID(-X2NEG)/AID(-X2POS)
        T = BID(-X2NEG)/AID(-X2POS)
        U = BID(-X2POS)/AID(-X2POS)
        F = C/D * (S - P) + T - Q
        E = U * (C/D * P + Q) - R * (C/D * S + T)
        RARR(I) = F/E
      END DO
      CALL EZXY(EARR,RARR,1000,'f/e')
C
C  DEACTIVATE AND CLOSE THE WORKSTATION
      CALL GDAWK (1)
      CALL GCLWK (1)
C  CLOSE GKS
      CALL GCLKS
      STOP
      END
```

REFERENCES

1. "The Quantum-Effect Device: Tomorrow's Transistor?", R. T. Bate, Scientific American, Vol 258, No 3, pp 96-100, March 1988

2. "Band Structure, Impurities and Excitons in Superlattices", M. Altarelli, Proceedings of Les Houches Winterschool in Semiconductor Superlattices and Heterojunctions, G. Allan, G. Bastard, N. Boccara, M. Lannoo and M. Voos, editors, Springer-Verlag, 1986

3. "Tunneling Phenomena in Solids", E. Burstein, S. Lundqvist, Plenum Press, 1969

4. "Band-Gap Engineering: From Physics and Materials to New Semiconductor Devices", F. Capasso, Science, Vol 235, pp 172-176, 9 January 1987

5. "Compositionally Graded Semiconductors and Their Device Applications", F. Capasso, Am. Rev. Mater. Sci., Vol 16, pp263-291, 1986

6. "Resonant Tunneling Through Double Barriers, Perpendicular Quantum Transport Phenomena in Superlattices, and Their Device Applications", F. Capasso, K. Mohammed, and A. Cho, IEEE J.Q.E., Vol QE-22, No. 9, pp1853-1869, September 1986

7. "Staircase Solid State Photomultipliers and Avalanche Photodiodes with Enhanced Ionization Ratios", F. Capasso, W. Tsang, and G. Williams, IEEE Transactions on Electron Devices, Vol. ED-30, No. 4, pp 381- 390, April 1983

8. "Observation of Resonant Tunneling Through Compositionally Graded Parabolic Quantum Well", S. Sen, F. Capasso, K. Mohammed, and A. Cho, Applied Physics Letters, November 1987

9. "Superlattice and Negative Differential Conductivity in Semiconductors", L. Esaki and R. Tsu, IBM J. Res. Devel., Vol 14, pp 61-65, 1970

10. "Resonant Tunneling in Semiconductor Double Barriers", L. Chang, L. Esaki, R. Tsu, App. Phys. Lett., Vol 24, pp 593-595, 1974 11. "Tunneling in a Finite Superlattice", R. Tsu and L. Esaki, App. Phys. Lett., Vol. 22, No. 11, pp 562-564, 1 June 1973

12. "New Phenomenon in Narrow Germanium p-n Junctions" , L. Esaki, Phys Rev., Vol. 109, No. 2, p603-604, January 15, 1958

13. "Probing Semiconductor-Semiconductor Interfaces", R.S. Bauer and G.Margaritondo, Physics Today, January 1987, pp 27-39

14. "Electronic Tunneling in GaAs/AlGaAs Heterostructures", A. C. Marsh, I.E.E.E. J.Q.E., Vol. QE-21, No. 4, pp 371-376, April 1987

15. "Interface Connection Rules for Effective Mass Wavefunctions at an Abrupt Heterojunction between Two Different Semiconductors" Qi-Gao Zhu, H. Kroemer, Phys. Rev. B, Vol. 27, No. 6, pp 3519-3526, 15 March 1983

16. "On the Interface Connection Rules for Effective-mass Wave Functions at an Abrupt Heterojunction between Two Semiconductors with Different Effective Mass", H. Kroemer and Qi-Gao Zhu, J. Vac. Sci. Tech., Vol 21, No. 2, pp 551-553, July/August 1982

17. "An Efficient Algorithm for Calculating Bound- and Resonant-energy Spectra ", C. Schwartz, Proceedings, IEEE Symposium on Quantum Wells and Heterojunction Superlattices, Vol 792, pp 257-263, 1986

18. "How Much Al in the AlGaAs-GaAs Laser?", D. L. Rode, J.A.P., Vol 45, No. 9, pp 3887-3891, September 1974

19. *Physics of Semiconductor Lasers*, G. B. H. Thompson, Wiley, 1980

20. *Quantum Mechanics*, E. Merzbacher, Wiley, New York, 1970

21. *Quantum Mechanics*, C. Cohen-Tannoudji, B. Diu, F. Laloe, Wiley-Interscience, 1977

22. *Semiconductor Statistics*, J. S. Blakemore, Dover, New York, 1987

23. "Transmission of Bloch Waves through Crystal Interfaces", P. J. Price, Proc. Int'l. Conf. on Physics of Semiconductors, pp 99-103, Exeter, July 1962

24. "A Ray Analysis of Optical Resonators Formed by Two Spherical Mirrors", I. A. Ramsay, J. J. Degnan, Applied Optics, Vol. 9, No. 2, pp 385-398, February, 1970

25. "The Effect of Electrode-Polymer Interfacial Layers on Polymer Conduction", A. Van Roggen and P.H.E. Meijer, IEEE Trans. on Electrical Insulation ,Vol. EI-21 No.3, pp 307-311, June 1986

26. "The Effect of Electrode-Polymer Interfacial Layers on Polymer Conduction. Part 2: Device Summary", A. Van Roggen and P.H.E. Meijer, Proc. Third Int. Symp. on Molecular Electronic Devices, October 1986, Elsevier, Amsterdam.

27. *Mathematical Handbook for Scientists and Engineers*, G. A. Korn and T.M. Korn, p 368, McGraw-Hill 1961.

28. "The Quantum Bouncer", R. I. Gibbs, American Journal of Physics, Vol. 43, pp 25-28, January 1975

29. "The Quantum Bouncer Revisited", R. D. Desko, D. J. Bord, Am. J. Phys., Vol 51, No. 1, pp 82-83, January 1983

30. "Quantum Bouncer in a Closed Court", V. C. Aguilera-Navarro, H. Iwamoto, E. Ley-Koo, A. H. Zimerman, Am. J. Phys., Vol. 49, No. 7, pp 648-651, July 1981

31. *Elementary Differential Equations and Boundary Value Problems*, Boyce and DiPrima, Wiley, 1977.

32. *Handbook of Mathematical Functions*, M. Abramowitz and I. Stegun, Dover, New York, 1970

33. *Solid State Physics*, J. S. Blakemore, W. S. Saunders, 1974

34. "An Empirical Pseudopotential Analysis of (100) and (110) GaAs-Al(x)Ga(1-x)As Heterojunctions", A. Marsh, J. Inkson, Journal of Physics C: Solid State Physics, Vol. 19, pp 43-52, 1986

35. "Theory of the Energy Band Lineup at an Abrupt Semiconductor Heterojunction", W. R. Frensley and H. Kroemer, Phys. Rev. B, Vol. 16, No. 6, pp 2642-2652, 15 September 1977

36. "Theory of Band Line-ups", W. A. Harrison, J. Vac. Sci. Tech. B, Vol. 3, No. 4, pp 1231-1238, July/August 1985

37. "Ionization Potentials, Electron Affinities,, and Band Offsets", J. A. Van Vechten, J. Vac. Sci. Tech. B, Vol. 3, No. 4, pp 1240- 1244, July/August 1985

38. "Deep-Level Impurities: A Possible Guide to Prediction of Band-Edge Discontinuities in Semiconductor Heterojunctions", J. M. Langer and H. Heinrich, Physical Review Letters, Vol.55, No. 13, pp 1414-1417, 23 September 1985

39. "On the Band Offsets of AlGaAs/GaAs and Beyond", W. I. Wang, Solid-State Electronics, Vol. 29, No. 2, pp 133-139

40. "Energy Band Alignment in GaAs:(Al,Ga)As Heterostructures: The Dependence on Alloy Composition, J. Batey and S. L. Wright, J. Appl. Phys., Vol. 59, No. 1, pp 200-209, 1 January 1986

41. "Electronic Structure of an Isolated GaAs-GaAlAs Quantum Well in a Strong Electric Field", E. J. Austin and M. Jaros, Phys. Rev. B. Vol. 31, No. 8, pp 5569-5571, 15 April 1985

42. "Variational Calculations on a Quantum Well in an Electric Field" G. Bastard, E.E. Mendez, L.L. Chang, and L. Esaki, Phys. Rev B, Vol. 28, No. 6, pp 3241-3245, 15 September 1983

43. "Electronic States in Semiconductor Heterostructures", G. Bastard and J. A. Brum, I.E.E.E. J.Q.E., Vol QE-22, No. 9, pp 1625-1644, September 1986

44. *Selected Problems in Quantum Mechanics*, D. Ter Haar, Academic Press, 1964

NASA
National Aeronautics and Space Administration

Report Documentation Page

1. Report No.	2. Government Accession No.	3. Recipient's Catalog No.
NASA TM-100726		

4. Title and Subtitle

Tunneling Calculations for $GaAsAl_xGa_{(1-x)}As$ Graded Band-Gap Sawtooth Superlattices

5. Report Date

April 1991

6. Performing Organization Code

723

7. Author(s)

Kathrine A. Forrest and Paul H.E. Meijer

8. Performing Organization Report No.

89B00121

10. Work Unit No.

RTOP 723-506-44-21

9. Performing Organization Name and Address

Goddard Space Flight Center
Greenbelt, Maryland 20771

11. Contract or Grant No.

13. Type of Report and Period Covered

Technical Memorandum

12. Sponsoring Agency Name and Address

National Aeronautics and Space Administration
Washington, D.C. 20546-0001

14. Sponsoring Agency Code

15. Supplementary Notes

This report is made from a thesis.
Dr. Paul H.E. Meijer is Professor of Physics, The Catholic University of America, Washington, D.C.

16. Abstract

Quantum mechanical tunneling calculations for sawtooth (linearly graded band-gap) and step-barrier AlGaAs superlattices were performed by means of a transfer matrix method, within the effective mass approximation. The transmission coefficient and tunneling current versus applied voltage were computed for several representative structures. Particular consideration was given to effective mass variations. The tunneling properties of step and sawtooth superlattices show some qualitative similarities. Both structures exhibit resonant tunneling, however, because they deform differently under applied fields, the J-V curves differ.

17. Key Words (Suggested by Author(s))

sawtooth superlattices, AlGaAs, tunneling, quantum wells

18. Distribution Statement

Unclassified - Unlimited

Subject Category 76

19. Security Classif. (of this report)	20. Security Classif. (of this page)	21. No. of pages	22. Price
Unclassified	Unclassified	152	